Studying the effect of differentiation therapy on osteosarcoma

Chara Dimitriadi Evgenidi (MRes)

A thesis submitted in part fulfilment of the requirements of the degree of Doctor of Philosophy

School of Chemistry

College of Science and Engineering

University of Glasgow

October 2024

Abstract

Lack of terminal differentiation is widely observed in bone cancer patients, yielding fast-proliferating, immature cancer cells. A potential strategy for cancer treatment is differentiation therapy, where the aim is to "reprogramme" cancer cell behaviour, by inducing differentiation. Around 150 people are diagnosed with osteosarcoma (OS) in England and Wales each year, which is a malignant primary bone cancer, with highest incidence in young people between the ages of 10-24. Identifying small molecules that can restore differentiation potential in OS cells was considered a promising strategy, so known osteogenic conditions for MSCs, including nanokicking, and a known osteogenic medium, containing ascorbic acid, dexamethasone and β-glycerophosphate, were applied on osteosarcoma cell lines MG-63 and SAOS-2, and MSCs. Mechanical and chemical stimulation appeared to drive differentiation in OS cells, as evident by upregulation of RUNX2, OSX and/or ONN in different conditions. After confirming differentiation, a metabolomics analysis was performed, to observe what groups of metabolites and pathways are involved in differentiation, and to identify metabolites of interest.

Mechanical and chemical stimulation were shown to drive metabolic reprogramming in OS cells, by altering bioenergetics, and employing metabolic pathways that are reported to be impaired in OS, including TCA metabolism. Cholesterol sulfate (CS) and taurine (TAU) levels were found to be significantly altered differentiation, so they were tested on OS cells, along with mineralocorticoid fludrocortisone acetate (FA). The small molecules were tested on SAOS-2 and MG-63 cells, and differentiation appeared to occur in a time, and dose dependent manner, with a concentration of 10 μM showing enhanced differentiation after 7 days.

A cancer targeting delivery approach was attempted for glucocorticoid, differentiation agent dexamethasone, where the small molecule was tethered to glucose, via a hydrazone cleavable linker. A hydrazone bond was formed at the C3 position of dexamethasone, and extensive purification was carried out to obtain the hydrazone, in a mixture of *cis-trans* isomers. The dexamethasone hydrazone was then coupled with the carboxylic acid of the glucose linker, which generated a mixture of *cis* and *trans* isomers, which were successfully separated via RP-HPLC. The novel small molecules were individually characterised, and the *cis* isomer was deprotected under strongly basic conditions, with the aim of obtaining the de-acetylated species. This led to degradation on the C20 sidechain of dexamethasone's D-

ring, but the small molecule was isolated, and characterised, and was found to exhibit biological activity, through initial testing. The small molecule induced a small decrease in viability of MG-63 and SAOS-2 cells, without inducing extensive cytotoxicity. The conjugate presented enhanced differentiation, compared to dexamethasone, in a dose dependent-manner, in MG-63 cells, while more limited response was observed in SAOS-2 cells. Overall, conditions were identified that could drive differentiation in OS cells, while a novel small molecule was successfully synthesised, characterised, and found to present biological response in OS cells.

Table of Contents

Acknowledgments

I would like to the Dr David France for the support, and the guidance you have offered me throughout the PhD. I am incredibly privileged to have received this opportunity. Thank you for the useful advice, for the patience, the support when I was feeling anxious, the impromptu science chats, and the quick and helpful feedback. Thank you for all the scientific advice, and for taking the time to teach me.

I would like to thank Dr Matthew Dalby for giving me a chance to join the original cohort of the lifETIME CDT, and for making us feel like we can make a difference. Your optimism, your support, your kind words, and your encouragement when I have not always felt my best has been the most wonderful thing. Thank you also for welcoming me in the lab, and for providing me with the resources, and the guidance to carry out my biology work. Coming from a chemistry background, it has been an incredible opportunity to truly immerse myself in a whole new discipline.

To Dr Monica Tsimbouri I want to thank you for everything. From teaching me different techniques, to providing constant guidance and support throughout the project, I cannot imagine having done this without you. Thank you for helping me with experimental design, and for helping me collect and analyse the metabolomics samples. You took in a chemist and gave me the tools, and skills that I needed. Your prompt answers and feedback have saved me more times than I can count. You have always been there for me and have supported me through some of the toughest times of my life. It would not have been the same without you. I will always cherish our funny chats, and our deep conversations, and I will miss having you around on my next steps.

I want to thank the technical staff for all their help throughout my PhD. I would like to thank Al and the technicians for always helping me if I had any questions, and for providing support in the lab. I would like to thank Alec Mungall for help with NRM experimental design, and for helping me set up 1D NOE experiments. To James McIver, thank you for letting me analyse my final compound on the NMR, and for helping me troubleshoot, so I can get my final data. To Dr Giovanni Rossi, thank you for analysing my high-res mass spectra, for the funny chats, and for helping me figure out how to best analyse. To Dr Mark

Sprott thank you for being so patient with me at the start, and for teaching me how to be a biologist, and helping with experiments.

To the France group past and present. Thank you for accepting me and welcoming me. I will really miss working with you. Thank you for the laughs, and thank you for the help both mentally, and scientifically with experimental data, and spectroscopic analysis. To Dr Amy Dodds, thank you for helping me so much in the lab, and for being patient about the hydrazones. Thank you for the mental support, and for telling me I can do this. To Dr Leanne Riley, thank you for all the chemistry help, and for indulging me and listening to my wild NMR ramblings. You have helped me so much. To Charlotte, Francesca, Lorna, Sarah, and Marta thank you for being the best queens. I will miss you. Francesca, you are my CDT, chemistry, biology and desk buddy. Thank you for being so supportive. To the Henderson lab, and the chemical biology lab, you have been so kind, and welcoming. To my CEMI friends, it has been a blast. Thank you for the fun chats, the vents, and the support in the lab. To CYTOCHROMA and Dr Kate Cameron, thank you for helping early on with liver experiments, and for the recipe for growth factor differentiation.

To my CDT friends, especially Lydia, Lauren, Maria Laura, Elaine, Hannah and Narina. Thank you for the funny chats, the support, and for making this experience all the more special. Thank you for being there during the good times and the hard times. You have been my support system, and I cannot wait to see what the future holds for all of us. Each of you is amazing. I will look back fondly to our time together, and we will have a bond for life.

To my friends and family. I couldn't have done it without you. Thank you for listening, for making me laugh, and for helping me forget the stress sometimes. To my parents, without your help this would not have been possible. Thank you for supporting me, pushing me to pursue my dreams, and being there when the times get tough. I love you so much. Mama thank you for taking care of me and being there always. To Jack. You have been my rock and cannot imagine having done this without you. You are the most patient man in the world, and soon we will go for swims, and walks, and pizza, and trips. Thank you for all the laughs, the late-night chats, the support through this insane time, and your love.

To lifETIME CDT, thank you for all the training, the funding, the retreats, the conferences, and the chance to develop as a scientist, and as a person. Thank you, Michelle and Aimee especially have made this experience, so special. I would like to thank EPSRC and SFI for

funding the lifETIME Centre for Doctoral Training. (EP/S02347X/1) and making this research possible.

To BCRT. Thank you for the support, for making this project possible with your kind contributions, and for allowing me to come to the patient conferences. You really changed my perspective and gave meaning to my work. I would especially like to thank Dr Zoe Davison and Dr Victoria Vinader for providing support throughout my PhD, providing helpful suggestions, and for being so lovely to me. To all the people I met at patient conferences. You have all been an inspiration, and I will never forget you. Your stories have touched my heart. I would like to extend my thanks to Florencia, Catherine and Charlene for the chats, and the feedback, and to little Lucy, may you find peace. You were taken too soon, and you will be missed. Until there is a cure.

Author's declaration:

This thesis represents the original work of Chara Dimitriadi Evgenidi, unless otherwise explicitly stated in the text. The research was conducted at the University of Glasgow, either within the School of Chemistry in the Henderson and Chemical Biology Labs under the supervision of Dr David J France, or at the Advanced Research Centre, at the Centre of Cellular Microenvironment, under the supervision of Prof Matthew Dalby, and Dr Monica P Tsimbouri. Research was conducted from October 2019 to June 2024.

List of abbreviations

Acetyl-CoA: acetyl coenzyme-A

ADCs: Antibody drug conjugates

AKT: Protein kinase B (Ak strain transforming)

ALP: Alkaline phosphatase

APL: Acute promyelotic leukemia

BMP2: Bone morphogenic protein 2

CAR T: Chimeric antigen receptor T-cell

COSY: Correlation Spectroscopy

CS: Cholesterol sulfate

DCM: Dichloromethane

DEX: Dexamethasone

DHAP: Dihydroxyacetone-phosphate

DNA: Deoxyribonucleic acid

EMT: Epithelial to mesenchymal transition

ERK: Extracellular signal-regulated kinase

EV: Extracellular vesicles

FA: Fludrocortisone acetate

FBS: Foetal bovine serum

Fructose-6P: Fructose-6-phosphate

Fructose-1,6-biP: Fructose-1,6-bisphosphate

GA3P: Glyceraldehyde-3-phosphate

GF: Growth factor

Glucose-6P: Glucose-6-phosphate

GLUT1: Glucose transporter-1

GSK-3 β: Glycogen synthase kinase-3 β

HA: Hydroxyapatite

HCC: Hepatocellular carcinoma

HDAC: Histone deacetylase

HER2: Human epidermal growth factor receptor 2

High res: High resolution

HMBC: Heteronuclear Multiple Bond Coherence

HPLC: High performance liquid chromatography

HPMA: N-(2-hydroxypropyl)methacrylamide

HSQC: Heteronuclear Single Quantum Coherence

Hz: Hertz

ICIs: Immune checkpoint inhibitors

ICW: In cell western

α-KG: α-Ketoglutarate

MAPKS: Mitogen-activated protein kinases

MCT: Monocarboxylate transporter

MHz: Megahertz

MPC: Mitochondrial pyruvate carrier

MSC: Mesenchymal stem cell

MTOR: Mammalian target of rapamycin

MW: Molecular Weight

NAD+: Oxidized nicotinamide adenine dinucleotide

NADH, H+: Reduced nicotinamide adenine dinucleotide

NK: Nanokicking

NMR: Nuclear Magnetic Resonance

NOE: Nuclear Overhauser Effect

NOESY: Nuclear Overhauser Effect Spectroscopy

OAA: Oxaloacetate

OGM: Osteogenic medium

ONN: Osteonectin

OPN: Osteopontin

OS: Osteosarcoma

OSC: Osteocalcein

OSX: Osterix

P53, TP53: Tumour suppressor tumour protein 53

PD-1: Programmed cell death protein 1

PDGFR: Platelet-derived growth factor receptor

PD-L1: Programmed death-ligand 1

PDX: Patient derived xenografts

3PG: 3-phosphoglycerate

PI: Propidium iodide

PLGA: Poly lactic-co-glycolic acid

PPAR-γ: Peroxisome proliferator-activated receptor-γ

Ppm: parts per million

PTH: Para thyroid hormone

RB1: Retinoblastoma protein 1

RNA: Ribonucleic acid

RP-HPLC: Reverse phase high performance liquid chromatography

RTKs: Receptor tyrosine kinases

RT-PCR: Reverse transcription polymerase chain reaction

RUNX2: Runt-related transcription factor 2

Succ-CoA: Succinyl-CoA

TAU: Taurine

TC: Tissue culture

TRIM14: Tripartite motif-containing 14 (TRIM14)

VEGF: Vascular endothelial growth factor

YAP: Yes-associated protein

Chapter 1: General introduction

1.1 Osteosarcoma

Between 124-150 people are diagnosed with osteosarcoma annually in England and Wales.[1] Osteosarcoma (OS) is a high-grade primary bone cancer that predominantly affects children and teenagers, with a second incidence in people over the age of 65.[2] The solid tumour mainly appears in the long bones, during rapid growth, especially during adolescence.[3] Risk factors include age, predisposition due to genetic disease, gender, bone defects, previous exposure to radiation,[4] and in over 80% of patients defects in osteogenic differentiation[5] (Figure 1.1). OS treatment typically involves limb-sparing surgery, combination chemotherapy, and radiotherapy in some cases.[6] Introduction of chemotherapy in 1975 increased the survival rate of OS patients from 22% in 1957 to near 60% nowadays.[7] The 5-year survival rate of localised OS patients is over 70%, for patients that don't present chemotherapy resistant OS.[8] OS patients present a high rate of metastasis, mainly to the lungs, which is associated with a very low survival rate of 25%, while others exhibit recurrent OS, which is resistant to the established chemotherapy regime.[9] Since one of the hallmarks of OS cells is a de-differentiated phenotype, which leads to high cell proliferation rates and cancer spread,[10] promoting further osteogenic differentiation in OS cells is an attractive strategy.

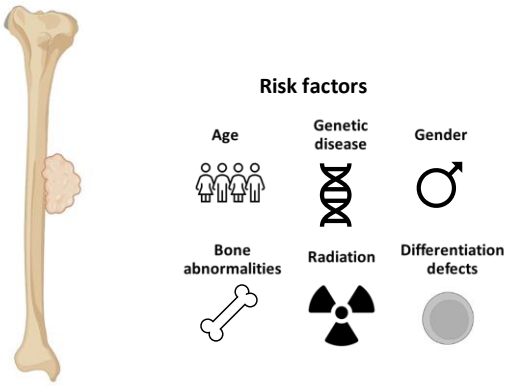

Figure 1.1: Risk factors associated with OS include age, predisposition due to genetic disease, gender, bone defects, previous exposure to radiation.[4]

1.1.1 Pathogenesis of osteosarcoma

Osteosarcoma is a complex disease, so there are limited characteristics that are observed across all tumours, raising questions about the pathogenesis of osteosarcoma. A number of genetic disorders have been linked to higher incidence rates amongst patients, with Li-Fraumeni syndrome, retinoblastoma, Bloom syndrome and Werner syndrome increasing the likelihood of OS development.[11] People with Li-Fraumeni syndrome have a mutation on the tumour suppressor tumour protein 53 (TP53 or p53) gene, which is a cell cycle regulator, that normally triggers cell cycle arrest and induces apoptosis.[12] p53 plays an important role in a number of cancers, as when this checkpoint protein is mutated, cell growth goes unchecked and uncontrolled proliferation occurs.[13] Mutation of the retinoblastoma protein 1 (RB1) tumour suppressor gene has been found to lead to retinoblastoma, which is a disease that makes patients more susceptible to cancer, and especially so for osteosarcoma.[14] A number of oncogenes have been found to be activated in some OS patient tumours, including c-Myc, c-Foc and tripartite motif-containing 14 (TRIM14).[15] One common point in at least 80% of osteosarcomas however, is an undifferentiated or partially differentiated phenotype, which gives rise to cells that are immature and highly proliferating.[5]

1.1.2 Current treatment

Current OS treatment involves a combination of chemotherapy, limb sparing surgery and/or radiotherapy.[16] Typical chemotherapy regimens (Figure 1.2) include the combination of multiple agents, including cisplatin, doxorubicin, methotrexate and/or ifosfamide.[17] Methotrexate is a folic acid analogue, that acts as a dihydrofolate reductase inhibitor, blocking the synthesis of DNA purines and pyrimidines and causing DNA damage.[18] Doxorubicin is an anthracycline, topoisomerase-II inhibitor, that acts as a DNA intercalating agent, that blocks DNA and RNA synthesis, leading to apoptosis.[19] Cisplatin is a platinum coordination complex, that acts by crosslinking DNA's purine bases, stopping cell division, and initiating apoptosis.[20] Ifosfamide and cyclophosphamide are prodrugs, that are activated in the liver by cytochrome P450, with the released nitrogen mustards alkylating the DNA of fast-dividing cells in the tumour, causing DNA damage.[21] Etoposide, is also employed in cases of metastatic osteosarcoma,[22] and it acts by stabilising the DNA-topoisomerase-II cleavage complex, breaking DNA strands, and triggering programmed cell death.[23] Multi-agent regimens have shown improved 5-year survival, but present significant side-effects, due to targeting any fast-dividing cells, while treatment is not standardised globally or

nationally.[24] Cytotoxicity problems from chemotherapy, including potential renal, cardiac, pulmonary, and hepatic failure, as well as nausea, neurotoxicity and immunosuppression pose severe risks to patients' survival and quality of life.[25] Severe adverse effects, high recurrence rates, and drug resistance,[26] make the pursuit of new therapeutic avenues critical.

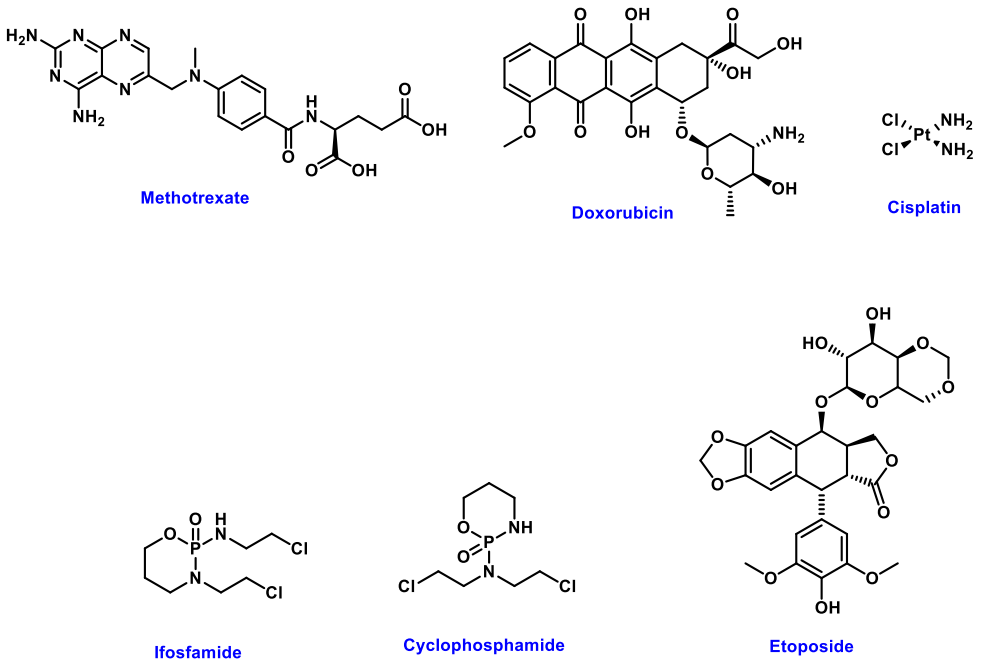

Figure 1.2: Chemotherapeutic agents used to treat osteosarcoma include methotrexate, doxorubicin, cisplatin, ifosfamide, cyclophosphamide and etoposide.

1.1.3 Osteosarcoma therapies and clinical trials

Therapies tested on OS have typically not been solely developed for bone sarcomas, but have previously proven effective in different cancer cell types, before being tested on OS.[27] Research into model systems enabling more accurate pre-clinical OS studies have proven valuable in identifying new drugs and pathways involved in cancer.[28] Recent clinical trials on OS have largely focused on immunotherapies, monoclonal antibodies, antibody-drug conjugates, tyrosine kinase inhibitors.[29] Targeted delivery methods are focused on accumulation of a therapeutic agent selectively in cancer cells, compared to healthy cells, as well as improved pharmacological properties.[30] Therapies investigated for OS have also been widely employed to treat different types of cancer, including hepatocellular carcinoma (HCC), which is an aggressive, malignant liver cancer.[31]

Tyrosine kinase targeting therapies

Receptor tyrosine kinases (RTKs) are enzymes that phosphorylate specific tyrosine sites in proteins, thus activating or deactivating the selected target.[32] Tyrosine kinases are involved in signal transduction, via phosphorylation of substrates, thus modulating cell proliferation, differentiation, invasion, and apoptosis.[33] Commonly investigated RTKs which are overexpressed, and/or mutated in OS include human epidermal growth factor receptor 2 (HER2),[34] epidermal growth factor receptor (EGFR), vascular endothelial growth factor (VEGF),[35] c-KIT, and platelet-derived growth factor receptor (PDGFR).[36] Tyrosine kinase therapies, whether they involve pathway inhibition, antibody-drug conjugates, or selective targeting via monoclonal antibodies, have found application in numerous cancers, including breast cancer, kidney cancer, hepatocellular carcinoma and osteosarcoma.[37] Tyrosine kinase inhibitors, including regorafenib,[38] sorafenib,[39,40] lenvatinib,[41] and apatinib, have been investigated in advanced OS, and have led to temporary disease stabilisation, though treatment has not proved curative.[42] Targeting multiple kinases simultaneously, and co-administering with etoposide, ifosfamide, or immunomodulatory drugs has led to improved outcomes.[42]

Modulating the immune environment

Thomas and Burnet established the "immune surveillance theory" in the 1960s after observing that the immune system recognised and attacked neoplasms in mice.[43] Cancer cells have adapted, to evade immune recognition and destruction, thus evading immune system modulated apoptosis.[69] According to Yao *et al.* there were more than 300 cancer immunotherapy clinical trials in either phase III, or IV in 2023.[44] CAR T therapies, oncolytic viruses, cytokines immune checkpoint inhibitors and monoclonal antibodies are amongst common strategies to modulate the immune environment, to attack cancer cells.[45] Immune checkpoint inhibitors (ICIs) seek to re-activate immune response, with the aim of T-cells attacking the cancer cells.[46] Common ICI targets in OS include targeting programmed cell death protein 1 (PD-1), and programmed cell death ligands PD-L1 or PD-L2.[47] Promising findings *in vitro.* have not translated to the clinic for OS, with partial response being achieved in 1 out of 17 patients, from PD-1 pathway inhibition, using mab pembrolizumab.[48] Further clinical trials on different ICIs have reported more limited response, ICI resistance, and severe side-effects,[49] thus highlighting the need to adapt strategies, and combine therapies.

Targeted delivery in osteosarcoma

Drug delivery is often hindered by poor pharmacological properties, rapid clearance, poor solubility and off-target effects.[50] Employing technologies that can enhance drug delivery to cancer cells and minimise distribution to healthy cells is a promising approach, for managing toxicities of established therapies.[51] Different approaches include the use of drug encapsulation, small molecule-drug conjugates, antibody-drug conjugates, and peptide drug conjugates (Figure 1.3). Targeted delivery strategies in osteosarcoma (OS) have largely focused on monoclonal antibody strategies and nanomedicine,[52] with more limited research on small molecule-drug conjugates.

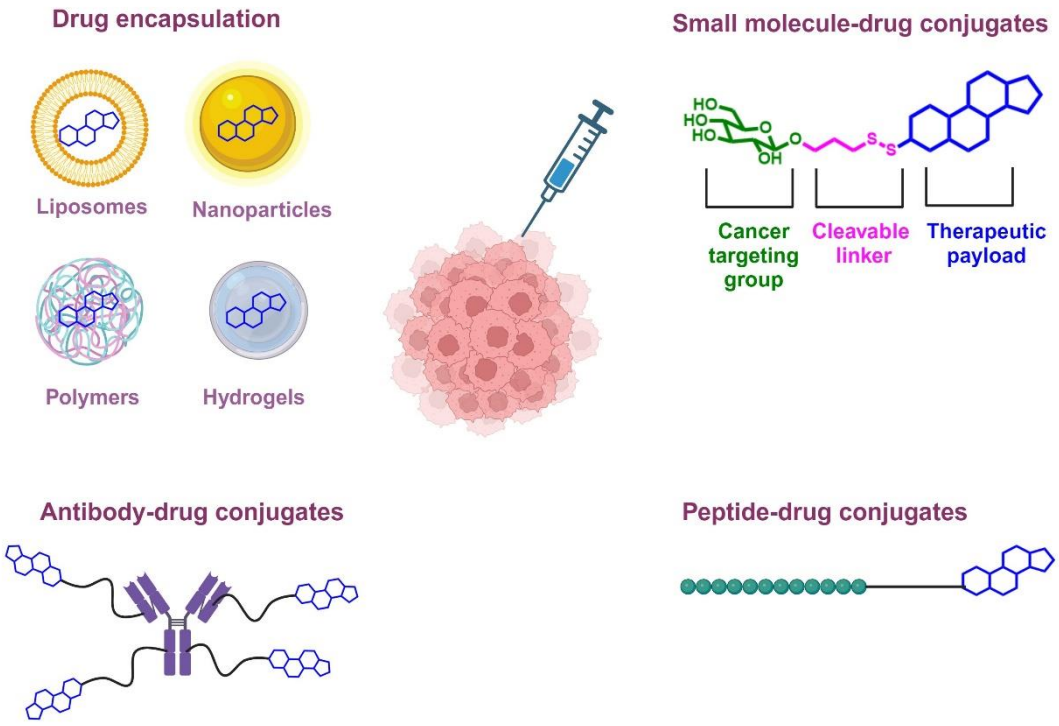

Figure 1.3: Targeted delivery approaches in cancer include encapsulation of a therapeutic agent in a targeted delivery system or conjugation of the drug to a cancer targeting group. Encapsulation strategies may involve the use of liposomes, nanoparticles, polymers and hydrogels. A drug may be conjugated to a cancer targeting antibody, small molecule or peptide. Figure created with biorender.com

In the US there has been a large focus on the surfaceome, and monoclonal antibody-based (mab) technologies to treat osteosarcoma.[53] Use of patient derived xenografts (PDX), as model systems of disease have provided a great platform to study efficacy of treatments, with mab.[54] Antibody drug conjugates (ADCs) have been studied in cancer, with the aim to achieve enhanced drug uptake in cancer cells, by tethering a cytotoxic drug, to a monoclonal

antibody, with specific activity for an antigen that is overexpressed at the tumour.[55] Lack of antigen specificity is a common issue, while there is no universally expressed OS cell surface marker in patients, that can be used for the antibody to target,[53] limiting use to specific patient phenotypes.

The use of nanomedicine to deliver drugs to cancer cells can improve solubility, minimise toxicity, and promote increased distribution of the drug in the cancer cells.[56] Mepact is a liposomal formulation of immunomodulating agent mifamurtide, that has shown improved efficacy in osteosarcoma patients, by releasing mimics of bacterial endotoxins, thus activating macrophage response.[57] Doxorubicin loaded, MSC derived exosomes have been previously used to promote enhanced drug accumulation of doxorubicin in MG-63 cells, and achieve controlled drug release in the cancer cells.[58] Enhanced cytotoxicity in MG-63 cells and low toxicity in cardiomyocytes was observed, suggesting selectivity towards cancer cells. Widespread use of extracellular vesicle-based therapies is currently constrained by trouble sourcing, isolating, purifying, and consistently characterising the vesicles.[59] Nanoparticles with different targeting sequences have also previously been employed to achieve targeted delivery in OS, including albumin, chitosan.[60]

Hydrogels have been employed in drug encapsulation strategies, to achieve controlled release in cancer cells, where the high water content of the gels, which can be crosslinked with polymers, can mimic tissue environment.[61] Doxorubicin loading in poly lactic-co-glycolic acid (PLGA)-based hydrogels in OS, previously showed lower toxicity in mice, but limited response in controlling tumour growth in lower doses, requiring 15 mg/kg to show improved efficacy.[62] Thermo-sensitive hydrogels, loaded with doxorubicin and palbociclib have also previously been described to achieve controlled release in OS.[63]

Tethering a pharmaceutical payload, to a cancer targeting group is a promising strategy for allowing better selectivity of the drug, more limited off-target effects, as well as an improved pharmacological profile.[64] Prodrugs are an example of this strategy, and have found particularly exciting applications on cancer therapeutics, by allowing the targeted release of therapeutic agents to the site of interest, minimising off-target effects.[65] Prodrugs are derivatives of pharmaceutical agents, which present limited biological activity, but undergo chemical or enzymatic transformation *in vivo*, to release the drug at the site of interest.[66] While the use of prodrugs is commonplace in cancer research,[67] more limited research was identified on small molecule drug conjugates for osteosarcoma. This prompted research into

targeted delivery of potential therapeutic agents in OS, using small molecule-drug conjugates, as will be discussed in chapter 6.

1.2 Cancer hallmarks

Osteosarcoma (OS) patients present phenotypic heterogeneity, yet common traits that define cancer cell behaviour, also apply in OS cells too. Weinberg and Hanahan published a seminal paper, in 2000, describing common characteristics in cancer cells, that aid them in sustaining their uncontrolled growth, and evading cell death.[68] They thus coined the term "hallmarks of cancer" to encompass those traits that promote carcinogenesis. Initial hallmarks included "uncontrolled proliferation, evading apoptosis, angiogenesis, and evading tumour suppression".[68] Metabolic reprogramming emerged as a hallmark of cancer, where cancer cells adapt, and use altered, and often energetically unfavourable metabolic pathways, to obtain essential building blocks, and sustain their uncontrolled proliferation.[69] In fact, OS cells commonly employ metabolic pathways that promote osteogenesis, with disease progression largely correlating to distinct pathways.[70] The presence of cancer stem cells, that may be involved in tumour initiation has also been considered to play a role in cancer initiation, invasion, and metastasis.[71] In 2020 Hanahan updated the list of cancer hallmarks, to include cancer cells' phenotypic plasticity, which includes cancer cells' lack of terminal differentiation.[71]

1.3 Osteogenic differentiation in healthy *vs* cancer cells

1.3.1 Healthy osteogenic differentiation of MSCs

Mesenchymal stem cells (MSCs) are multipotent, stromal, self-renewing cells, which can differentiate to various cell types, with the main classes being osteoblasts, chondrocytes, adipocytes, and myoblasts[72] (Figure 1.4). These cells are typically isolated from bone marrow or adipose tissues, amongst other sources. Depending on the activation of different genes, different differentiation pathways are activated. Adipogenesis is mainly regulated by peroxisome proliferator-activated receptor-γ (PPAR-γ), while osteogenesis is regulated by runt-related transcription factor 2 (RUNX2).[73] Osteogenic differentiation towards mature osteoblasts and osteocytes, occurs through various progenitor stages, and is regulated by a cascade of signalling molecules and proteins.[74] Different genes are involved in the different stages of differentiation, with earlier progenitors being more proliferative, and more mature

cells presenting a more differentiated phenotype, that promotes mineralisation.[75] Bone morphogenic proteins (BMPs) are involved in early stages of osteogenic differentiation and play a role in bone remodelling and repair, while alkaline phosphatase (ALP), type I collagen (Col1a1), osteopontin (OPN), and osteocalcin (OCN) are common markers of osteogenesis.[74] Osteoblasts are involved in bone deposition, mineralisation and resorption, and dysfunction in osteoblast formation is closely linked to bone disease and bone cancers.[76].

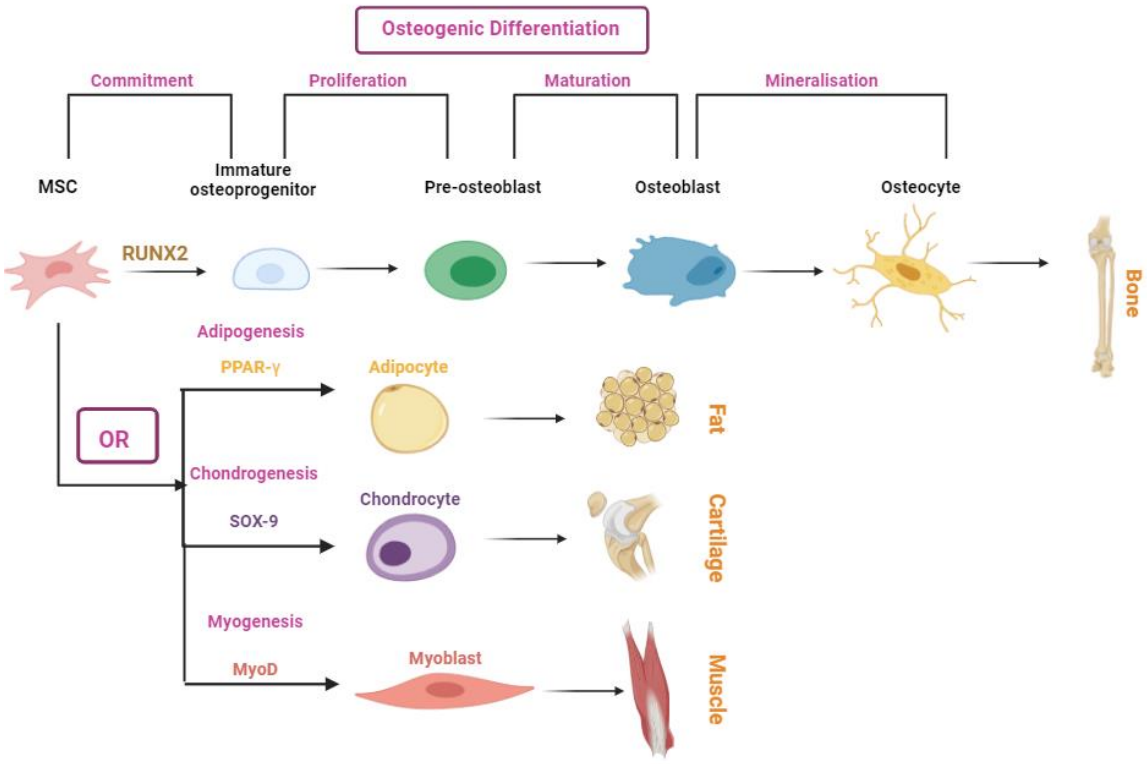

Figure 1.4: MSCs are multipotent cells, that can differentiate into osteocytes, adipocytes, chondrocytes or myoblasts, depending on the activation of different signalling pathways.[72] Osteogenic differentiation of MSCs occurs through intermediate osteo-progenitors, of different levels of maturity. Osteoblastic commitment is followed by a proliferative phase, subsequent maturation, and then mineralisation, to produce osteocytes, and eventually bone.[72] (created with biorender.com)

1.3.2 Aberrant osteogenic differentiation on osteosarcoma

Incomplete osteoblastic differentiation and uncontrolled proliferation are observed in at least 80% of osteosarcomas.[5] While osteogenic differentiation of MSCs occurs through various intermediate osteoprogenitor cells, in osteosarcoma osteogenesis stops before the cells become mature osteoblasts. Stem cells and "immature" osteosarcoma progenitor cells possess increased potential for self-renewal and expansion.[77] As seen in Figure 1.5, the degree of differentiation, largely dictates the proliferative capacity of the cancer cells and

the degree of malignancy. Osteosarcoma cells that are closer to the phenotype of a stem-cell like immature progenitor, are more malignant, faster proliferating, and possess lower levels of late osteogenic markers.[78] On the other hand, osteosarcoma cells which are more differentiated, and closer to a more mature pre-osteoblast progenitor, are slower growing, and less malignant.[79] The regulation between differentiation and proliferation that occurs in healthy differentiation, is disrupted in osteosarcoma, shifting the balance towards faster proliferating, immature cells.[80] Phenotypic cell plasticity is another ability cancer cells possess, that aids them to adapt to their environment and survive.[81] Consequently, inducing further differentiation in osteosarcoma may hold promising therapeutic potential.

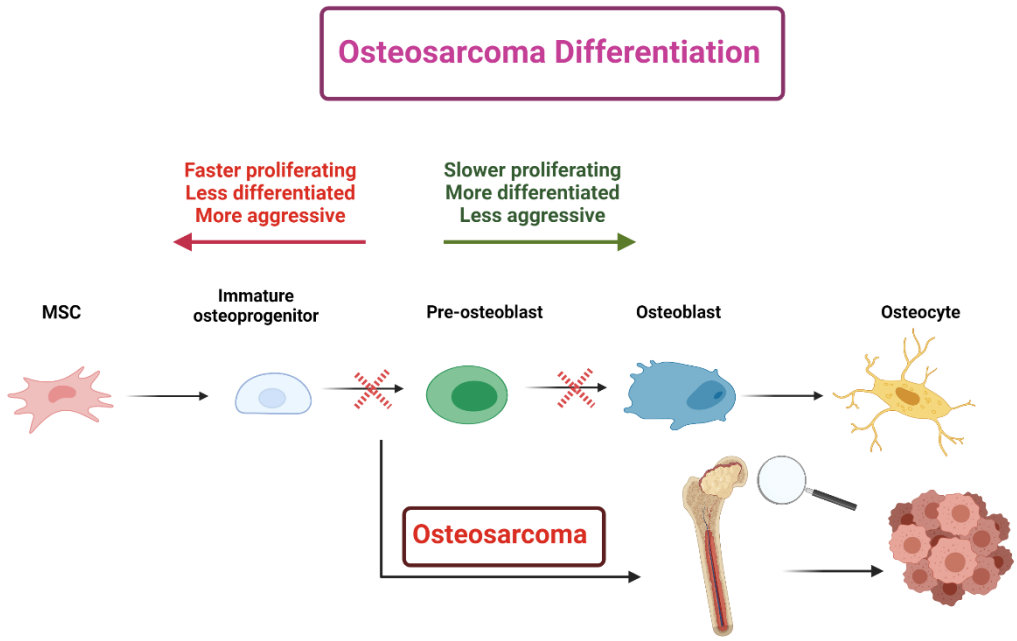

Figure 1.5: Osteogenic differentiation of MSCs is disrupted in osteosarcoma, with the degree of maturity affecting the proliferation capacity and malignancy of osteosarcoma. (created with biorender.com)

1.3.3 Differentiation therapy

As previously mentioned, a non-terminally differentiated phenotype is a hallmark of cancer, that yields immature, fast-proliferating cancer cells, whose phenotype more closely resembles immature progenitors, than terminally differentiated cells.[82] Differentiation therapy seeks to restore differentiation drive in cancer cells, and "reprogramme" cell behaviour, thus suppressing cancer proliferation, and sensitising cells to chemotherapy.[81] All trans retinoic acid (ATRA) (Figure 1.6) and arsenic trioxide were amongst the first

molecules used to induce differentiation of acute promyelotic leukemia (APL) cells and are still employed for the treatment of APL.[83]

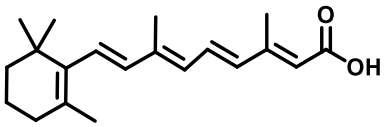

All trans-retinoic acid

Figure 1.6: Historic differentiation therapy agent all trans-retinoic acid.

Differentiation therapy was first found to be effective on APL cells, where retinoids induced terminal differentiation of leukemic cells, where retinoid pathway dysregulation was found to play a key role in de-differentiation in APL cells.[84] ATRA induced differentiation was found to induce cell maturation, slow down self-renewal and reduce tumour bulk. This exciting finding led researchers and clinicians to investigate this therapeutic strategy on various cancers including hepatocellular carcinoma,[85] prostate cancer[86] and OS.[87] Furthermore, differentiation drugs have shown reduced toxicity compared to chemotherapy regimens, making them attractive therapeutics.[83]

1.3.4 Differentiation therapy in osteosarcoma

Differentiation therapy is a promising therapeutic strategy in cancer, but the success on haematological cancers has not been replicated clinically on more complex solid tumours[88] and sarcomas. OS presents a more complex cancer with a heterogeneous phenotype, with signalling pathways presenting pleiotropic effects on cancer growth, and differentiation.[89] Moreover, mutations in osteogenesis regulator RUNX2 in OS, and aberrant expression has introduced challenges in applying differentiation therapy in OS.[90] Inducing terminal differentiation in OS cells is a promising approach for treating OS in conjunction with traditional chemotherapy. [91]

Differentiation of osteosarcoma cells on materials

Relatively slow-growing SAOS-2 OS cells were found to differentiate on nanocrystalline diamond films, when they were treated with ascorbic acid.[92] Cells were also found to adhere well to this material, grow, promote bone mineralisation, and deposit extracellular matrix. Diamon like coatings, coated with chromium were previously described to promote enhanced cell adhesion and osteogenesis in SAOS-2 cells,[93] with an observation of decreased

differentiation, with increase in Cr content. A silk fibroin hydroxyapatite-based material was found to support differentiation of MG-63 cells.[94] This fibroin blend is biocompatible for bone defect grafts, and was found to promote osteogenic differentiation, according to an ALP increase. Biomaterials that are used in bone grafts have also been seen to drive differentiation in SAOS-2 cells, as evident by ALP upregulation.[95] Titanium implant integration[96] and TiO_2[97,98] based materials have also been widely researched and found to improve adhesion and promote differentiation in OS cell lines. OS cell lines have mostly been used as model systems for osteoblasts, in materials studies, with a focus on developing substrates that can promote improved osteoinduction in bone grafts.[92,95,96,97,98] Hence there was a more limited focus on the effect of those materials on the cancerous phenotype, and driving terminal differentiation.

BMP2 driven differentiation in osteosarcoma

Growth factors are commonly included in differentiation supplements for osteogenic,[99] hepatic,[100] and adipogenic[101] differentiation. Bone morphogenic proteins (BMPs) are members of the TGF-β superfamily, that regulate early stages of osteogenesis, with BMP2 being a common osteogenic differentiation supplement.[102] BMP2 is an early differentiation marker, and is known to promote bone regeneration, so BMP2 has previously been employed in bone graft surgery, to aid bone viability.[103] Kendal *et al.* reported that cell phenotype affects OS cell response to BMP2 treatment, with BMP2 slowing proliferation, and inducing further differentiation in more mature OS cells.[104] On the other hand, poorly differentiated cancer cells displayed increased proliferation, and lack of differentiation, when treated with BMP2. Tian *et al.* also discovered that BMP2 could promote a malignant phenotype in OS cells, through epithelial to mesenchymal transition.[105] Gill et *al*. reported that BMP2 did not appear to promote invasion and metastasis in patient derived xenograft (PDX) models. BMP2 is sometimes included in bone grafts, to support bone regeneration, but more careful consideration should be given to grafts meant for OS patients, to avoid this invasive observation.

Flavonoid driven differentiation in osteosarcoma

Flavonoids are natural products with polyphenolic structures, that are naturally found in fruits, vegetables, and plants.[106] Flavonoids have interesting medicinal properties, including antioxidant, antipyretic, anti-inflammatory,[107] anti-neurodegenerative[108] and anti-carcinogenic effects.[109] A variety of those molecules have been reported to promote

osteogenic differentiation of MSCs,[110,] and have been tested in OS cell lines (Figure 1.7), as a form of differentiation therapy. Hyperoside was found to induce differentiation in U2OS and MG-63 cells within 7 days, whilst also inducing cell cycle arrest and slowing down proliferation of these OS cells.[111] Quercetin was found to suppress invasiveness in OS cells, and thought to differentiate the cells, which was evaluated by a decrease in matrix metalloproteinase.[112] The group did not look at more osteogenic markers, that would indicate the degree of osteogenic differentiation. Nobiletin has also been reported to drive differentiation in MG-63 cells, via the RUNX2/BMP2 pathway.[113] Galangin is a flavonoid, derived from the herbal plant *Alpinia officinarum*, that has also been shown to induce OS differentiation by modulation of TGF-β function.[114] Genistein, which is an isoflavone isolated from soy beans, induced MG-63 differentiation, as measured by increased ALP activity, whilst differentiation led to cell cycle arrest.[115] Kaempferol was also found to induce osteogenic differentiation of SAOS-2 cells, in a dose respondent manner, through the Wnt/β-catenin pathway.[116] TGF-β was involved in genistein, galangin and hyperoside driven OS differentiation, and TGF-β is also known to regulate Wnt/β-catenin signalling in osteoblast differentiation.[117] This confirms the most common pathways involved in flavonoid induced OS differentiation. Direct treatment with TGF- β[118] and BMP-2[119] has been reported to slow cell growth and promote differentiation in OS cells.

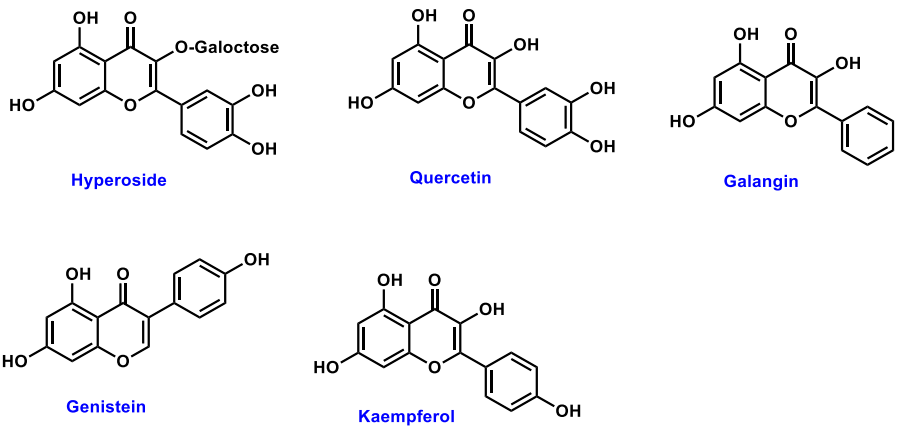

Figure 1.7: Flavonoids quercetin, galangin, genistein, kaempferol, and hyperoside, were found to induce osteosarcoma differentiation. Flavonoids are polyphenolic compounds, that are naturally found in plants, and possess medicinal properties.[107]

Despite the potential of various flavonoids for OS differentiation, as seen by the *in vitro.* experiments mentioned above, clinical application could be limited, by potential assay interference. A number of flavonoids are considered as "nuisance compounds", or Pan Assay INterference compoundS (PAINS).[120,121] They have been found to decrease membrane

fluidity, form aggregates, and solubilise other molecules, leading to false positive results in certain biological assays. Hence, whilst flavonoids have been shown to induce OS differentiation *in vitro*, questions may be raised as to the validity, due to potential assay interference.

Nuclear receptor agonist driven osteosarcoma differentiation

Several nuclear receptor agonists have been investigated for differentiation of OS cells, with retinoids being commonly employed in stem cell differentiation.[122] Tretinoin or 9-*cis*-retinoic acid (Figure 1.8), interacts with the retinoic acid receptor (RAR) and retinoid X receptor (RXR), which are involved in signalling pathways including Akt, MAPK and PKA,[123] and regulate genes that modulate differentiation.[124] ATRA is an isomer of tretinoin, that it has been found to induce differentiation in a variety of cancer cells, sparking interest in those molecules.[83] Induction of PPAR-γ, RXRα, and/or RARα has been found to slow down proliferation of OS cells synergistically, or individually.[125] Nuclear receptor agonists have also been found to induce osteogenic differentiation in PS cell lines, apart from slowing down their growth.[126] Modulators of nuclear receptors have also been reported to slow OS growth, through the mTOR pathway,[127] though information on the differentiation of the cells was not provided.

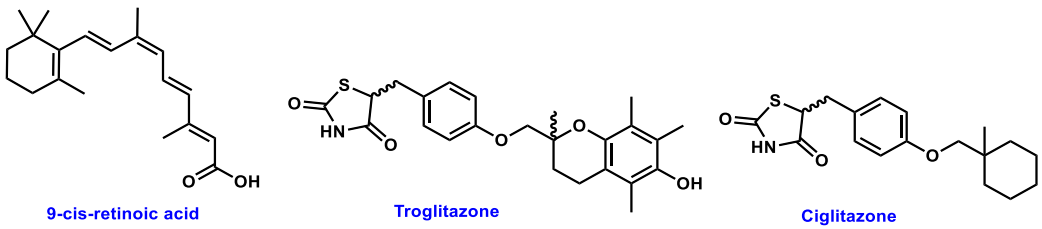

Figure 1.8: Nuclear receptor agonists have been found to induce osteosarcoma differentiation.

Retinoid 9-*cis*- retinoic acid, and PPAR-γ agonists troglitazone and ciglitazone (Figure 1.8), appeared to be driving OS differentiation and reducing cell proliferation in multiple OS lines.[128] Whilst both compounds promoted osteogenesis individually, when combined they appeared to form a synergistic effect, that enhanced differentiation. Haydon *et al.* further investigated PPAR-γ driven differentiation in OS and found that osteogenesis may be induced though BMP2-independent pathways.[129] Isoflavone genistein also appears to slow cell proliferation and induce OS differentiation through the PPAR-γ pathway.[115] Moreover, combining cisplatin with PPAR-γ agonists, has been found to decrease chemoresistance in OS cells.[130] Stereochemistry was not defined, and though racemates of thiazolidine

compounds present biological activity, the *S*-enantiomer shows stronger affinity for PPAR-γ.[131] The synergistic effect of retinoid receptors and PPAR-γ can offer a promising potential therapeutic avenue for OS differentiation.

Differentiation strategies involving chemotherapeutics and the immune environment

Trabectedin is a particularly exciting example of differentiation therapy. Trabectedin is a chemotherapeutic agent, that has been approved for treatment of soft tissue sarcomas, including liposarcoma, and leiomyosarcoma.[132] Trabectedin is a marine alkaloid, that showed promising response in OS, by modulating the immune environment, slowing proliferation, and inducing terminal differentiation, through DNA alkylation.[133] Toll like receptor agonists were found to suppress tumour invasion and suppression, with the added observation, of induction of differentiation and mineralisation on the OS cells.[134] Sciandra, Manara *et al*. reported that CD99 was able to drive terminal differentiation on multiple OS cell lines via the ERK1/2 pathway.[135] Transfection of SAOS-2 cells with CD99 was found to promote differentiation, and reduce proliferation, while driving G0/G1 cell cycle arrest. Terminal differentiation instead of senescence was confirmed by negative galactosidase staining.

Steroid driven osteosarcoma differentiation

Dexamethasone (Figure 1.9) is a synthetic glucocorticoid steroid, that can alter multiple cellular processes and functions by modulating the glucocorticoid pathway.[136] Dexamethasone presents strong anti-inflammatory action, and it is one of the most commonly prescribed drugs, for a variety of ailments.[137] Dexamethasone has also been widely used to promote further osteogenic differentiation in MSCs and OS cells, alongside differentiation agents ascorbic acid, and β-glycerophosphate.[138]

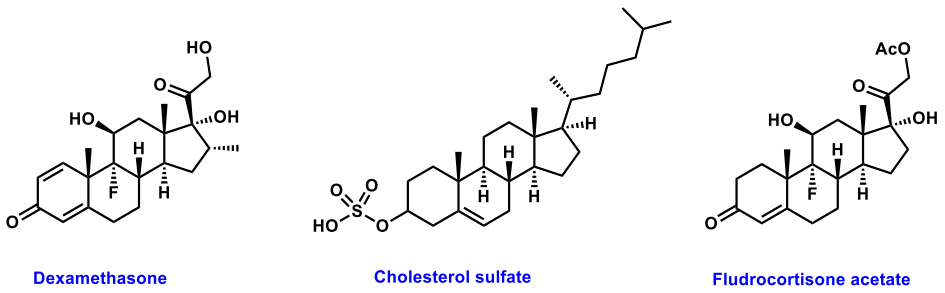

Figure 1.9: Steroids dexamethasone, cholesterol sulfate and fludrocortisone acetate have been found to induce osteogenic and/or osteosarcoma differentiation.

The rat OS cell line ROS 17/2.8, and human OS cell line U-2 OS were treated with the glucocorticoid dexamethasone (Figure 1.9), to study its effect on osteogenic differentiation of OS cells.[139] Dexamethasone was found to induce osteogenic differentiation, as evidenced by nodule formation and increased expression of bone specific proteins. Whilst this was an encouraging result, this glucocorticoid was found to also increase expression of astrocyte, oligodendrocyte, and hepatocyte specific markers in the OS cells, indicating a lack of selectivity. In addition, dexamethasone has also been found to induce OS cell differentiation in combination with retinoic acid.[138] Given the involvement of this glucocorticoid in several signalling pathways,[140] the activation of competing pathways is expected, but this also highlights the need for identifying compounds that can induce more selective osteogenesis.

Metabolomics was previously employed by the group, to identify small molecules that are involved in the osteogenic differentiation of MSCs, as well as to study the effect of glucocorticoid vs mineralocorticoid molecules on MSC metabolism.[141] Cells were treated with a known osteogenic medium or nanovibrated at 1000 HZ, 30 nm, using a proprietary equipment called nanokicking, to induce osteogenic differentiation. Metabolites promoting differentiation in the samples were identified using metabolomics, and it was discovered that the glucocorticoid pathway played an important role in osteogenic differentiation of MSCs. The steroid cholesterol sulfate (Figure 1.9) was identified as a metabolite of interest, using bioinformatics tools, and pathway analysis tools. It was found to induce differentiation MSCs, but not selectively, so structure activity relation (SAR) studies were carried out. These studies led to the identification of fludrocortisone acetate, as a molecule of interest, as it was found to induce more potent and selective osteogenic differentiation of MSCs. The group's previous work on steroid induced osteogenic differentiation of MSCs, and clinical research on dexamethasone induced OS differentiation, led to a focus on testing steroids on OS cells in this thesis. Studying alterations in metabolism, during osteogenic differentiation can provide important information on cell behaviour, and pathways involved in bone formation, while it is a useful tool for identifying bioactive metabolites. Therefore, cell metabolism was studied during differentiation of OS cells in this thesis, in chapter 4.

1.4 Cancer cell metabolism

Altered cell metabolism is a hallmark of cancer cells, that aids cells in evading apoptotic signals, and adapting their processes, to support their uncontrolled cancer growth and proliferation.[71] Cancer cells require increased numbers of metabolites, to maintain their

proliferative drive, which includes lipids for membrane formation, and vehicular transfer, amino acids for protein synthesis and for nucleotide formation for DNA synthesis.[142] Cells are known to undergo metabolic reprogramming during osteogenic differentiation,[143] which made it of interest to study cell metabolism during differentiation of OS cells (chapter 4). Metabolomics is a powerful tool, that can be used to quantify metabolites in a biological sample and obtain information on cell phenotype.[144]

1.5 Overall aim

Motivated by the previous success of differentiation therapy in haematological cancers, discussed above, this thesis sought to investigate whether OS cells can be driven to terminally differentiate, whether this would slow cell proliferation and to synthesise and test small molecules that could promote terminal differentiation.

- One of the objectives was to study whether known osteogenic differentiation conditions for MSCs also promote osteogenic differentiation in OS cells. The study specifically aimed to examine whether mechanical and chemical stimulation lead to similar distinct changes in cell phenotype and metabolic activity in OS cells compared to MSCs.
- A further objective was to design, synthesise and test a set of small molecules that were expected to promote osteogenic differentiation in OS cells, and show enhanced uptake in cancer cells, compared to healthy cells.

1.6 Summaries of chapter content

Chapter 3 studied the effect of mechanical vs chemical stimulation on OS cells and MSCs. Cells were nanovibrated at 1000 Hz, 30 nm, using nanokicking as means of mechanical stimulation, while an osteogenic medium containing dexamethasone, ascorbic acid, and β-glycerophosphate was used as means of chemical stimulation. Biological response was assessed by assays that measured cell viability, differentiation proteins and genes, and cell cycle progression.

Chapter 4 studied the effect of mechanical vs chemical stimulation on cell metabolism of OS cells, and MSCs. Metabolomics was used as a tool for quantifying metabolite changes in biological samples, and bioinformatics tools were used to study specific metabolites, and metabolic pathways involved in differentiation.

Chapter 5 studied the effect of identified metabolites, and related compounds on the differentiation of OS cells. Small molecules were tested at different concentrations, and further biological assays were carried out to study cell response.

Chapter 6 studied the synthesis of a steroid-glucose conjugate, through a hydrazone cleavable linker, with focus on devising a synthetic route towards a novel molecule, purifying it, characterising it, and testing its response on OS cells.

Chapter 7 included a general discussion of this thesis' findings, as well as the general conclusions that can be drawn from this research

Chapter 2: Materials and methods

2.1 Software and resources

Biorender.com	
Chemdraw 20.0	PerkinElmer Informatics
Fiji	
FlowJo v 10.9.0	BD Life Sciences
Graphpad Prism 10.1.2	
IDEOM	
ImageStudio	Li-Cor Biosciences
Ingenuity Pathway Analysis (IPA)	Qiagen
Imaris Viewer 10.1.0	Oxford Instruments
MetaboAnalyst 6.0	
Zotero 6.0.36	

Table 2.1: Software used in this thesis

2.2 Cell culture

MSC cells were obtained from Promocell. MG-63 and SAOS-2 cells were obtained from the American Type Cell Collection (ATCC). Cells were cultured in Dulbecco's modified essential medium (DMEM) (Sigma) supplemented with 5% Foetal Bovine Serum (FBS; Sigma), 1% (v/v) L-glutamine (200 mM, Gibco) and 2% antibiotics (6.74 U/mL penicillin-streptomycin, 0.2 µg/mL fungizone) (Sigma), unless otherwise specified. Cells were grown in a T75 flask, to approximately 70% confluence, media was changed every 3-4 days, and cells were split 1-2 times a week, depending on confluence. For differentiation studies cells were grown in a T75 flask, washed with PBS, trypsinised, counted with a haemocytometer, and resuspended in appropriate amount of DMEM. Cells were then seeded on multiwell plates and treated at a defined timepoint.

2.3 Alamar blue metabolic assay

Samples were washed with warm PBS, and 400 µL of 10% v/v of Alamar blue reagent (Biorad) in DMEM were added to each well. Cells were incubated at 37 ^{o}C, in an incubator, in the dark for 4 hours. 150 µL of the alamar solution were added to a 96 well plate for each

condition in duplicate, and absorbance was measured at 570 nm and 600 nm, on a microplate reader spectrophotometer. Viability was measured via % alamar reduction of treated cells, compared to the untreated cell control, using equation 3 from the BioRad website.[145]

2.4 Immunostaining recipes and antibodies

Buffer	Ingredients
Formaldehyde fixative	10 mL of Formaldehyde solution (37% v/v), 90 mL PBS, 2 g sucrose
Blocking buffer (1% BSA) for immunofluorescence	100 mL PBS, 1% w/v PBS
Permeabilization buffer	100 mL PBS, 0.1 % w/v Sucrose, 50 mM NaCl, 3 mM $MgCl_2.6H_2O$, 20 mM HEPES, 0.5 % v/v Triton X-100. pH adjusted to 7.2
Blocking buffer (1% Milk powder) for ICW	100 mL PBS, 1% w/v milk powder

Table 2.2: Immunostaining buffer recipes

Reagent	Company	Description	Dilution
RUNX2 primary antibody	Santa Cruz Biotechnology	RUNX2 (F-2) mouse monoclonal IgG_1 antibody (sc-390351)	1:200
OSX primary antibody	Santa Cruz Biotechnology	OSX (F-3) mouse monoclonal IgG_1 antibody (sc-393325)	1:200
ONN (SPARC) primary antibody	Santa Cruz Biotechnology	SPARC (D-2) mouse monoclonal IgG_1 antibody (sc-398419)	1:200
OPN primary antibody	Santa Cruz Biotechnology	Osteopontin/OPN/SPP1 x5 mouse monoclonal antibody (AKm2A1) (sc-21742)	1:200

Table 2.3: Immunostaining primary antibodies

Reagent	Company	Description	Dilution
Phalloidin Oregon green	Molecular Probes	Oregon Green™ 488 Phalloidin (O7466)	1:600 of 6.6 µM stock in methanol
Goat anti-mouse secondary antibody	Vector Labs (2B Scientific)	Horse Anti-Mouse IgG Antibody (H+L), Texas Red® (TI-2000-1.5)	1:200
Goat anti-rabbit secondary antibody	Vector Labs (2B Scientific)	Goat Anti-Rabbit IgG Antibody (H+L), Texas Red™ (TI-1000-1.5)	1:200
DAPI	Vector Labs (2B Scientific)	VECTASHIELD® Antifade Mounting Medium with DAPI (H-1200-10)	2 drops

Table 2.4: List of immunofluorescence secondary antibodies

2.5 Immunofluorescence

Samples were washed with PBS and fixed with 4% formaldehyde at 37 °C for 15 min. They were then washed with PBS and permeabilised using a permeabilisation buffer solution (Table 2.2) at 4 °C for 5 min. The buffer was removed, and the cells were incubated at room temperature for 1 hour in a 1% BSA/PBS blocking buffer. Primary antibody (Table 2.3) was prepared in 1% BSA, added to the relevant samples and left on a shaker overnight at 4 °C. The samples were then washed 4 times with 0.5% Tween 20/PBS and cells were incubated for 1 hour at 37 °C, and 30 minutes at room temperature on a shaker, with the relevant secondary antibody (Table 2.4) and Oregon green phalloidin (Table 2.4), in the dark. Cells were washed 4 times with 0.5% Tween 20/PBS, nuclear stain Hoechst or DAPI was added and then washed with PBS. 50 % glycerol in PBS was added to wells, and a coverslip was mounted on top. Cells were imaged with EVOS microscope, at 20x magnification, and images were processed using Imaris Viewer, unless stated otherwise.

2.6 In cell western

Samples were washed with PBS and fixed with 4% formaldehyde at 37 °C for 20 min. They were then washed with PBS and permeabilised using a permeabilization buffer solution (Table 2.2) at 4 °C for 5 min. The buffer was removed, and the cells were incubated at room temperature for 1.5 hours in a 1% milk powder/PBS blocking buffer. Primary antibody (Table 2.3) solutions were prepared in 1% milk powder/PBS and added to the samples and left overnight at 4 °C. The samples were then washed 4 times with 0.1% Tween 20/PBS and cells were incubated for 1.5 hours at 37 °C, with 1:1,000 secondary antibody IRDye 800CW, and 1:1,000 CellTag 700 Stain (LICOR). Cells were washed 5 times with 0.1% Tween 20/PBS, samples were dried, and the plate was imaged, at 800 nm using the LICOR Odyssey system. Images were processed using ImageStudio software. Protein expression was calculated as a ratio of antibody/celltag readings. The fold-change expression of the protein calculated as a ratio against the untreated cell control for the respective protein and timepoint was reported, with the control having an assigned value of 1, after normalisation.

2.7 Quantitative polymerase chain reaction with reverse transcription (qRT-PCR).

After 3 and 7 days, media was removed from the samples, they were washed with PBS and lysed with RLT buffer. The lysates were collected in RNA-free Eppendorf tubes, and stored

at -80 ^{o}C, until the PCR experiment was carried out. RNA was extracted from this solution using the Qiagen RNAeasy extraction kit, followed by the DNAse step, according to the Qiagen's protocols. The RNA was eluted in nuclease-free water and quantified using the Nanodrop instruments. After RNA normalisation calculations, the cDNA was prepared by reverse transcription using the Qiagen Quantitect Kit, according to Qiagen's protocols. cDNA concentration was normalised to 4 ng μL^{-1} by dilution in nuclease-free water. Using the 7500 real-time PCR system from Applied Biosystems, qRT-PCR was performed using the Quantifast SYBR green qRT-PCR kit (Qiagen) and the appropriate gene primers, (Eurofins Genomics). Gene primer sequences were obtained from the OriGene Technologies website. Gene values were quantified using the $2^{-\Delta\Delta Ct}$ method, for treatments against the individual timepoint control.[146]

Gene	Forward primer	Reverse primer
GAPDH	TCAAGGCTGAGAACGGGAA	TGGGTGGCAGTGATGGCA
RUNX2	GGTCAGATGCAGGCGGCCC	TACGTGTGGTAGCGCGTGGC
ALP	AGAACCCCAAAGGCTTCTTC	CTTGGCTTTTCCTTCATGGT
RPL13a	CTCAAGGTGTTTGACGGCATCC	TACTTCCAGCCAACCTCGTGAG
COL1A	GATTCCCTGGACCTAAAGGTGC	AGCCTCTCCATCTTTGCCAGCA
OSX	GGCAAAGCAGGCACAAAGAAAG	AATGAGTGGGAAAAGGGAGGG
OPN	AGCTGGATGACCAGAGTGCT	TGAAATTCATGGCTGTGGAA

Table 2.5: List of Primers purchased from Eurofins genomics. Primer sequence obtained from the OriGene Technologies website.

2.8 Flow cell cycle staining and analysis

Cells were trypsinised, counted, and cell numbers were normalised accordingly, to keep uniform cell populations. Cells were resuspended, centrifuged, and fixed in 80% ethanol, 20% PBS for 15 minutes at -20 ^{o}C. Cells were then centrifuged, and stored in PBS at 4 ^{o}C, until the time of analysis. Cells were resuspended, centrifuged, and the supernatant was discarded. 500 µl of FxCycle™ PI/RNase Staining Solution (Invitrogen) was added to each condition, and the cells were left to stain in the dark for 15 minutes. For each condition, two experimental replicates, and triplicate analytical replicates were added to a round bottomed 96 well plate. Unstained and stained controls for each cell line and timepoint were also collected, to carry out the gating on the instrument. The Attune flow cytometer was used to carry out cell cycle analysis, with BL3 bead compensation carried out, for calibration.

FlowJo software was used to analyse cell cycle data, with individual gating, and threshold parameters described in chapters 3 and 5.

2.9 Statistical analysis

Graphs were prepared, and statistical analysis was performed, using the GraphPad Prism Software (v10.1.2; GraphPad Software Inc.). All treatments were compared against the untreated control using the appropriate t-test or u-test, to answer the question of whether the treatment promoted differentiation or altered cell viability. First, the Shapiro-Wilk test was used to assess normality of the data, with a $p<0.05$ signifying that the sample is not normally distributed. The Shapiro-Wilk test is considered useful for smaller sample numbers of $n<50$,[147] which made this an appropriate test for the datasets in this thesis. Fold-expression was assessed for protein and gene expression, where the data were normalised against the untreated control, which had an assigned value of 1. Alamar reduction for different treatments was measured against an untreated cell control of the respective timepoint, with the untreated control having an assigned value of 100%. When data passed the normality test, a parametric t-test with Welch's adjustment was used to compare the fold-expression of the protein of the gene of the treatment, compared to the control=1, or alamar reduction against the control=100%. When data failed the normality test, a non-parametric Mann-Whitney U-test was carried out for the treatment vs the control=1, or control=100% for the alamar reduction. Differences of $p<0.05$ were considered statistically significant.

Chapter 3: Effects of mechanical vs chemical stimulation on osteosarcoma differentiation.

3.1 Introduction

As previously discussed, a lack of terminal differentiation is a hallmark of cancer.[5] Differentiation therapy (DT) aims to restore differentiation potential of the cancer cells and sensitise the cancer to chemotherapy.[81] This treatment has found application in haematological cancers, in combination with traditional chemotherapy, leading to improved prognosis for APL patients.[83] Restoring the differentiation potential of cancerous cells has proved to be more complicated in solid tumours, and the same success for haematological tumours has not been replicated.[88] Given osteosarcoma (OS) has previously been described a differentiation disease, identifying conditions that can push OS cells to further differentiation, is worth investigating. To identify whether conditions are indeed driving osteogenesis, it is important to assess cell viability, and osteogenic differentiation markers.

3.1.1 Osteogenic differentiation markers

RUNX2 (Runt-related transcription factor 2) is a transcription factor that is a master regulator of osteogenesis. As previously discussed, RUNX2 co-ordinates the osteogenic differentiation of MSCs, by triggering relevant signalling pathways and regulating osteogenesis and mineralisation.[148] Overexpression of RUNX2 has been linked to an increase in proliferation of OS cells *in vitro*, poor clinical outcome, and poor response to chemotherapeutic regimens.[149] From this it is evident that RUNX2's role in OS is complicated. Knockdown of RUNX2 has been reported to sensitise OS cells to chemotherapy, and lead to apoptosis of OS cells.[150] RUNX2 mediated osteogenic differentiation is disrupted in OS,[151] which could in part account for the undifferentiated phenotype of OS cells. Moreover, abnormal function of RUNX2 in OS, including RUNX2

mutations and dysregulation, has been linked to impaired osteogenic differentiation of OS cells.[148]

Osterix (OSX) is a zinc finger containing transcription factor, that is a marker of early to mid- osteogenic differentiation, and is modulated by RUNX2.[152] OSX regulates the expression of late-stage differentiation markers, including osteocalcin and osteopontin.[153] OSX expression is decreased in OS,[154] leading to incomplete osteogenic differentiation of OS cells. When OSX is knocked down no osteogenesis occurs in mice, confirming the key role of this transcription factor in bone formation and remodelling.[152]

The expression of markers of later osteogenic differentiation and mineralisation, including osteonectin, osteopontin and osteocalcin is regulated by RUNX2,[148] and OSX.[153] Osteonectin (ONN), or secreted protein acidic and rich in cysteine (SPARC, BM-40) is a matricellular protein with a key role in osteogenesis, and bone remodelling.[155] ONN levels correlate to parathyroid hormone (PTH) activity, with Wnt signalling regulating the production of ONN.[156] ONN plays a key role in calcification of collagen in bone, synthesis of extracellular matrix and the promotion of changes to cell shape.[157] Aberrant ONN expression is associated with osteogenesis imperfecta, which is a congenital disease that can lead to bone fragility and bone fractures.[157] Osteopontin (OPN) is a late-stage osteogenic differentiation marker, playing a key role in differentiation and bone mineralisation, matrix deposition and resorption.[158] Its role in OS is complicated, as reduced expression has been linked to OS, whilst overexpression under hypoxia, also can trigger OS.[159] OPN is also a marker for metastasis in OS cells.[160]

3.1.2 Osteosarcoma cell lines

Different model systems are used to study OS, including patient derived xenograft (PDX) models,[161] biomimetic and 3D models,[162] and animal models.[163] Immortalised OS cell lines such as SAOS-2 and MG-63 are often used as model systems for osteoblasts and osteogenic differentiation.[164] This is because they possess some osteogenic markers and characteristics, and they are fast-growing.[165] However, they bear major differences to healthy osteoblasts, due to their invasive-cancer properties, their increased proliferation and their relatively immature phenotype.[166] Whilst this presents limitations for studies of normal osteogenic differentiation, they are invaluable for studies of the effect of differentiation therapy on OS, as they are an unlimited resource, compared to cells freshly derived from a patient's

tumour.[167] Apart from the immortalised cancer cell lines, mesenchymal stem cells (MSCs) were also used as a control group for healthy osteogenic differentiation, in early experiments.

MG-63 is an OS cancer cell line, isolated from a 14-year old's tumour, and established in 1977 by Billiau *et al.*[168] MG-63 is a fast proliferating, aggressive cancer, that resembles poorly differentiated pre-osteoblast progenitors, more than mature osteocytes. RUNX2 expression is reduced in fast-proliferating cell lines, such as MG-63.[169] OSX expression in MG-63 cells has been found to be significantly downregulated,[164] which further confirms this poorly differentiated phenotype, and aberrant differentiation pathway. The cells also express high levels of OPN, with OPN knockdown triggering programmed cell death.[170] SAOS-2 is an OS cell line that was isolated from a patient's tumour and characterised by Fogh *et al*. in 1975.[171] It is an osteoblastic cell line, that presents a relatively mature phenotype, and it is relatively slower growing in comparison to the faster growing MG-63.[164] While RUNX2 is detected in low levels in MG-63 cells, it is expressed in high levels in the more mature SAOS-2 cells.[149] SAOS-2 cells also express intermediate levels of OPN,[172] and OSX,[173] making it a good model system for studying differentiation of more differentiated OS.

3.1.3 Chemical stimulation of osteosarcoma cells

Overall, a lack of terminal differentiation is a hallmark of OS,[5] and while different techniques have been employed, there is no gold standard, that has undisputedly been employed in the differentiation and mineralisation of OS. The use of small molecules to drive differentiation has been investigated in stem cell differentiation, as well as cancer cell differentiation.[174] Benefits include typically lower molecular weights, favourable pharmacokinetic properties, as well as defined chemical structures, standardised purity, and usually more reproducible action, compared to biological factors.[175] As discussed in chapter one, numerous small molecules have been employed, with the aim to drive differentiation in OS, with varying degrees of success. This includes different classes of small molecules, including flavonoids,[114] retinoids[122] and glucocorticoids.[139] What will be referred to as osteogenic medium (OGM) in this report, is a small molecule containing medium, that has been extensively used in cell-based assays in literature, to induce osteogenic differentiation of MSCs.[176,177] The small molecule cocktail contains ascorbic acid, β-glycerophosphate and dexamethasone. Ascorbic acid induces osteogenic differentiation and mineralisation, by increasing markers such as osteocalcin and alkaline phosphatase (ALP), and depositing

collagen into the extracellular matrix.[178] β-Glycerophosphate promotes osteogenic differentiation, nodule formation and osteocyte mineralisation,[179] by acting as an inorganic phosphate source for bone mineralisation.[180] Dexamethasone is a synthetic steroid, that induces differentiation through the glucocorticoid signalling pathway, and enhances the action of other components in the mixture.[181] This OGM will be used to induce osteogenic differentiation of MSCs and OS cells, through chemical stimulation. Identifying small molecules that drive differentiation in OS cells is one of the main aims of this thesis.

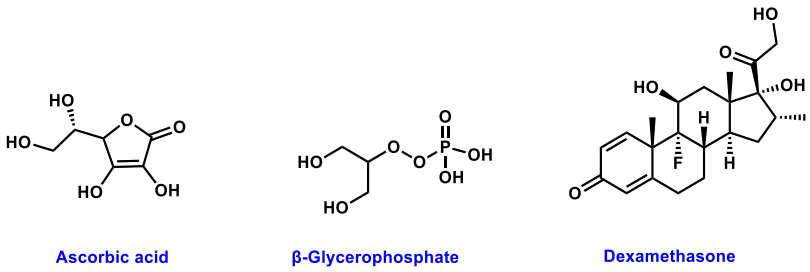

Figure 3.1: Osteogenic medium (OGM) contains ascorbic acid, β-glycerophosphate and dexamethasone.

3.1.4 Mechanotranduction and mechanical stimulation in stem cells and osteosarcoma

Mechanically modulating the cell environment is a promising strategy for driving differentiation in MSCs. Mechanotransduction refers to the cells' ability to sense changes in their mechanical environment and transform that into a biological response, according to the signal they receive.[182] Mechanotransduction also plays an important role in bone formation, resorption, and regeneration. Injuries and sports are known to apply mechanical force onto the bone, with literature reports of athletes not only showing increased muscle mass in their predominant hand, but also an increased bone density.[183] When mechanical force is applied on bone, it can lead to changes in the microenvironment, activation of ROCK and FAK, cytoskeleton reorganisation, and formation of focal adhesions.[184]

There is a fine balance in tuning the microenvironment, with stiffness playing an important role, as adipogenesis is promoted in soft surfaces, and osteogenesis is promoted in hard surfaces.[185] Controlling stem cell fate through mechanotransduction, to drive osteogenesis is a widely researched topic with electrical, magnetic, and mechanical stimulation being different approaches, to achieve that.[186] Modulating the cellular environment using biomaterials, is a further way to control the mechanical environment of the cells. Cao *et al.* reported that a combination of electrical pulse stimulation on nanocomposites PLDA showed

enhanced differentiation.[187] Hardy *et al.* also found that a combination of electrical stimulation on biomaterials induced enhanced differentiation.[188] Electrically stimulating stem cells using polypyrrole based electrodes was reported to drive osteogenic differentiation, when the signal provided was continuous.[189] Professor Adam Curtis published seminal work on how altering surface topography and material properties can lead to directing cell behaviour and stem cell fate,[190] with a later focus on nanotopography, and the piezoelectric effect.[191] Dalby *et al.* employed lithography to compose nanotopographies, to drive stem cell differentiation, and observed osteogenic differentiation.[192] Through RNA sequencing studies, similarities between pathways involved in dexamethasone and nanotopographies treatments were identified.

While harnessing effects of mechanotransduction to drive differentiation has proven successful on MSCs, the same level of research has not been carried out on OS cells. Luu *et al.* published a review, which focused on changes in the mechanical environment of OS.[193] Most research carried out on the field has focused on how treatment alters the mechanical environment, rather than directly mechanically stimulating the cancer cells. MG-63 cells, which are less differentiated were reported to be smaller in size, with a more spindle-like morphology, reduced matrix stiffness, fewer thick filaments, as well as a more disorganised actin cytoskeleton, compared to MSCs and osteoblasts.[194] OS cells present changes in their microenvironment that lead to aberrant mechanical properties, while the decreased stiffness, and smaller size[195] are thought to be linked to OS's invasive metastatic tendencies and poor differentiation.[196] Singh *et al.* have previously studied the piezoelectric effect on MG-63 cells, but their focus was on bone viability, and the antimicrobial properties of the material, rather than the induction of osteogenesis.[197]

Nanokicking is a proprietary technique co-developed by Curtis, Dalby *et al.* at the University of Glasgow, where MSC cells are stimulated with nanovibrations, to differentiate into osteoblasts.[198] The reverse piezo actuator transforms the generated electronic signal into a mechanical signal, which in turn induces a nanovibration.[141] Both the frequency and the amplitude of the vibration has been found to have a significant effect on the degree of differentiation. Nikukar *et al.* reported that a frequency of 1000 Hz showed statistically significant increase in osteogenesis, compared to 500 Hz, as this 1000 Hz frequency mimics the bones' natural frequency.[199] Different displacements have been tested, with *Orapiriyakul et al.* reporting that a 90 nm displacement showed differentiation and inflammation, while postulating that this inflammation was a contributor to the mineralisation.[200] Rho-associated

kinase (ROCK) was found to be a main driver of osteogenesis via mechanical stimulation. In the case of nanokicking, a ceramic material is used to harness the reverse piezo-electric effect, and induce selective osteogenic differentiation of the cells, through mechanical deformations. Tsimbouri *et al.* demonstrated in 2017 that 3D mineralised bone could efficiently be produced from MSCs, by stimulating MSC cells on a nano-bioreactor, on a collagen gel, without the need for additional growth factors.[198] This technique has great potential for clinical applications for bone healing, whilst it is also scalable, doesn't require added osteogenic molecules or growth factors, and it is compatible with the typical cell culture setup. [201] The nanovibrations apply mechanical stress to the stem cells, which in turn induces differentiation through mechanotransduction. This was found to enhance mineralised matrix formation, and an initial increase was observed for early markers ALP and RUNX2, followed by a decrease after 21 days, where later marker osteocalcin was expressed. The absence of additional osteogenic supplements might limit artifacts, that could produce false positives in planned metabolomic experiments. Preliminary data on primary OS cells indicate that NK affects gene expression, cell proliferation and metabolism of fast-growing cancer cells. (Tsimbouri *et al*, manuscript in preparation)

Figure 3.2: Nanokicking: MSCs are mechanically stimulated for 28 days using a nanokicker, to generate 1000 Hz, 30 nm nanodisplacements, and produce osteoblasts in vitro.

3.2 Aims and objectives

The aim of this chapter is to investigate whether OS cells can be driven to further differentiation and maturation, by employing techniques known to drive osteogenesis in MSCs. A small molecule cocktail containing β-glycerophosphate, dexamethasone and ascorbic acid was employed as a means of chemical stimulation, as it is known to drive differentiation and mineralisation in MSCs. Nanokicking was employed as a means of mechanical stimulation. The aim was to observe the effect of mechanical vs chemical

stimulation on the OS cells, compared to MSCs. Observing how the pre-existing degree of differentiation of the cells affects the cells' response to treatment was a further objective, so MG-63 cells were used to represent poorly differentiated OS, and SAOS-2 cells were used to represent more osteoblastic OS. A further objective was to assess whether osteogenic conditions were cytotoxic to the cells, and what degree of differentiation could be achieved.

3.3. Materials and methods

3.3.1 Cell culture and differentiation conditions

Cells were cultured using protocols described in chapter 2. Osteogenic differentiation medium contained basal medium, Dulbecco's modified essential medium (DMEM) (Sigma) supplemented with 5% Foetal Bovine Serum (FBS; Sigma), 1% (v/v) L-glutamine (200 mM, Gibco) and 2% antibiotics (6.74 U/mL penicillin-streptomycin, 0.2 μg/mL fungizone) (Sigma), supplemented with 200 μM ascorbic acid (Sigma-Aldrich), 100 nM dexamethasone (Sigma-Aldrich), and 10 mM β-glycerophosphate (Sigma-Aldrich). Nanovibration (30-nm displacement; 1000 Hz, using nanokickers) was applied to MSCs, SAOS-2 and MG-63, and cells were cultured in their respective basal media.

3.3.2 Nanokicking bioreactor setup

A nanokicker was used, with the design described by Hodgkinson *et al.*[141] TC-treated 24-well plates or 6-well plates were attached to a magnetic adhesive strip (NeoFlex Flexible Neodymium Magnetic Sheet, 3M, MN, USA), that covered the whole cell-growth area. The plate was then magnetically attached to the nanokicker. The nanokicker consists of an aluminium block, which is layered with an array of multilayer piezo actuators (NAC2022, Noliac A/S CTS, Denmark). On top of the piezo-array lays a ferromagnetic vibration top plate, to which the cell culture plate is attached. The piezo array is connected to a signal generator integrated circuit (AD9833, Analog Devices, MA, USA) to produce 1000-Hz sinusoidal waves, which are amplified using custom audio amplifiers (TDA7293, STMicroelectronics, Geneva, Switzerland). Monitoring of the nanokicker apparatus were carried out by Dr Monica Tsimbouri using an accelerometer in-house. Laser interferometry was used, in order to calibrate the nanokickers, to deliver 30 nm amplitude sine waves. Calibrations were carried out at the University of Strathclyde by Dr Paul Campsie, using a laser interferometric vibrometer (wavelength = 632.8 nm, CW power; 5mW; SIOS, Technik

GmbH, Germany), which was connected to an oscilloscope (72-6800 model; Tenma, UK).[201] This set up produces 30 nm, 1000 Hz vertical, sinusoidal vibrations on the attached plates.

3.3.3 Differentiation experiments

Cells were cultured to approximately 70% confluency and detached using trypsin/EDTA solution, before seeding. Cells were then centrifuged, and the cell concentration was determined using a haemocytometer, and resuspensions with the appropriate density were prepared in cell culture medium. Cells were seeded onto 24-well plates to allow attachment. After 24-48 hours the appropriate samples were treated with osteogenic medium, or nanovibrated. 4 experimental replicates were set up for each condition. For initial experiments MG-63 cells were seeded at 1,000 cells/ cm^2, and MSCs and SAOS-2 cells were seeded at 2,000 cells cm^2, for initial experiments. For subsequent experiments a seeding density of 2,000 cells/cm^2 for MG-63 cells, and 4,000 cells/cm^2 was employed for SAOS-2 cells.

3.3.4 Alamar blue metabolic assay

Cell viability was assessed after 3 and 7 days (n=2 experimental replicates, n=2 analytical replicates), by using the alamar blue assay, as was described in chapter 2. %Alamar reduction was quantified against the untreated cell control for the individual cell line and timepoint, using equation 3 from Bio-Rad.[145]

3.3.5 Quantitative polymerase chain reaction with reverse transcription (qRT-PCR).

Cells were treated for 3 or 7 days, and lysed using appropriate amount of RLT buffer, depending on well size. RNA, and cDNA were prepared, and gene levels were measured using the protocol described in chapter 2. qRT-PCR reactions were carried out using 8 ng of cDNA, in 20 µL reactions. Gene expression was quantified using the $2^{-\Delta\Delta CT}$ method, by comparing gene expression for the treated group against the untreated cell control group of the same timepoint.[146]

3.3.6 Immunofluorescence

Immunofluorescence staining and imaging was carried out following the general protocol described chapter 2. Cells were seeded, treated with NK or OGM, and fixed after 3 or 7 days. RUNX2, OSX, ONN or OPN primary monoclonal bodies were used. Cells were imaged on

EVOS M7000 microscope, at a 20x magnification. Images were processed using Imaris Viewer.

3.3.7 In-cell western (ICW)

ICW staining was carried out following the protocol described in chapter 2. In brief, cells were treated with control, NK or OGM, and fixed after 3 or 7 days. RUNX2, OSX, ONN or OPN primary monoclonal antibodies were used. Following staining, samples were imaged using the LICOR Odyssey SA, and protein expression was normalised to CellTag, and the untreated control.

3.3.8 Flow cytometric cell cycle

Cells were seeded on 6-well plates, at a density of 2,000 cells/cm^2 for MG-63 cells, and 4,000 cells/cm^2 for SAOS-2 cells. Cells were allowed to attach overnight and treated after two days, according to the previously described differentiation protocol. Cells were collected after 3 and 7 days, and stained, using the flow cytometry protocol described in chapter 2. For each condition 2 technical and 3 analytical replicates were used. Cell numbers were normalised, to analyse uniform populations. Cell cycle analysis was carried out using FlowJo software (Figure 3.3). First, gating was carried out to select single cell populations, by plotting the forward scatter vs side scatter area and selecting the live population. A second gating was carried out by looking at the FSCH vs FSCA, to select single cells, and exclude dye artifacts and dimers. Populations to the upper right quadrant were unviable, cell debris, dimers, and artifacts. The same gating was then applied to all cell populations, for different conditions, to be able to compare representative comparable cell populations. Histograms were then generated on the BL3-H channel, and the same thresholds were applied, to all groups, to quantify the number of cells in the sub-G1, G0/G1, S and G2/M phase.

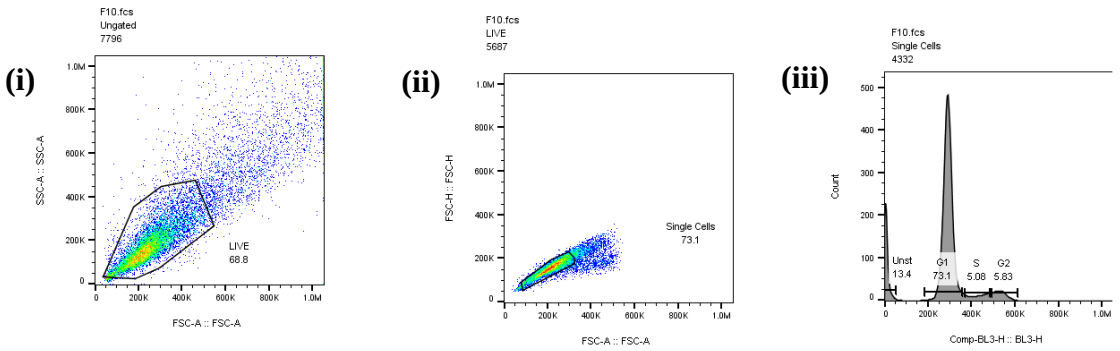

Figure 3.3: Cell cycle analysis gating strategy included (i) Plotting SSC-A vs FSC-A, and selective the live cell population. (ii) Plotting FSC-H vs FSC-A, to select the single cell population, and exclude dimers and artifacts. (iii) Plotting histograms of DNA content, to quantify cells in the sub-G1, G0/G1, S and G2/M phase.

3.3.8 Statistical analysis

Statistical comparison was carried out for different treatments, against their untreated cell control, using statistical tests described in chapter 2. For ICW and qPCR data a treatment's fold-expression of a specific gene of protein was measured against the untreated cell control of the respective timepoint. Fold-expression was statistically compared to a control=1, using the Mann-Whitney u-test for data that failed the Shapiro-Wilk normality test, or Welch's adjusted t-test for data that passed the Shapiro-Wilk normality test. For alamar blue data treatments' calculated alamar reduction was statistically compared to a control=100%.

3.4 Results and discussion

Nanokicking was employed as means of mechanical stimulation, and an osteogenic medium (OGM) containing ascorbic acid, dexamethasone, and β-glycerophosphate was used as means of chemical stimulation. MG-63 cells were used as an example of poorly differentiated OS cells, SAOS-2 as an example of more mature OS cells, and MSCs were included to study healthy osteogenic differentiation. Cell density is known to affect cell growth, and cells' response to differentiation.[202] Different cell densities were used for the different cell lines, depending on their proliferation rate. Cell crowding can commit cells to adipogenic differentiation, while nanotopographies that promote cell spreading and focal adhesions, can commit cells to osteogenic differentiation.[199] For MSCs cells were seeded at 1,000-2,000 cells/cm^2, SAOS-2 cells were grown at 2,000-4,000 cells/cm^2. MSCs were seeded at 4,000 cells/cm^2. Variation in cell density was due to issues in cell growth in certain instances and will be highlighted in respective experiments.

3.4.1 MG-63 mechanical vs chemical stimulation

Cell morphology and viability

First, there was a need to establish whether the treatments were cytotoxic to the cancer cells. Cell growth was assessed regularly via microscopy, during culture, as well as by Hoechst nuclear staining, after 3 and 7 days. Cells were trypsinised and counted after 3 and 7 days, with the limitation of a small number of technical replicates, of n=2. The cytoskeleton and actin were visualised via phalloidin green staining. Viability was assessed via alamar blue, which is a non-cytotoxic assay, where the reduction of the active ingredient, resazurin (blue) to resorufin (pink), indicates the presence of metabolically active cells.[203] The reduction of Alamar blue was quantified relative to the untreated control group, so a reduction of less than 100%, could indicate that growth is inhibited by the treatment. A reduction above 100% would indicate that there are more metabolically active cells in the treatment group than the control, which may translate to increased proliferation.

Cell density was not uniform across the whole growth area, but cells still had space to spread at 3 days (Figure 3.4), and adjust to their environment, meaning they might be more receptive to mechanotransduction effects. Cell numbers visibly appeared to be comparable for the control, the nanokicked, and the osteogenic group, from the Hoescht staining, with some cytoskeletal reorganisation observed, according to the phalloidin staining. Cell density appeared to have a major effect on the cell structure. Cell counts of trypsinised samples revealed similar numbers of collected cells, between the control and the treatments. Finally, alamar blue indicated that the presence of metabolically active cells was very similar between the control and the treatments, with very small deviation. A statistically significant decrease in reduction of alamar in the NK group may suggest inhibition of cell growth, while the statistically significant increase of alamar reduction in the OGM group, may suggest the presence of more metabolically active cells. After 7 days confluent monolayers were formed, with cell crowding observed, for all conditions, as seen by Hoechst nuclear staining. Some differences in actin cytoskeletal organisation were observed again, but due to cell crowding, the differences were not as evident. MG-63 cells are highly proliferative cancer cells, which explains the rapid cell growth, and formation of confluent monolayers. From trypsinised cell counts, comparable cell numbers were observed in the control and the OGM group after 7 days, while an increase was observed in the nanokicked group. Limitations include a lack of cell detachment of all cells during trypsinisation, as well as a smaller sample number, which

does not allow statistical observations. Alamar blue showed comparable reduction between the control and the treatment after 7 days too, with a small, but a statistically significant increase in reduction of alamar in the NK group, and a statistically significant decrease in the OGM group. MG-63 cells are rapidly proliferating, with high cell numbers present after 3 days, and a confluent monolayer being formed within 7 days, in all conditions. All those observations confirmed that the differentiation conditions were not cytotoxic, and cells were still viable, which matches observations on stimulation of MSCs.[198] Identifying conditions that can drive differentiation on OS cells is the main aim of this project, so differentiation was then assessed, via qPCR, immunofluorescence and ICW.

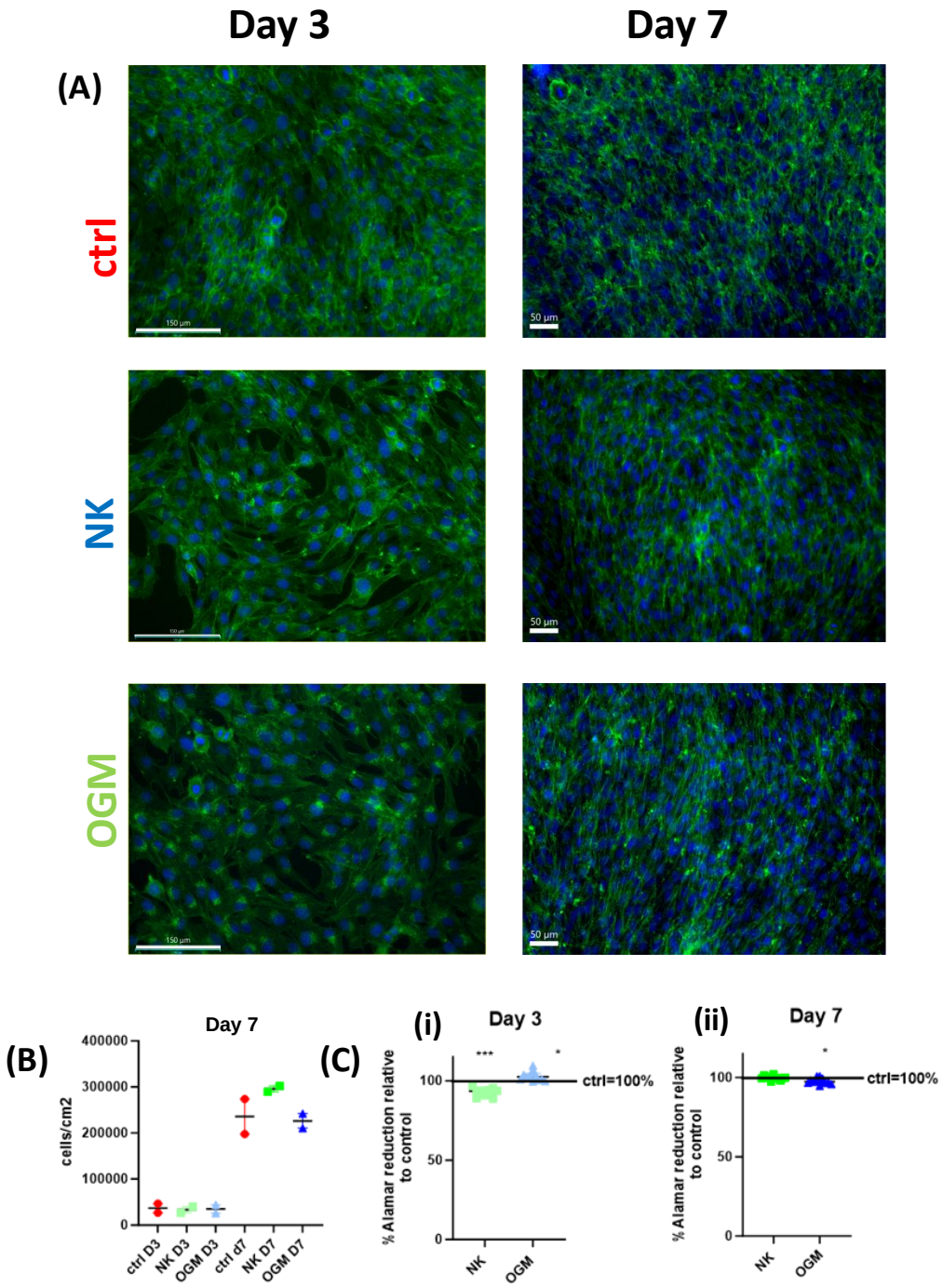

*Figure 3.4: Cell numbers during differentiation. 2,000 cells/cm^2 MG-63 cells were seeded, and then treated after 2 days, with NK or OGM for 3, or 7 days. (A) Immunofluorescence staining showing cell numbers and morphology: (N-1 biological replicate, N=8 experimental replicates) Cells were stained with Hoechst (blue) and phalloidin (green) and imaged on EVOS at 20x magnification. Images processed on Imaris viewer. Scale bars: 150 µm for day 3, and 50 µm for 7 days. (B) Trypsinised cell counts, after 3 and 7 days (N=1 biological replicate, N=2 experimental replicates) (C) %Alamar reduction measured against individual untreated MG-63 control, of day (i) 3 and day (ii) 7 timepoint respectively. Welch's adjusted t-test was used to statistically compare treatments' alamar reduction vs control=100%. N=1 biological replicate, N=4 experimental replicates, and N=3 analytical replicates each. (blank=ns=p>0.05, *=p<0.05, **=p<0.01, ***=p<0.001)*

Quantification of osteogenic genes via qPCR for MG-63 cells

Differentiation was first assessed via qPCR, where osteogenic potential was measured by comparing osteogenic gene expression levels between the untreated control, and the treatments. RUNX2 and OSX were chosen to screen differentiation conditions at first, due to their role in regulating differentiation. While changes in OSX were measured, low endogenous expression of OSX in MG-63 cells is a limitation,[164] as to how representative that increase would be. Experimental variability is a well-documented issue in molecular biology, especially so in cancer cell lines.[204,205] Superplots were used to assess variability between biological replicates, and to assess statistical significance, following Lord *et al.*'s described procedure.[206] Data points of the same colour represent replicates from the same experiment, while different coloured points represent different experiments. Variations in numbers of replicates reflect sample limitations, RNA numbers, or technical issues.

After 3 days of nanokicking, a large, statistically significant decrease in RUNX2 was observed, as well as a small decrease in OSX and ONN (Figure 3.5). For the OGM group, a decrease in RUNX2 was observed after 3 days, and a statistically significant decrease of OSX and ONN. Those findings would indicate a lack of differentiation, an early timepoint, or earlier differentiation, under both mechanical and chemical stimulation. On the other hand, after 7 days of nanokicking, a small upregulation of RUNX2 and OSX was observed, and downregulation of ONN. This may indicate that mechanical stimulation drove earlier differentiation, evident by the increase of osteogenesis regulators. Chemical stimulation also appeared to drive differentiation after 7 days. A statistically significant upregulation of RUNX2 gene expression indicates initiation of differentiation, while the observed statistically significant increase in ONN indicates mineralisation. Variance was observed between experiments, which may be due to biological heterogeneity, but some trends could still be observed. Initial trends in differentiation were observed, so the panel of osteogenic genes was expanded for a set of biological samples. Mechanical and chemical stimulation both demonstrated differentiation after 7 days, with observed differences in the gene profiles, while a day 3 timepoint seemed too early to observe differences. To confirm this finding protein expression and localisation of osteogenic markers was assessed via immunofluorescence.

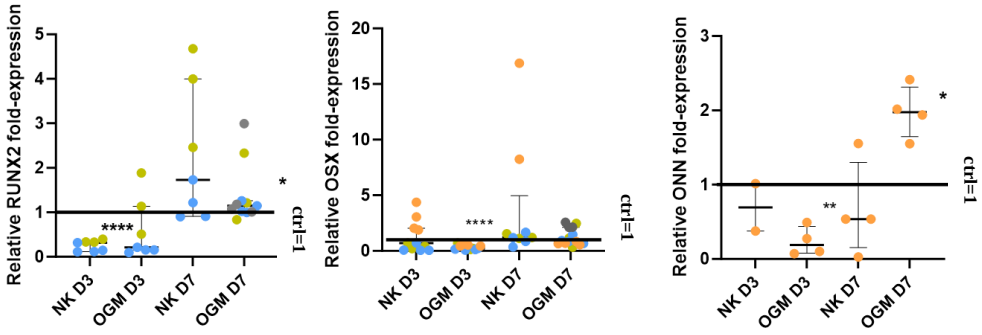

Figure 3.5: Gene fold-expression quantified by qPCR: MG-63 cells were seeded at a density of 1,000 cells/cm^2, treated with NK or OGM for 3 or 7 days. RUNX2, OSX and ONN gene levels were normalised against untreated MG-63 D3 or D7 control. N numbers variable, but data from N=1-3 biological repeats. Mann Whitney u-test was used to statistically compare treatments' gene fold-expression vs untreated control=1 (p>0.05=ns=blank, p<0.05=, p<0.01=**, p<0.0001=****).*

In order to further understand the osteogenic response of cells to the treatments, a deeper analysis into a wider panel of osteogenic genes was carried out on a single dataset. A small, yet statistically significant increase of COL1 was observed after 3 days of nanokicking (Figure 3.6), which could indicate initiation of differentiation and mineralisation. No clear discernible changes in COL1 levels were seen under chemical stimulation, or after 7 days of mechanical stimulation. A small, but not statistically significant increase in alkaline phosphatase (ALP) levels was observed for the nanokicked sample after 3 and 7 days, as well as for the OGM group after 7 days. RUNX2, which is a key of osteogenesis, was upregulated during chemical stimulation yet downregulated during mechanical stimulation. ONN expression was not changed after 7 days. OPN expression was elevated after 7 days of treatment, with NK treatment showing more of an increase than regulator OGM treatment, with increase in OPN indicates later differentiation and mineralisation. Overall, though changes in osteogenic genes were not statistically significant, they overall would show trends in osteogenic differentiation, with limitations of biological variance.

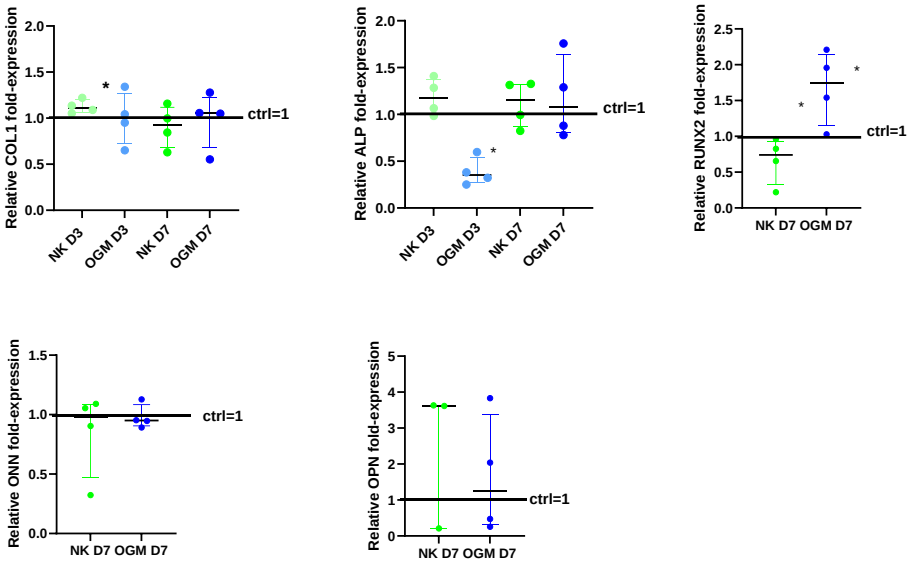

*Figure 3.6: Gene fold-expression was quantified via qPCR: MG-63 cells were seeded at 2,000 cells/cm^2 and treated after two days. Cells were nanokicked (NK) or treated with osteogenic medium (OGM) for 3 or 7 days. COL1, ALP, RUNX2, ONN and OPN gene levels were normalised against untreated MG-63 D3 or D7 control. N=1 biological replicate. N=3-4 experimental replicates, 2 analytical replicates. Mann Whitney u-test was used to statistically compare treatments' gene fold-expression vs untreated control=1 (blank=ns=p>0.05, *=p<0.05)*

Visualisation and localisation of osteogenic proteins during differentiation

Immunofluorescence can provide valuable information on protein expression, cell morphology, as well as the localisation of the protein,[207] which offers insights as to the activity and function of the said protein. Cytoplasmic and perinuclear expression of RUNX2 was observed in MG-63 cells (Figure 3.7). Inhomogeneous protein expression was generally observed, with pink arrows pointing to areas of increased protein expression. Higher levels of RUNX2 are visible in the nanokicked group, compared to the control and the OGM group, which is further indication of differentiation. In this specific instance OGM treatment did not show increased RUNX2 expression. Protein expression was further quantified via the in-cell western assay.

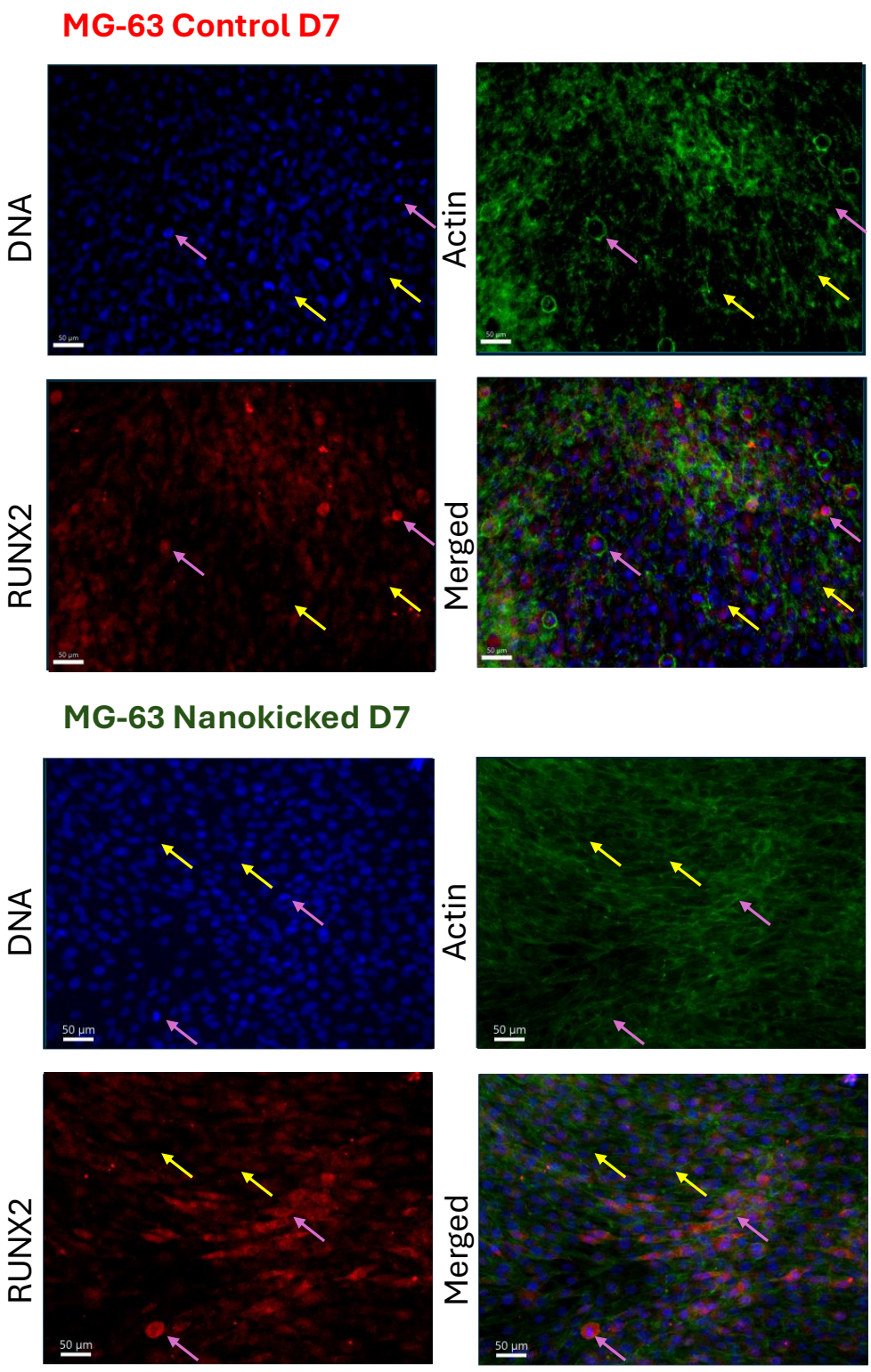
MG-63 Control D7
DNA
Actin
RUNX2
Merged
MG-63 Nanokicked D7
DNA
Actin
RUNX2
Merged
50 µm

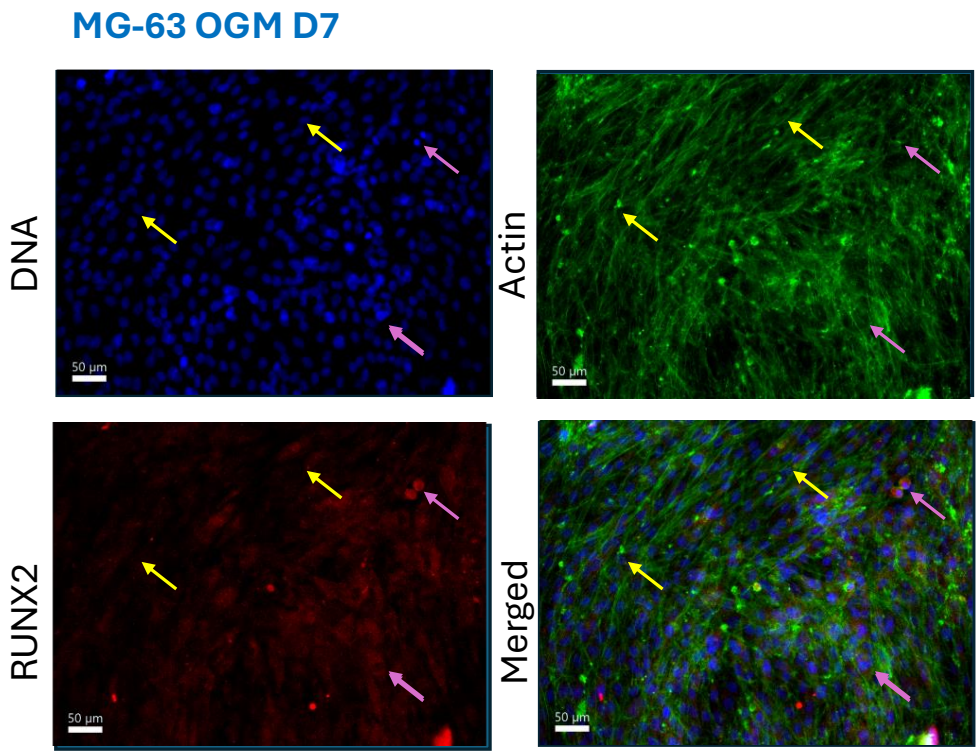

Figure 3.7:Immunofluorescence staining: MG-63 cells were treated with nanokicking (NK), or OGM for 7 days. Nuclei were stained with Hoechst (blue), phalloidin (green), and RUNX2 (red), and imaged on EVOS at 20x magnification. Images processed on imartis viewer. Scale bars: 50 µm. Yellow arrows point to areas of decreased RUNX2 expression, and pink arrows point to areas of increased RUNX2 expression. N=1 biological replicate, N=2 experimental replicates.

Low endogenous expression of OSX has been documented in literature for MG-63 cells,[164] which was visually confirmed in this case via immunofluorescence. MG-63 cells present a more fibroblastic, more poorly differentiated phenotype. OSX was found to be expressed in a small number of cells (Figure 3.8). A small upregulation of OSX was observed for both the nanokicked and the OGM treated samples (pink arrows), despite the abnormally low expression of the protein (yellow arrows), compared to osteoblasts, and differentiating MSCs. Only visual observations were made, as protein expression was later quantified via ICW.

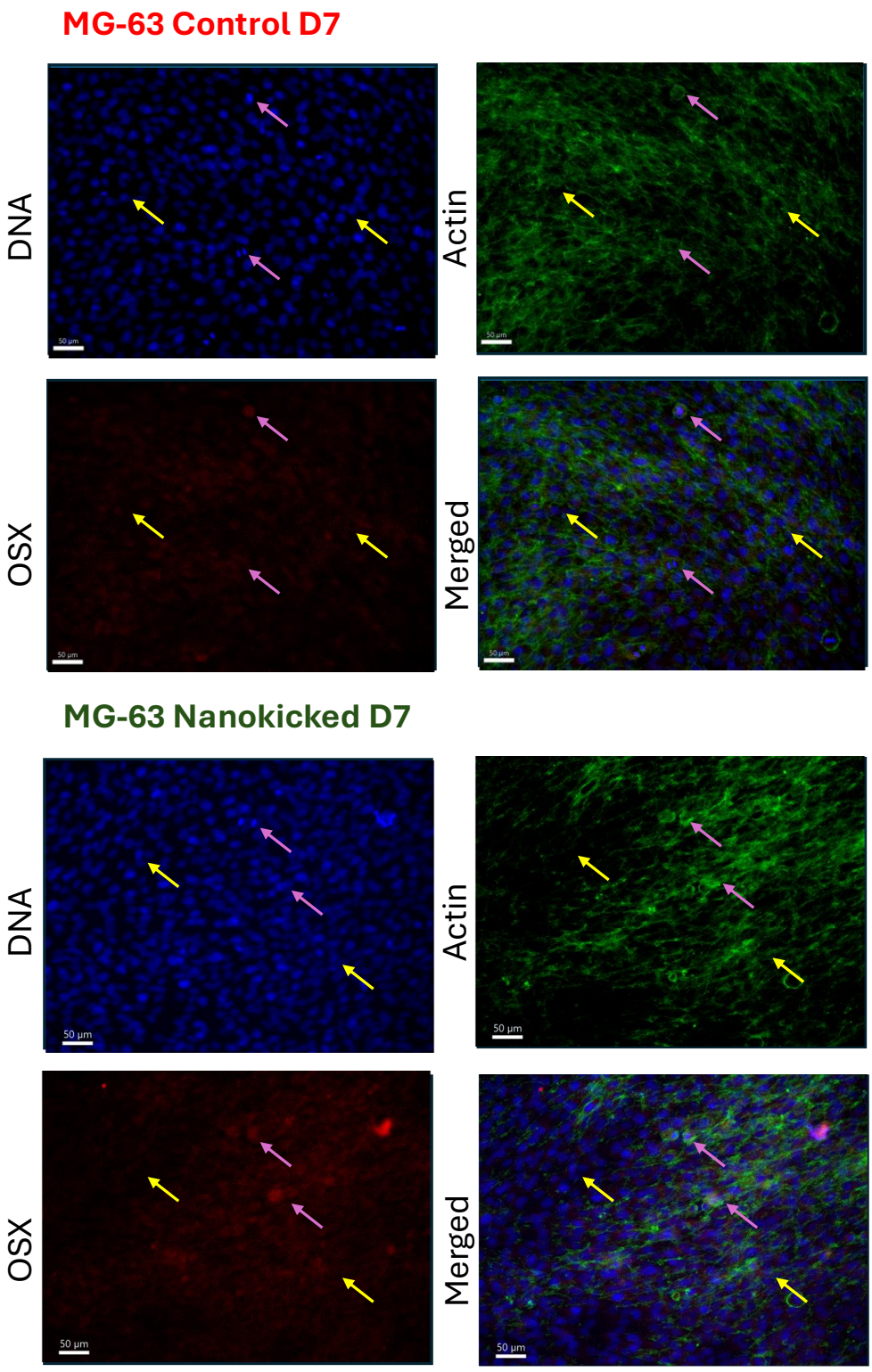
MG-63 Control D7
DNA
Actin
OSX
Merged
MG-63 Nanokicked D7
DNA
Actin
OSX
Merged
50 µm

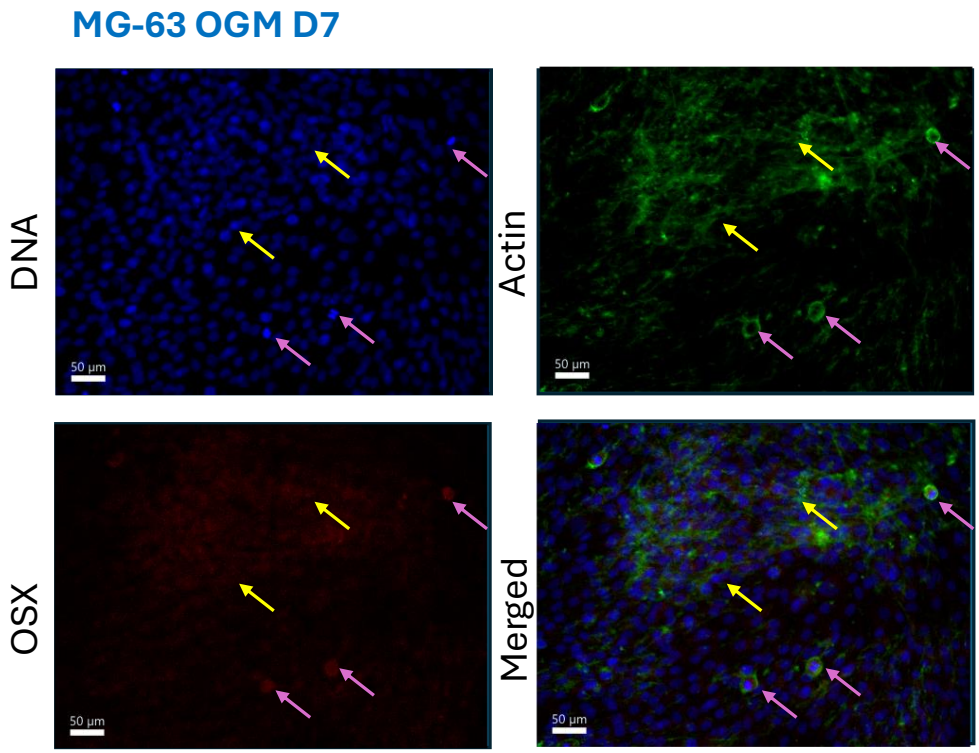

Figure 3.8: Immunofluorescence staining: MG-63 cells were treated with nanokicking (NK), or OGM for 7 days. Nuclei were stained with Hoechst (blue), phalloidin (green), and OSX (red), and imaged on EVOS at 20x magnification. Images processed on Imaris viewer. Scale bars: 50 µm. Yellow arrows point to areas of decreased OSX expression, and pink arrows point to areas of increased OSX expression. N=1 biological replicate, N=2 experimental replicates.

While OSX expression was very low for MG-63 cells, osteonectin (ONN) which is a later differentiation/mineralisation marker appeared to be more abundant (Figure 3.9). ONN presented perinuclear localisation, as was observed for RUNX2, with some heterogeneity in cell populations. Cells that were nanokicked appeared to show higher expression of ONN. Treatment with osteogenic medium seemed to show enhanced expression of the matricellular protein, with areas of higher cluster formation showing upregulated ONN. Overall, both mechanical and chemical stimulation appeared to drive differentiation, as seen by the increase of this late mineralisation marker.

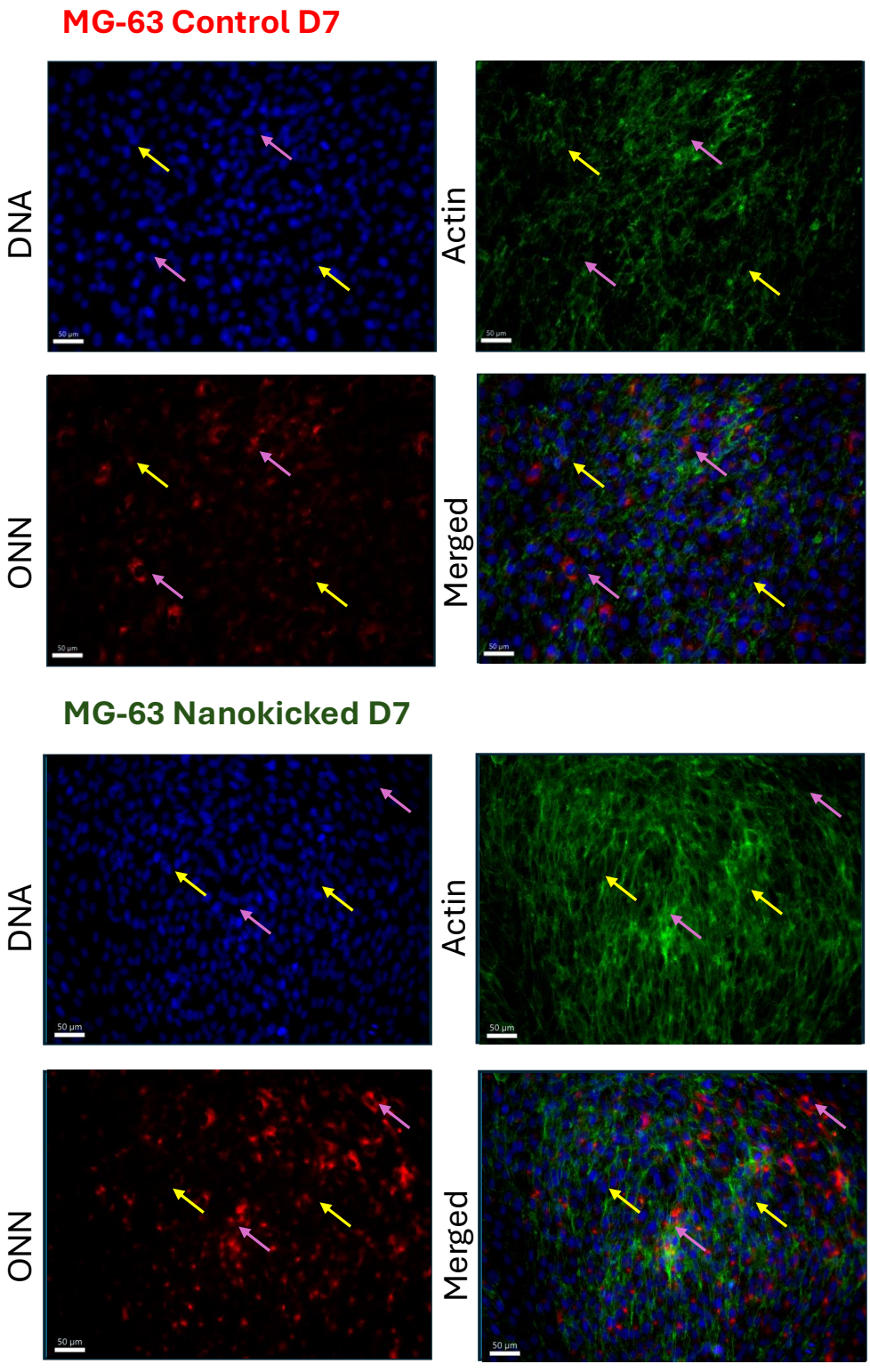
MG-63 Control D7
DNA
Actin
ONN
Merged
MG-63 Nanokicked D7
DNA
Actin
ONN
Merged

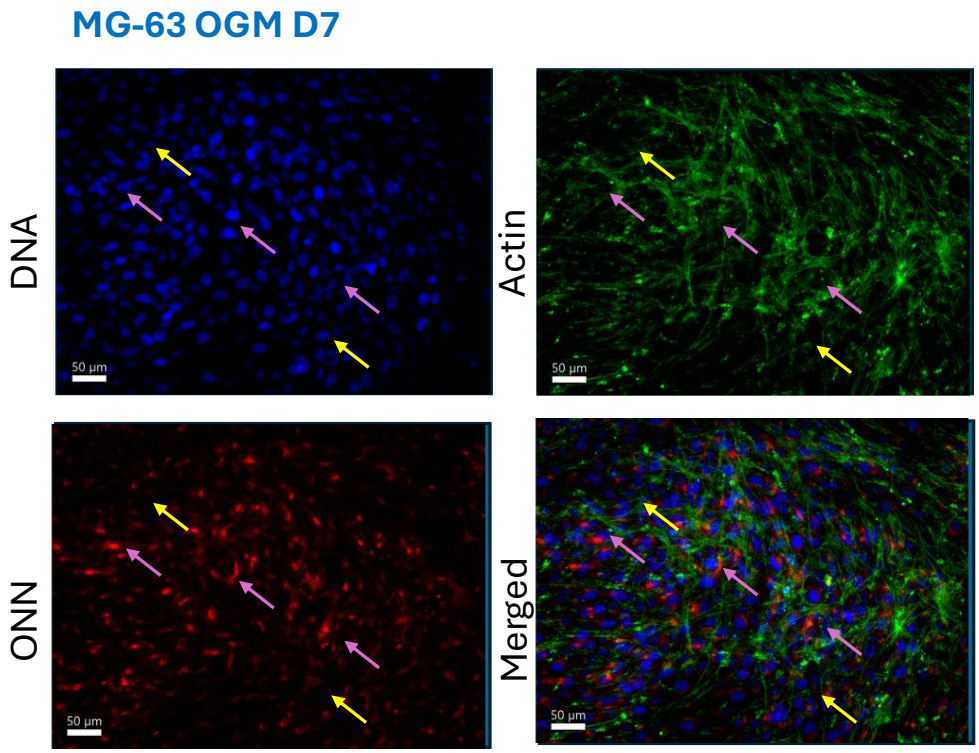

Figure 3.9: Immunofluorescence staining: MG-63 cells were treated with nanokicking (NK), or OGM for 7 days. Nuclei were stained with Hoechst (blue), phalloidin (green), and ONN (red), and imaged on EVOS at 20x magnification. Images processed on Imaris viewer. Scale bars: 50 µm. Yellow arrows point to areas of decreased ONN expression, and pink arrows point to areas of increased ONN expression. N=1 biological replicate, N=2 experimental replicates.

As previously discussed, osteopontin (OPN) is a matricellular protein, that is overexpressed in MG-63 cells.[170] Upregulation of OPN is also an indicator of later osteogenic differentiation in MSCs and in OS cells.[158] OPN expression was found to be cytoplasmic, and in a smaller number of cells perinuclear (Figure 3.10). Areas of cluster formation showed increased OPN expression. Overall, some increase in osteogenic markers could be observed visually for mechanical and chemical stimulation, but the protein expression was later quantified via in-cell western (ICW).

MG-63 Control D7

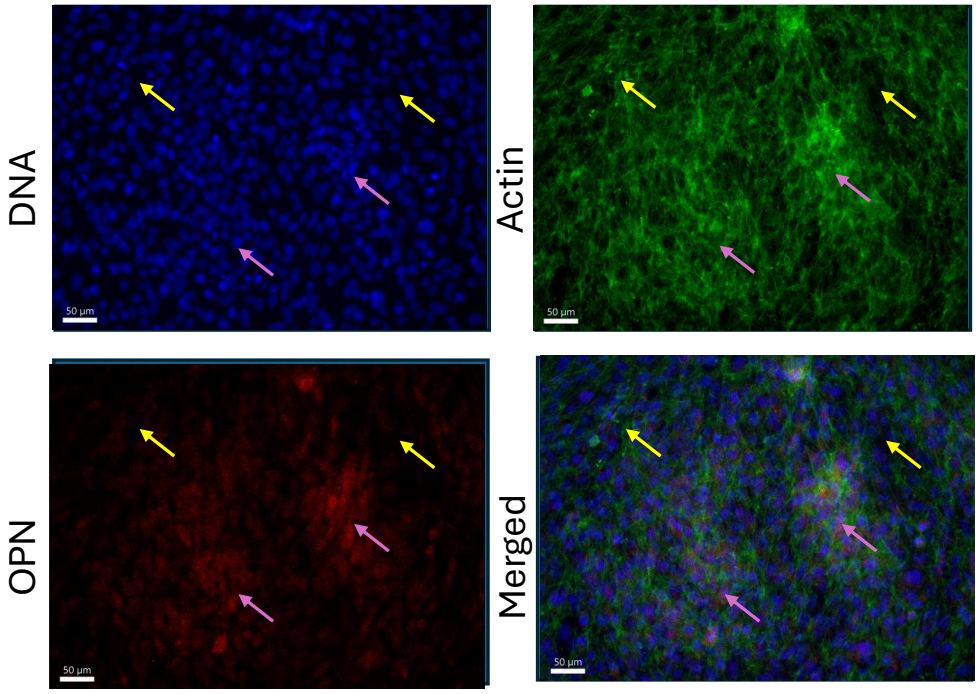

MG63 Nanokicked D7

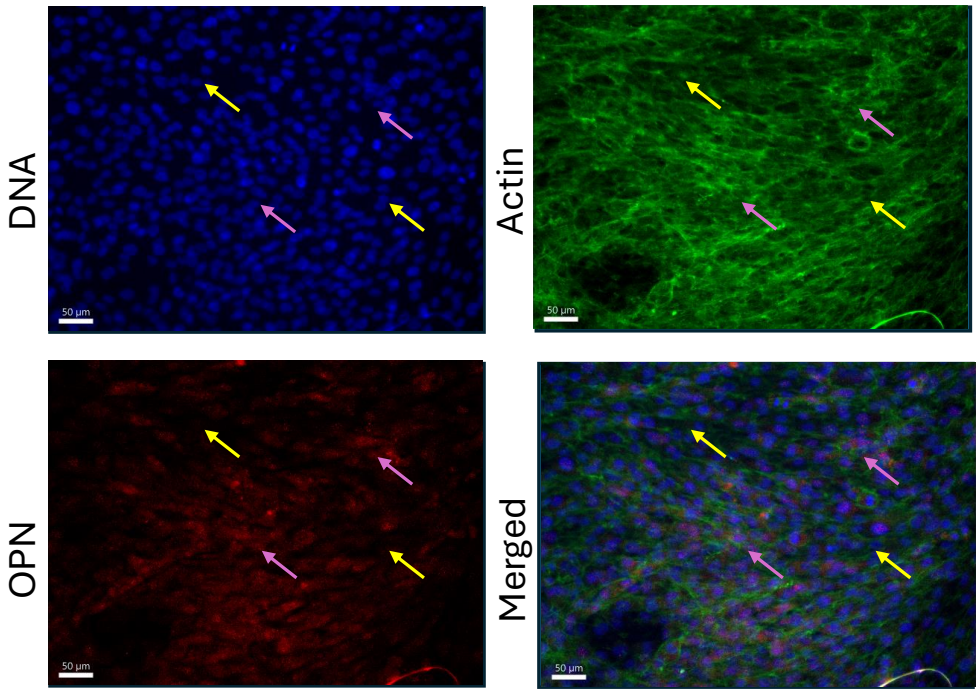

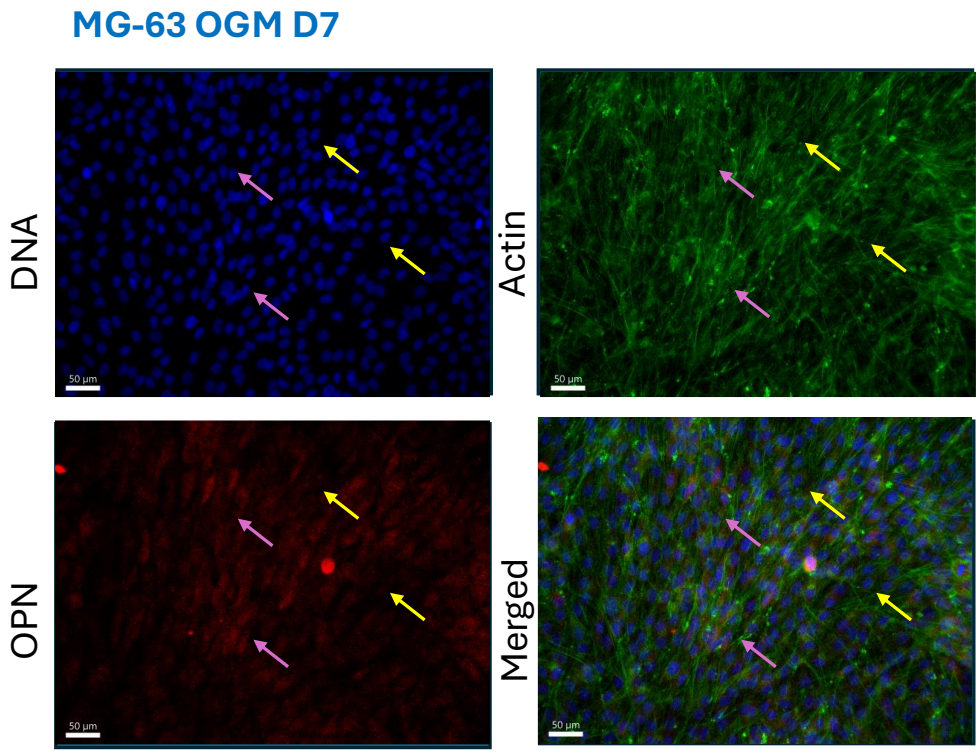

Figure 3.10: Immunofluorescence staining: MG-63 cells were treated with nanokicking (NK), or OGM for 7 days. Nuclei were stained with Hoechst (blue), phalloidin (green), and ONN (red), and imaged on EVOS at 20x magnification. Images processed on Imaris viewer. Scale bars: 50 µm. Yellow arrows point to areas of decreased OPN expression, and pink arrows point to areas of increased OPN expression. N=1 biological replicate, N=2 experimental replicates.

Overall, perinuclear, and diffuse cytoplasmic localisation was observed for the different osteogenic proteins, in MG-63 cells. RUNX2 was found to be abundant both in treated and untreated MG-63 cells. OSX expression was found to be very low, and below limits of detection for this technique in some areas. The matricellular proteins ONN, and OPN were found to be more highly expressed in areas of cluster formation, with an indication of some increase from treatments. Inhomogeneous expression of osteogenic markers was identified in the samples, which has previously been described for different OS cells, including MG-63.[75] This variation is a common characteristic of the bone cancer cells but may also be an indication that while further differentiation may have been induced, it was not terminal. Nonetheless, the analysis was mostly qualitative, and hence protein expression was then quantified via a quantitative immunofluorescence technique, called in-cell western (ICW).

Quantification of osteogenic markers during differentiation

To study protein expression, in-cell western (ICW) was used, which is a quantitative immunofluorescence technique, used to study protein expression.[208] The IR dyes were previously described in literature to show decreased background fluorescence, allowing for more accurate quantification of the protein.[209] Values were normalised against cellTag, which is a fluorescent dye, that is used to measure the number of cells. RUNX2 and OSX are indicators of earlier differentiation, with ONN and OPN being included to measure later differentiation, and mineralisation. Data from two separate experiments was plotted, with different shape symbols and colours denoting different experiments. After 3 days the nanokicked group did not show an increase in osteogenic markers, with a statistically significant decrease in ONN being observed (Figure 3.11). This lack of differentiation is in line with the qPCR data, that also demonstrated that perhaps a day 3 timepoint might be too early to see a significant osteogenic response. Cells treated with osteogenic medium (OGM) however showed an increase in OSX and OPN after 3 days, which was not statistically significant, but could indicate cells undergoing differentiation.

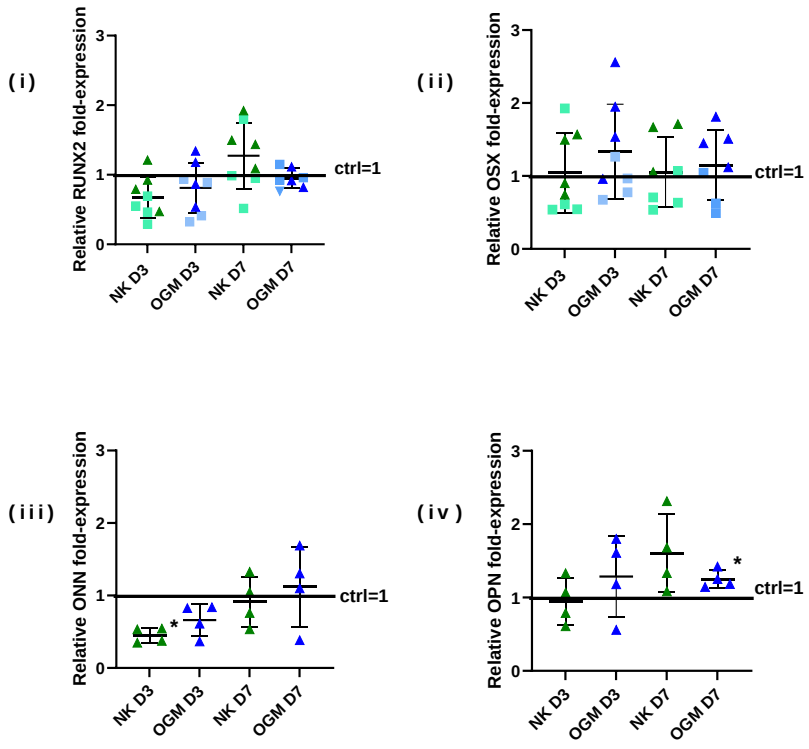

Figure 3.11: ICW analysis of protein fold-expression: MG-63 cells were seeded at 1,000 cells/cm^2 (square symbols) or 2,000 cells/cm^2 (triangle symbols) and after 2 days were nanokicked (NK) or treated with osteogenic medium (OGM). Protein fold-expression for (i) RUNX2, (ii) OSX, (iii) ONN and (iv) OPN was quantified against untreated D3 or D7 MG-63 control, via ICW. Welch's adjusted t-test was used to statistically compare treatments' protein fold-expression vs control=1. (p>0.05=blank=ns, p<0.05=). N=1-2 biological replicates. N=4 experimental replicates.*

After 7 days of nanokicking an increase in RUNX2 and a more visible increase in OPN was observed, which shows a trend of nanokicking driving osteogenic differentiation. The qPCR findings and the ICW findings corroborate that mechanical stimulation can induce differentiation in the highly proliferative, and poorly differentiated MG-63 cells. It is also noteworthy that albeit being poorly differentiated, MG-63 cells already express some osteogenic markers. Osteogenic medium was used as a positive control of differentiation, so there are more replicates, compared to other conditions. Cells treated with osteogenic medium for 7 days, showed a statistically significant upregulation of RUNX2, and a statistically significant increase in OSX, ONN, and OPN, which would also be consistent with osteogenic differentiation. Moreover, both the gene and protein data for the nanokicked and the osteogenic group, showed some statistically significant increase in osteogenic genes, and markers respectively. This would strongly suggest that differentiation occurred in MG-

63 cells both under chemical and mechanical stimulation after 7 days, albeit at different rates, as seen by the different marker profiles.

Cell cycle distribution during differentiation

Cell cycle analysis was carried out for the control and the treatments, by measuring DNA content, via flow cytometry, using a propidium iodide (PI), intercalating, fluorescent dye.[210] First, the gating strategy described in section 3.3.8 was employed, to ensure single cell analysis, and exclude dimers, and debris. Histograms were arranged by DNA content. Analysis revealed that for the untreated control group 73.88% of cells were in the G0/G1 phase, 6.58% of cells were in the S phase, and 8.85% of cells were in the G2/M phase (Figure 3.12). The portion of cells in the G0/G1 phase demonstrates the osteoblastic commitment of the cells, which is within reason of the partial differentiation of the cancer cells. Overlapping histograms for the control, the nanokicked and the osteogenic group showed a shift in G0/G1 phase in the treatment groups compared to the control. The shift was more significant for the osteogenic group. Moreover, more cells were in the G1, G2 phases and fewer cells were in the S phase compared to the untreated control group, indicating fewer cells undergoing DNA synthesis. Lengthening of the G0/G1 phase, as well as an increase of cells in that phase is a sign of commitment to differentiation. A small increase of cells in the G2 was also observed, which typically indicates stemness. A small increase of cells in G1 phase was observed in the NK and OGM treated group, but the increase was not statistically significant. According to Muhr *et al*, a lengthening of the G1 phase, as well as an increase of portion of cells in the G1 phase may indicate stem cells differentiating.[211]

(i)

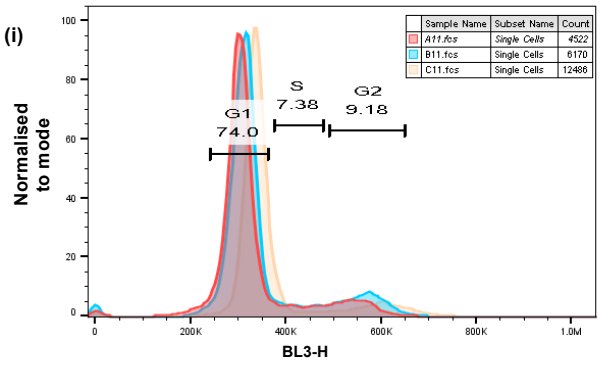

(iii)

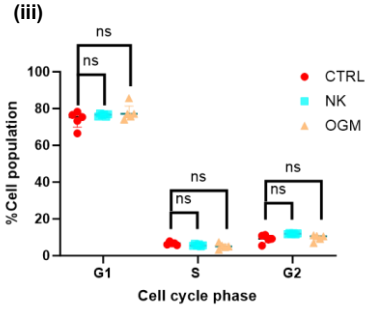

(ii)

	ctrl mean	ctrl SD	NK mean	NK SD	OGM mean	OGM SD
G1	73.88	4.09	76.61	0.58	76.20	0.74
S	6.58	0.73	5.51	0.38	5.54	0.660
G2	8.85	2.08	11.90	0.30	11.32	0.73

Figure 3.12: Flow cell cycle distribution: (i) BL3-H histograms assessed cycle distribution of NK and OGM treated MG-63 cells after 7 days. (ii) Table showing cell cycle distribution for control and treatments. (iii) Graph showing cell cycle distribution. Welch's adjusted t-test revealed no statistical significance. N=1 biological replicate, N=2 experimental replicates, N=3 analytical replicates.

3.4.2 The effect of mechanical vs chemical stimulation on SAOS-2 cells

Cell morphology and viability

SAOS-2 cells are more osteoblastic, further differentiated OS cells,[164] compared to the more poorly differentiated MG-63 cells. Similar assays used for MG-63 cells were used for SAOS-2 cells, with viability being assessed via Alamar blue. Microscopic observations were also made, where within each well there was a level of variability, in terms of confluence (Figure 3.13). Observations after 7 days were made by studying the cell numbers, and morphology, via HOESCHT DNA staining, and phalloidin actin staining, respectively. Extensive cell death occurred in the cells that were treated with osteogenic medium, as observed microscopically (iii). A statistically significant decrease in metabolically active cells was observed, according to the alamar blue assay, confirming that OGM reduced metabolic activity (iv). This degree of cell death was not previously observed in MG-63 cells, with the differing response. For the nanokicked group, cell numbers were comparable between the treated group (ii) and the untreated control (i), while statistically significant decrease in metabolic activity was observed (iv). While the treatment may have slowed proliferation, cell death was not as significant as for the OGM group.

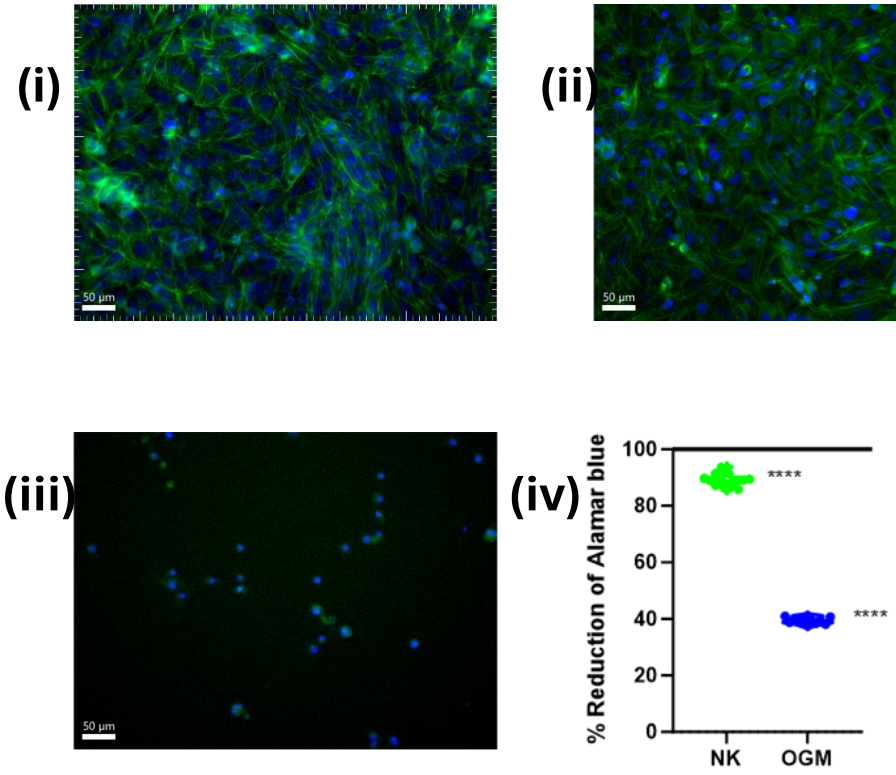

*Figure 3.13: SAOS-2 cell numbers assessed by fluorescent imaging: Cells were treated with NK or OGM for 7 days. Hoechst stained the nuclei (blue), and phalloidin (green) stained the cytoskeleton. (i)control, (ii)NK, (iii)OGM, Scale bars=50 µm. (iv) Alamar blue used to quantify metabolic activity in NK and OGM treated cells after 7 days, against untreated SAOS-2 D7 control. N=1 biological replicate, N=4 experimental replicates, N=3 analytical replicates of each technical. Mann Whitney u test was used to statistically compare treatments' alamar reduction vs untreated control=100% (****=p<0.0001).*

Quantification of osteogenic genes via qPCR for SAOS-2 cells

Differentiation was assessed in the more osteoblastic SAOS-2 cells using the assays previously described in section 3.4.1. Gene expression for different biological replicates was compared using previously described superplots.[206] RUNX2 increase was found to be statistically significant for the nanokicked and osteogenic groups after 7 days, with no statistically significant increase being observed after 3 days (Figure 3.14). It is important to note that cell numbers, and consequently RNA levels were low for the osteogenic group, so extensive analyses were not carried out for SAOS-2. Fold-expression was increased for RUNX2 for the nanokicked and the osteogenic group for different replicates, but there was variation, as to the degree of increase. The increase in RUNX2, and to a lesser degree increase in OSX and ONN, would indicate that differentiation occurred in the SAOS-2 cells,

both under mechanical and chemical stimulation. This observation was further verified using ICW analysis.

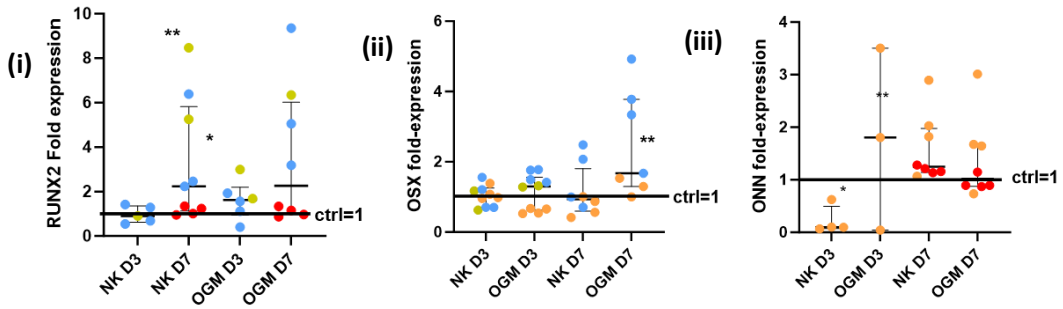

Figure 3.14: Gene fold-expression assessed by qPCR: SAOS-2 cells were seeded at a density of 1,000 cells/cm^2, treated with NK or OGM for 3 or 7 days. (i) RUNX2, (ii) OSX and (iii) ONN fold-expression was quantified against the untreated SAOS-2 D3 or D7 control. . Different colours signify data points from different biological repeats. N numbers variable. N=1-4 biological repeats. Mann Whitney u test used to statistically compare treatments' protein gene-expression vs control=1 (p>0.05=ns=blank, p<0.05=, p<0.01=**).*

To assess the degree of differentiation, a panel of osteogenic genes were used. As previously observed, 3 days of nanokicking appeared to be insufficient for inducing differentiation in SAOS-2 (Figure 3.15). COL1 was found to be the most upregulated gene after 7 days of nanokicking, which is an indication of collagen production, and early differentiation. ALP and RUNX2 levels were also increased, which would further corroborate earlier differentiation, with RUNX2 upregulation also being shown on Figure 3.14. No clear changes were observed in OSX and ONN expression. Overall, some trends in osteogenic genes could be observed after a week of mechanical stimulation, albeit not being statistically significant. Differentiation was further assessed by studying protein expression and localisation via immunofluorescence, while protein expression was later quantified ICW.

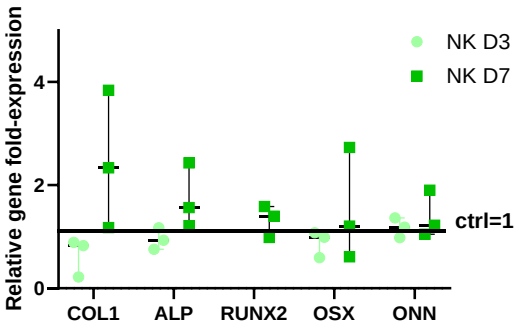

Figure 3.15: Gene fold-expression assessed by qPCR: 4,000 cells/cm^2 SAOS-2 cells were seeded and then treated with NK for 3 or 7 days. Relative fold-expression of COL1, ALP, RUNX2, OSX and ONN was quantified against the untreated SAOS-2 D3 or D7 control. N=1 biological replicate, N=3 experimental replicates Mann Whitney u test was used to statistically compare treatments' gene fold-expression vs control=1. No statistical significance observed.

Visualisation and localisation of osteogenic proteins on SAOS-2 cells

Immunofluorescence was used to study osteogenic protein expression and localisation in mechanically stimulated SAOS-2 cells. Varying levels of RUNX2 were observed both in the control and the nanokicked group (Figure 3.16), which would indicate cells within the population are differentiated to varying degrees. Areas of higher density, and particularly clusters appeared to express higher protein levels, which was a common observation in MG-63 cells too. RUNX2 was found to be localised in the nucleus, which is in line with SAOS-2 cells being more mature and expressing RUNX2 already. Cells within the population expressed varying levels of RUNX2, which would indicate they were undergoing differentiation. As previously discussed, RUNX2 localisation was found to be perinuclear in most cells for MG-63. This difference between the two cell lines is interesting, as this is another indication of the degree of differentiation of the cells dictating the cell behaviour, and response to chemical and mechanical stimulation. SAOS-2 cells being further differentiated and already expressing higher levels of RUNX2, would account for the localisation that was not present in the MG-63 cells.

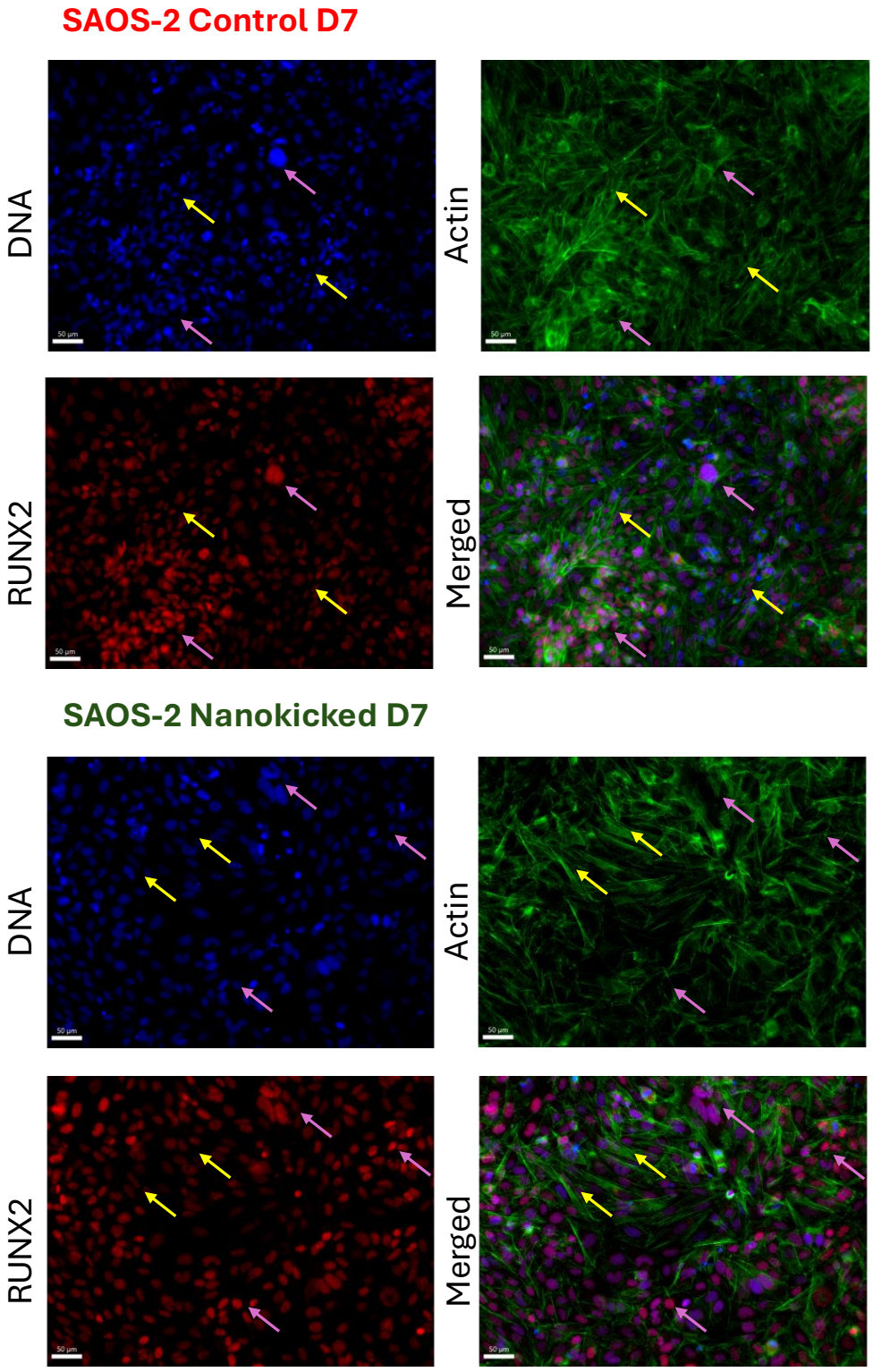

Figure 3.16: Immunofluorescence staining: SAOS-2 cells were treated with nanokicking (NK) for 7 days. Nuclei were stained with Hoechst (blue), phalloidin (green), and RUNX2 (red), and imaged on EVOS at 20x magnification. Images processed on Imaris viewer. Scale bars: 50 µm. Yellow arrows point to areas of decreased RUNX2 expression, and pink arrows point to areas of increased RUNX2 expression. N=1 biological replicate, N=2 experimental replicates

SAOS-2 cells displayed nuclear localisation of the osteogenic regulator OSX, with some cell populations expressing higher levels of OSX (pink arrows), and some expressing lower OSX levels (yellow arrows) (Figure 3.17). Nuclear translocation of OSX has previously been described during early differentiation in healthy cells, [212] with this localisation further highlighting the cells' more mature phenotype. Immunofluorescence was used as a qualitative tool, and protein expression was later quantified via ICW, though certain areas of increased protein levels were evident, as indicated by the pink arrows.

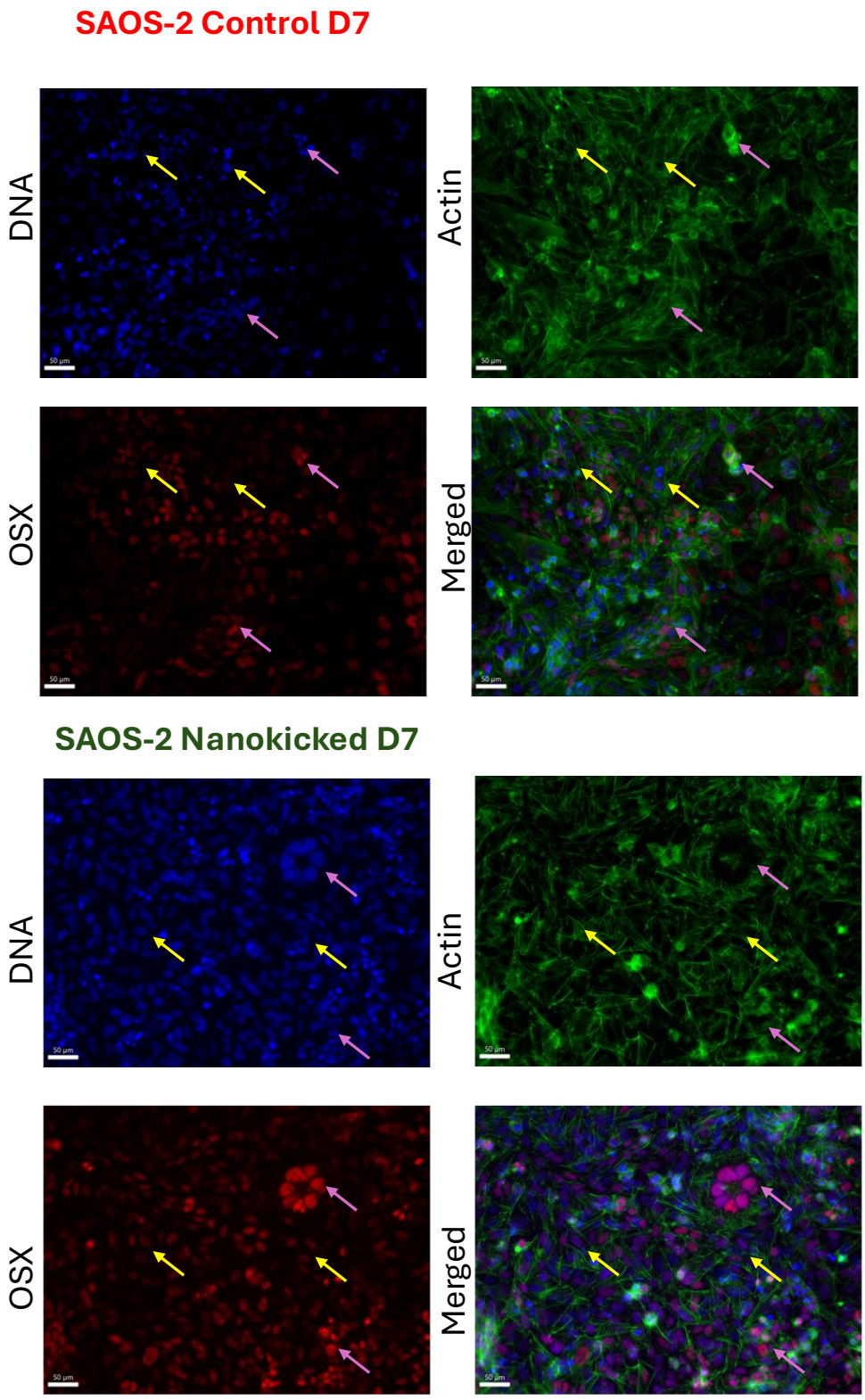

Figure 3.17: Immunofluorescence staining: SAOS-2 cells were treated with nanokicking (NK) for 7 days. Nuclei were stained with Hoechst (blue), phalloidin (green), and OSX (red), and imaged on EVOS at 20x magnification. Images processed on Imaris viewer. Scale bars: 50 µm. Yellow arrows point to areas of decreased OSX expression, and pink arrows point to areas of increased OSX expression. N=1 biological replicate, N=2 experimental replicates

ONN was found to display perinuclear localisation in SAOS-2 cells (Figure 3.18), as was observed for MG-63 cells, with heterogeneous protein labelling. Nuclear polymorphism was evident. Areas of higher density, and cluster formation presented increased levels of ONN, which was more evident in the control group, but was also previously observed in MG-63 cells. Expression of ONN was higher in the control in this instance, compared to the nanokicked group, which may be attributed to the increased cluster formation.

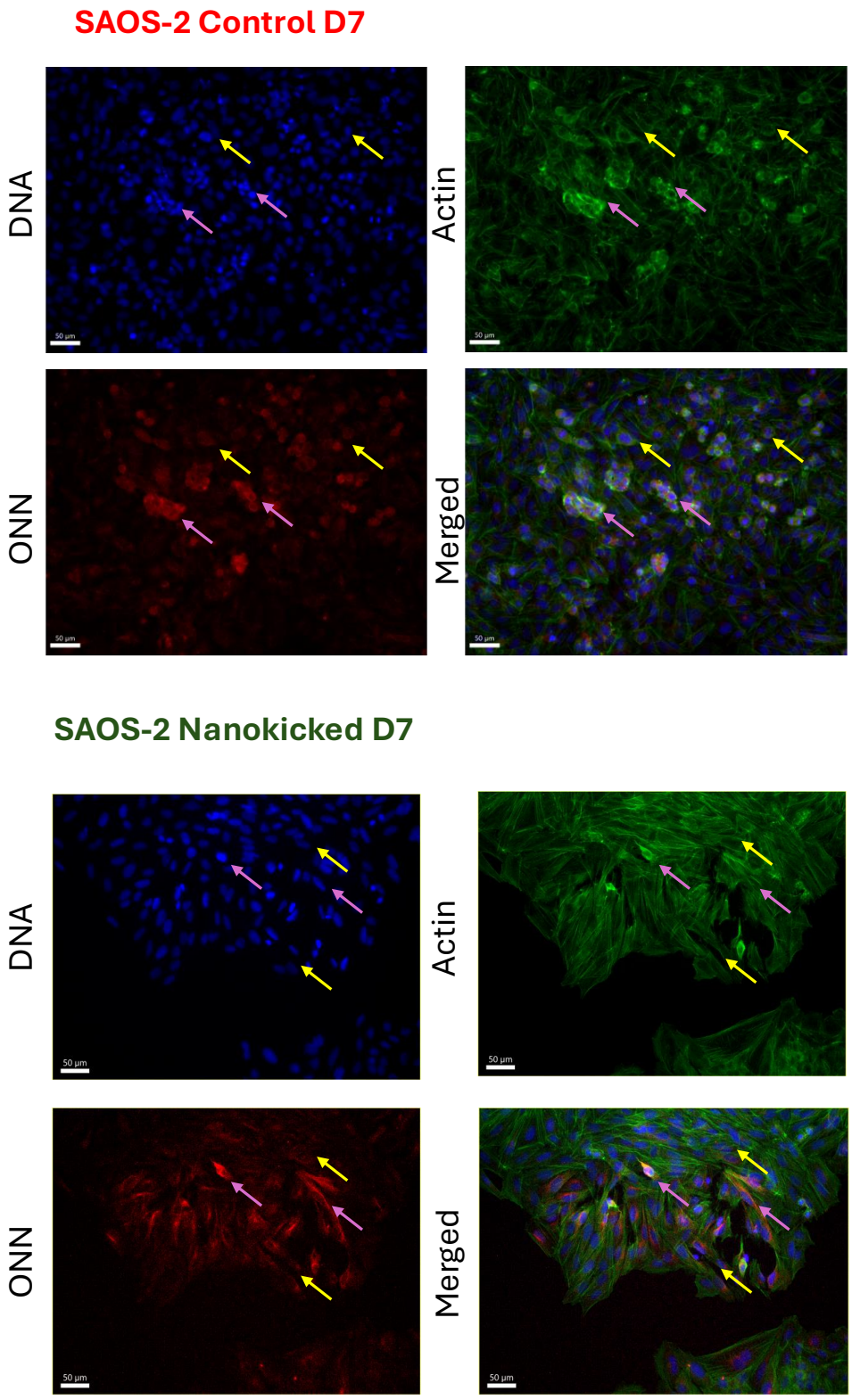

Figure 3.18: Immunofluorescence staining: SAOS-2 cells were treated with nanokicking (NK) for 7 days: Cells were stained with Hoechst (blue), phalloidin (green), and ONN (red), and imaged on EVOS at 20x magnification. Images processed on Imaris viewer. Scale bars: 50 µm. Yellow arrows point to areas of decreased ONN expression, and pink arrows point to areas of increased ONN expression. N=1 biological replicate, N=2 experimental replicates

OPN was not as highly expressed, with nuclear localisation observed for some cells, while for others, both perinuclear, and cytoplasmic expression was also observed (Figure 3.19). Nanokicking appeared to also have an effect on cell morphology, with cells that expressed higher levels of OPN, appearing to have more rounded morphology, as seen by the actin cytoskeleton organisation. Moreover, clusters of cells appeared to also express increased levels of osteopontin, which further highlights that through "macromolecular interactions" cell to cell contact may induce increased mineralisation, even in the absence of treatment.[213]

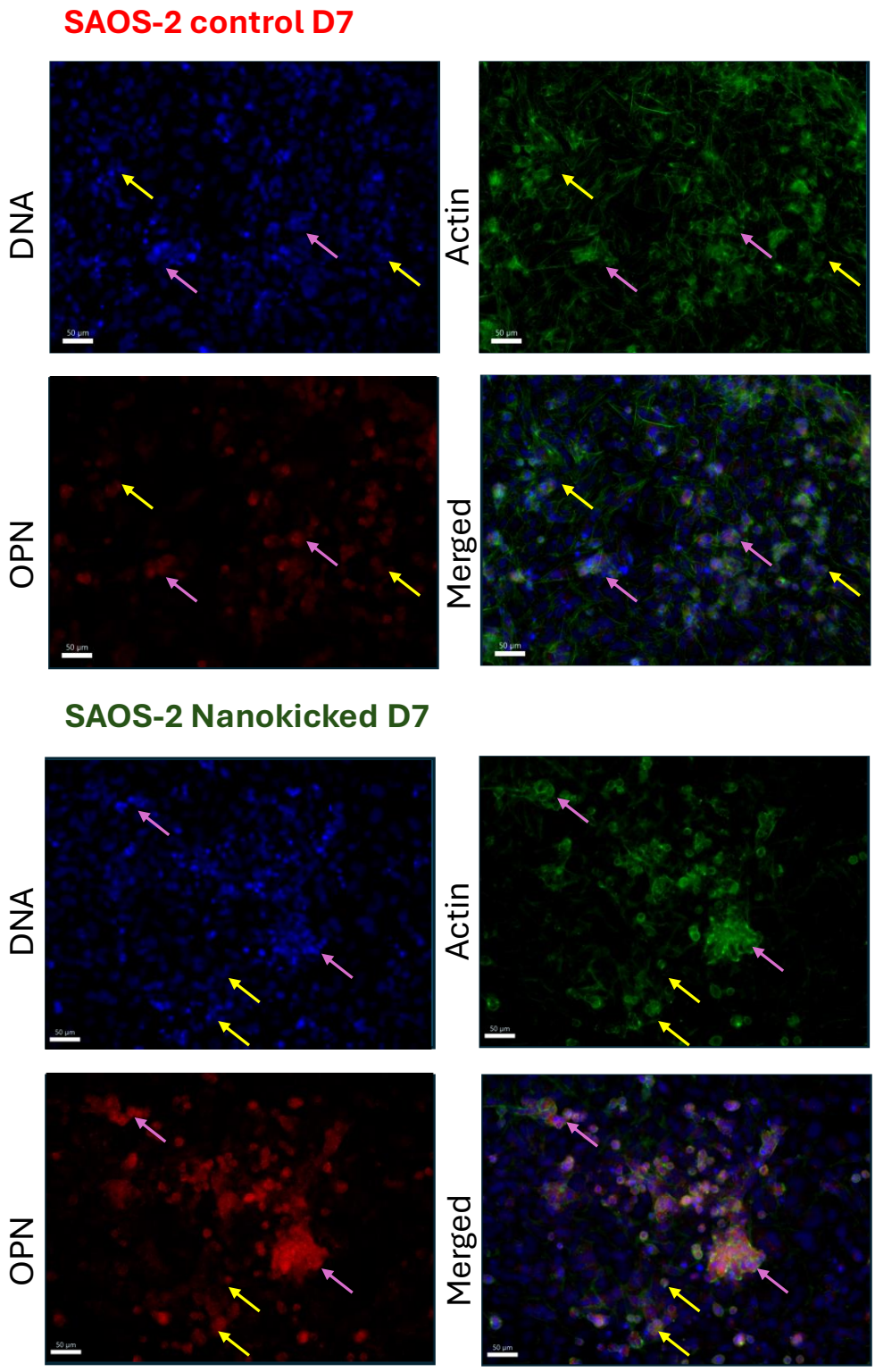

Figure 3.19: Immunofluorescence staining: SAOS-2 cells were treated with nanokicking (NK) for 7 days. Cells were stained with Hoechst (blue), phalloidin (green), and OPN (red), and imaged on EVOS at 20x magnification. Images processed on Imaris viewer. Scale bars: 50 µm. Yellow arrows point to areas of decreased OPN expression, and pink arrows point to areas of increased OPN expression. N=1 biological replicate. N=2 experimental replicates.

Quantification of osteogenic markers during differentiation

Nanokicking for 7 days led to statistically significant upregulation of RUNX2, and OPN (Figure 3.20). Given RUNX2 is a regulator of osteogenesis, the increase in RUNX2, could facilitate the downstream expression of more mature markers,[148] such as osteopontin (OPN), in this instance. No statistically significant changes were observed for OSX and ONN. On the other hand, RUNX2, OSX and OPN were downregulated, when SAOS-2 cells were nanovibrated for 3 days, indicating that it may be too early to study differentiation. Treatment with OGM for 7 days led to a non-statistically significant increase of RUNX2, and OSX, with further studies not including OGM treatment, due to cell death. Both SAOS-2 cells and MG-63 cells showed enhanced differentiation after 7 days, when they were mechanically stimulated. Cells showed limited differentiation after 3 days, as previously observed.

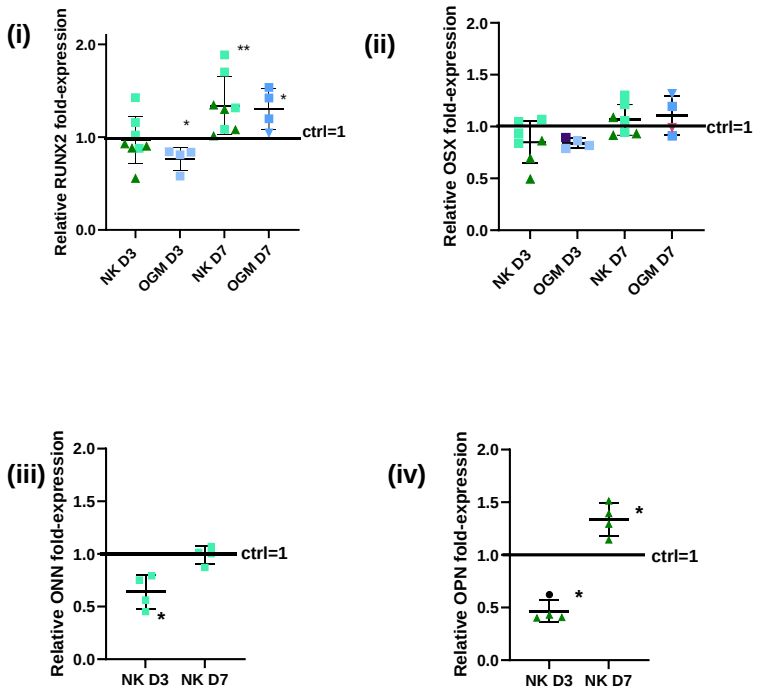

Figure 3.20: ICW analysis of protein expression: SAOS-2 cells were seeded at 2,000 cells/cm^2 (triangle), or 4,000 cells/cm^2 (square). Cells were treated with OGM or nanokicked (NK) for 3 or 7 days, and protein fold-expression was quantified against untreated SAOS-2 D3 or D7 control, via ICW. RUNX2, OSX, ONN and OPN levels were normalised against cell tag, followed by normalisation against the untreated D3 or D7 SAOS-2 control. (n=1 biological replicate, n=4 experimental replicates), Mann Whitney u test used to statistically compare treatments' protein fold-expression vs control=1. (p>0.05=ns=blank, p<0.05=, p<0.01=**).*

Cell cycle analysis

Cell cycle analysis was carried out to study the effect of nanokicking and the osteogenic medium, on the cell cycle distribution. The same gating strategy that was described for MG-63 cells was employed on the SAOS-2 cells. In the untreated, control cells 64% of cells were in the G0/G1 phase, 6.5% of cells were in the S phase and 5.99% of cells were in the G2/M phase (Figure 3.21). Moreover, 18% of cells were in the sub-G1 phase, which may correspond to unstained apoptotic fragments, which contain smaller DNA fragments.[214] Some dead cells were visually observed in cell culture, which matches with this result. Overall, most of the cells were in the G0/G1 phase, which is expected for SAOS-2 cells, given they are further differentiated, and have committed to the osteogenic pathway, though cells are not terminally differentiated. For the nanokicked group there was a statistically significant increase of cells in the G1 phase, while there was a smaller portion of cells in the G2/M and the S phase. G0/G1 phase also appeared during nanokicking treatment, which is in agreement with increase in osteogenic gene and protein expression, previously described. The lengthening of the G1 phase and increase of cells in that phase of the cell cycle was also observed in MG-63 cells, which shows a degree of agreement between cell lines, in this aspect. For the osteogenic medium group, which corresponds to the H10 orange peak on the histogram, all cells were located in the sub-G1 region. Apoptotic cells contain smaller fragments of DNA, and hence will appear earlier on the plot, indicating less stained content.[214] This was further evidence of the extensive cell death that was observed for this treatment for the SAOS-2 cells. In the future carrying out Annexin V and caspase-3 staining, would confirm that cells were truly apoptotic.

(i)

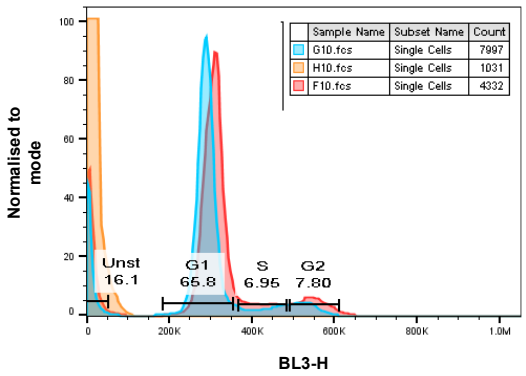

(iii)

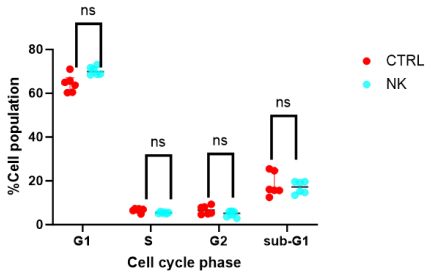

(ii)

	ctrl mean	ctrl SD	NK mean	NK SD
G1	64.4%	3.9%	70.0%	1.8%
S	6.5%	0.9%	5.5%	0.3%
G2	6.0%	1.5%	4.4%	1.2%
sub-G1	18.1%	4.9%	16.7%	2.6%

Figure 3.21: Flow cytometric cell cycle analysis of SAOS-2 cells: (i) Overlapped BL3-H histograms for control (red), nanokicked (blue), and OGM (orange), (ii) Table showing cell cycle distribution for control and treatments. (iii) Graph showing cell cycle distribution. Welch's adjusted t-test revealed no statistical significance. N=1 biological replicate. N=2 experimental replicates. N=3 analytical replicates.

3.4.3 The effect of mechanical vs chemical stimulation on MSCs

MSC differentiation was studied alongside OS cell differentiation, to study the effect on healthy cells. Promo MSC cells were used, which are sourced from different donors, and donor variation can lead to variability from batch to batch.[215,216] Faster proliferating MSCs present reduced differentiation potential. First, differentiation was observed by studying gene expression. After 3 days there was a statistically significant decrease in OSX, and a small increase in RUNX2, in the osteogenic medium (Figure 3.22, A). RUNX2 and OSX were upregulated after a week in the osteogenic medium, which would indicate that differentiation was occurring, despite the lack of statistical significance. For the nanokicked group an increase in RUNX2 was observed after 3 days, which would indicate differentiation occurred earlier. However, a decrease in OSX was seen at both timepoints, with the limitation of fewer replicates to give the full picture. Both mechanical and chemical stimulation appeared to drive differentiation, but at different rates. Protein expression was also studied, to verify whether differentiation was occurring, via in-cell western (B). No statistically significant increase in RUNX2 or OSX was observed for either condition after 3 or 7 days. This provides no meaningful insights into the differentiation of MSCs, but it could either indicate a lack of differentiation or a need to expand the panel of osteogenic proteins, to reflect the differentiation stage. The increase in the osteogenic genes that was

previously described indicated that differentiation had occurred overall, but in the future expanding gene and protein panels would provide more information on the cell behaviour. Further tests were not run, as previous research in the group has widely explored osteogenic differentiation of MSCs when nanokicked.[198,199,200,201] Overall MSCs were included alongside OS cell lines, to study differentiation. preliminary data was collected, that indicated differentiation. Prior research on the effect of nanokicking and the osteogenic medium on MSCs had shown that differentiation occurred, but lengthier differentiation protocols were used, to achieve maturity and mineralisation.

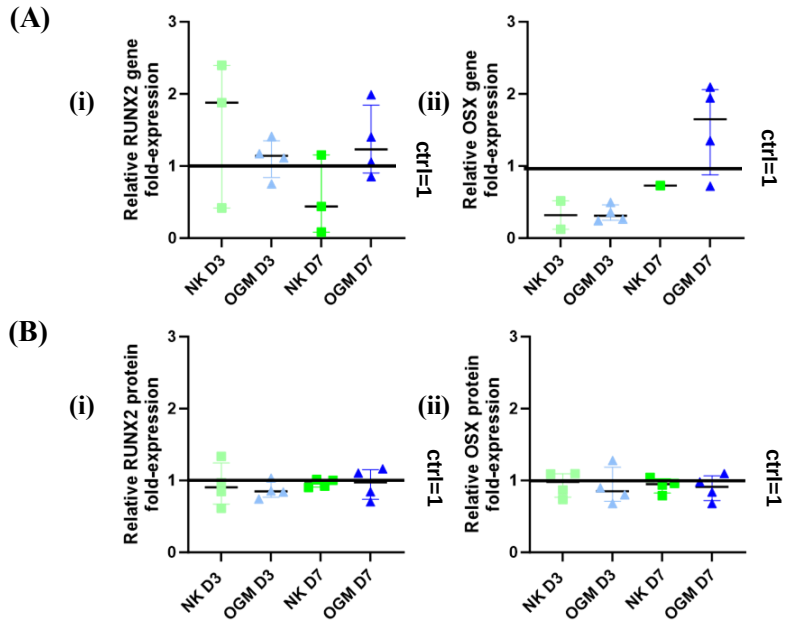

Figure 3.22: MSC osteogenesis assessed via (A) qPCR and (B) ICW: (A) Gene fold-expression of (i) RUNX2 and (ii) OSX normalised against untreated D3 or D7 MG-63 control for nanokicked (NK) and osteogenic medium (OGM) group, after 3 and 7 days. Protein expression of (i) RUNX2 fold expression, (ii) OSX fold expression. Mann Whitney u-test was used to statistically compare treatments' gene or protein fold-expression vs control=1, and showed no statistically significant changes between control and treatments.

3.5 General discussion

Known differentiation conditions for MSC osteogenesis were tested on OS cells. The aim was to observe the effect of mechanical vs chemical stimulation, and whether both conditions can drive differentiation. MG-63 cells represented a more undifferentiated, highly proliferative OS cell line. SAOS-2 cells represented a more differentiated, slower proliferating cell line. MSCs were used to study the response of differentiation conditions on healthy cells, compared to the cancerous cell lines. It was exciting to see that both

chemical and mechanical stimulation promoted differentiation, despite differences in protein expression patterns.

First, it was observed that nanokicking promoted a small decrease in metabolic activity for MG-63 and SAOS-2 cells, though cells still divided rapidly, given their cancerous phenotype. Some initial observation of changed cell morphology would translate to cells adapting to changes in their mechanical environment, though mechanical properties would need to be studied in the future. The cells' degree of differentiation clearly has some bearing on cellular morphology, as would be expected.

Research into OS and mechanotransduction has shown greater focus on characterisation of mechanical properties, rather than directly mechanically stimulating the cancer cells. Nagayama *et al.* observed that during differentiation of SAOS-2 cells, using a small molecule cocktail, mechanical changes occurred, including nuclear shrinkage and stiffening.[217] Rounding of nuclei, actin stress fibres, and nuclei was observed for the differentiated group, while they reported a plateau in Alizarin production, after 20 days. Griffin *et al.* electrically stimulated SAOS-2 cells for 28 hours, and observed enhanced differentiation and mineralisation, without increased proliferation.[218] making it a promising approach for mechanically inducing osteogenesis in cancer cells. Interested in how external mechanical stimulation alters the mechanical environment of the OS cells, Alloisio *et al.* applied 1 Hz cyclic stretch stimulation to SAOS-2 cells for 24 hours.[219] They reported that while there were changes in the mechanical environment, no differentiation was apparent after 24 hours, though one should consider that this is an early timepoint. While this study was the closest identified to the scope of this project, direct comparison could not be drawn, given the differences in length of treatment, as well as difference in stimulus. Choi *et al.* also used compression stimulation HA/PLGA scaffolds, on MG-63 cells, but did not make observations on differentiation and mineralisation.[220] Chen, Jeng *et al.* applied cyclic stretch stimulation (15% elongation, 0.5 Hz) to MG-63 cells, and reported apoptotic effects, due to the increased mechanical loading.[221] It is interesting to see how different sources of mechanical stimulation significantly affect cell response, as cyclic stretch stimulation had apoptotic effects on OS cells, while nanokicking did not present apoptotic effects. Wang, Kingshott *et al.* reported that culturing OS cells on substrates with nanotopography patterns can improve cell attachment and increase differentiation.[222] Mechanical stimulation appeared to induce changes in integrins in OS cells,[223] while FAK was also found to play an important role in mechanotransduction of OS cells.[224] It would be interesting to carry out

characterisation of mechanical properties of OS cells, during nanokicking, to observe what pathways may govern mechanotransduction. Instead, the focus on this thesis was to characterise differentiation of OS cells under the different stimuli, to better understand cell behaviour, and later identify small molecules that could promote osteogenesis.

MG-63 cells showed no significant alterations in viability when treated with OGM, while extensive cell death was observed in SAOS-2 cells, though differentiation had also been previously seen in some biological replicates. Osteogenic medium cocktails containing β-glycerophosphate, ascorbic acid and dexamethasone are typically used to drive differentiation in MSCs.[176,177] Use of the same conditions in OS cells is more complicated, with different cell lines showing differing response, based on their phenotype. While MG-63 cells showed few alterations in cell growth after 7 day of treatment, cell death and/or differentiation was observed in the more osteoblastic SAOS-2 cells. Yevlashevskaya *et al.* reported that osteogenic medium can drive differentiation in MG-63, while for the further differentiated SAOS-2 cells they reported apoptosis.[225] This was in line with observations that were made in the OGM group after 7 days of treatment for both cell lines. MG-63 cells remained viable and differentiated, while SAOS-2 presented reduced metabolic activity, though differentiation was observed in remaining viable cells. Orimo *et al.* also observed that the use of inorganic phosphate could drive differentiation in SAOS-2 cells, which was also accompanied by observations of cell death.[226] Cmoch *et al.* also reported that medium supplementation with β-glycerophosphate and ascorbic acid drove apoptosis in SAOS-2 cells. This literature behaviour of differentiation, and apoptosis in OGM treated SAOS-2 cells matched findings of extended cell death under those conditions. While OGM treatment drove extensive cell death in SAOS-2 cells, mechanical stimulation did not show the same effect, with a small decrease proliferation observed in NK stimulated cells, with cells still appearing viable.

Distinct cell morphologies, protein expression profiles, and localisation for the different cancer cell lines were observed from immunofluorescence. Nuclear polymorphism was more evident in SAOS-2 cells, compared to MG-63 cells, with more variation in nuclear size, shape, as well as cells within the population presenting abnormally enlarged nuclei. A link has been reported between nuclei sizes and patient outcomes in OS.[227] Worse prognosis was observed in patients that present smaller cell morphology, as they were more likely to present chemoresistance. According to fluorescent staining SAOS-2 cells, which are further differentiated present larger nuclei compared to MG-63 cells, which are less differentiated,

with smaller nuclei and a more spindle-like elongated cell morphology. The degree of differentiation clearly has some bearing on cellular morphology.

Overall RUNX2 and OSX were abundant in SAOS-2, with nuclear localisation of both proteins, which indicate active expression. Tai *et al.* used GFP-OSX, to study OSX localisation during differentiation, and reported that during early differentiation OSX was located in the cytoplasm, and after 7 days of treatment, OSX translocated to the nucleus.[212] MG-63 cells did not show this localisation pattern or high expression of OSX, which is both reported in literature, and can be explained by the cell line's "immature" phenotype, compared to the SAOS-2 more osteoblastic phenotype. Perinuclear localisation of matricellular proteins ONN and OPN was observed for both cell lines. Cell clusters tended to display higher levels of osteogenic proteins, which may be linked to macromolecular interactions, and increased mineralisation.[213]

Nanokicking MG-63 cells drove an increase in RUNX2 gene expression after 7 days, as well as an increase in RUNX2, OSX and OPN protein expression, which would strongly differentiation. The osteogenic medium drove an increase in RUNX2, OSX and OPN gene expression, as well as an increase in OSX, ONN and OPN protein expression, which indicate further differentiation. Earlier osteogenic genes such as RUNX2 and ALP were found to be upregulated after 7 days of mechanical stimulation, with some overall trends being observed for differentiation, but not statistical significance. RUNX2 and OPN protein levels were also found to be upregulated after 7 days of treatment, though changes were not statistically significant. Chemical stimulation also drove differentiation after 7 days of treatment, with statistically significant increase in gene expression of RUNX2 and ONN, and trends showing increase in ALP and OPN. This indicated further differentiation from chemical compared to mechanical stimulation. Flow cytometric propidium iodide-based cell cycle analysis showed an increase of cells in the G0/G1 phase and G2/M phase, from mechanical and chemical stimulation, though changes were not significant. Overall, despite the lack of statistical significance in some instances, the different assays strongly indicated that the MG-63 cells can be pushed to further differentiated from chemical and mechanical stimulation.

For SAOS-2 cells RUNX2 gene levels were found to be upregulated after 7 days of chemical and mechanical stimulation, while OSX was also upregulated for the OGM treated sample. COL1, ALP, RUNX2 were also upregulated after nanokicking for 7 days, though changes were not statistically significant. The nuclear localisation of RUNX2 and OSX reflect the more mature phenotype of SAOS-2 cells, compared to MG-63. A statistically significant

increase of RUNX2 and OPN after 7 days of nanokicking strongly suggested that mechanical stimulation drove differentiation, while a smaller increase of RUNX2 and OSX was observed for OGM treatment. SAOS-2 cells appeared to respond more consistently to mechanical stimulation compared to MG-63 cells, showing that cell phenotype can affect cell response to osteogenesis. Cell cycle analysis also showed that there were more cells in the G0/G1 phase from nanokicking compared to the control, while osteogenic group was localised in the sub-G1 region, which is an indicator of apoptosis.[214]

Overall, mechanical and chemical stimulation both appeared to drive differentiation in MG-63 cells. For SAOS-2 cells mechanical stimulation led to enhanced osteogenesis, but chemical stimulation led to decrease in metabolic activity. Mechanically modulating the environment is a promising approach for promoting osteogenic differentiation in OS cells, with limited previous information on the osteogenic response identified.

3.6 Conclusions

Nanokicking and osteogenic medium treatment did not appear to alter cell proliferation and viability in MG-63 cells, while some changes in cell morphology could be observed. For SAOS-2 cells, differing response was observed to the stimuli. While OGM led to decrease in metabolic activity, and fewer cell numbers in SAOS-2 cells, mechanical stimulation did not induce cytotoxicity. Increase in osteogenic genes and proteins would strongly suggest that the nanokicking induced differentiation, which was an exciting finding. 3 days of treatment appeared to be insufficient to drive osteogenic differentiation, for the different cell lines, and the different treatments, which led to future studies focusing on 7-day differentiation protocols. Given promising initial results, the next aim was to identify small molecules that can drive differentiation in the OS cells. To do this, metabolomic analysis was carried out, to identify metabolites that are involved in differentiation, as well as predicted changes in metabolite compositions, and pathways (chapter 4).

3.7 Future work

Future work may involve comparison studies in 2D cultures, 3D cultures, and spheroids, to better understand cell response to mechanical stimuli. Collecting more information on mechanical markers, and applying further methodologies for studying mechanotransduction of MSCs, on OS cell lines would be beneficial. Studying signalling pathways such as the FAK and ROCK pathway, and mechanical markers, such as piezo-1 would be beneficial.

Obtaining further information on integrins, and YAP/TAZ localisation can provide further information on how cells adapt to changes in their mechanical environment. To further assess changes in the mechanical environment, AFM, can be employed to obtain information on structure. Vinculin and talin could provide information on focal adhesion formation, while integrins can provide valuable information. Overall further information on changes in the mechanical environment and effects of mechanotransduction on OS cells, would provide a deeper understanding of differentiation, and cell response.

Chapter 4: Effects of chemical vs mechanical stimulation on OS cell metabolism

4.1 Introduction

4.1.1 Cancer cell metabolism

Cancer cells exhibit unique traits, that support their uncontrolled growth, and tumour formation, including increased levels of oncogenes, reduced function and/or mutations of tumour suppressor genes, and metabolic alterations.[71] Rapid-growing cancer cells present increased energy demands, which they support by using alternative metabolic pathways, including aerobic glycolysis, fatty acid oxidation and glutaminolysis.[228] Carbohydrate metabolism plays an important role in osteogenic differentiation and in cancer. The Warburg effect refers to cancers' enhanced glucose consumption[229] and increased lactate accumulation,[230] that was first reported in landmark research by Warburg and Cori.[231] Warburg observed that while healthy cells rely on the more energetically efficient oxidative phosphorylation to generate adenine triphosphate (ATP), as a source of energy, cancer cells more extensively rely on the less efficient aerobic glycolysis. He had also postulated at the time that the mitochondrial oxidative phosphorylation pathway is irreversibly impaired in cancer cells, which promotes aerobic glycolysis in cancer cells.[232] However, later research has extensively investigated the active role of tricarboxylic acid (TCA) cycle metabolites in cell survival and maintenance, which would disprove the hypothesis of inactive oxidative phosphorylation.[233] The TCA cycle is a biochemical pathway that is employed by cells to produce to replenish biosynthetic blocks (Figure 4.1), such as lipids, carbohydrates and amino acids, and to generate energy.[234] Carbohydrates, including TCA metabolites are involved in osteogenic differentiation, while impaired carbohydrate metabolism has previously been reported in OS.

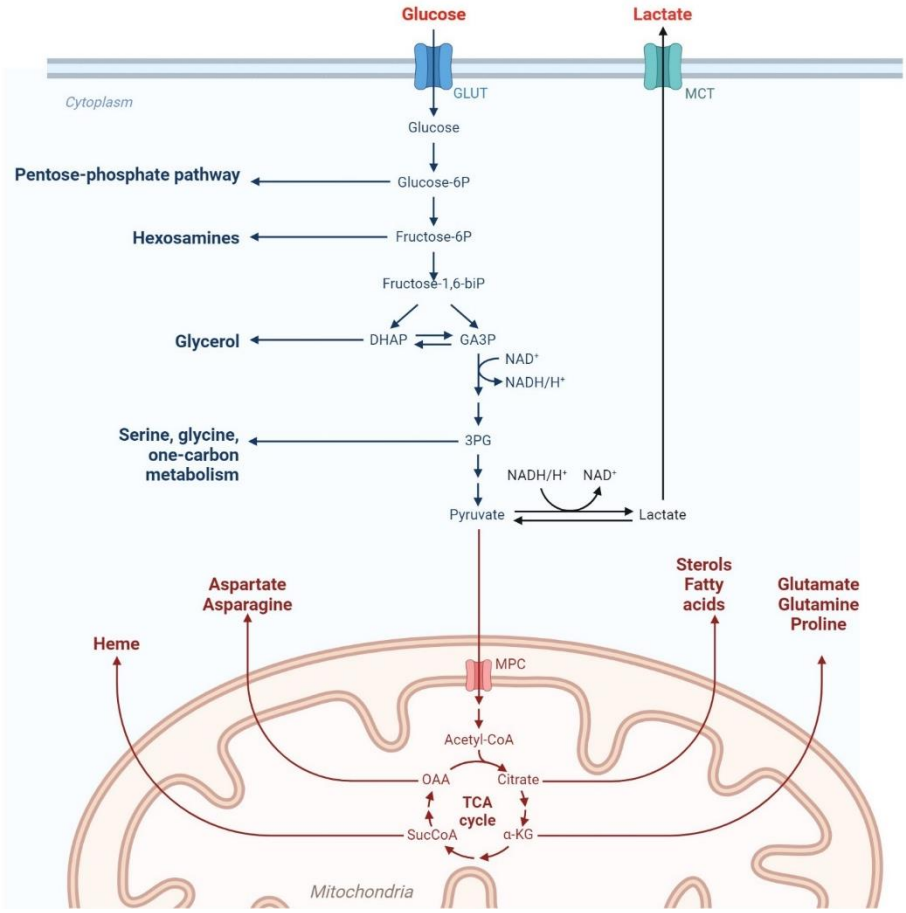

Figure 4.1: Role of glycolysis and TCA metabolic pathways in metabolite anaplerosis, including amino acids and lipids. Abbreviations: Glucose transporter (GLUT), monocarboxylate transporter (MCT), mitochondrial pyruvate carrier (MPC), glucose-6-phosphate (glucose-6P), fructose-6-phosphate (fructose-6P), fructose-1,6-bisphosphate (fructose-1,6-biP), dihydroxyacetone-phosphate (DHAP), glyceraldehyde-3-phosphate (GA3P), 3-phosphoglycerate (3PG), acetyl coenzyme-A (acetyl-CoA), α-ketoglutarate (α-KG), succinyl-CoA (Succ-CoA), oxaloacetate (OAA), oxidized nicotinamide adenine dinucleotide (NAD+), reduced nicotinamide adenine dinucleotide (NADH, H+) Tricarboxylic acid (TCA). Figure adapted from DeBerardinis et al.,[235] using biorender.com. Figure reproduced with permission from Springer Nature.

Amino acids are important metabolic products, used as a source of nitrogen, as an energy source, as building blocks for protein synthesis, and as anaplerotic metabolites.[236] Amino acids are involved in cell survival and osteogenic differentiation,[237] with proline playing a role in RUNX2 regulation and collagen biosynthesis.[238] Glutamine is the most abundant amino acid in the body, with cancer cells extensively using glutamine as a source of energy and nitrogen in biosynthetic pathways.[239] Amino acid and glutathione metabolism have also been found to be enriched in OS, to sustain the uncontrolled growth and proliferation.[240] Glucose deprived OS cells were previously described to switch to glutaminolysis as a source of energy, with glutamine starved cancer cells presenting reduced proliferation.[241]

Lipids are hydrophobic metabolites that play an important role in cell signalling, hormone regulation, small molecule transport, and membrane biogenesis.[242] Lipid metabolism is altered in cancer to provide energy and biosynthetic building blocks, with increased lipid uptake, and fatty acid synthesis and oxidation being observed.[243] Cholesterol and its derivatives have previously been described to drive dose dependent osteogenic differentiation.[244] Moreover, cholesterol is involved in signal transduction, and is one of the main components of cell membranes, aiding in the maintenance of membrane integrity and fluidity .[245] The TCA pathway is involved in metabolite anaplerosis in cells, connecting the carbohydrate and lipid biosynthetic pathways, with cancer cells displaying enhanced lipid catabolism.[246]

4.1.2 Metabolomics

Metabolites are low molecular weight molecules required for key cellular functions in a biological substrate.[247] Metabolomics is a powerful high-throughput technique, that utilises analytical chemistry techniques to quantify all metabolites in a biological sample.[248] Metabolomics analyses can generate data on thousands of molecules, so different bioinformatics tools have to be used to study trends in the data, and identify metabolites of interest for testing.[249] Targeted metabolomics is employed in hypothesis driven studies, to measure and analyse a defined group of metabolites in a biological sample, associated with specific metabolic pathways.[250] Fingerprinting or untargeted metabolomics can be employed to map the full metabolome of a biological sample, and to detect alterations in small molecule composition due to disease or treatment.[250] One advantage of metabolomics is that while the genome is in flux, the metabolome can be a snapshot of ongoing cell activity, showing the current small molecules involved in a specific cell process.[251]

Different analytical techniques may be employed to study metabolite levels, based on sample availability, intended application, and pathway of interest. High resolution mass spectroscopy can provide invaluable information, as to the accurate mass and fragmentation of a metabolite.[252] Coupling chromatography techniques to mass spectrometry can offer improved metabolite separation, while information on retention times on optimised conditions, aids in metabolite identification.`[253] Gas chromatography is preferable for analysis of volatile metabolites, as derivatisation techniques are otherwise required, to extend the pool of metabolites that can be tested.[254] Nuclear magnetic resonance (NMR) spectroscopic analysis of biological samples is also often employed for the metabolic analysis of clinical samples, including blood and urine, providing greater detail on

metabolite structure.[255] LC-MS is particularly useful for untargeted metabolomics, as it allows for the quantification of a wider range of metabolites, compared to GC-MS, where the compounds must be volatile, and NMR where there is often spectral overlap of metabolites.[256] Hydrophilic interaction liquid chromatography (HILIC) columns can be employed to quantify a wider set of metabolites, and can offer superior separation, compared to regular reverse phase columns.[257] The field of metabolomics is a particularly growing and exciting one, as there is a big portion of the metabolome that is untapped, while the biological function of a significant number of known metabolites is not fully understood.

Metabolomic research on OS is more limited compared to more prevalent cancers, with a greater focus on biomarker identification,[258] as well as the link between metabolism, and disease progression.[259,260,] Analyses of the metabolome of patients with localised, or metastatic OS disease have previously shown that tumours can be classified on their metabolic characteristics,[261,262,259] though no standardised, universal classification system has been uncovered. Moreover, studies have focused on changes in OS metabolism, in response to chemotherapeutic agents.[263,264,] as well as ionising radiation.[265] OS studies have also investigated altered metabolism in OS cancer stem cells,[266] as well as the role of MSCs, and the microenvironment in OS tumour initiation, and progression.[267,268] Transcriptomic and metabolomic analysis of SAOS-2 cells previously revealed that culturing conditions play a significant role in cancer cell metabolism.[269] Different 2D and 3D methodologies revealed distinctive metabolic and phenotypic profiles, thus revealing the importance of employed model systems in cancer studies. Metabolic alterations have also been reported, when RUNX2 was silenced in OS cells.[270]

A limited number of studies on changes in cell metabolism during OS differentiation were identified,[271] while there is little research into the effects of mechanical stimulation on the OS metabolome.[272] A GC-MS based study Fanelli *et al.* studied the effect of mechanotransduction, through 24 hour-1 Hz cyclic stretch, on SAOS-2 cell metabolism, with a focus on reactive oxygen species.[272] They observed depletion of TCA metabolites upon mechanical stimulation of the OS cells. Given the link between cell metabolism and cancer, and previous observations of mechanically induced OS maturation (chapter 3), it is worth studying the link between mechanotranduction, differentiation, and metabolic reprogramming in OS. OS cells display altered lipid, amino acid, and carbohydrate metabolism, to provide energy and precursors for building blocks, that will support the cancer's uncontrolled growth and proliferation.[70] Studying changes in putative metabolic groups, and mapping metabolites involved in major pathways, such as the TCA cycle,

glutaminolysis, and fatty acid metabolism can offer insights into the bioenergetics of differentiation.

4.2 Aims and objectives

The main aim of this chapter was to study the effect of mechanical versus chemical stimulation on the metabolome of OS cells vs healthy MSCs and identify metabolic and signalling pathways involved in differentiation. As limited previous research was identified on metabolites involved in OS differentiation, a further objective was to detect changes in carbohydrates, amino acids and lipids, and discern some initial observations on the bioenergetics of differentiation. It was sought to discover how the degree of differentiation of OS cells may affect their metabolic response to the different stimuli. Identifying specific bioactive metabolites that are involved in differentiation, and testing them on OS cells, to drive osteogenesis was the final aim.

4.3 Materials and methods

A multistep protocol was followed to isolate and identify metabolites, and to study associated metabolic pathways (Figure 4.2). First, cells were cultured and then treated for 3 or 7 days with osteogenic medium or nanokicking, and metabolites were extracted and submitted for chromatographic and bioinformatics analysis to Glasgow Polyomics.[273] The data output was received from the facility as an excel interface file, called the IDEOM, for further bioinformatics analysis. IDEOM is a Microsoft Excel interface employed by Glasgow Polyomics, which employs features of mzMatch and XCMS, to filter out noise, and assign metabolites.[274] Analysis was carried out, by breaking down the data into separate cell lines, and then comparing treatments to their own timepoint no treatment control. MetaboAnalyst was used to carry out multivariate statistics, generate plots, identify metabolites of interest and to study overall trends on what metabolic groups each treatment employs.[275] Peak intensities were assessed relative to the control group, and data was $\log_{10}$-transformed on MetaboAnalyst, before generating plots. Ingenuity pathway analysis (IPA) software was then used to look for trends in the type of metabolism employed, canonical pathways[276] and metabolic reactions cells may employ to promote differentiation or cell survival. The software also identified networks and pathways involved in differentiation, whether treatment is predicted to be activated or inactivated, and what metabolites are involved in this pathway identification.

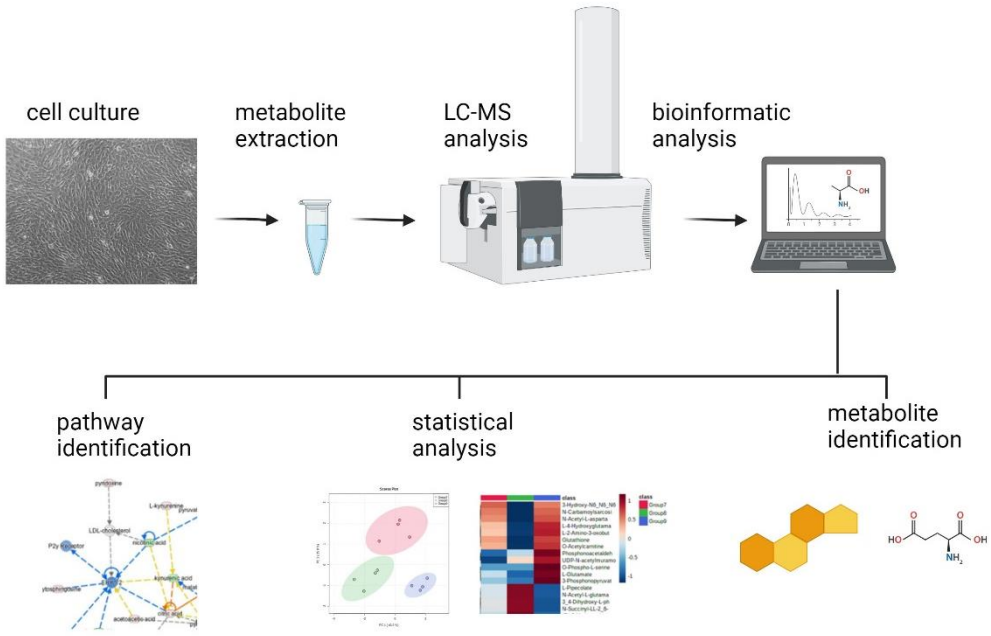

Figure 4.2: Metabolomics workflow: First cells were seeded, treated, and samples were lysed after 3 or 7 days. Samples were then analysed using LC-MS, to measure metabolite levels, and bioinformatic tools were used to carry out statistical analysis, metabolite identification, and pathway identification. (created with biorender.com)

4.3.1 Cell culture

Differentiation of MSCs, MG-63 and SAOS-2 cells was carried out using nanokicking or osteogenic medium, and differentiation was assessed via assays described in chapter 3, and cell culture protocols from chapter 2. Cells were seeded at densities of 1,000 cells/cm^2 for MG-63, and 2,000 cells/cm^2 for SAOS-2 and MSC cell lines. Cells were nanokicked or treated with osteogenic medium for 3 or 7 days, and samples were harvested for subsequent analysis.

4.3.2 Metabolite extraction

An extraction buffer containing chloroform:methanol:water (1:3:1, v/v) was prepared. Cells were washed once with cold PBS for 5 minutes, liquid was aspirated, and 500 µL of ice-cold extraction solvent was added to each well of the 24 well plate, on ice. The plate was wrapped in parafilm, kept on ice, and agitated gently (300 rpm) on a shaker for 1 hour at 4 ˚C. Cells were then scraped, and the lysate was transferred to clean Eppendorf tubes. Samples were subsequently centrifuged at 13,000 g for 5 minutes, the supernatant transferred into clean Eppendorf tubes and stored at -80 ˚C until ready for chromatographic analysis by Glasgow Polyomics. For each condition N=1 biological replicate, and N=4 experimental replicates

were collected, and data was compared to each individual cell line's control group, at the specific time point.

4.3.3 Chromatographic analysis

Sample preparation was carried out with the help of Dr Monica Tsimbouri. Quality control analysis, as well as sample analysis was carried out by Dr Clement Regnault at the Glasgow Polyomics facility.[273] Metabolite quantification was carried out using hydrophilic interaction liquid chromatography (HILIC), on a Dionex UltiMate 3000 RSLC instrument (Thermo Fisher Scientific, Hemel Hempstead, UK) using a ZIC-pHILIC column (150 mm × 4.6 mm, 5 µm column, Merck Sequant). HPLC grade solvents were used, with 20 mM $(NH_4)_2CO_3$ in H_2O, and CH_3CN being used. The column was maintained at 40 °C during analysis. 10 µL of sample were injected, and sample was analysed using the gradient reported in Table 4.1.

Mass spectrometric analysis was carried out on Thermo Orbitrap QExactive (Thermo Fisher Scientific), in polarity switching mode. Analysis was carried out on positive ion electrospray ionisation, and negative mode electro-ionisation.

Time (minutes)	%Acetonitrile	%Water
0	80	20
15	20	80
15	5	95
17	5	95
17	80	20
25	80	20

Table 4.1: Solvent gradient used for chromatographic analysis of metabolites, via HILIC.

Data was initially processed by Dr Clement Regnault using the IDEOM MS Excel interface.[274] Individual IDEOM files were created for each cell line and timepoint.

4.3.4 Biostatistical analysis using MetaboAnalyst software

MetaboAnalyst was used to carry out statistical analyses, generate plots, identify metabolites of interest and to study overall trends on what metabolic groups each treatment employs.[275] Peak intensities were assessed relative to the control group, and data was $\log_{10}$-transformed in MetaboAnalyst, before generating plots. Principle component analysis (PCA) plots were used as statistical tools, with the x-axis corresponding to PC1, and y-axis belonging to PC2. Heatmaps were generated from normalised data using the ward clustering algorithm, with a Euclidean distance measure. ANOVA, and ANOVA with Tukey's adjustment were used as statistical tools.

4.3.5 Biostatistical analysis via ingenuity pathway analysis software

SAOS-2 and MG-63 metabolic pathways were analysed for the day 7 timepoint, by comparing fold-expression of a treatment group versus the control was assessed using IPA software.[276] Each treatment was individually compared to the control, with observation 1 referring to NK treatment, and observation 2 referring to OGM treatment.

4.4 Results and discussion

Nanokicking has previously been described to drive selective osteogenic differentiation of MSCs, while as discussed in chapter 3, nanovibrating cells at 30 nm for 7 days appeared to drive osteogenic differentiation in OS cells. An osteogenic medium (OGM), containing β-glycerophosphate, ascorbic acid, and dexamethasone was used as means of chemical stimulation, and was found to drive differentiation. Chemical stimulation drove differentiation in poorly differentiated MG-63 cells, while for the more osteoblastic SAOS-2 cells, treatment appeared to induce differentiation, in some biological replicates, but reduce metabolic activity. Upon confirming that differentiation was occurring through a variety of assays, metabolomic analysis was carried out, to identify small molecules of interest and relevant pathways. Analysis of different classes of metabolites, such as amino acids, carbohydrates and lipids was first carried out after 3, and 7 days of treatment, to assess changes in the metabolome.

4.4.1 Metabolic profile of MG-63 cells

While both mechanical and chemical stimulation drove differentiation in MG-63 cells, they did so at different rates. As previously mentioned, in chapter 3, nanokicking drove upregulation of earlier markers, such as RUNX2, while osteogenic medium treatment drove upregulation of earlier markers, such as RUNX2, and later markers such as OPN. Those slight differences were even more evident from the metabolomic data. Metabolic changes were assessed after 3 and 7 days, by comparing the untreated control for that timepoint, with the nanokicked or the osteogenic medium treated sample. Statistical analysis revealed that one of the technical replicates of MG-63 cells nanokicked for 7 days was a significant outlier, and it was thus excluded from further analyses. MetaboAnalyst was first used to study cell behaviour for putative metabolites, including amino acids, carbohydrates and lipids. IPA software was then used to identify pathways involved in osteogenesis, and study how metabolic alterations can alter downstream pathways.

Carbohydrates

One way ANOVA analysis revealed that 50/68 analysed carbohydrates were significantly altered in MG-63 cells after 3 days of treatment, while 40/70 of them were significantly altered after 7 days of differentiation. PCA plots revealed distinct groupings at the day 3 timepoint, showing significant log-increase along PC2 axis in the NK group compared to the control (Figure 4.3, (A)). More subtle changes were observed after 7 days, according to PCA (A, ii). Heatmap analyses confirmed those findings, showing significant accumulation of carbohydrates after 3 days, followed by subtler changes after 7 days (B), with individual metabolites being depleted or upregulated. Positive fold-change across PC1 was observed at both timepoints for the OGM group, while changes across PC2 were further observed at the day 3 timepoint (A). Significant accumulation of carbohydrates was observed at both timepoints, with smaller clusters of metabolites being depleted. Accumulation of carbohydrates was observed for both treatments after 3 days, though heatmap observations highlighted that cells employ different clusters of metabolites during differentiation. Different carbohydrate expression patterns were observed for the NK and the OGM groups, suggesting differing metabolic pathways, and distinctive cell phenotypes, between the control, the mechanically induced group, and the chemically induced group. Changes in TCA, and glycolysis metabolism were further studied, to obtain more information on the bioenergetics of OS differentiation.

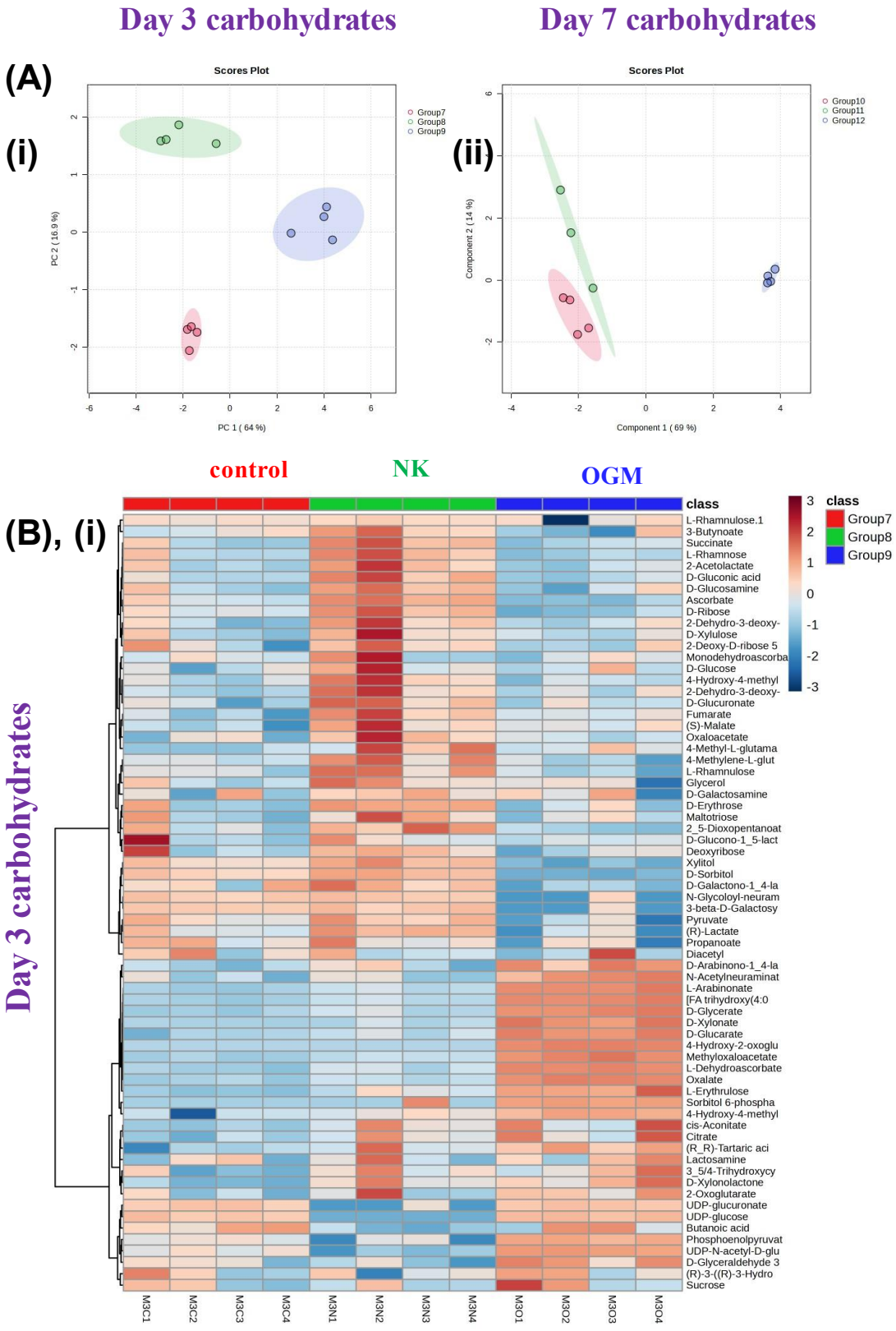
Day 3 carbohydrates
Day 7 carbohydrates
(A)
(i)
(ii)
Scores Plot
Group7
Group8
Group9
PC 1 (64 %)
PC 2 (16.9 %)
Group10
Group11
Group12
Component 1 (69 %)
Component 2 (14 %)
control
NK
OGM
(B), (i)
Day 3 carbohydrates
class
L-Rhamnulose.1
3-Butynoate
Succinate
L-Rhamnose
2-Acetolactate
D-Gluconic acid
D-Glucosamine
Ascorbate
D-Ribose
2-Dehydro-3-deoxy-
D-Xylulose
2-Deoxy-D-ribose 5
Monodehydroascorba
D-Glucose
4-Hydroxy-4-methyl
2-Dehydro-3-deoxy-
D-Glucuronate
Fumarate
(S)-Malate
Oxaloacetate
4-Methyl-L-glutama
4-Methylene-L-glut
L-Rhamnulose
Glycerol
D-Galactosamine
D-Erythrose
Maltotriose
2_5-Dioxopentanoat
D-Glucono-1_5-lact
Deoxyribose
Xylitol
D-Sorbitol
D-Galactono-1_4-la
N-Glycoloyl-neuram
3-beta-D-Galactosy
Pyruvate
(R)-Lactate
Propanoate
Diacetyl
D-Arabinono-1_4-la
N-Acetylneuraminat
L-Arabinonate
[FA trihydroxy(4:0
D-Glycerate
D-Xylonate
D-Glucarate
4-Hydroxy-2-oxoglu
Methyloxaloacetate
L-Dehydroascorbate
Oxalate
L-Erythrulose
Sorbitol 6-phospha
4-Hydroxy-4-methyl
cis-Aconitate
Citrate
(R_R)-Tartaric aci
Lactosamine
3_5/4-Trihydroxycy
D-Xylonolactone
2-Oxoglutarate
UDP-glucuronate
UDP-glucose
Butanoic acid
Phosphoenolpyruvat
UDP-N-acetyl-D-glu
D-Glyceraldehyde 3
(R)-3-((R)-3-Hydro
Sucrose
M3C1
M3C2
M3C3
M3C4
M3N1
M3N2
M3N3
M3N4
M3O1
M3O2
M3O3
M3O4
class
Group7
Group8
Group9

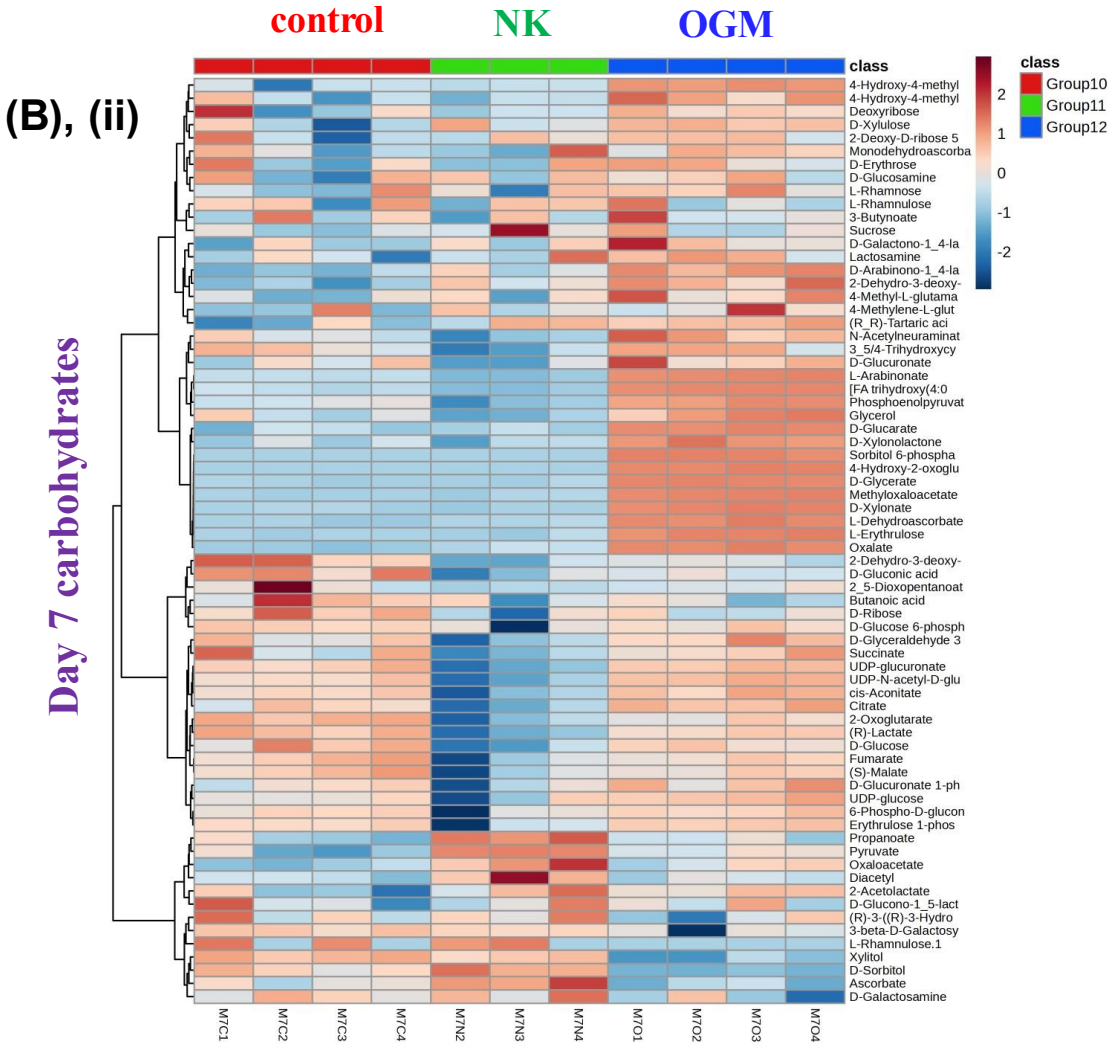

Figure 4.3: Carbohydrate profile of MG-63 cells treated with NK or OGM for 3 or 7 days: (A) PCA plots were generated after (i) 3 and (ii) 7 days using MetaboAnalyst, with groupings shown across PC1 and PC2. Ellipses represent boarders of different groups, including the untreated MG-63 control (red), the NK group (green), and the OGM group (blue). (B) Heatmaps of top 70 most changed carbohydrates (calculated by t-test p-value) were generated using MetaboAnalyst after 3 (i), and 7 days (ii). Colour represents a metabolite's z-score. Individual metabolites shown in darker red were most upregulated, while individual metabolites in dark blue were most downregulated. N=1 biological replicate, N=3-4 experimental replicates.

Due to the role of carbohydrates on biosynthesis and bioenergetics in cancer growth and differentiation, fold-expression of TCA and glycolytic metabolites was assessed against individual timepoint controls, using heatmaps (Figure 4.4). Increased expression of TCA metabolites, followed by depletion after 7 days was observed in the NK group (Figure 4.4), highlighting the active role of this pathway in mechanically induced osteogenesis. *Cis*-aconitate and citrate showed the largest fold-increase in the NK group after 3 days. This was followed by significant fold-decrease in the analysed TCA and glycolytic metabolites after 7 days, except for an accumulation of oxaloacetate. Significant citrate accumulation was observed for both NK and OGM treated cells after 3 days, which was followed by depletion

in NK and accumulation in the OGM group, to a lesser degree. Citrate is a key TCA metabolite, that is involved in osteogenesis of MSCs.[277] Glucose and lactate were accumulated after 3 days in the NK, which was followed by depletion of glucose, pyruvate, and lactate after 7 days, suggesting a role of glycolysis in mechanical stimulation. After observing that carbohydrates were involved in the differentiation of MG-63, amino acids were analysed.

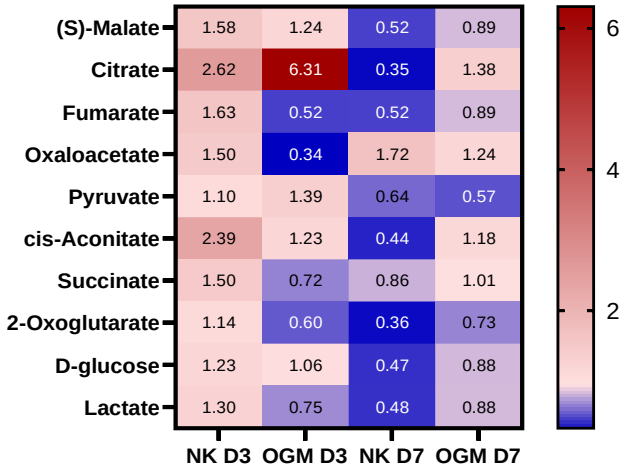

Figure 4.4: TCA metabolites altered during differentiation of MG-63: MG-63 cells were treated with NK or OGM for 3 or 7 days, and fold-presence of TCA metabolite levels was assessed as a ratio against individual untreated cell control. N=1 biological replicate, N=4 experimental replicates.

Amino acids

Amino acid metabolism was found to be altered in MG-63 cells during differentiation. One way ANOVA analysis revealed that 85/171 of the analysed amino acids were significantly altered after 3 days of treatment and 79/171 of the amino acids were significantly altered after 7 days of treatment. PCA plots revealed heterogeneity in amino acid distribution, for the different NK D3 replicates, (Figure 4.5, (A, i)) thus providing limited statistical insights. On the other hand, heatmap analysis showed significant changes in amino acids after 3 days of nanokicking MG-63 cells (B, i). One cluster of metabolites was significantly depleted, and a smaller cluster was upregulated after 7 days of nanokicking, according to the heatmap (B, ii), while PCA analysis showed more significant changes from the control, across PC2 (A, ii). More uniform distribution was observed across both time points, for the OGM group, while significant changes across PC2 were observed (A). Small clusters of metabolites showed variation from the control group, but overall, the metabolic profiles of OGM treated cells and the control group were more similar after 7 days, compared to the NK group (B,

ii). Changes in proline metabolism, which is an amino acid involved in osteogenesis,[238] were observed after 7 days of treatment (C). Insignificant accumulation of proline was observed 3 days of OGM treatment, which was followed by significant depletion after 7 days, while more significant fold-decrease in proline levels was observed after 7 days of nanokicking. Changes in glutamine metabolism were observed, as evident by small accumulation of glutamine (C) after 7 days for both treatments, while glutamate levels were depleted after 7 days of NK and accumulated after 3 days of OGM induction.

Day 3 amino acids

Day 7 amino acids

(A)

(i)

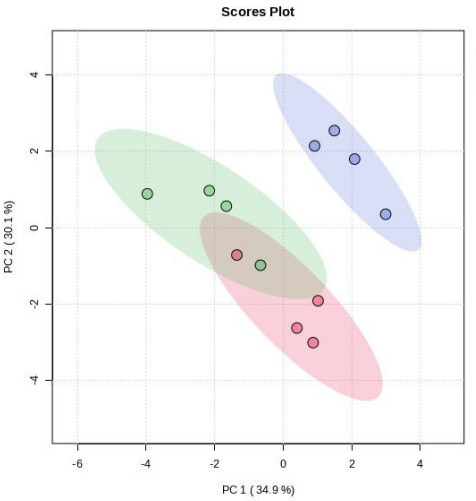

(ii)

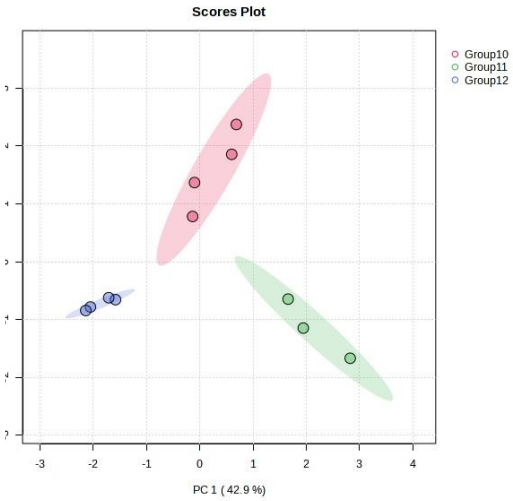

(B)

(i)

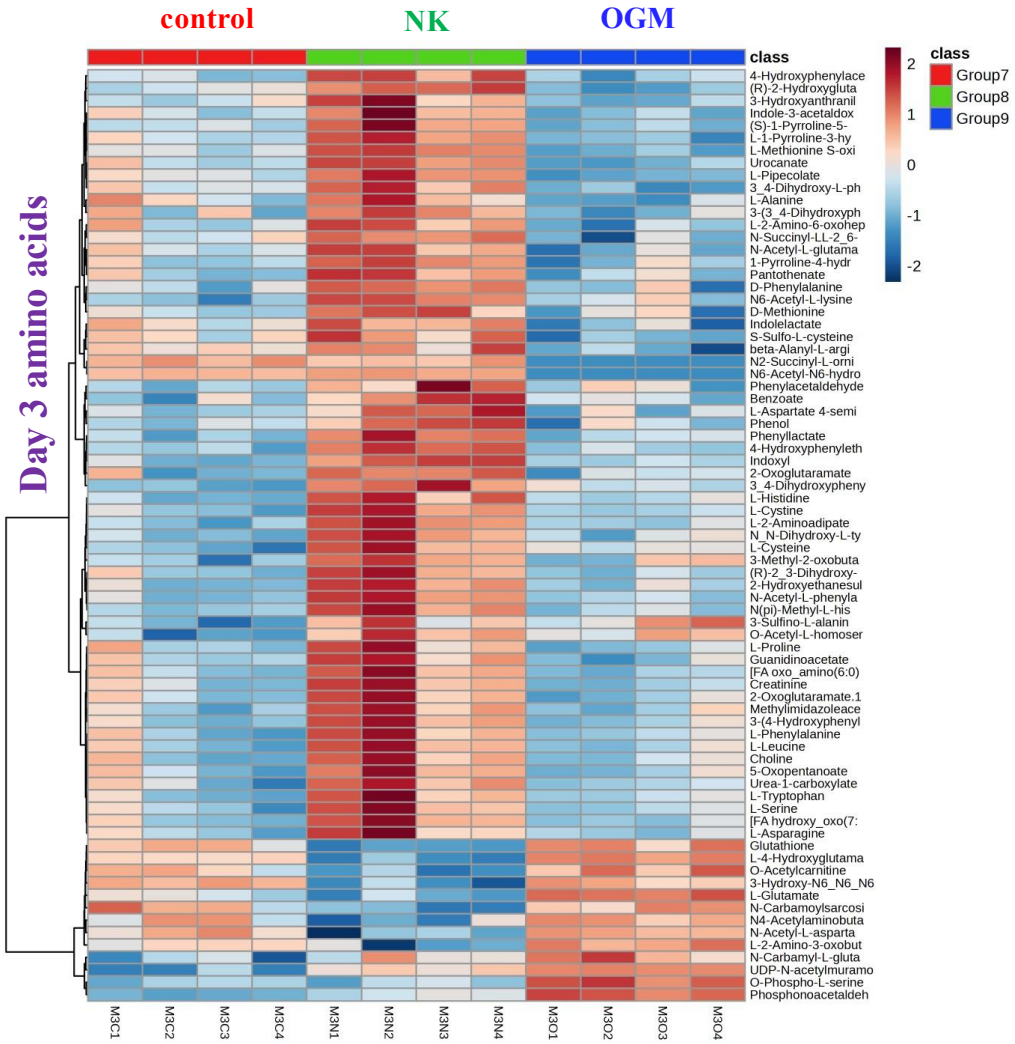

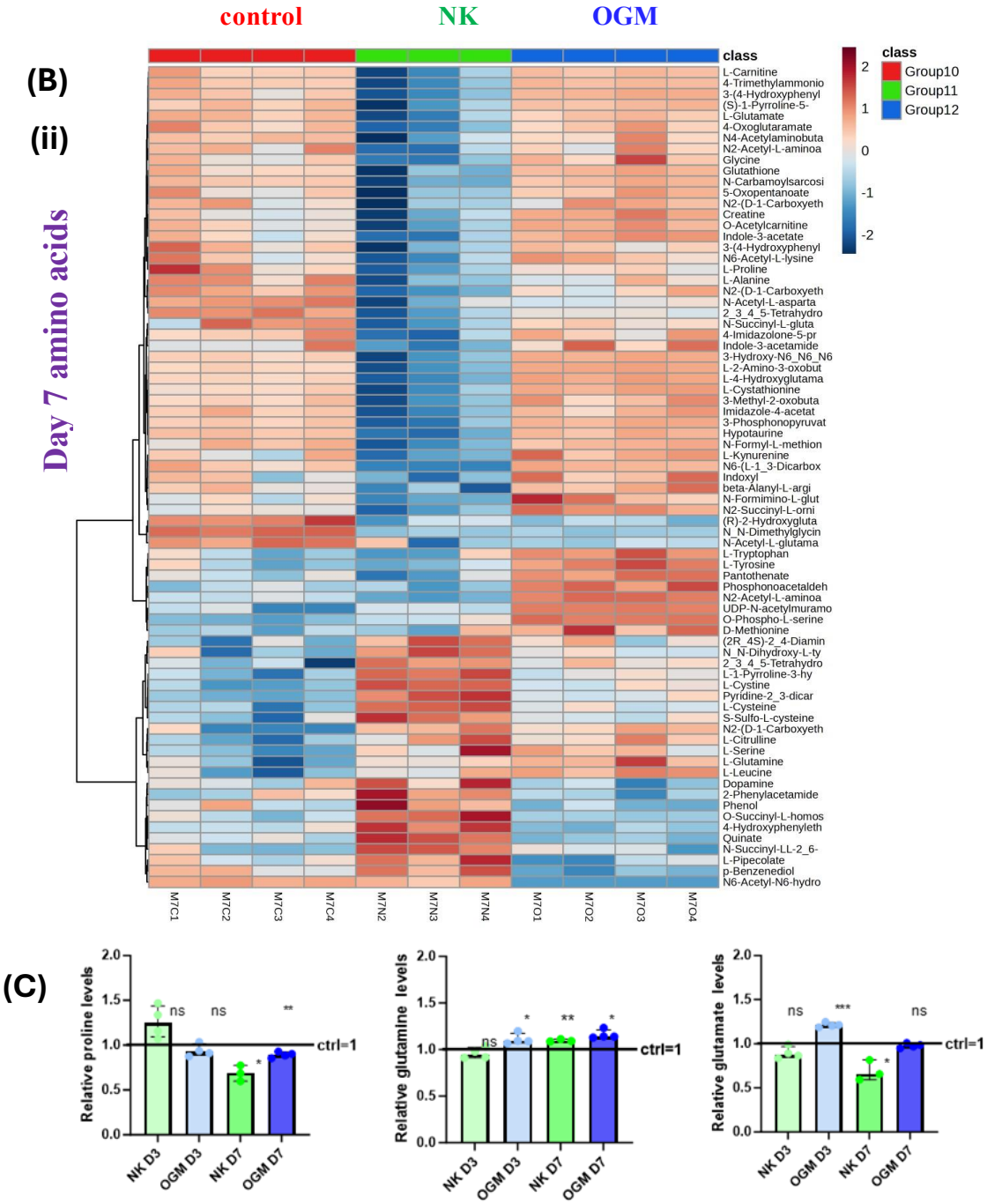

*Figure 4.5: Amino acid profile of MG-63 cells treated with NK or OGM for 3 or 7 days: (A) PCA plots were generated after (i) 3 and (ii) 7 days using MetaboAnalyst, with groupings across PC1 and PC2. Ellipses represent boarders of different groups, including the untreated MG-63 control (red), the NK group (green), and the OGM group (blue). (B) Heatmaps of top 70 most changed amino acids (calculated by t-test p-value) were generated using MetaboAnalyst after 3 (i), and 7 days (ii). Colour represents a metabolite's z-score. Individual metabolites shown in darker red were most upregulated, while individual metabolites in dark blue were most downregulated. (C) Fold-presence of proline, glutamine, and glutamate was assessed against individual untreated MG-63 control for the respective timepoint. Stats by adjusted Welch t-test. Each group's metabolite fold-expression was assessed against ctrl=1. (blank=ns=p>0.05, *= p<0.05, **=p<0.01. ***=p<0.001). N=1 biological replicate, N=3-4 experimental replicates.*

Lipids

One-way ANOVA revealed that 57/105 analysed lipids were significantly altered after 3 days of treatment, while 39/92 analysed lipids were significantly changed after 7 days of differentiation in MG-63 cells. PCA also showed alterations in lipid expression in cells that were nanokicked after 3 days, as evidence by log-decrease along PC1 and PC2 against the control (Figure 4.6, (A,i)) Heatmaps also revealed that NK treated cells employed lipids to differentiate, with one cluster of metabolites being significantly accumulated after 3 days, and a second cluster being significantly depleted (B, i). Similar observations on lipid expression patterns were observed in NK cells after 7 days too, according to heatmap analysis (B, ii), while a small log-increase along PC1 and no perceivable changes along PC2 (A, ii). OGM treatment also appeared to show more significant changes along PC1 and PC2 after 3 days, compared to 7 days of induction (A). Heatmaps of the OGM group showed a smaller increase in lipids after 3 days, followed by subtler changes after 7 days, showing more changes in individual metabolites (B). Overall, closer similarities were observed in the metabolite profile of OGM and control group, while in the NK group opposite observations were made on accumulated or consumed metabolites. Both the nanokicked and the osteogenic medium treated group showed significant changes after 7 days. Significant changes were observed in fatty acid, phospholipid and steroid metabolism under mechanical and chemical stimulation.

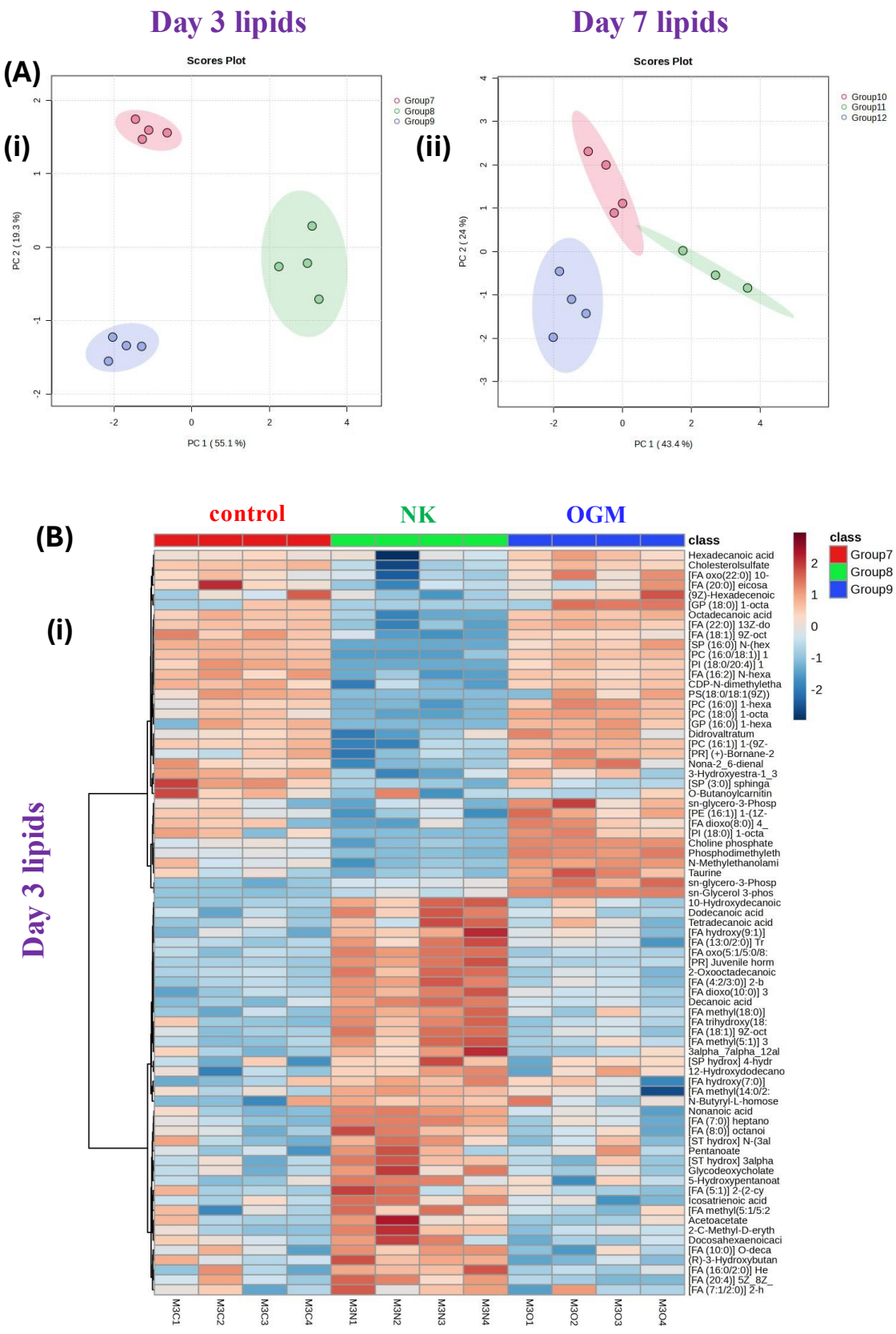
Day 3 lipids
Day 7 lipids
(A)
(i)
(ii)
Scores Plot
Group7
Group8
Group9
Group10
Group11
Group12
PC 1 (55.1 %)
PC 2 (19.3 %)
PC 1 (43.4 %)
PC 2 (24 %)
(B)
control
NK
OGM
Day 3 lipids
class
Group7
Group8
Group9
M3C1
M3C2
M3C3
M3C4
M3N1
M3N2
M3N3
M3N4
M3O1
M3O2
M3O3
M3O4

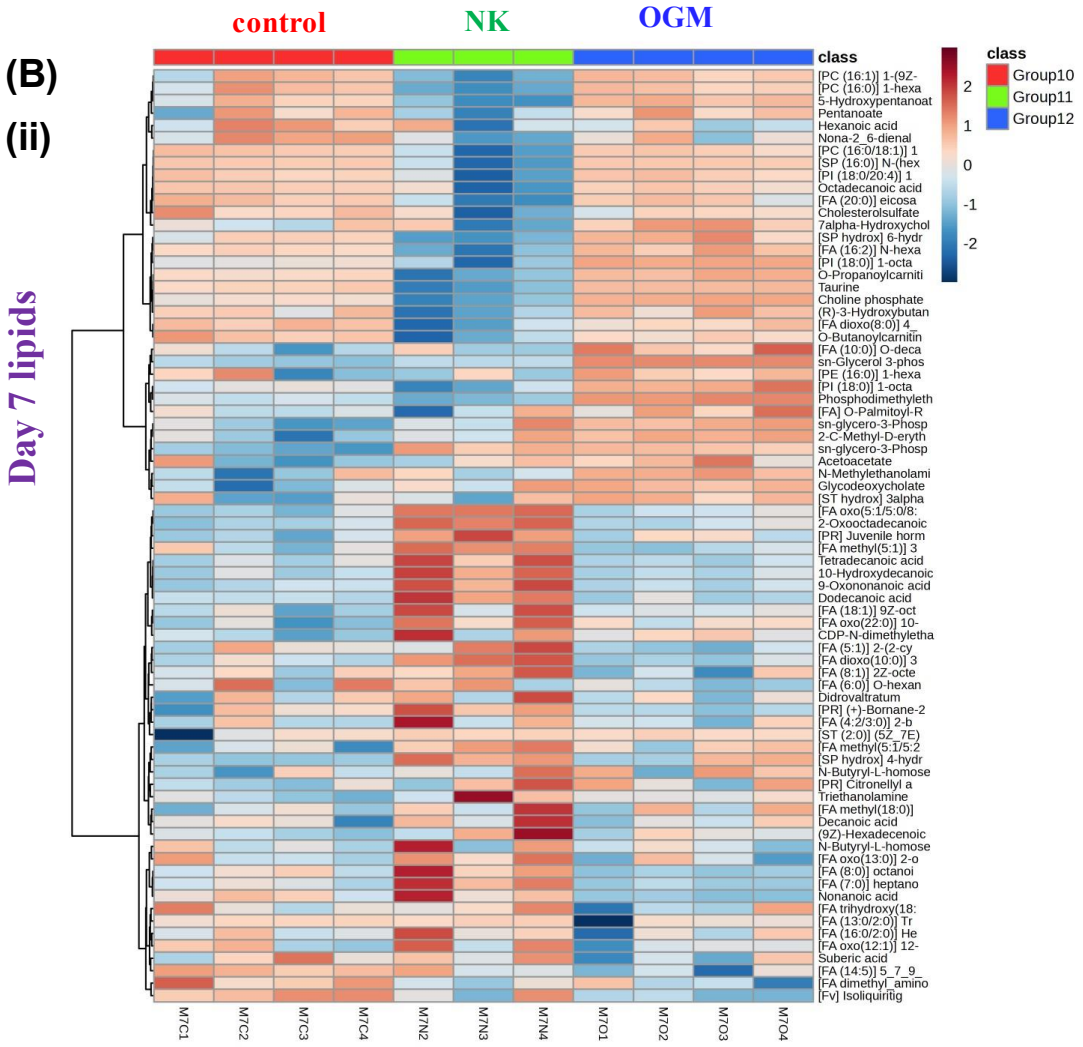

Figure 4.6: Lipid profile of MG-63 cells treated with NK or OGM for 3 or 7 days: (A) PCA plots were generated after (i) 3 and (ii) 7 days using MetaboAnalyst, with groupings shown across PC1 and PC2. Ellipses represent boarders of different groups, including the untreated MG-63 control (red), the NK group (green), and the OGM group (blue). (B) Heatmaps of top 70 most changed lipids (calculated by t-test p-value) were generated using MetaboAnalyst after 3 (i), and 7 days (ii). Colour represents a metabolite's z-score. Individual metabolites shown in darker red were most upregulated, while individual metabolites in dark blue were most downregulated. N=1 biological replicate, N=3-4 experimental replicates.

Signalling pathways

The ingenuity pathway analysis (IPA) software was used to predict how changes in the metabolome may cause downstream effects on signalling pathways, after 7 days of treatment. Both mechanical and chemical stimulation, were predicted to inhibit ERK ½, which is a key signalling pathway (Figure 4. 7). ERK plays a pleiotropic role in cancer, regulating both increased proliferation and tumourigenesis,[278] as well as differentiation, and apoptosis.[279]

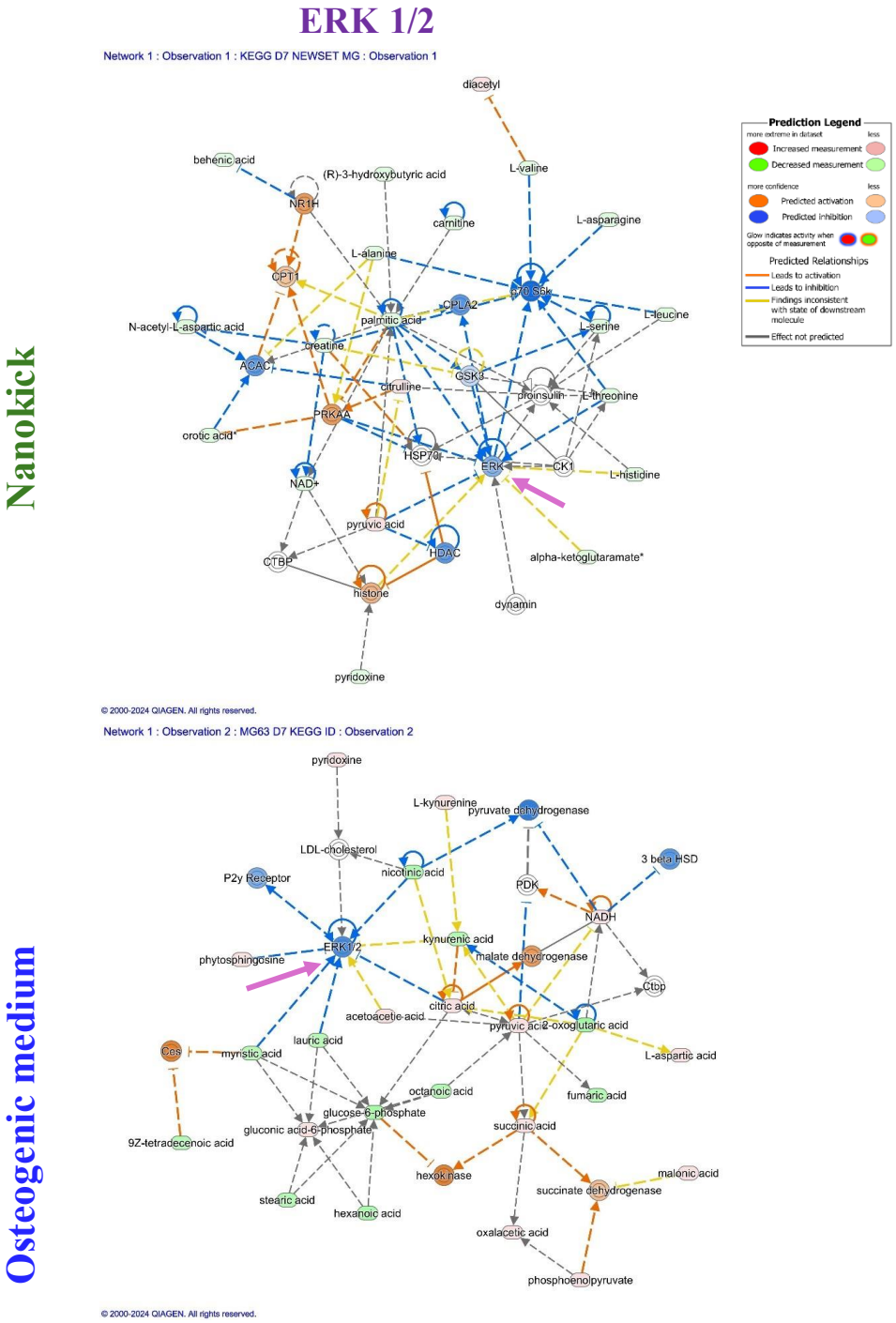

Figure 4. 7: Predicted changes in ERK ½ MG-63 activity in NK and OGM treated SAOS-2 cells after 7 days: Plots were created using IPA software. Blue nodules represent predicted pathway inhibition, and orange represents predicted pathway activation. Green nodules represent depleted metabolites, and red nodules represent accumulated metabolites. N=1 biological replicate, N=4 experimental replicates.

JNK is a MAPK that regulates osteogenic differentiation, proliferation, and apoptosis.[280] JNK was predicted to be activated in nanokicked MG-63 cells (Figure 4. 8), suggesting that this MAPK plays an active role in mechanically induced osteogenesis of OS cells. On the other hand, JNK was predicted not to be involved according to the IPA software in OGM

treated MG-63 cells. This further highlights that mechanically and chemically stimulated OS cells may employ different signalling pathways to differentiate.

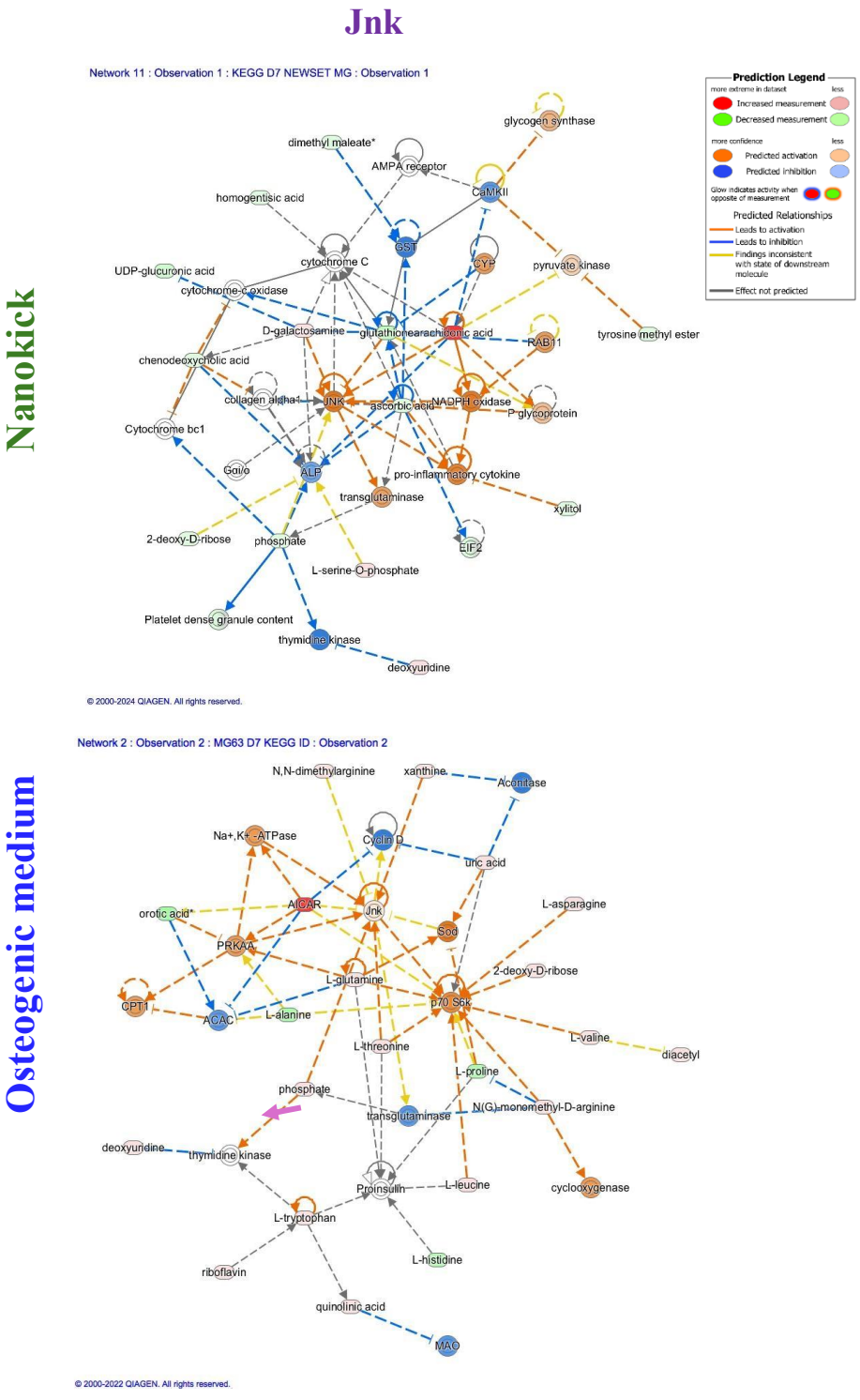

Figure 4. 8: Predicted changes in JNK MG-63 activity in NK and OGM treated SAOS-2 cells after 7 days: Plots were created using IPA software. Blue nodules represent predicted pathway inhibition, and orange represents predicted pathway activation. Green nodules represent depleted metabolites, and red nodules represent accumulated metabolites. N=1 biological replicate, N=4 experimental replicates.

Akt was predicted to be inhibited in the nanokicked group after 7 days (Figure 4. 9), drawing a link to observations of decreased proliferation in chapter 3. Given the activation of JNK, and predicted inhibition of ERK ½, and Akt, it would be interesting to test agonists and inhibitors of those putative signalling pathways, and study their role in differentiation, and proliferation in OS. More significant changes in amino acid metabolism were observed for NK cells, which may explain why stronger predictions were made for signalling pathways. As the control and the OGM group bore more similarities in their metabolic profiles, more limited predictions on pathway activation were made using the IPA algorithm.

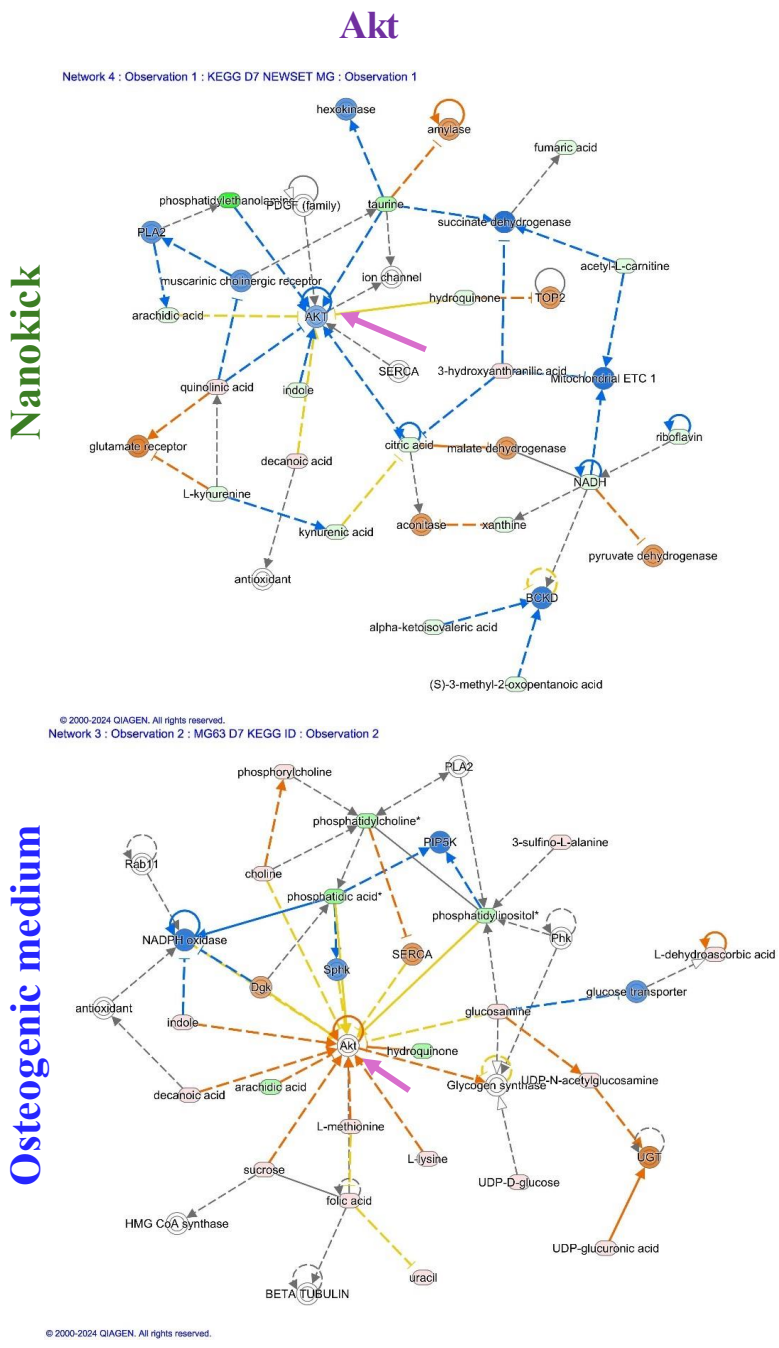

Figure 4. 9: Predicted changes in Akt MG-63 activity in NK and OGM treated SAOS-2 cells after 7 days: Plots were created using IPA software. Blue nodules represent predicted pathway inhibition, and orange represents predicted pathway activation. Green nodules represent depleted metabolites, and red nodules represent accumulated metabolites. N=1 biological replicate, N=4 experimental replicates.

4.4.2 SAOS-2 effect of mechanical vs chemical stimulation on metabolism

Carbohydrates

One way ANOVA revealed that 39/65 analysed carbohydrates were significantly altered after 3 days of treatment, while 50/66 Carbohydrates were statistically changed after 7 days of treatment. PCA revealed close similarities in carbohydrate metabolism between the control and the nanokicked group after 3 days (Figure 4.10, (A,i)), which was confirmed by heatmap analysis (B, i), which revealed subtle changes in carbohydrate metabolism. At the day 7 timepoint distinctive groupings, and significant changes from the control and the OGM group were observed via PCA (A, ii). Heatmap analysis revealed depletion of carbohydrates after 7 days of NK (B, ii). 3 days of OGM treatment induced significant changes in carbohydrate metabolism, as evident by the positive fold-increase along PC1 (A, i), while heatmap analysis revealed significant carbohydrate accumulation in a cluster of metabolites (B, i). The day 7 timepoint showed more distinct groupings, and significant changes between the OGM group, the control, and the NK group, according to PCA (A, ii). Heatmap analysis revealed significant depletion of carbohydrates, while a cluster of metabolites revealed accumulation (B, ii). Overall, more significant changes in carbohydrate usage, compared to the control was observed in chemically stimulated cells, while mechanically stimulated cells showed subtler changes in carbohydrate metabolism.

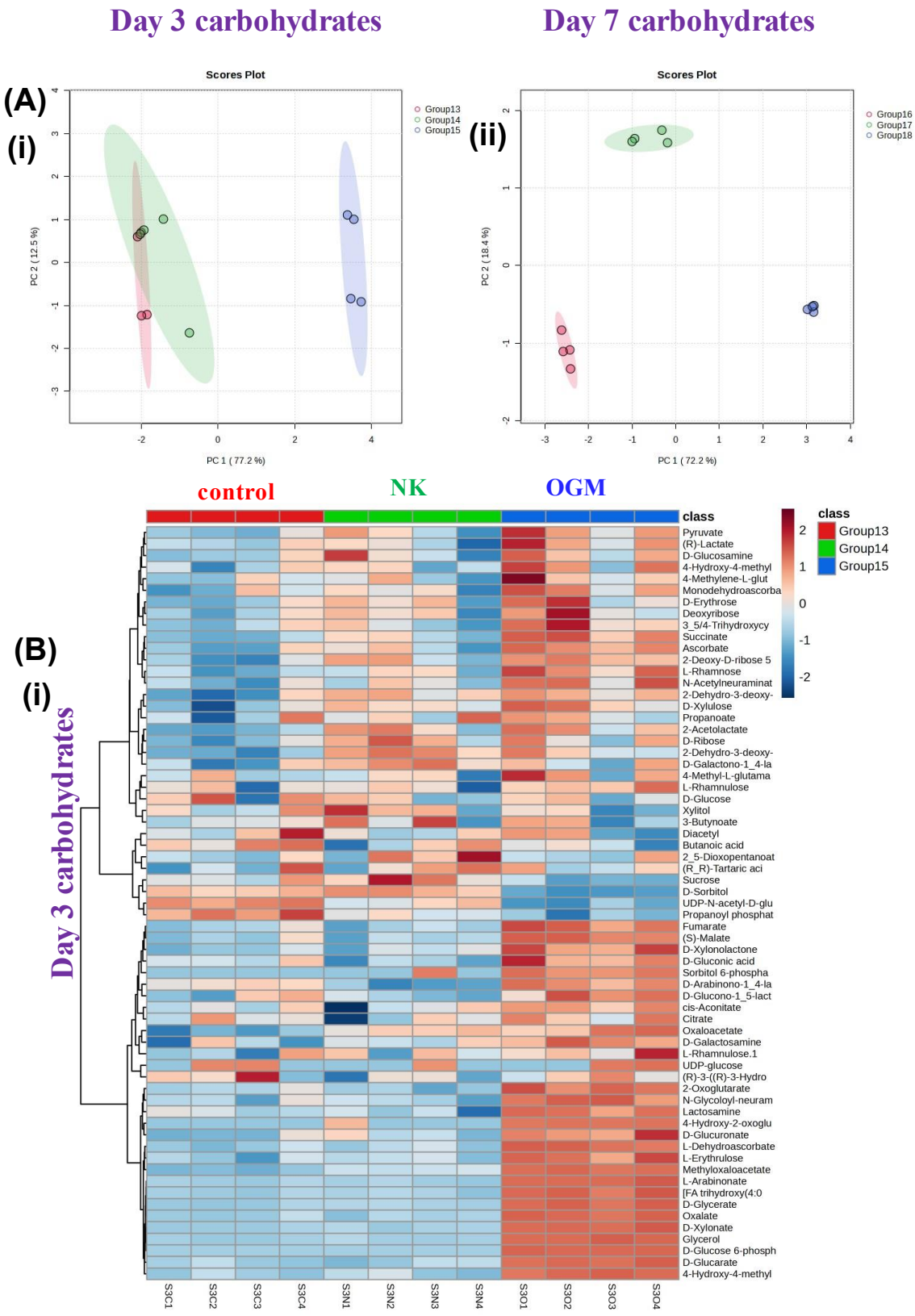
Day 3 carbohydrates
Day 7 carbohydrates
(A)
(i)
Scores Plot
Group13
Group14
Group15
PC 2 (12.5 %)
PC 1 (77.2 %)
(ii)
Scores Plot
Group16
Group17
Group18
PC 2 (18.4 %)
PC 1 (72.2 %)
(B)
(i)
Day 3 carbohydrates
control
NK
OGM
class
Group13
Group14
Group15
Pyruvate
(R)-Lactate
D-Glucosamine
4-Hydroxy-4-methyl
4-Methylene-L-glut
Monodehydroascorba
D-Erythrose
Deoxyribose
3_5/4-Trihydroxycy
Succinate
Ascorbate
2-Deoxy-D-ribose 5
L-Rhamnose
N-Acetylneuraminat
2-Dehydro-3-deoxy-
D-Xylulose
Propanoate
2-Acetolactate
D-Ribose
2-Dehydro-3-deoxy-
D-Galactono-1_4-la
4-Methyl-L-glutama
L-Rhamnulose
D-Glucose
Xylitol
3-Butynoate
Diacetyl
Butanoic acid
2_5-Dioxopentanoat
(R_R)-Tartaric aci
Sucrose
D-Sorbitol
UDP-N-acetyl-D-glu
Propanoyl phosphat
Fumarate
(S)-Malate
D-Xylonolactone
D-Gluconic acid
Sorbitol 6-phospha
D-Arabinono-1_4-la
D-Glucono-1_5-lact
cis-Aconitate
Citrate
Oxaloacetate
D-Galactosamine
L-Rhamnulose.1
UDP-glucose
(R)-3-((R)-3-Hydro
2-Oxoglutarate
N-Glycoloyl-neuram
Lactosamine
4-Hydroxy-2-oxoglu
D-Glucuronate
L-Dehydroascorbate
L-Erythrulose
Methyloxaloacetate
L-Arabinonate
[FA trihydroxy(4:0
D-Glycerate
Oxalate
D-Xylonate
Glycerol
D-Glucose 6-phosph
D-Glucarate
4-Hydroxy-4-methyl
S3C1
S3C2
S3C3
S3C4
S3N1
S3N2
S3N3
S3N4
S3O1
S3O2
S3O3
S3O4

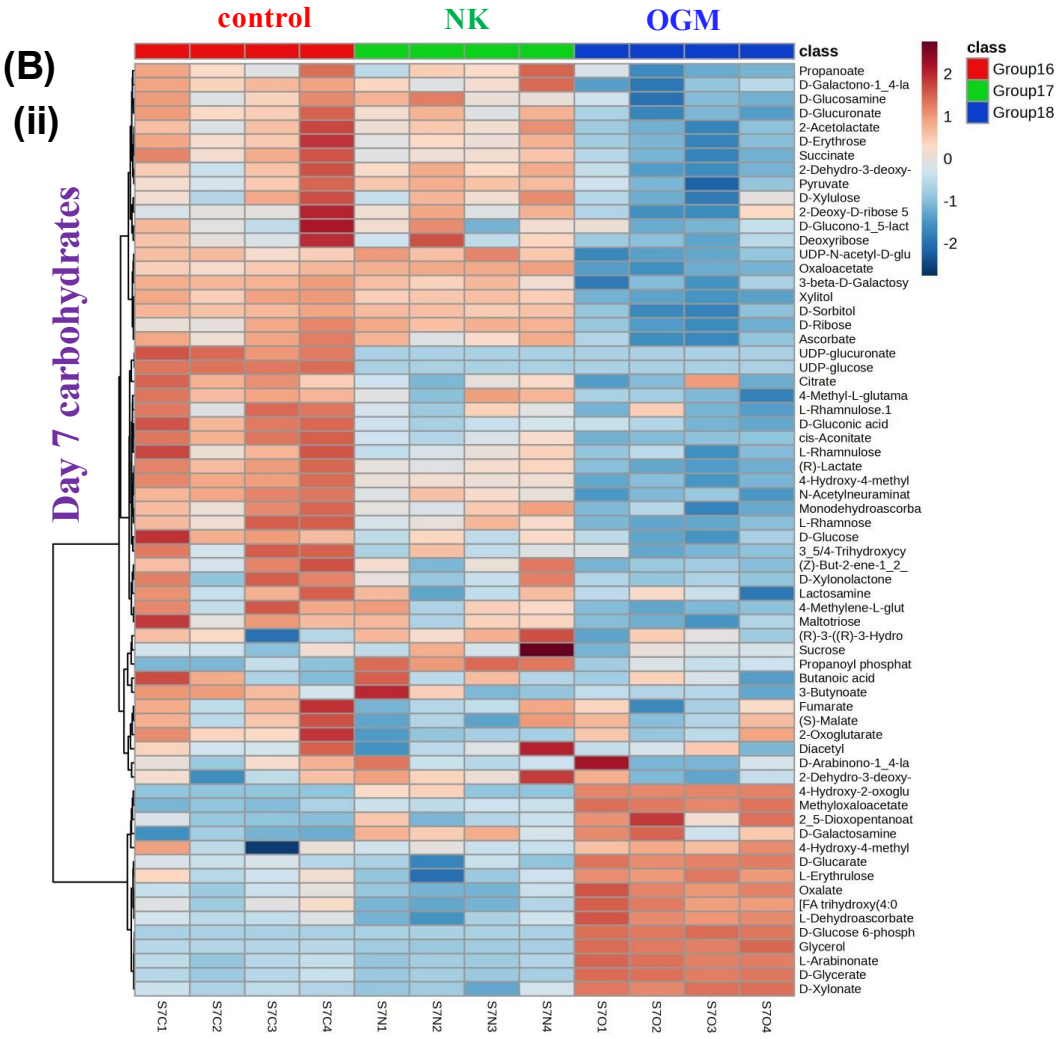

Figure 4.10: Carbohydrate profile of SAOS-2 cells treated with NK or OGM for 3 or 7 days: (A) PCA plots were generated after (i) 3 and (ii) 7 days using MetaboAnalyst, with groupings shown across PC1 and PC2. Ellipses represent boarders of different groups, including the untreated SAOS-2 control (red), the NK group (green), and the OGM group (blue). (B) Heatmaps of top 70 most changed carbohydrates (calculated by t-test p-value) were generated using MetaboAnalyst after 3 (i), and 7 days (ii). Colour represents a metabolite's z-score. Individual metabolites shown in darker red were most upregulated, while individual metabolites in dark blue were most downregulated. N=1 biological replicate, N=4 experimental replicates.

Glucose and lactate depletion was observed after 7 days, for both treatments (Figure 4.11). while, depletion of pyruvate was also observed after 7 days of OGM treatment, following the small accumulation that was observed after 3 days. After 7 days, lactate levels were decreased under both chemical and mechanical stimulation, with a more significant fold-decrease during OGM treatment. further highlighting that mechanical and chemical stimuli employ different metabolic pathways. Significant accumulation of oxaloacetate was observed across both timepoints in the nanokicked group, while other TCA metabolites were depleted after 7 days. Oxaloacetate on the other hand showed the largest depletion in OGM

treated cells after 7 days, though general impaired carbohydrate metabolism was observed. Malate accumulation was observed in the OGM treated cells after 3 days. Overall significant changes in TCA metabolism were observed, with the OGM group showing more significant fold-decrease in TCA metabolites after 7 days.

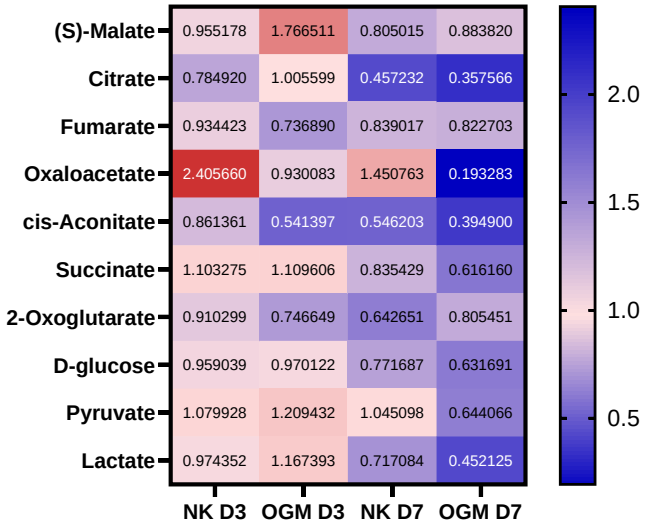

Figure 4.11: TCA metabolites altered during differentiation of SAOS-2: SAOS-2 cells were treated with NK or OGM for 3 or 7 days, and TCA levels were assessed as a ratio against individual untreated cell control. N=1 biological replicate, N=4 experimental replicates.

Amino acids

Amino acid metabolism was significantly altered during SAOS-2 cell differentiation. According to a one-way ANOVA analysis 69/169 of the analysed amino acids were significantly altered after 3 days of treatment, while 136/170 amino acids were significantly changed after 7 days. For the nanokicked group, more subtle changes were observed on the PCA after 3 days, with a small decrease along PC2 axis, with one replicate showing more significant changes (Figure 4.12, (A, i)). After 7 days, changes along PC1, and PC2 demonstrated that nanokicking significantly altered the amino acid composition in SAOS-2 cells (A, ii). Heatmap analysis revealed subtler changes in metabolite composition after 3 days of treatment, with a small cluster of metabolites showing upregulation in the heatmap (B, i). This was followed by a trend in depletion of amino acids, compared to the control after 7 days (B, ii). OGM treated cells showed significant changes after 3, and 7 days of stimulation, with PCA revealing a more significant fold-increase along the PC1 after 7 days, compared to the day 3 timepoint (A). Heatmaps revealed upregulation of a significant cluster of metabolites, which was followed by significant depletion of amino acids (B). So as was

observed for MG-63 cells, there was a difference in metabolic profiles of SAOS-2 cells treated with OGM compared to NK cells. Specific amino acids of interest included proline, glutamine and glutamate (C). Small accumulation in proline was observed for the OGM D3 group, which is linked to bone formation,[238] while glutamine was also upregulated. After 7 days of treatment both proline, and glutamate were depleted under chemical and mechanical stimulation, indicating that while each treatment displayed their own metabolic profile, there were some common threads. More significant changes in amino acid metabolism were observed in the OGM group compared to the NK group.

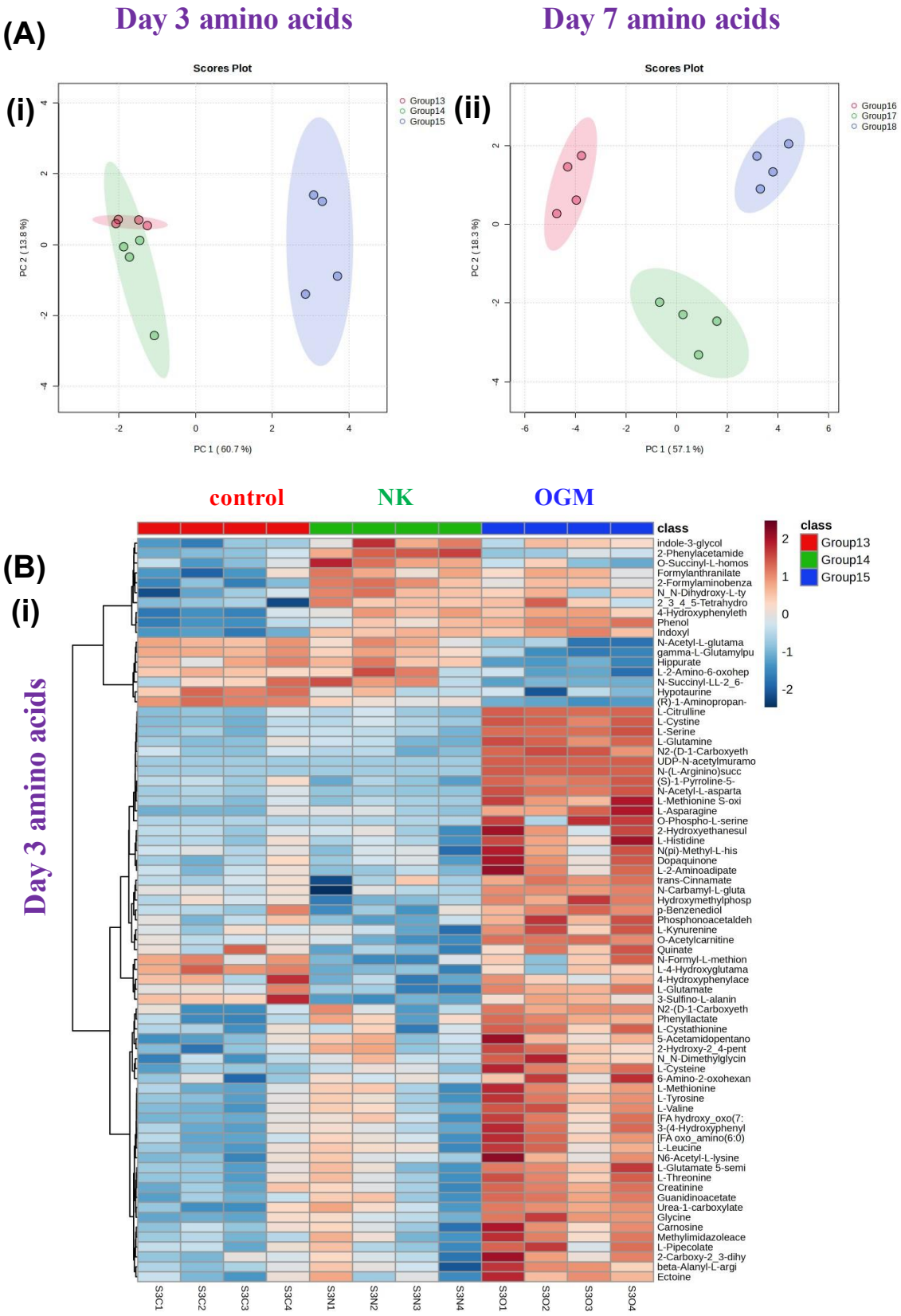
(A)
Day 3 amino acids
Day 7 amino acids
(i)
(ii)
Scores Plot
Group13
Group14
Group15
Group16
Group17
Group18
PC 2 (13.8 %)
PC 1 (60.7 %)
PC 2 (18.3 %)
PC 1 (57.1 %)
control
NK
OGM
(B)
(i)
Day 3 amino acids
class
indole-3-glycol
2-Phenylacetamide
O-Succinyl-L-homos
Formylanthranilate
2-Formylaminobenza
N_N-Dihydroxy-L-ty
2_3_4_5-Tetrahydro
4-Hydroxyphenyleth
Phenol
Indoxyl
N-Acetyl-L-glutama
gamma-L-Glutamylpu
Hippurate
L-2-Amino-6-oxohep
N-Succinyl-LL-2_6-
Hypotaurine
(R)-1-Aminopropan-
L-Citrulline
L-Cystine
L-Serine
L-Glutamine
N2-(D-1-Carboxyeth
UDP-N-acetylmuramo
N-(L-Arginino)succ
(S)-1-Pyrroline-5-
N-Acetyl-L-asparta
L-Methionine S-oxi
L-Asparagine
O-Phospho-L-serine
2-Hydroxyethanesul
L-Histidine
N(pi)-Methyl-L-his
Dopaquinone
L-2-Aminoadipate
trans-Cinnamate
N-Carbamyl-L-gluta
Hydroxymethylphosp
p-Benzenediol
Phosphonoacetaldeh
L-Kynurenine
O-Acetylcarnitine
Quinate
N-Formyl-L-methion
L-4-Hydroxyglutama
4-Hydroxyphenylace
L-Glutamate
3-Sulfino-L-alanin
N2-(D-1-Carboxyeth
Phenyllactate
L-Cystathionine
5-Acetamidopentano
2-Hydroxy-2_4-pent
N_N-Dimethylglycin
L-Cysteine
6-Amino-2-oxohexan
L-Methionine
L-Tyrosine
L-Valine
[FA hydroxy_oxo(7:
3-(4-Hydroxyphenyl
[FA oxo_amino(6:0)
L-Leucine
N6-Acetyl-L-lysine
L-Glutamate 5-semi
L-Threonine
Creatinine
Guanidinoacetate
Urea-1-carboxylate
Glycine
Carnosine
Methylimidazoleace
L-Pipecolate
2-Carboxy-2_3-dihy
beta-Alanyl-L-argi
Ectoine
S3C1
S3C2
S3C3
S3C4
S3N1
S3N2
S3N3
S3N4
S3O1
S3O2
S3O3
S3O4
class
Group13
Group14
Group15

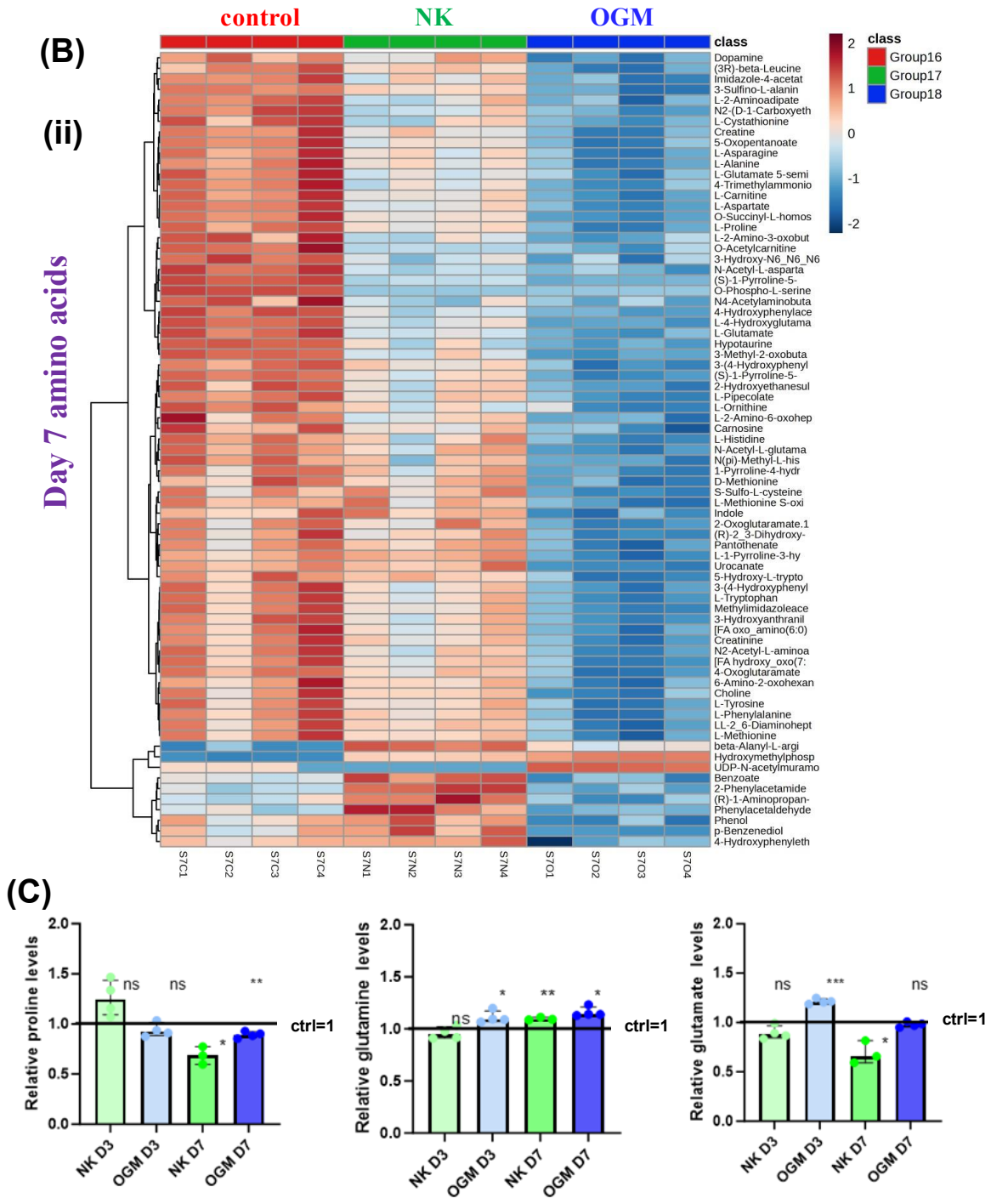

*Figure 4.12: Amino acid profile of SAOS-2 cells treated with NK or OGM for 3 or 7 days: (A) PCA plots were generated after (i) 3 and (ii) 7 days using MetaboAnalyst, with groupings across PC1 and PC2. Ellipses represent boarders of different groups, including the untreated SAOS-2 control (red), the NK group (green), and the OGM group (blue). (B) Heatmaps of top 70 most changed amino acids (calculated by t-test p-value) were generated using MetaboAnalyst after 3 (i), and 7 days (ii). Colour represents a metabolite's z-score. Individual metabolites shown in darker red were most upregulated, while individual metabolites in dark blue were most downregulated. (C) Fold-presence of proline, glutamine, and glutamate was assessed against individual untreated SAOS-2 control for the respective timepoint. Each was statistically compared against ctrl=1, using Mann Whitney u-test. (blank=p>0.05 ns, *= p<0.05). N=1 biological replicate, N=4 experimental replicates.*

Lipids

One way ANOVA analysis revealed that 40/106 analysed lipids were significantly altered after 3 days of treatment, while 73/113 lipids were significantly changed after 7 days of treatment. An outlier for the day 7 control was observed for the lipid metabolism, but the replicate was not an outlier for the different metabolic pathways, so it was not excluded (Figure 4.13). PCA revealed closer groupings between the control and the treatment after 3 days of nanokicking (A, i), while heatmap map analysis showed a cluster of metabolites being accumulated and another depleted, though changes were subtle overall (B, i). More significant changes were observed in the OGM treated group, with PCA revealing significant changes across PC1 at both timepoints (A). Heatmap revealed accumulation of a cluster of metabolites after 3 days, which was followed by significant depletion after 7 days of OGM, with a small cluster of metabolites showing significant accumulation (B). Overall, more significant changes in lipid metabolism were observed after 7 days. Changes in phospholipids and fatty acid metabolism was generally observed.

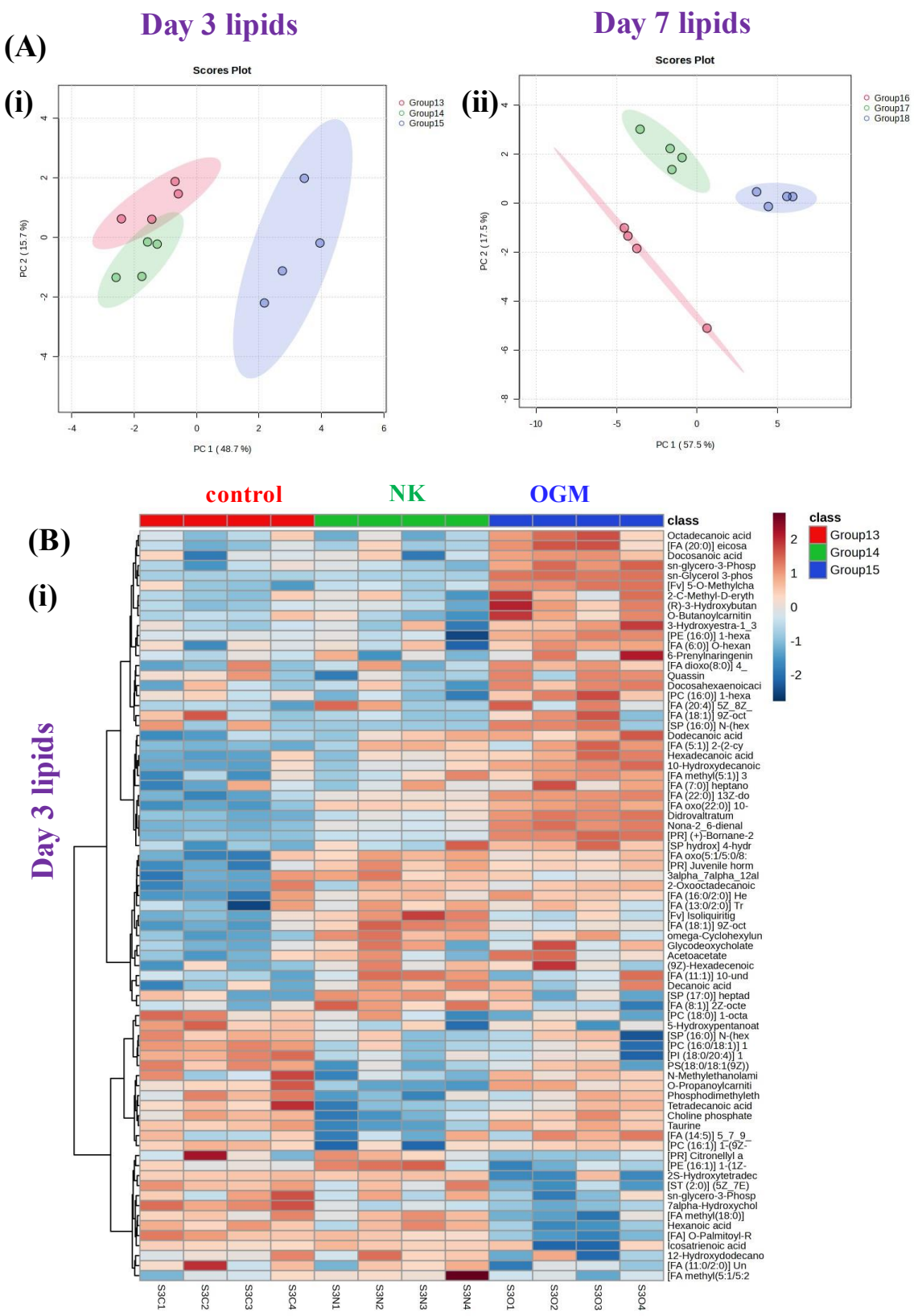
(A)
Day 3 lipids
Day 7 lipids
(i)
(ii)
Scores Plot
Group13
Group14
Group15
Group16
Group17
Group18
PC 2 (15.7 %)
PC 1 (48.7 %)
PC 2 (17.5 %)
PC 1 (57.5 %)
(B)
(i)
control
NK
OGM
Day 3 lipids
class
Octadecanoic acid
[FA (20:0)] eicosa
Docosanoic acid
sn-glycero-3-Phosp
sn-Glycerol 3-phos
[Fv] 5-O-Methylcha
2-C-Methyl-D-eryth
(R)-3-Hydroxybutan
O-Butanoylcarnitin
3-Hydroxyestra-1_3
[PE (16:0)] 1-hexa
[FA (6:0)] O-hexan
6-Prenylnaringenin
[FA dioxo(8:0)] 4_
Quassin
Docosahexaenoicaci
[PC (16:0)] 1-hexa
[FA (20:4)] 5Z_8Z_
[FA (18:1)] 9Z-oct
[SP (16:0)] N-(hex
Dodecanoic acid
[FA (5:1)] 2-(2-cy
Hexadecanoic acid
10-Hydroxydecanoic
[FA methyl(5:1)] 3
[FA (7:0)] heptano
[FA (22:0)] 13Z-do
[FA oxo(22:0)] 10-
Didrovaltratum
Nona-2_6-dienal
[PR] (+)-Bornane-2
[SP hydrox] 4-hydr
[FA oxo(5:1/5:0/8:
[PR] Juvenile horm
3alpha_7alpha_12al
2-Oxooctadecanoic
[FA (16:0/2:0)] He
[FA (13:0/2:0)] Tr
[Fv] Isoliquiritig
[FA (18:1)] 9Z-oct
omega-Cyclohexylun
Glycodeoxycholate
Acetoacetate
(9Z)-Hexadecenoic
[FA (11:1)] 10-und
Decanoic acid
[SP (17:0)] heptad
[FA (8:1)] 2Z-octe
[PC (18:0)] 1-octa
5-Hydroxypentanoat
[SP (16:0)] N-(hex
[PC (16:0/18:1)] 1
[PI (18:0/20:4)] 1
PS(18:0/18:1(9Z))
N-Methylethanolami
O-Propanoylcarniti
Phosphodimethyleth
Tetradecanoic acid
Choline phosphate
Taurine
[FA (14:5)] 5_7_9_
[PC (16:1)] 1-(9Z-
[PR] Citronellyl a
[PE (16:1)] 1-(1Z-
2S-Hydroxytetradec
[ST (2:0)] (5Z_7E)
sn-glycero-3-Phosp
7alpha-Hydroxychol
[FA methyl(18:0)]
Hexanoic acid
[FA] O-Palmitoyl-R
Icosatrienoic acid
12-Hydroxydodecano
[FA (11:0/2:0)] Un
[FA methyl(5:1/5:2
S3C1
S3C2
S3C3
S3C4
S3N1
S3N2
S3N3
S3N4
S3O1
S3O2
S3O3
S3O4
class
Group13
Group14
Group15

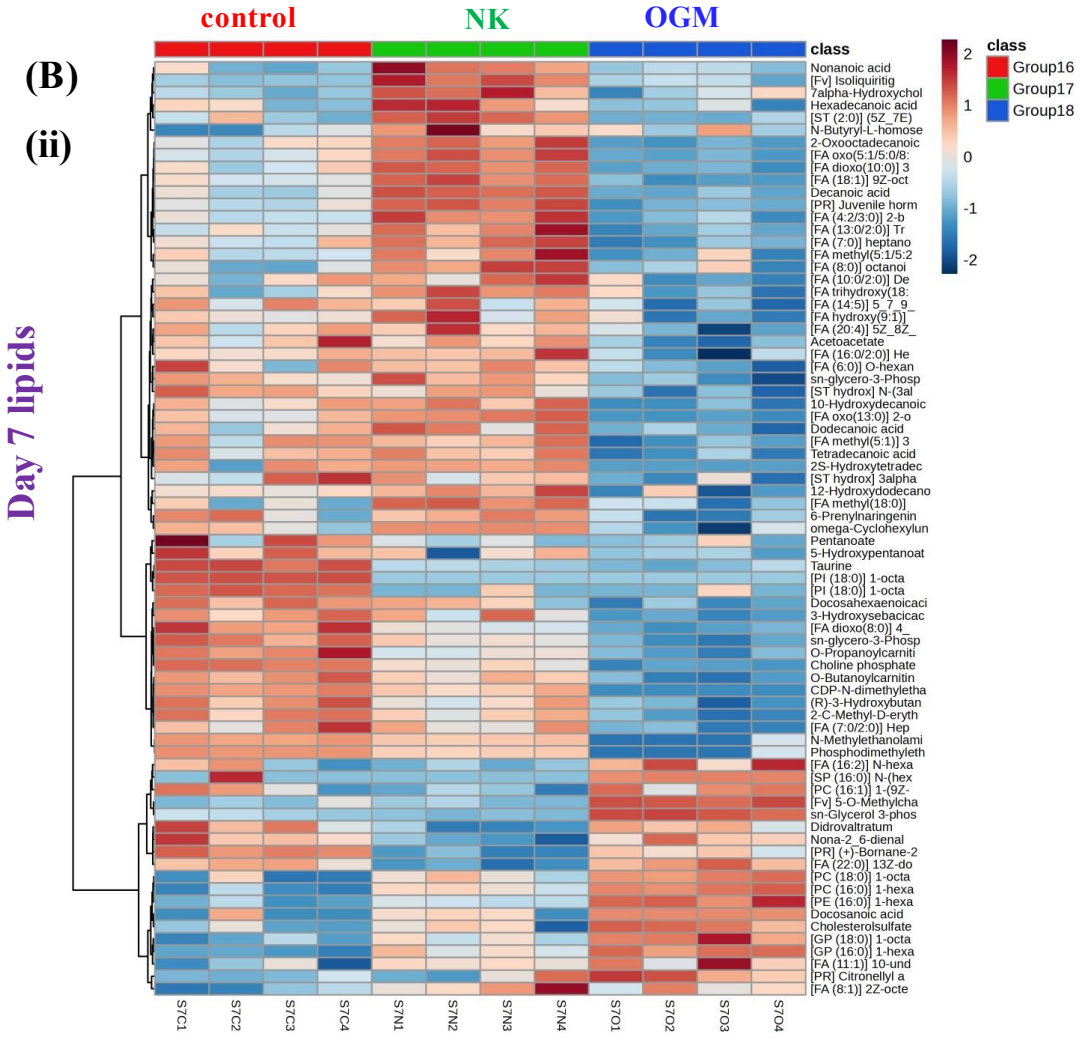

Figure 4.13: Lipid profile of SAOS-2 cells treated with NK or OGM for 3 or 7 days: (A) PCA plots were generated after (i) 3 and (ii) 7 days using MetaboAnalyst, with groupings shown across PC1 and PC2. Ellipses represent boarders of different groups, including the untreated SAOS-2 control (red), the NK group (green), and the OGM group (blue). (B) Heatmaps of top 70 most changed lipids (calculated by t-test p-value) were generated using MetaboAnalyst after 3 (i), and 7 days (ii). Colour represents a metabolite's z-score. Individual metabolites shown in darker red were most upregulated, while individual metabolites in dark blue were most downregulated. N=1 biological replicate, N=4 experimental replicates.

Signalling pathways

Predicted changes in signalling pathways were assessed using the IPA software, where ERK was predicted to be activated in nanokicked SAOS-2 cells (Figure 4. 14). This may indicate that mechanically induced differentiation in the SAOS-2 cells is regulated via the ERK/MAPK pathway. This pathway has been widely reported to be involved in osteogenesis, with ERK inhibition inhibiting terminal osteogenesis, while ERK is known to play a role in early stages of osteogenesis, regulating RUNX2 function.[281] and be inactivated in mature osteoblasts. While ERK was predicted to be activated in NK cells, it was predicted

to be inhibited in OGM treated cells. Reduced metabolic activity was observed in OGM treated SAOS-2 cells, as confirmed in chapter 3 via the alamar blue assay, and the by depletion of a significant cluster of amino acids, carbohydrates and lipids. Multiple signalling pathways associated with cell survival were predicted to be inhibited in this group, which may be linked to the observed reduced metabolic activity.

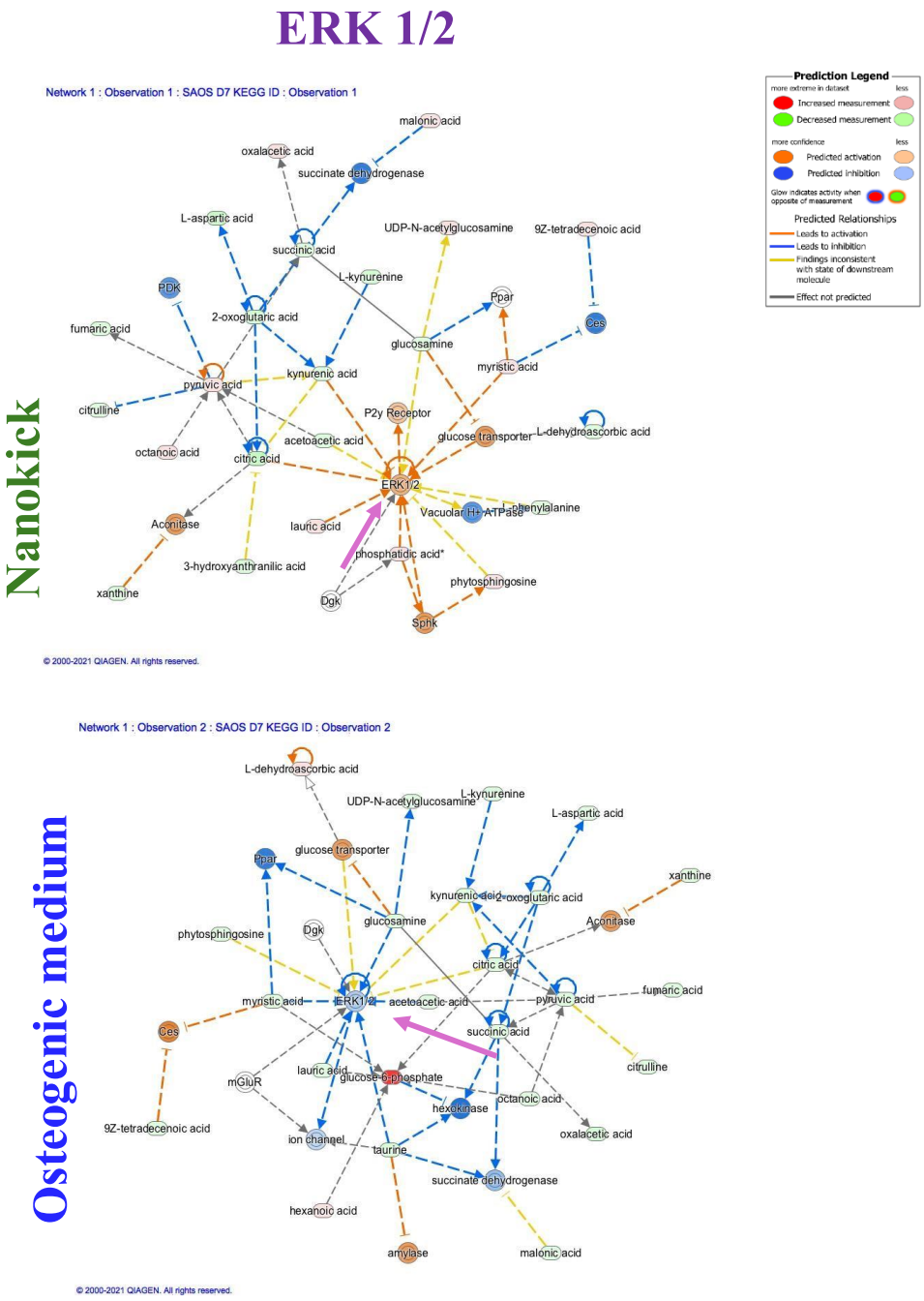

Figure 4. 14: Predicted changes in ERK1/2 activity in NK and OGM treated SAOS-2 cells after 7 days: Plots were created using IPA software. Blue nodules represent predicted pathway inhibition, and orange represents predicted pathway activation. Green nodules represent depleted metabolites, and red nodules represent accumulated metabolites. N=1 biological replicate, N=4 experimental replicates.

Akt, which belongs to the mTOR pathway[282] was predicted to be inhibited in both mechanically and chemically stimulated cells (Figure 4. 15). Akt activation is linked to proliferative signals, and Akt activation may drive cancer progression.[283] Akt was predicted to be inhibited in both chemically and mechanically stimulated cells, which may suggest an anti-proliferative effect of both treatments. Nanokicked SAOS-2 cells were previously discovered to slow cell growth, while extensive cell death observed in OGM treated cells would corroborate the prediction of Akt inhibition in SAOS-2 cells. JNK is another MAPK known to play a role in osteogenesis.**Error! Bookmark not defined.**

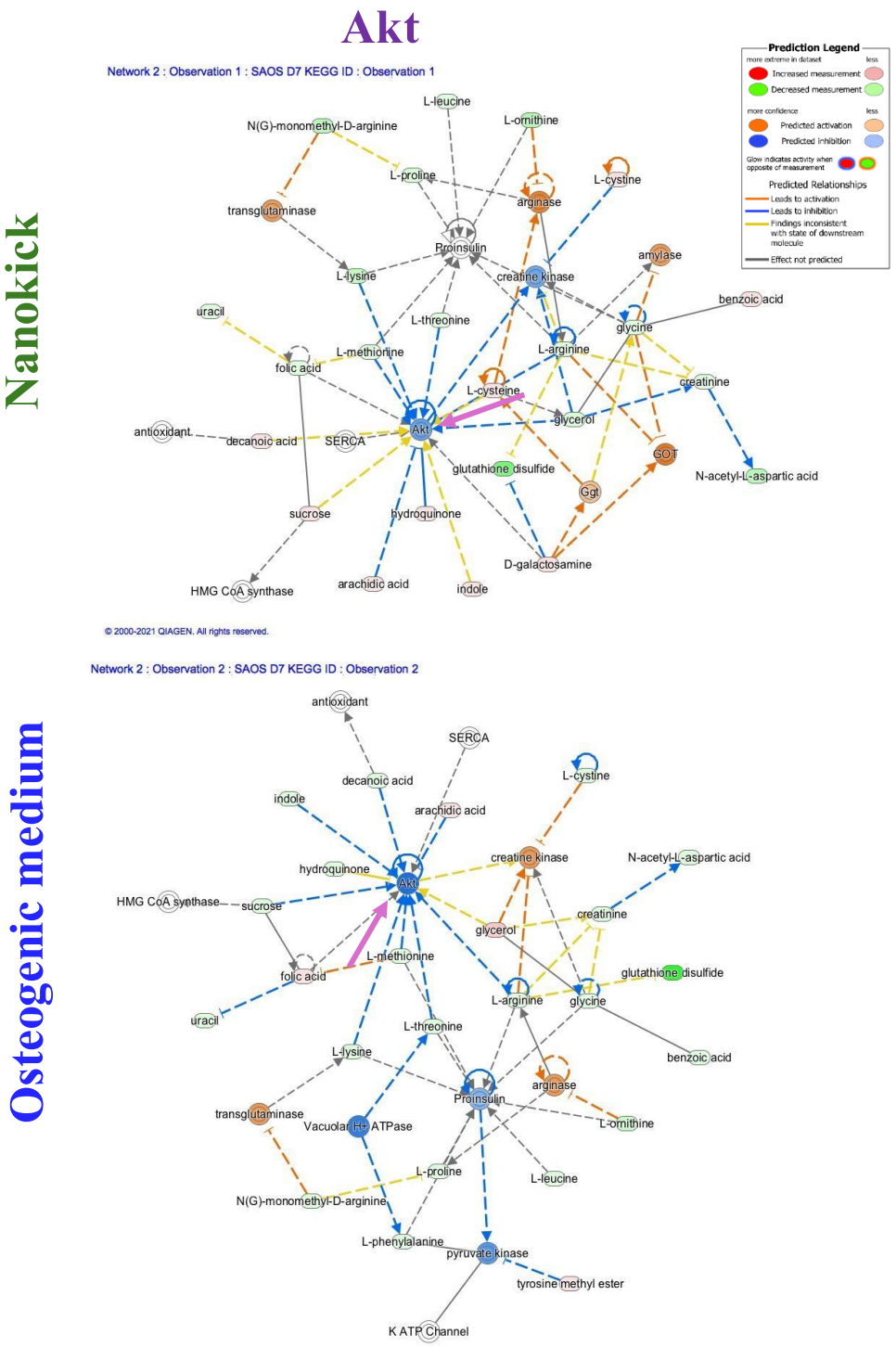

Figure 4. 15: Predicted changes in Akt activity in NK and OGM treated SAOS-2 cells after 7 days: Plots were created using IPA software. Blue nodules represent predicted pathway inhibition, and orange represents predicted pathway activation. Green nodules represent depleted metabolites, and red nodules represent accumulated metabolites. N=1 biological replicate, N=4 experimental replicates.

JNK was predicted to be inactive in nanokicked cells, suggesting that JNK may not regulate mechanically induced osteogenesis in SAOS-2 cells (Figure 4.16). On the other hand, JNK as well as ERK were also predicted to be inhibited in SAOS-2 cells, and while osteogenesis

was observed, cell death was extensive. Apoptotic effects previously observed in OGM treated SAOS-2, may contribute more to the inhibition of MAPK.

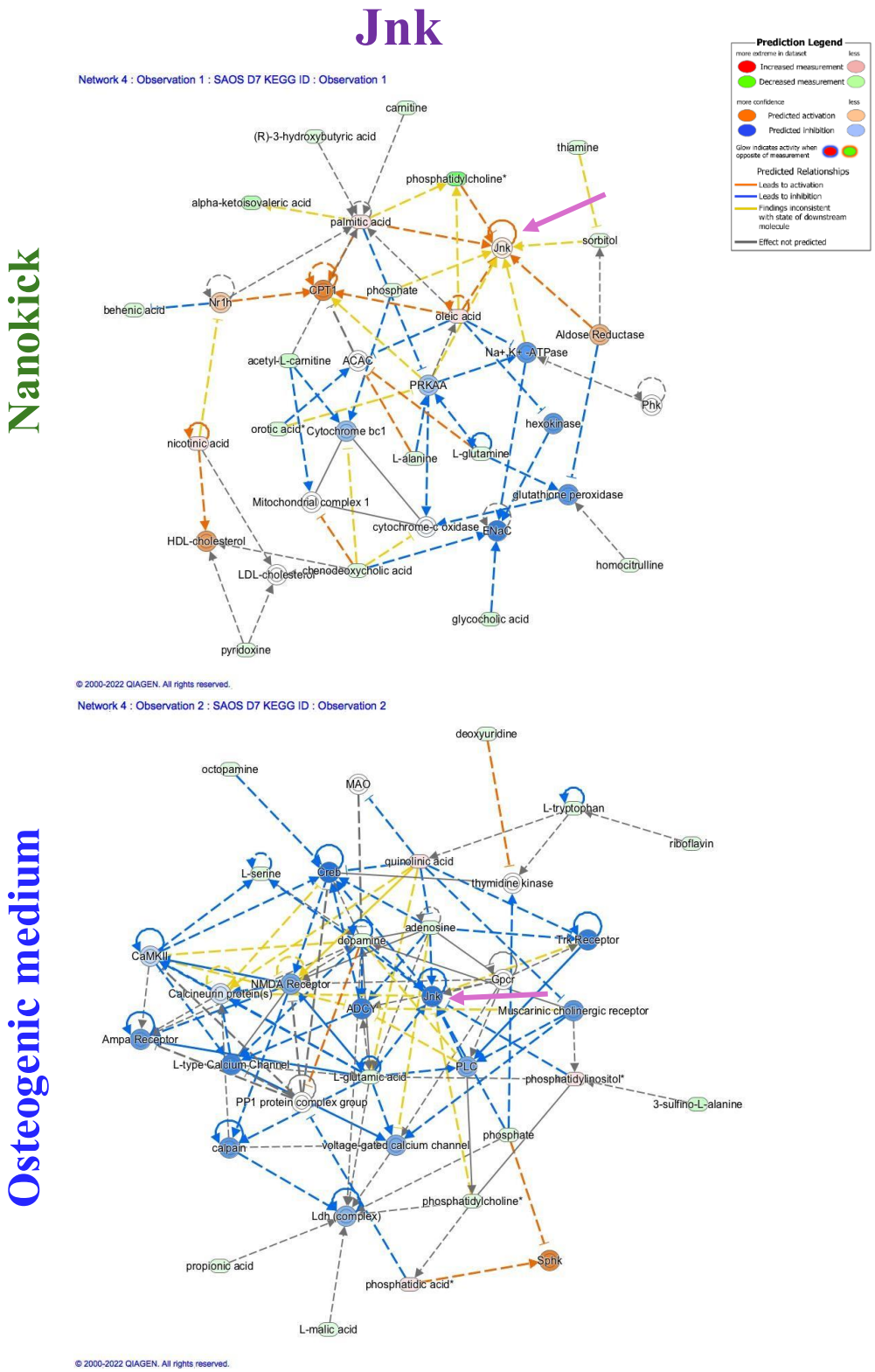

Figure 4.16: Predicted changes in Jnk activity in NK and OGM treated SAOS-2 cells after 7 days: Plots were created using IPA software. Blue nodules represent predicted pathway inhibition, and orange represents predicted pathway activation. Green nodules represent depleted metabolites, and red nodules represent accumulated metabolites. N=1 biological replicate, N=4 experimental replicates.

4.4.3 MSC metabolism

Carbohydrates

Changes in MSC metabolism were observed, to compare response to differing stimuli in healthy cells, compared to cancer cells. As previously discussed, carbohydrates are essential sources of energy, with TCA metabolites, and glycolysis metabolites playing a role in cell survival.[284] NK and OGM treatment induced changes in carbohydrate metabolism, as seen in Figure 4.17. Nanokicking for 3 days showed variability within the group, with no fold-change observed on PC1 axis, and a negative, insignificant foldchange observed on PC2 (A, i), which was visually confirmed on the heatmap (B, i). 7 days of treatment showed more dramatic differences from the control, with a significant fold-decrease on PC1, and a less significant decrease on PC2 (A, ii). Carbohydrates levels were found to be significantly downregulated, according to heatmap analysis (B, ii), which would suggest either pathway inhibition, from differentiation, or the consumption of carbohydrates by differentiating cells. PCA analysis showed positive fold-increase along PC1, and more limited variation along PC2 (A, i), for the OGM day 3 group, which was visually confirmed by the upregulation of carbohydrates from the heatmap (B, i). Positive fold-change on PC1, and a less significant negative fold change on PC2 were observed after 7 days of treatment (A, ii), with more variation being observed in clusters of metabolites from the heatmap (B, ii).

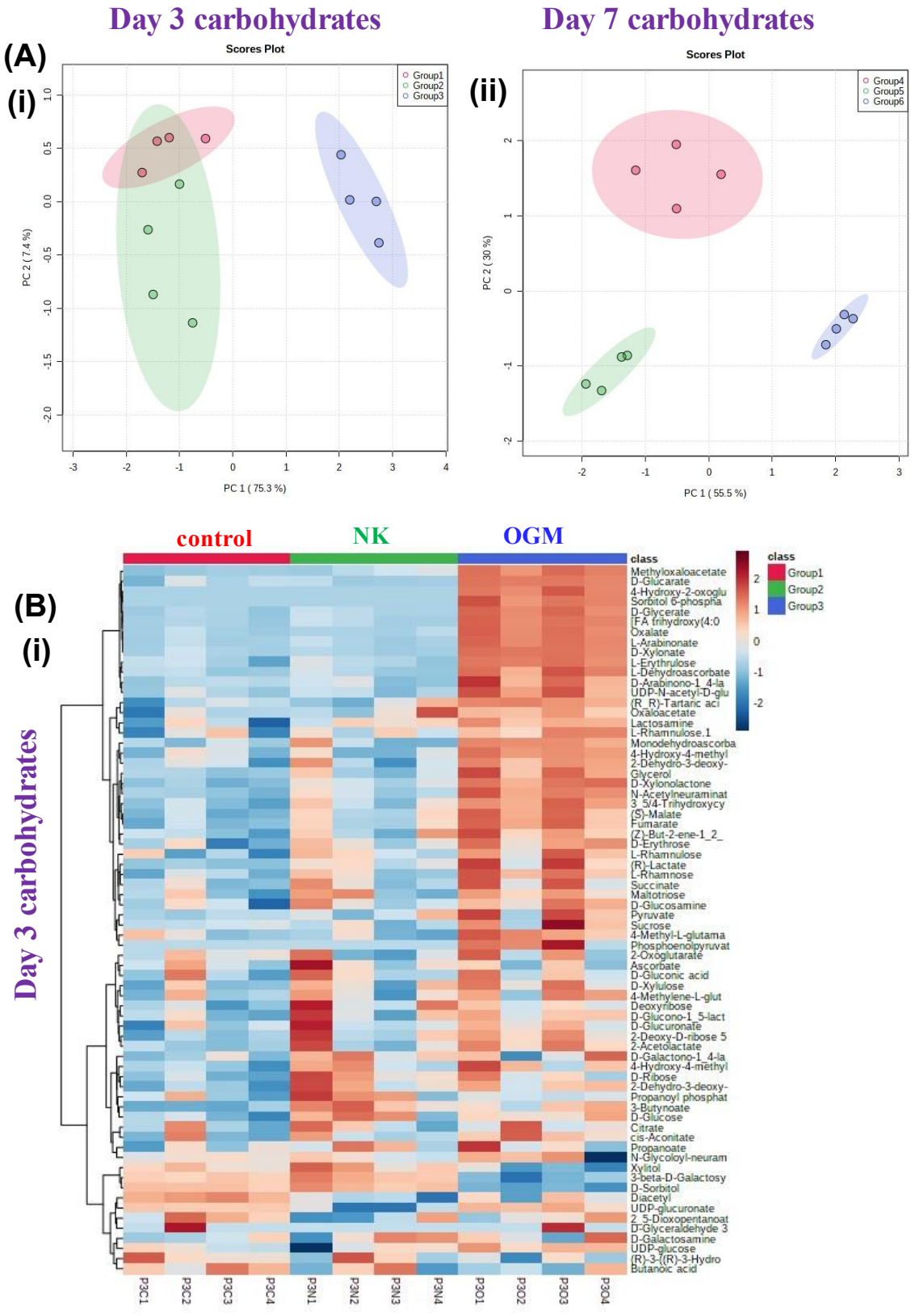
Day 3 carbohydrates
Day 7 carbohydrates
(A)
(i)
(ii)
Scores Plot
Group1
Group2
Group3
Group4
Group5
Group6
PC 2 (7.4 %)
PC 1 (75.3 %)
PC 2 (30 %)
PC 1 (55.5 %)
control
NK
OGM
(B)
(i)
Day 3 carbohydrates
class
Methyloxaloacetate
D-Glucarate
4-Hydroxy-2-oxoglu
Sorbitol 6-phospha
D-Glycerate
FA trihydroxy(4:0
Oxalate
L-Arabinonate
D-Xylonate
L-Erythrulose
L-Dehydroascorbate
D-Arabinono-1_4-la
UDP-N-acetyl-D-glu
(R_R)-Tartaric aci
Oxaloacetate
Lactosamine
L-Rhamnulose.1
Monodehydroascorba
4-Hydroxy-4-methyl
2-Dehydro-3-deoxy-
Glycerol
D-Xylonolactone
N-Acetylneuraminat
3_5/4-Trihydroxycy
(S)-Malate
Fumarate
(Z)-But-2-ene-1_2_
D-Erythrose
L-Rhamnulose
(R)-Lactate
L-Rhamnose
Succinate
Maltotriose
D-Glucosamine
Pyruvate
Sucrose
4-Methyl-L-glutama
Phosphoenolpyruvat
2-Oxoglutarate
Ascorbate
D-Gluconic acid
D-Xylulose
4-Methylene-L-glut
Deoxyribose
D-Glucono-1_5-lact
D-Glucuronate
2-Deoxy-D-ribose 5
2-Acetolactate
D-Galactono-1_4-la
4-Hydroxy-4-methyl
D-Ribose
2-Dehydro-3-deoxy-
Propanoyl phosphat
3-Butynoate
D-Glucose
Citrate
cis-Aconitate
Propanoate
N-Glycoloyl-neuram
Xylitol
3-beta-D-Galactosy
D-Sorbitol
Diacetyl
UDP-glucuronate
2_5-Dioxopentanoat
D-Glyceraldehyde 3
D-Galactosamine
UDP-glucose
(R)-3-[(R)-3-Hydro
Butanoic acid
P3C1
P3C2
P3C3
P3C4
P3N1
P3N2
P3N3
P3N4
P3O1
P3O2
P3O3
P3O4

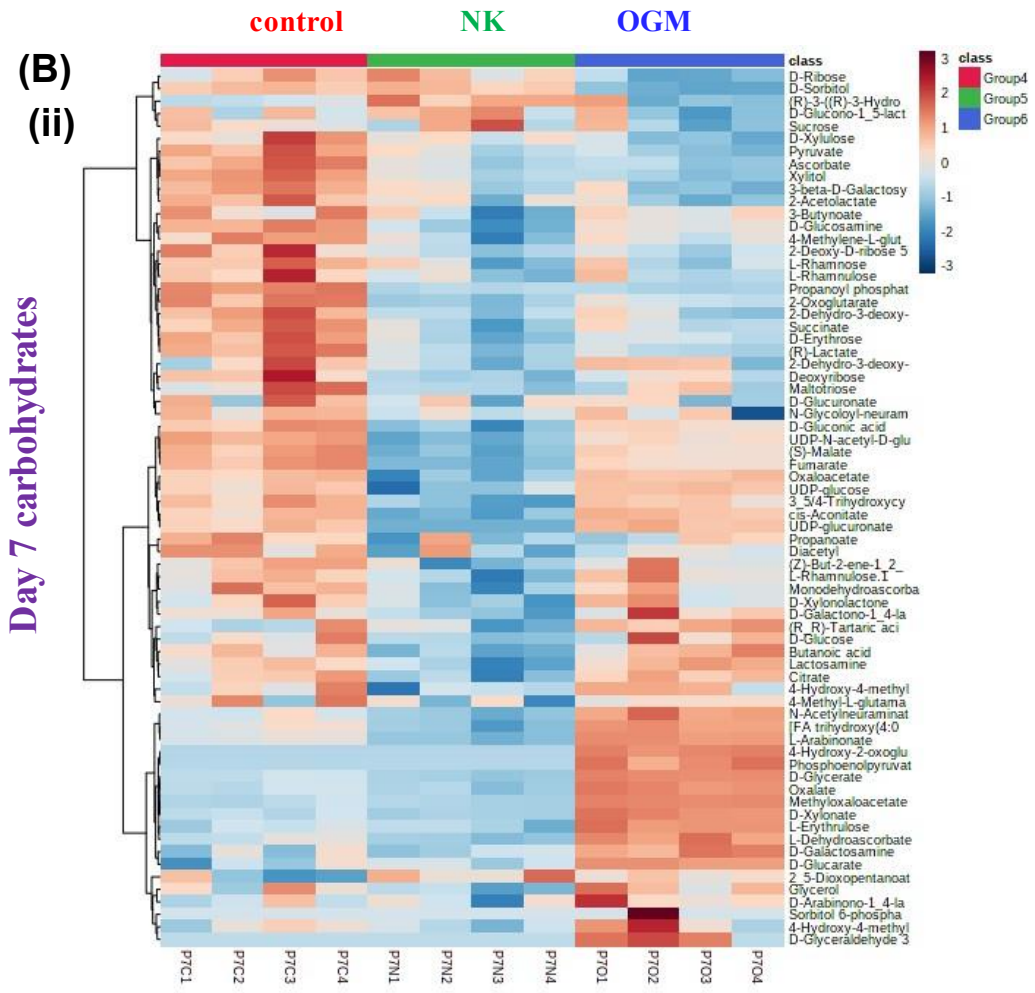

Figure 4.17: Carbohydrate profile of MSCs treated with NK or OGM for 3 or 7 days: (A) PCA plots were generated after (i) 3 and (ii) 7 days using MetaboAnalyst, with groupings across PC1 and PC2. Ellipses represent boarders of different groups, including the untreated MSC control (red), the NK group (green), and the OGM group (blue). (B) Heatmaps of top 50 most changed carbohydrates (calculated by t-test p-value) were generated using MetaboAnalyst after 3 (i), and 7 days (ii). Colour represents a metabolite's z-score. Individual metabolites shown in darker red were most upregulated, while individual metabolites in dark blue were most downregulated. N=1 biological replicate, N=4 experimental replicates.

Further analysis was carried out, with a focus on the TCA and glycolysis pathways (Figure 4.18). The fold-change against the individual timepoint control was assessed for the different conditions. TCA metabolites were found to be accumulated after 3 days of nanokicking, and significantly depleted after 7 days of stimulation. 3 days of treatment with osteogenic medium led to more significant upregulation of TCA metabolites, while a more varied observation was made after 7 days of treatment, with some metabolites being depleted, some remaining unchanged, and some accumulating. The TCA cycle plays an important role in cancer.[285] Accumulation of TCA metabolites was observed after 3 days, followed by depletion after 7 days for both groups. Malate, fumarate and *cis*-aconitate were the most

accumulated metabolites in the OGM group, with citrate accumulation observed. Citrate fold-increase was not as large as was observed in MG-63, but accumulation was observed at both timepoints.

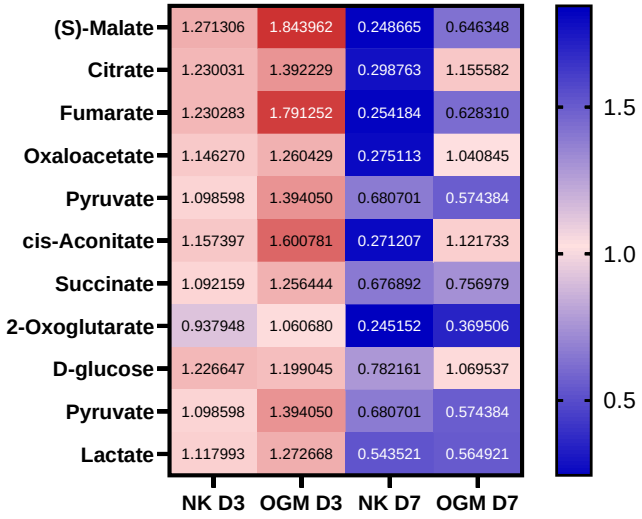

Figure 4.18: TCA metabolites altered during differentiation of MSCs: MSCs were treated with NK or OGM for 3 or 7 days, and TCA levels were assessed as a ratio against individual untreated cell control. N=1 biological replicate, N=4 experimental replicates.

Amino acids

52/171 of the analysed amino acids were found to be significantly altered in MSCs after 3 days of treatment, and 133/170 were found to be depleted after 7 days of treatment in MSCs, according to a one-way ANOVA analysis. Subtler changes were observed in the NK group after 3 days, according to PCA (Figure 4.19, (A, i), with the heatmap analysis corroborating that (B, i). After 7 days significant changes were observed between the control and the NK group according to PCA (A, ii), with heatmap analysis revealing significant depletion of amino acids, during differentiation (B, ii). In the OGM group more significant changes were observed according to PCA (A, i), with the heatmap revealing significant accumulation of amino acids after 3 days (B, i). 7 days of chemical stimulation induced depletion of amino acids in a cluster of metabolites, and significant accumulation in a smaller cluster (B, ii). Amino acids appeared to be consumed when MSCs were nanovibrated for 7 days, while more significant enrichment of amino acids was observed in chemically stimulated MSCs. This highlighted that amino acids play an active role in osteogenic differentiation in MSCs.

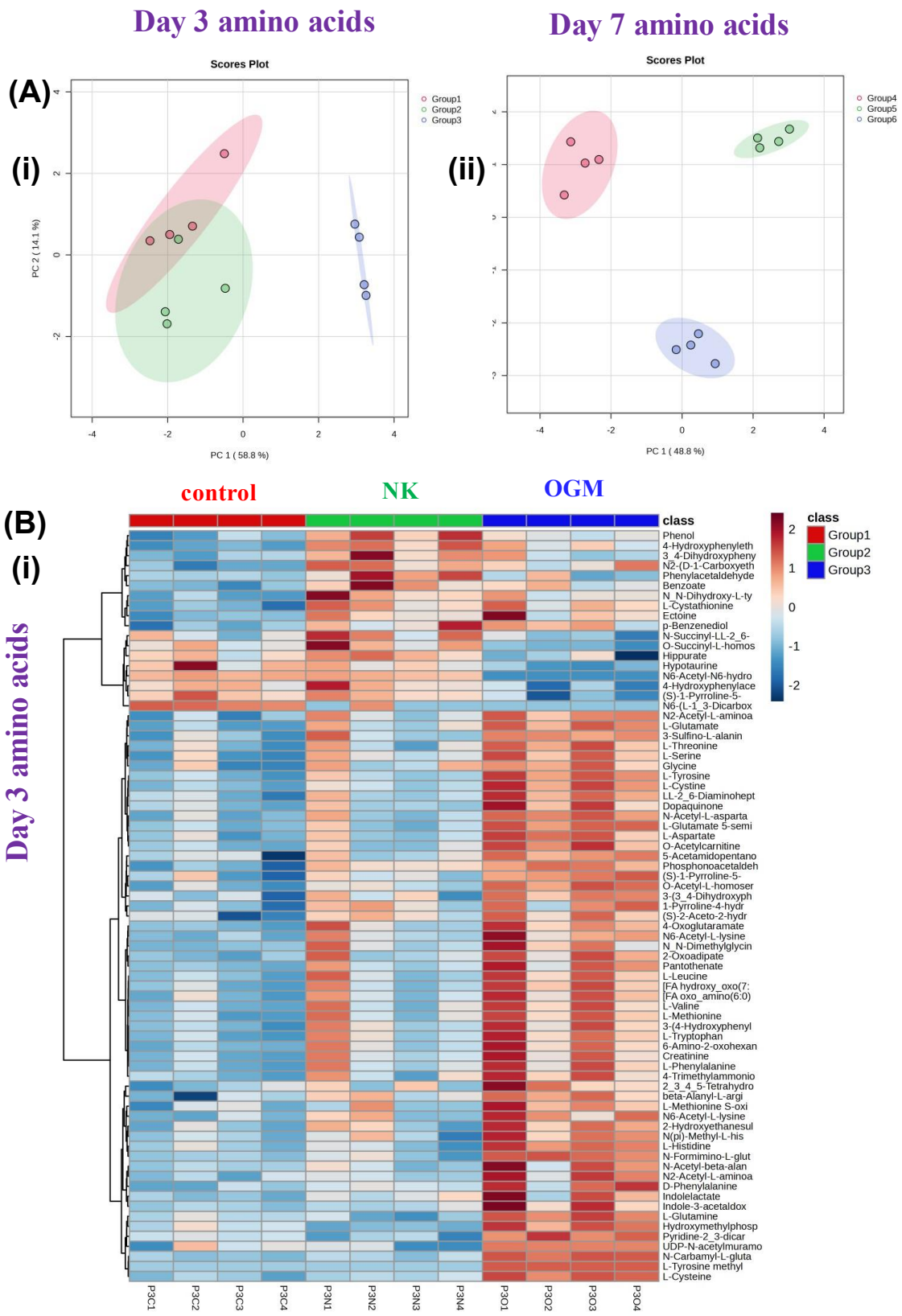
Day 3 amino acids
Day 7 amino acids
(A)
(i)
(ii)
Scores Plot
Group1
Group2
Group3
Group4
Group5
Group6
PC 1 (58.8 %)
PC 2 (14.1 %)
PC 1 (48.8 %)
control
NK
OGM
(B)
(i)
Day 3 amino acids
class
Group1
Group2
Group3
P3C1
P3C2
P3C3
P3C4
P3N1
P3N2
P3N3
P3N4
P3O1
P3O2
P3O3
P3O4

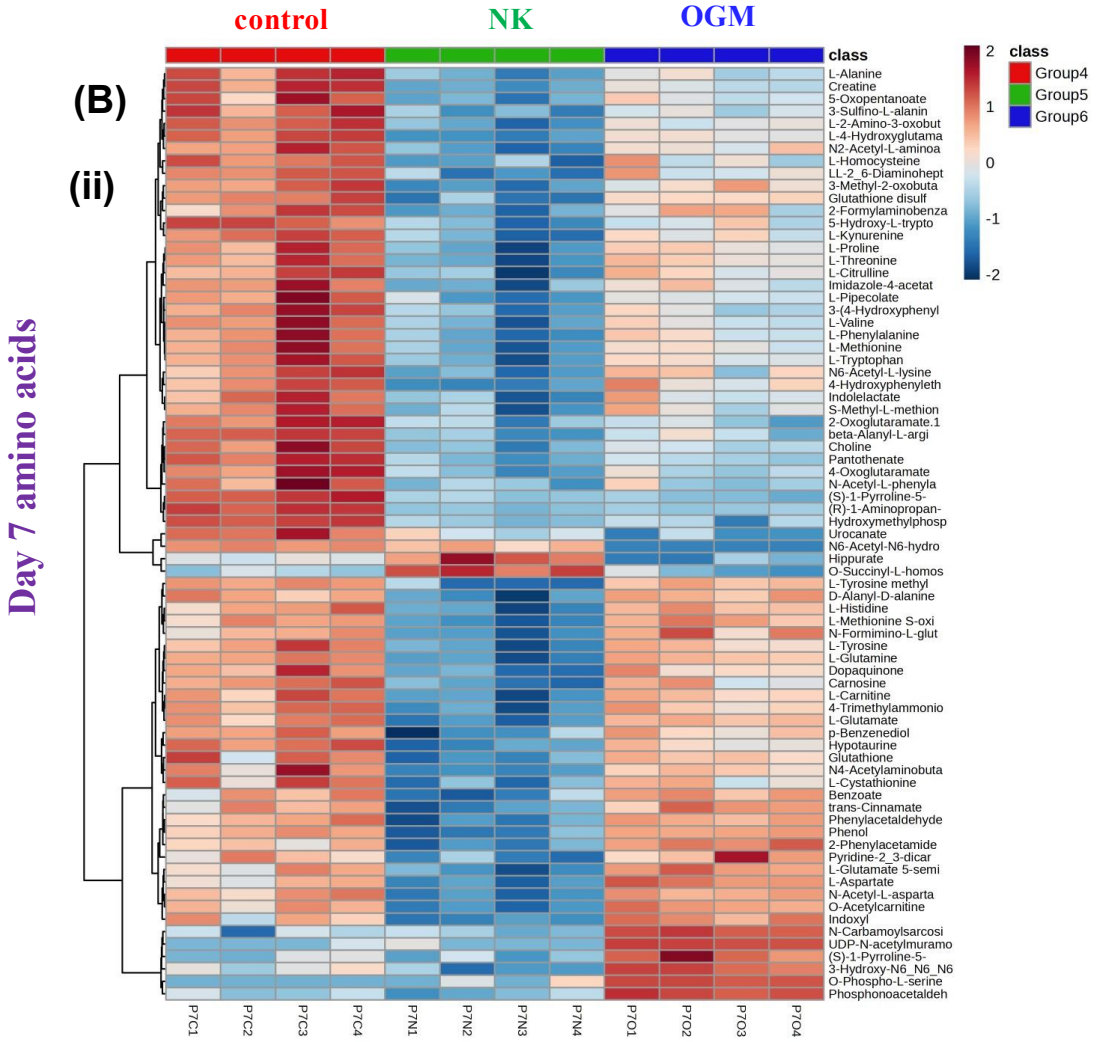

Figure 4.19: Amino acid profile of MSC cells treated with NK or OGM for 3 or 7 days: (A) PCA plots were generated after (i) 3 and (ii) 7 days using MetaboAnalyst, with groupings across PC1 and PC2. Ellipses represent boarders of different groups, including the untreated MSC control (red), the NK group (green), and the OGM group (blue). (B) Heatmaps of top 70 most changed amino acids (calculated by t-test p-value) were generated using MetaboAnalyst after 3 (i), and 7 days (ii). Colour represents a metabolite's z-score. Individual metabolites shown in darker red were most upregulated, while individual metabolites in dark blue were most downregulated. N=1 biological replicate, N=4 experimental replicates.

Lipids

59/108 analysed lipids were found to be significantly altered after 3 days of treatment, while 52/107 of the analysed lipids were significantly altered after 7 days, according to one way ANOVA of MSCs. Subtle changes in the NK lipid profile were observed according to PCA (Figure 4.20 (A)) Lipid accumulation was observed for the nanokicked group after 3 days of stimulation, with a cluster of metabolites being depleted during treatment (B, i). After 7 days of mechanical stimulation a statistically significant fold-increase along PC1, and statistically significant log-decrease along PC2 was observed, indicating that the NK group possessed a

distinctive lipid profile, from the control (A, ii). Indeed, heatmap analysis revealed that a cluster of lipids accumulated during mechanical stimulation, but a more significant cluster was depleted, as a result of the treatment (B, ii). Cells treated with osteogenic medium showed variation from the control group after 3 days, according to PCA, with a more significant decrease along PC1, and PC2 (A, i). Cells treated with osteogenic medium showed significant depletion of lipids after 3 days, which was followed by significant accumulation after 7 days, according to the heatmap (B). Studying the clusters of lipids involved in osteogenic differentiation of MSCs, it was evident that different groups of metabolites were employed by NK and OGM cells, to differentiate, as evident by distinctive clusters.

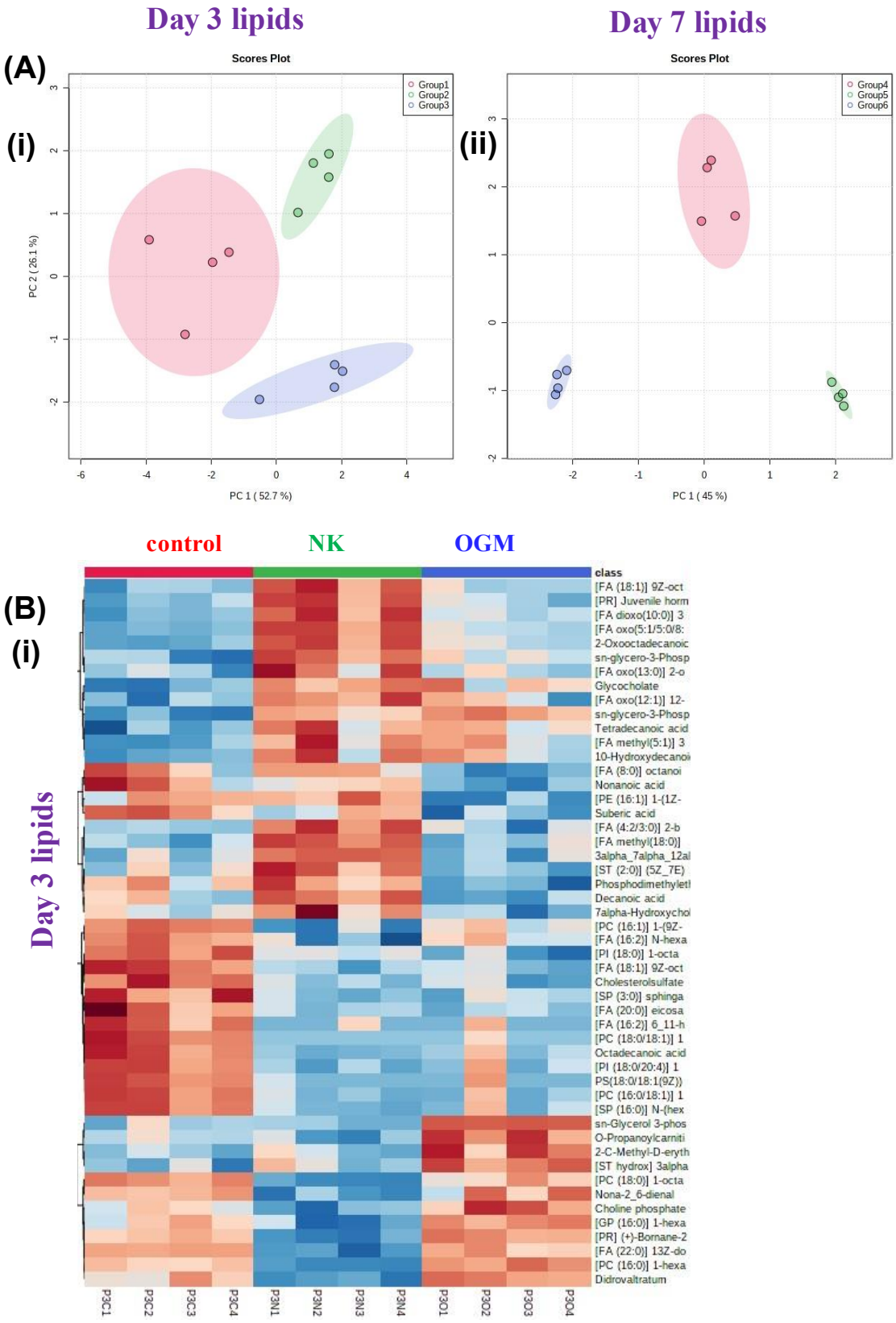
Day 3 lipids
Day 7 lipids
(A)
(i)
(ii)
Scores Plot
Group1
Group2
Group3
Group4
Group5
Group6
PC 2 (26.1 %)
PC 1 (52.7 %)
PC 1 (45 %)
control
NK
OGM
(B)
(i)
Day 3 lipids
class
[FA (18:1)] 9Z-oct
[PR] Juvenile horm
[FA dioxo(10:0)] 3
[FA oxo(5:1/5:0/8:
2-Oxooctadecanoic
sn-glycero-3-Phosp
[FA oxo(13:0)] 2-o
Glycocholate
[FA oxo(12:1)] 12-
sn-glycero-3-Phosp
Tetradecanoic acid
[FA methyl(5:1)] 3
10-Hydroxydecanoi
[FA (8:0)] octanoi
Nonanoic acid
[PE (16:1)] 1-(1Z-
Suberic acid
[FA (4:2/3:0)] 2-b
[FA methyl(18:0)]
3alpha_7alpha_12al
[ST (2:0)] (5Z_7E)
Phosphodimethyleth
Decanoic acid
7alpha-Hydroxycho
[PC (16:1)] 1-(9Z-
[FA (16:2)] N-hexa
[PI (18:0)] 1-octa
[FA (18:1)] 9Z-oct
Cholesterolsulfate
[SP (3:0)] sphinga
[FA (20:0)] eicosa
[FA (16:2)] 6_11-h
[PC (18:0/18:1)] 1
Octadecanoic acid
[PI (18:0/20:4)] 1
PS(18:0/18:1(9Z))
[PC (16:0/18:1)] 1
[SP (16:0)] N-(hex
sn-Glycerol 3-phos
O-Propanoylcarniti
2-C-Methyl-D-eryth
[ST hydrox] 3alpha
[PC (18:0)] 1-octa
Nona-2_6-dienal
Choline phosphate
[GP (16:0)] 1-hexa
[PR] (+)-Bornane-2
[FA (22:0)] 13Z-do
[PC (16:0)] 1-hexa
Didrovaltratum
P3C1
P3C2
P3C3
P3C4
P3N1
P3N2
P3N3
P3N4
P3O1
P3O2
P3O3
P3O4

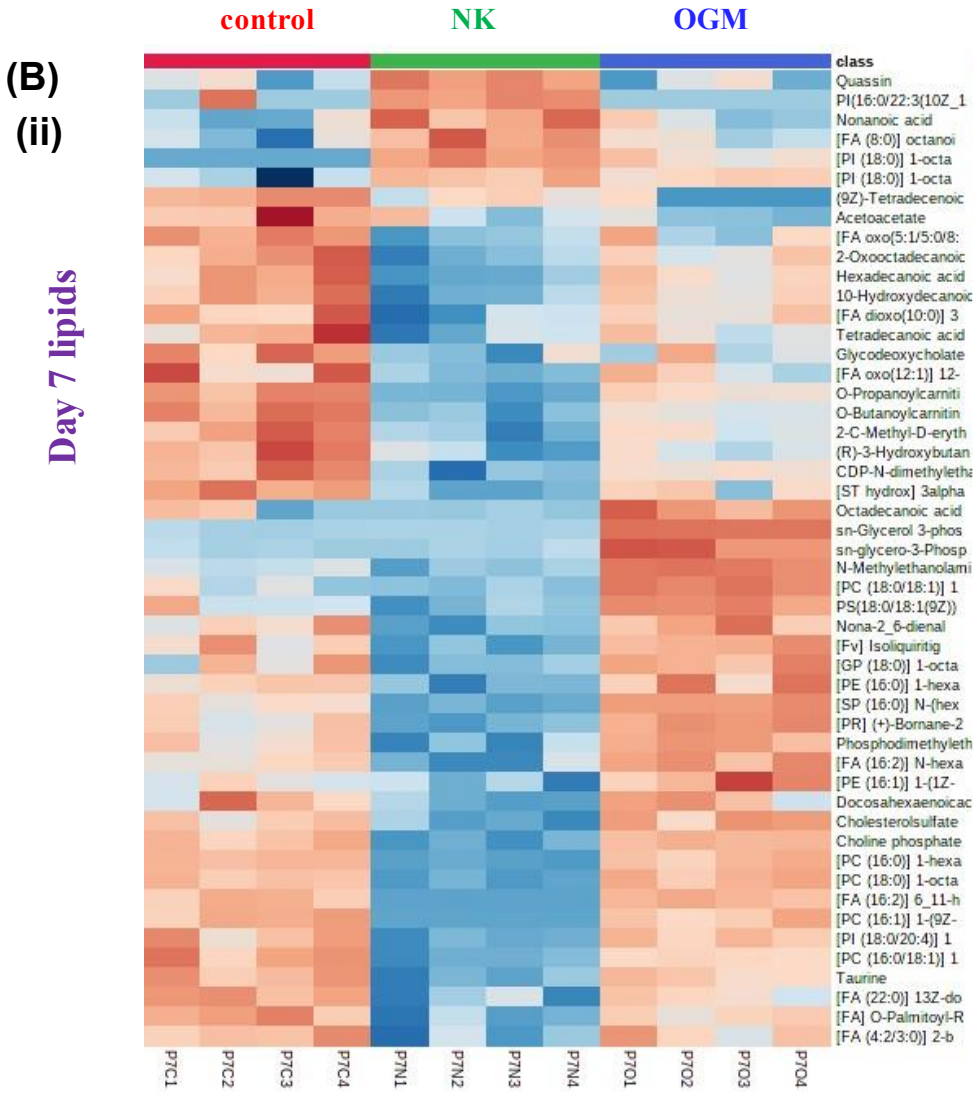

Figure 4.20: Lipid profile of MSC cells treated with NK or OGM for 3 or 7 days: (A) PCA plots were generated after (i) 3 and (ii) 7 days using MetaboAnalyst, with groupings across PC1 and PC2. Ellipses represent boarders of different groups, including the untreated MSC control (red), the NK group (green), and the OGM group (blue). (B) Heatmaps of top 50 most changed lipids (calculated by t-test p-value) were generated using MetaboAnalyst after 3 (i), and 7 days (ii). Colour represents a metabolite's z-score. Individual metabolites shown in darker red were most upregulated, while individual metabolites in dark blue were most downregulated. N=1 biological replicate, N=4 experimental replicates.

4.4.4 Metabolite identification

Bioinformatics tools MetaboAnalyst and IPA aided in uncovering trends in metabolite changes, and in the discovery of specific metabolic pathways involved in osteogenic differentiation of MSCs and OS cells. A further aim was to identify small molecules that are transformed during differentiation, and assess their bioactivity, by testing them on OS cells, and assessing their osteogenic effects. There was a special focus on metabolites that are depleted during osteogenesis, and significantly altered in the different cell types.

One way ANOVA with Tukey's post-hoc highlighted taurine as a significantly altered metabolite in all tested groups, apart from MSCs after 7 days of treatment (Table 4.2). Martins *et al.* previously reported that taurine was depleted in MG-63 cells, when they were treated with Pt and Pd chelate drugs, according to their NMR based metabolomics analysis.[286] Initial statistical analysis revealed most statistically significant changes in taurine levels in MG-63 cells after 7 days, with an f value of 86.506 and in SAOS-2 cells after 7 days, with an f value of 146.65. Taurine, or 2-aminoethane sulfonic acid, is a metabolite, that can be obtained through diet or biosynthetically derived from cysteine or methionine.[287] Taurine is involved in bile acid conjugation, signal transduction, and cardiac regulation,[288] and is a known bioactive molecule, so it was further investigated for its role in osteogenesis.

	f.value	**p.value**
MG-63 Day 3	24.849	2.1643 E-4
MG-63 Day 7	86.706	3.7818 E-6
SAOS-2 Day 3	52.186	1.1189*E-5
SAOS-2 Day 7	146.65	1.3648*E-7
MSC Day 3	45.407	1.9849 E-5
MSC Day 7	ns	ns

Table 4.2: Statistical significance in taurine expression: The individual control for each timepoint and cell line was compared to NK or OGM treated cells for MG-63, SAOS-2 and MSCs after 3 and 7 days. Statistical significance assessed via one-way ANOVA with Tukey's post-hoc. N=1 biological replicate, N=4 experimental replicates.

Cholesterol sulfate (CS) was also identified as a significantly altered metabolite in MSCs, and SAOS-2 cells, according to ANOVA, with Tukey's post-hoc (Table 4.3). Significant alterations were observed at both timepoints for MSCs, with a lower f and p value observed for SAOS-2 cells after 7 days. This statistical analysis did not identify changes in CS expression for MG-63 cells at either timepoint, or for SAOS-2 cells at the day 3 timepoint. Previous research in the group, as discussed in chapter 1, had highlighted CS as a bioactive metabolite, that drove osteogenic differentiation in MSCs.[141] Furthermore, a more thorough look into individual treatments highlighted CS indeed was altered during differentiation for the different cell lines, prompting further analysis for the metabolite.

	f.value	p.value
MG-63 Day 3	ns	ns
MG-63 Day 7	ns	ns
SAOS-2 Day 3	ns	ns
SAOS-2 Day 7	6.846	0.015347
MSC Day 3	32.085	8.0277 E-5
MSC Day 7	18.951	5.9394 E-4

Table 4.3: Statistical significance in cholesterol sulfate expression: The individual control for each timepoint and cell line was compared to NK or OGM treated cells for MG-63, SAOS-2 and MSCs after 3 and 7 days. Statistical significance assessed via one-way ANOVA with Tukey's post-hoc. N=1 biological replicate, N=4 experimental replicates.

CS was significantly depleted both under mechanical and chemical stimulation after 3 days for MSCs (Figure 4.21). After 7 days, the metabolite was still being used by the nanokicked group to differentiate, while CS levels were increased in the osteogenic group. The highly proliferative OS cell line MG-63 exhibited a similar behaviour, with both chemical and mechanical stimulation leading to depleted levels of CS after 3 and 7 days of treatment. NK treatment showed more significant consumption of CS, as was observed in MSCs. On the other hand, the more differentiated SAOS-2 cell line showed increased levels of cholesterol sulfate after 7 days of treatment, with OGM treatment inducing more significant fold-increase in CS levels.

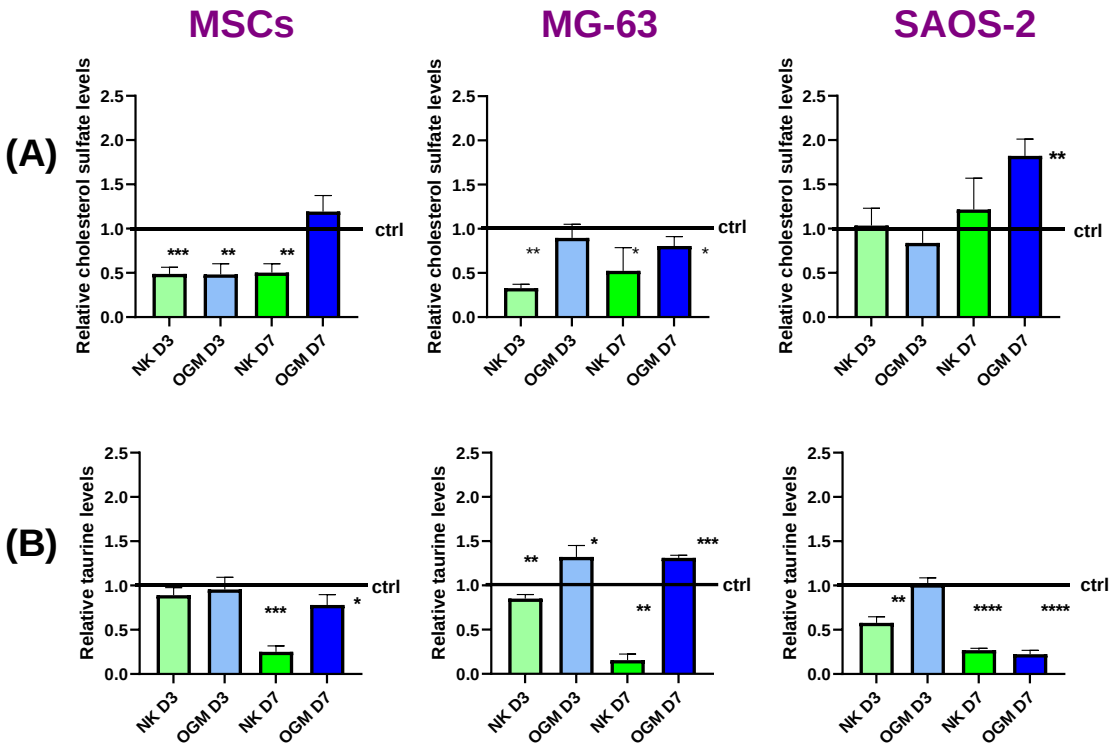

Figure 4.21: Metabolomic relative abundance of cholesterol sulfate (A), and taurine (B) levels, against individual timepoint and cell line control for (i) MG-63 cells, (ii) SAOS-2 cells, and (iii) MSC cells. Adjusted Welch t test was used to statistically compare treatments' metabolite fold-presence vs control=1. N=1 biological replicate N=4 experimental replicates (n=3 for MG-63 NK D7 group).

3 days of treatment drove small downregulation of taurine in MSCs, which was followed by more significant depletion after 7 days (Figure 4.21, (B)). Cells appeared to consume taurine during osteogenic differentiation under both treatments, but most significant fold-decrease in taurine levels was observed for the nanokicked group. Differing response was observed in the more poorly differentiated MG-63 cells, with taurine depleted during mechanical stimulation, and accumulated during chemical stimulation. For the NK group most significant, larger fold-decrease was evident after 7 days, while more significant accumulation of taurine was observed after days of OGM treatment. For SAOS-2 cells taurine was depleted across both conditions and timepoints, with most significant decrease after 7 days of treatment. OGM treatment elicited different response on the metabolite expression for the different cell lines. NK treatment induced depletion of taurine in both healthy and OS cells, highlighting a common metabolite in mechanically induced differentiation. It was thus considered of interest to observe whether the identified metabolites would promote osteogenic differentiation in both the poorly differentiated MG-63, and the more mature SAOS-2 cells.

4.5 General discussion

While metabolomics is an established field with great potential for understanding cell behaviour, there is more limited research on the osteosarcoma (OS) metabolome. Research has focused on OS microenvironment,[269] OS cancer stem cells,[266] biomarker identification,[258] response to treatment,[264] and metabolic profiling of OS cancer progression.[260] A key objective has been to identify metabolites associated with OS progression, and metastasis, to aid in tumour metabolic classification.[261,262,263] Through metabolomic studies Ren *et al.* previously reported a link between inositol metabolism, and metastasis,[260] and further observed that interrupted ezrin phosphorylation has inhibited metastatic potential in OS cells.[289] Wu *et al.* employed metabolomics, to study the tumour immune microenvironment, and identify phenotypes that would be most likely to respond to immune checkpoint inhibitors.[290] They identified that ST3GAL4 knockdown could inhibit proliferation in OS, and inhibit proliferation and macrophage polarisation, while vitamin metabolism was identified to be significant. Vitamin metabolism has been reported to be involved in OS,[291,292] with research into 1,25-dihydroxyvitamin D_3 metabolism revealing a link to cancer cell differentiation.[293] Thus, studying links between metabolism and differentiation, may be a promising approach to identifying agents that may restore differentiation potential in OS. Limited research was identified on metabolic reprogramming during OS differentiation,[271] therefore a further objective was to identify changes in carbohydrates, amino acids, and lipids. Through untargeted metabolomics, information on cell behaviour, and involvement of different classes of metabolites, was also obtained. This led to better understanding of OS cell behaviour, and biological processes involved in differentiation. Bioinformatic tools were used to study trends in metabolite biotransformation during differentiation, and to infer biological relevance from the generated high-dimensional data.

TCA metabolites were found to be significantly altered during differentiation of OS cells, and MSCs. Zhong *et al.* previously reported that OS cells presented decreased TCA, and glutathione metabolic activity, compared to healthy cells, while amino acid metabolism, including arginine, aspartate was generally enriched.[266] The general implication was that mitochondrial metabolism was impaired in OS. Zhang *et al.* reported that amino acid, glutathione, and polyamine metabolism was enriched in OS, while lipid metabolism, and carbohydrate metabolism, which included glycolytic and TCA metabolites, were inhibited.[240] Conflicting results on glutathione metabolism may be linked to different

instrumentation, analytical methods, as well as individual patient phenotypes. Smith *et al.* reported that MSCs employed oxidative phosphorylation, more so than glycolysis, as a source of energy, to undergo differentiation.[282]

While increased glucose consumption in cancer cells is often followed by significant accumulation of lactate, this was not what was observed in OS cells that were mechanically or chemically stimulated for 7 days. Both mechanical, and chemical stimulation of MSCs, MG-63 and SAOS-2 cells appeared to induce changes in TCA metabolites. accumulation of different metabolites downstream of glycolysis was observed for the different treatments. Significant depletion of TCA metabolites was observed both for SAOS-2, and MG-63 cells, after 7 days of mechanical stimulation, though accumulation of carbohydrates was observed at an early timepoint.

Oxaloacetate was the most accumulated TCA metabolite in SAOS-2 and MG-63 cells, that were nanokicked for 3 days. Oxaloacetate is involved in amino acid, and lipid metabolism, linking glutaminolysis,[294] the urea cycle,[295] and fatty acid synthesis, to the TCA cycle.[296,297] Accumulation of oxaloacetate is a driving force of fatty acid synthesis, while oxaloacetate treatment of MSCs was reported to induce osteogenic differentiation.[298] The observed accumulation of oxaloacetate in different mechanically induced cells may suggest a common osteogenic pathway in mechanically induced differentiation in OS cells. In MG-63, oxaloacetate, was depleted after 3 days of OGM treatment, while glutamate accumulation was observed in this group. For SAOS oxaloacetate was depleted at both timepoints, while glutamine accumulation was observed after 3 days, which was followed by significant depletion after 7 days. This may indicate the glutamate pathway was involved in chemical stimulation of MG-63 cells.

There is a fine balance between anaplerosis and cataplerosis in the TCA cycle, that helps balance biosynthesis, and bioenergetics.[299] Citrate is a key TCA metabolite, that is mostly deposited in bone, regulates energy metabolism, and has been described to be a driver of osteogenesis in MSCs.[277] Citrate was the most altered TCA metabolite, after 3 days of treating MG-63 cells with OGM, showing large accumulation. MSCs also displayed citrate upregulation after 3 days of OGM treatment, though fold-change was not as significant. Citrate remained accumulated after 7 days of treatment for both cell lines. On the other hand, nanokicking induce citrate accumulation both MSCs, and MG-63 after 3 days, though this was followed by depletion. SAOS-2 cells showing less significant changes in citrate expression after OGM treatment, which may be linked to previously observed reduced

metabolic activity (chapter 3). The more significant accumulation of citrate in OGM treated cells may be linked to mineralisation, induced from the supplementation of OGM with β-glycerophosphate. Fu *et al.* reported that osteogenic supplementation with ^{13}C labelled glucose, led to ^{13}C labelled citrate deposition in hydroxyapatite crystals leading to mineralisation.[300] This research demonstrated that MSCs utilise TCA intermediates, to drive differentiation, more so than glycolysis, with Zn uptake playing an important role in differentiation. The active role of citrate in osteogenic differentiation was confirmed during chemical stimulation of MSCs, and MG-63 further corroborating observations of increased osteogenesis. Though TCA cycle has been reported to play a more limited role in cancer, studies have proven TCA intermediates are also used as an energy source and building blocks for macromolecules.[301] Osteogenic differentiation is an energetically demanding process,[282] which may explain the observed increased activity in carbohydrate metabolism, both in the healthy MSCs, and the OS cell lines.

Fanelli *et al*. had previously reported that mechanically stimulation of SAOS-2 cells led to significant depletion of TCA metabolites, after 24 hour-1 Hz cyclic stretch.[272] This study was relevant to this research, as there is limited information on metabolic alterations during mechanical stimulation of OS cells. While both approaches focused on the effects of mechanical stimulation, there were differences in length of treatment, as well as frequency, where they employed 1 Hz frequency, while 1000 Hz frequency was employed in this thesis, to more closely mimic bone. This may explain differing observations on metabolic pathways involved in mechanotransduction of SAOS-2.

NK treated MG-63 cells had shown accumulation of amino acids after 3 days, which was followed by significant depletion in a large cluster of metabolites. OGM treatment showed more subtle changes in amino acid metabolism, compared to the control, according to heatmap analysis. For SAOS-2 cells more significant changes in amino acid metabolism was observed in the OGM group, compared to the nanokicked group. Significant depletion of amino acids including proline and glutamate was observed after 7 days of nanokicking, with OGM treatment inducing a more significant fold-decrease in metabolite expression. Changes in proline metabolism were observed for both cell lines. A statistically significant accumulation of proline was observed after 3 days of NK treatment in MG-63 cells, which was followed by depletion after 7 days both in the NK and the OGM groups. Shen *et al.* reported that proline is essential for osteoblastic commitment, with osteogenesis regulators RUNX2 and OSX showing significant enrichment of proline pathways, compared to other cell types.[238] Proline also plays a role in collagen biosynthesis, and in extracellular matrix

deposition.[302] Shen *et al.* theorised that rather than proline being further metabolised, it is directly involved in synthesis of osteogenic proteins like RUNX2, COL1, and osteocalcin. Given proline's role in osteogenesis and RUNX2 regulation, it was interesting to observe changes in proline metabolism, and it may be of interest to study amino acid metabolism more thoroughly.

GC-MS studies into OS differentiation, by Sunjic *et al.* previously revealed increased fatty acid metabolism.[271] Palmitic acid, stearic acid, and oleic acid were found to be abundant in both treated and untreated OS cells, which would be expected given enhanced fatty acid metabolism in OS cells. 5,8,11-eicosatrienoic acid was found to be significantly altered compared to untreated cells, suggesting a role of C20 metabolism in OS differentiation. Lipids play an important role in molecule transfer and signal transduction, and are implicated in cancer progression, as well as osteogenic differentiation. One way ANOVA for MG-63 and SAOS-2 cells identified choline phosphate, taurine, carnitine, decanoic acid, oxodecanoic acid, as significantly altered metabolites. Taurine is known to be involved in signalling pathways, while cholesterol sulfate (CS) has previously been described to promote osteogenic differentiation.[141] CS was found to be depleted both under mechanical and chemical stimulation after 3 days for MSCs. Previous research in the group had identified CS as a metabolite of interest in stem cell differentiation,[141] so this finding corroborates that. MG-63 also showed significant depletion of CS under mechanical and chemical stimulation, further highlighting commonalities between the 2 poorly differentiated cell lines. Lipid metabolism was screened in this metabolomics dataset, and while some general observations were made on lipids, expression levels for multiple lipids were below the limit of detection of the instrument. HILIC chromatography was employed, which offers enhanced separation, and allows for detection of diverse sets of metabolites, but this system is better suited for polar metabolites, than hydrophobic ones.[303] Global lipidomic analysis may be carried out in the future to obtain further information on hydrophobic metabolite involvement on OS differentiation.

While mechanically induced osteogenesis was predicted to be driven through the JNK pathway in MG-63 cells, through the IPA algorithm, nanokicking was predicted to drive osteogenesis in SAOS-2 cells through the ERK pathway. Decreased metabolic activity in OGM treated cells was previously observed in SAOS-2 cells, according to the alamar blue assay (chapter 3), which was reflected by the decreased metabolic activity according to metabolomics. This may potentially be linked to the depleted levels of carbohydrates, amino acids and lipids, as well as predicted inhibition of ERK, JNK and AKT. Nonetheless several

metabolites including malate were enriched in cells that were chemically stimulated, with impaired metabolic activity potentially being linked to apoptotic effects.

4.6 Conclusions

Mechanical and chemical stimulation were previously found to drive differentiation both on MSCs, and OS cells. Further maturity was achieved under both conditions, employing separate metabolic pathways, though metabolites in common were also identified. Amino acid metabolism was found to be significantly altered during differentiation for MSCs and OS cells, though the different stimuli appeared to employ different types of metabolites to induce osteogenic response. Citrate accumulation was observed in OGM treated MSCs, and MG-63 cells, which is an indication of mineralisation. Significant accumulation of oxaloacetate was observed when SAOS-2 and MG-63 cells were nanokicked for 3 days, showing a shared link in mechanically induced differentiation. Further osteogenic differentiation in OS cells appeared to induce metabolic reprogramming, and lead to cells employing pathways, such as TCA, that were previously described to be impaired in OS. Taurine and cholesterol sulfate were identified as metabolites of interest to be tested on OS cells, which will be described in chapter 5.

4.7 Future work

Initial observations were made on bioenergetics of OS differentiation on a metabolic level. Studying enzymes involved in glycolysis, glutaminolysis, and oxidative phosphorylation may provide further information on the bioenergetics and enzymatic pathways involved in differentiation, in the future. Some major signalling pathways predicted to be involved in OS differentiation, included JNK, ERK, Akt, so carrying out inhibitor studies in the future could help deconvolute which biological pathways are drivers, or suppressors of osteogenesis. Moreover, pairing further omics studies, such as RNA-sequencing or proteomics with the metabolomics would further highlight what are the most important pathways that drive maturation in OS. Testing some of the identified metabolites of interest from this dataset, on OS cells, is a promising strategy in assessing bioactivity of metabolites. Hence, in the following chapter, MG-63 and SAOS-2 cells were treated with cholesterol sulfate and taurine, to identify whether they would indeed promote differentiation.

Chapter 5: Small molecule driven differentiation in osteosarcoma

5.1 Introduction

As discussed in chapter 4, metabolomics was used to study metabolic pathways, and small molecules involved in differentiation. The aim of this chapter was to test metabolites that were identified from the comprehensive metabolomics data set and observe if they can drive differentiation in osteosarcoma (OS) cells. Cholesterol sulfate and taurine were identified from the metabolomic screen, while fludrocortisone acetate was also screened (Figure 5.1), due to previous research in the group.[141] Cholesterol sulfate (CS) and fludrocortisone acetate (FA) both possess a steroid scaffold.

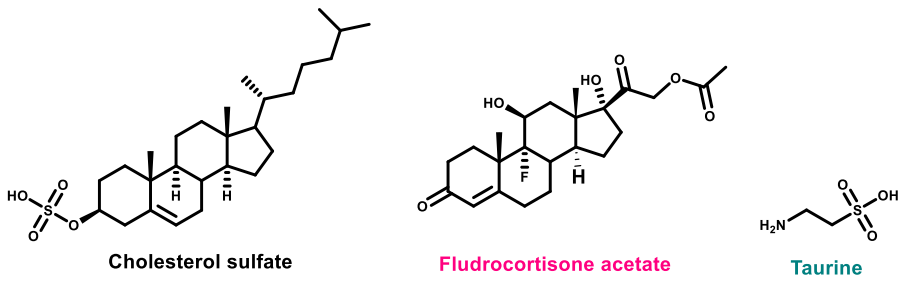

Figure 5.1: Small molecules screened in chapter 5 include cholesterol sulfate, fludrocortisone acetate and taurine.

Taurine (TAU) is an endogenous metabolite, biosynthetically derived from amino acids such as methionine and more commonly cysteine, though vertebrates typically obtain taurine from their diet.[304] Taurine is an amine sulfonic acid, that modulates lipid metabolism, and liver detoxification, by forming conjugates with bile acids, leading to the formation of easier to clear salts.[305] Taurine presents wide bioactivity, modulating calcium homeostasis, osmoregulation, central nervous system regulation and lipid membrane modulation.[306] Taurine has been reported to drive *in vitro*, and *in vivo.* tumour suppression in breast cancer, colon cancer, lung cancer, and nasopharyngeal cancer.[307] Overall, taurine is a wide acting metabolite, that modulates signalling, with taurine deficiency being linked to ageing.[308]

Cholesterol sulfate (CS) is an endogenous metabolite, that is an abundant cell membrane lipid, and plays a role in signal transduction.[309] CS is synthesised via the reversible sulfation

of cholesterol, in the presence of 3′-phosphoadenosine-5′-phosphosulfate (PAPs), as a sulfate donor, and SULT, as a catalyst.[310] CS is abundant in rodent brains and is thought to be a precursor to other sulfated steroids, such a pregnenolone sulfate.[311] CS binds to matrisylin-7[312,313] and has also been reported to be a retinoid orphan receptor (ROR) agonist, which is a nuclear hormone receptor.[314] ATRA, which has been employed in differentiation protocols for a number of cancers, including OS and acute myeloid leukaemia also presents biological activity through retinoid receptors.[315] Previous research in the group identified CS as a metabolite involved in osteogenic differentiation of MSCs, through glucocorticoid activity.[141] As discussed in chapter 1, the same research concluded that structurally related, fludrocortisone acetate (FA) presented enhanced, selective osteogenic differentiation, through mineralocorticoid activity.

Fludrocortisone acetate (FA) is a synthetic mineralocorticoid receptor agonist, that regulates salt homeostasis,[316] and has been used to treat adrenal failure, in combination with glucocorticoids.[317] FA has been shown to present more potent mineralocorticoid receptor (MR), than glucocorticoid receptor (GR) activity,[318] and has been reported to present a safe pharmacological profile. MR and GR can be activated due to stress, and play an important role in hormone homeostasis, with low affinity GR binding, and high-affinity MR binding.[319] It was considered of interest to observe osteogenic response of the different steroid receptor agonists on osteogenic induction of OS cells.

5.2 Aim

Literature search suggests that there is no previous published research on the effect of cholesterol sulfate or fludrocortisone acetate on differentiation in OS. The aim of this chapter was to assess whether steroid fludrocortisone acetate and metabolites cholesterol sulfate and taurine can drive differentiation in OS. Further objectives included assessing whether the small molecules could induce differentiation in a dose-dependent manner, and how they would affect viability of OS cells.

5.3 Materials and methods

5.3.1 Dose response experiment

MG-63 and SAOS-2 cells were cultured, plated and maintained, using protocols described in chapter 2. Cells were grown in a T75 flask, trypsinised, counted, and resuspended in DMEM. Due to growth rate differences MG-63 cells (faster) were seeded at a density of

1,000 cells/cm^2, and SAOS-2 cells (slower) were seeded at 2,000 cells/cm^2, in basal medium, in a 48 well plate. Cells were treated the following day with cholesterol sulfate (CS), fludrocortisone acetate (FA), or taurine (TAU) at 0.1, 1 or 10 µM, for 7 days. Viability was assessed after 3 and 7 days, via the Alamar blue assay, while protein expression was assessed via the ICW assay.

5.3.2 Timepoint experiment

Cells were grown in a T75 flask, trypsinised, counted, resuspended in DMEM, and plated at 10,000 cells/cm^2 for SAOS-2 and 5,000 cells/cm^2 for MG-63. Cells were grown into monolayers over a week, and subsequently treated with 10 µM CS, FA or TAU, or with OGM (recipe in chapter 3). Media was changed every 3 days, and cells were fixed with 4% formaldehyde in PBS, after 3, 7, 14 and 28 days. For each marker 4 experimental replicates were used, and protein fold-expression against the control, was quantified via ICW.

5.3.3 Alamar blue

Cells were treated according to the protocol described for the dose response experiment. Alamar blue was used to measure the metabolic activity of cells, after 7 days of treatment, using the protocol described in chapter 2. %Alamar reduction was measured against an untreated cell line control, using equation 3, reported on the Bio-Rad website.[145]

5.3.4 In cell western

Cells were treated with 10 µM of CS, FA or TAU. Cells were fixed in 4% formaldehyde, and stained for in-cell western analysis, using the reagents, and methods described in chapter 2. Monoclonal antibodies against proteins including RUNX2, OSX, ONN and OPN were used. Protein expression was quantified using LICOR ODYSSEY SA instrument, and protein expression was quantified for treatments by normalisation against CellTag, followed by normalisation against relevant untreated cell controls, for each cell line and timepoint.

5.3.5 Quantitative polymerase chain reaction with reverse transcription (qRT-PCR).

Cells were seeded in 24 well plates, at a density of 2,000 cells/cm^2 for MG-63, and 4,000 cells/cm^2 for SAOS-2. Cells were treated with 10 µM of CS or FA after 2 days, and cells were washed and lysed after 7 days of treatment, using protocols described in chapter 2. qRT-PCR was employed to quantify osteogenic gene expression during small molecule treatment, using protocols from chapter 2.

5.3.6 Immunofluorescence

Cells were seeded in 6-well plates at a density of 2,000 cells/cm^2 for MG-63 and 4,000 cells/cm^2 for SAOS-2, and treated with 10 μM CS, FA, or TAU, after 2 days. Cells were fixed after 7 days and stained using the immunofluorescence protocol described in chapter 2. Monoclonal antibodies against proteins including RUNX2, OSX, ONN and OPN were used. Cells were imaged on EVOS M7000 microscope at 20x magnification, and images were processed on Imaris Viewer.

5.3.7 Cell cycle assessment using flow cytometry

Cells were seeded in TC-treated 6-well plates at cell concentrations of 2,000 cells/cm^2 for MG-63 cells, and 4,000 cells/cm^2 for SAOS-2 cells. Cells were allowed to attach overnight and treated after two days, according to the previously described differentiation protocol. Cells were collected after 7 days, using the protocol described in chapter 2. For each condition 2 technical and 3 analytical replicates were used. Cell numbers were normalised, to analyse uniform populations. Cell cycle analysis was carried out using FlowJo software, and the gating strategy described in chapter 3 was employed, to eliminate artifacts, and dimers, and analyse single cells.

5.3.8 Statistical analysis

Statistical tests described in chapters 2, and 3 were used to compared treatments protein or gene expression, or alamar reduction, compared to respective untreated cell control.

5.4 Results and discussion

5.4.1 Effect of small molecule concentration on MG-63 cells

As previously discussed, cholesterol sulfate and taurine were identified as metabolites of interest from our metabolomic screen. Given these small molecules have not previously been described to have been tested on OS cells, to my knowledge, it was first essential to assess cytotoxicity, and the effect of concentration on the MG-63 cells. Viability was assessed via the alamar blue assay. Cell numbers were further assessed via cell counts, upon trypsinisation. Cell morphology and confluence was further assessed via immunofluorescence microscopy.

Treating MG-63 cells with CS did not cause changes in viability at 0.1 and 10 μM after 3 days, but after 7 days decreased alamar blue reduction was observed for the lowest concentration, and increased alamar blue reduction was observed at the highest concentration (Figure 5.2, A, (i)). More metabolically active cells were present after 3 days of 1 μM CS treatment while after 7 days viability was comparable to the control (A, ii). FA treatment showed a dose dependent increase in alamar blue reduction after 3 days, while 7 days of 1 μM treatment led to a statistically significant increase in metabolically active cells. TAU did not appear to affect cell viability, with comparable reduction in alamar blue for both timepoints, apart from an observed statistically significant increase in reduction after 3 days of 1 μM induction. Increased cell numbers were observed after CS treatment, and decreased cell numbers were observed from FA and TAU treatment, after trypsinisation compared to the control (B). Given confluent monolayers were formed across the different conditions after 7 days, and the limited number of replicates, there is a limitation, as to how representative those numbers are. To confirm that cells were viable after 7 days of 10 μM treatment, fluorescent staining was also carried out (C). DAPI staining was used to assess cell numbers, and phalloidin staining was used to assess cell spread and morphology. Fluorescent staining confirmed formation of confluent monolayers after 7 days, both for the control group, and the different treatments, which was in line with observations from chapter 2. Overall MG-63 cells tolerated CS, FA and TAU treatment, at the tested range of concentrations, with no cytotoxicity observed. The small increase in alamar reduction may be an indicator of increased proliferation from the small molecule stimulation, which was not previously observed for nanokicking or osteogenic medium.

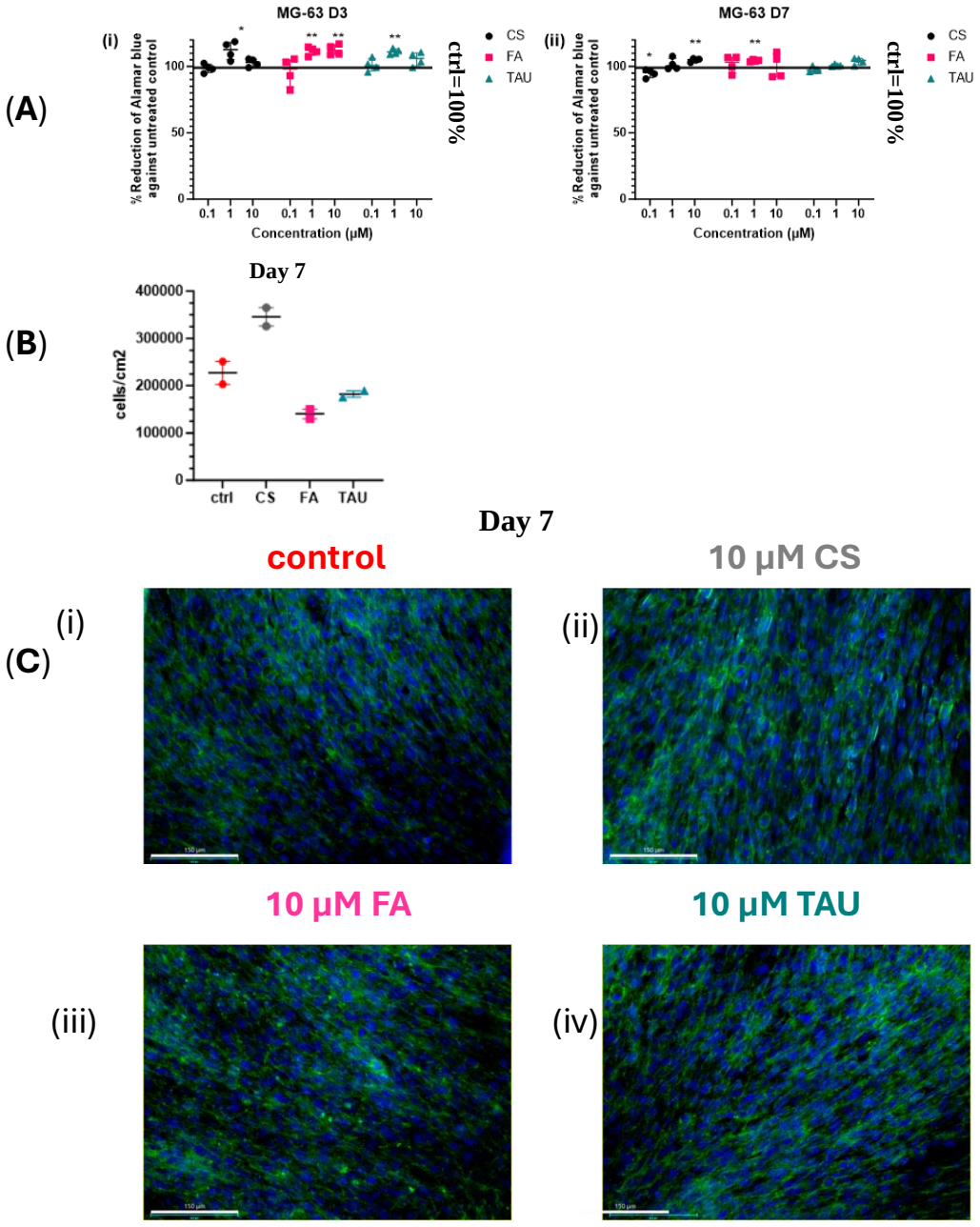

*Figure 5.2: Concentration effect of CS, FA and TAU on SAOS-2 viability: A) %Alamar reduction of CS, FA and TAU against untreated MG-63 cell control, of (i) D3 and (ii) D7 timepoints. N=2 experimental replicates, N=2 analytical replicates, Welch adjusted t-test was used to statistically compare treatments' alamar reduction vs control=100%, (blank=ns=p>0.05, *=p<0.05, **=p<0.01) (B) Cell numbers after cell trypsinisation. Cells were treated for 7 days with 10 μM of CS, FA or TAU, trypsinised and counted., N=1 biological replicate, N=2 experimental replicates (C) Fluorescent images showing cell distribution during differentiation. MG-63 cells were (i) untreated or treated with 10 μM of (ii) CS, (iii) FA or (iv) TAU for 7 days. DAPI (blue) stained nuclei, and phalloidin (green) stained actin cytoskeleton. 150 μm scale bar. N=1 biological replicate, N=6 experimental replicates*

After observing that cells were viable at the tested range of concentrations, protein expression was assessed via the previously discussed in-cell western (ICW) assay. From

earlier observations in chapter 3, cells had not typically achieved differentiation in 3 days, so osteogenic protein expression was quantified after 7 days. ICW was the main screening technique that was chosen, due to the increased throughput capability, as well as the perceived accuracy of the readings, caused by the lower background from IR dyes. Protein expression was normalised against the CellTag fluorescent cellular readout, and fold-expression was quantified, relative to the untreated MG-63-day 7 control. RUNX2 expression was measured, as an increase in RUNX2 is required to initiate differentiation, and downstream expression of osteogenic proteins. OSX expression was also measured, as OSX is also a regulator of osteogenesis, that acts downstream of RUNX2.

All tested small molecules showed signs of osteogenic differentiation, as evident by a pattern of increased RUNX2 and/or OSX expression (Figure 5.3). At the lowest tested concentration, CS did not appear to drive differentiation, with comparable protein expression to the control observed for RUNX2 (A, (i)) and OSX (B, (i)). Treatment with 1 μM of the metabolite showed a small increase in RUNX2 and OSX. An increase in RUNX2 and OSX was observed after 7 days of 10 μM CS treatment, which would suggest the glucocorticoid small molecule could drive osteogenesis. Overall upward trends in osteogenic markers were observed, even though statistical significance was absent. Fludrocortisone acetate was tested under the same range of concentrations, with insignificant differentiation observed at 0.1 μM and no observable changes at 1 μM. Insignificant increase in fold-expression was observed for RUNX2 and a statistically significant increase in OSX was observed at the highest tested concentration. This would strongly indicate that treatment with 10 μM FA induces osteogenic differentiation, in a concentration-dependent manner.

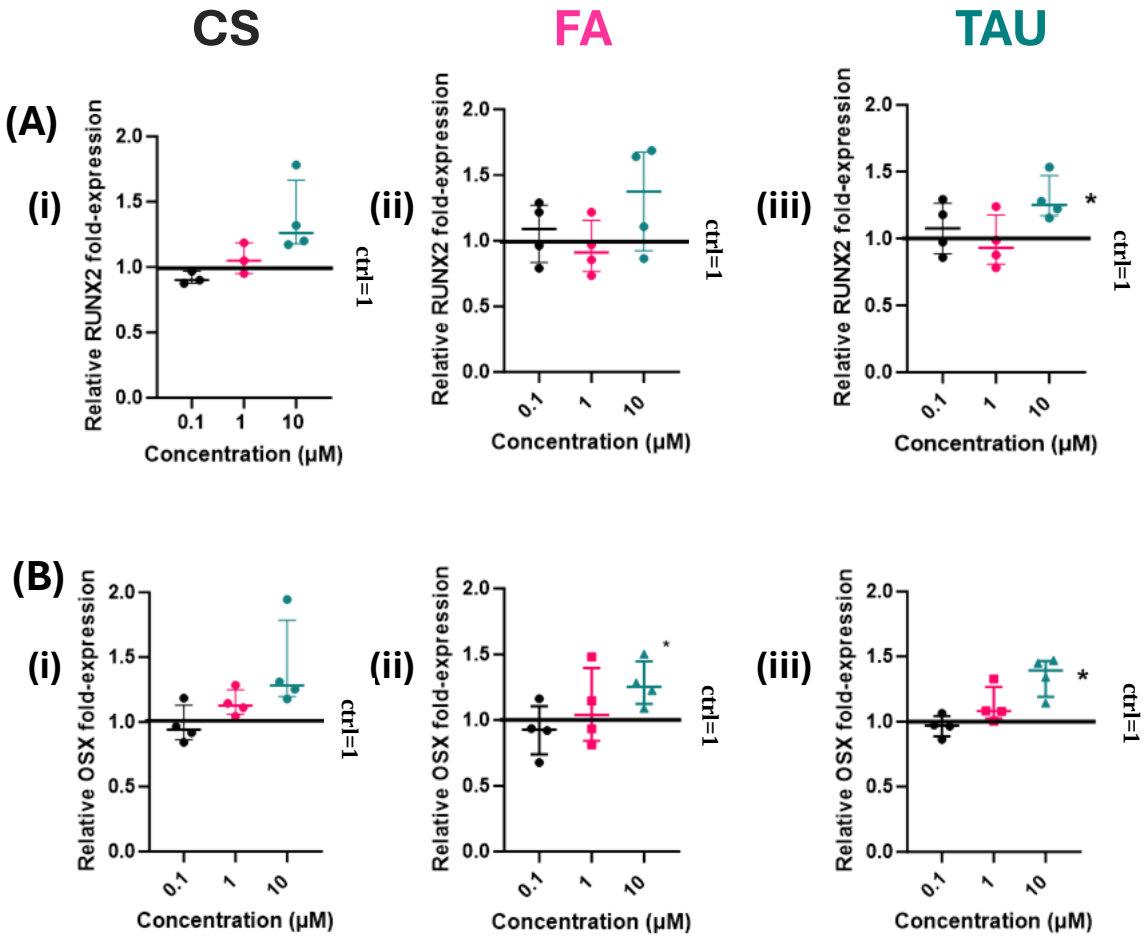

*Figure 5.3: ICW protein expression. Protein fold-expression of (A) RUNX2 and (B) OSX was normalised against untreated MG-63 control treatment after 7 days. MG-63 cells were treated with 0.1, 1 or 10 μM of (i) CS, (ii) FA or (iii) TAU. Welch's adjusted t-test was used to statistically compare treatments' protein fold-expression vs control=1 (blank=ns=p>0.05, *=p<0.05). N=1 biological replicate. N=4 experimental replicates.*

Given the gradual increase in osteogenic proteins, with the increase in small molecule concentration, a dose dependent response was observed for CS, FA and TAU, with 10 μM treatment showing the most significant differentiation. Glucocorticoids are often included in osteogenic cocktails,[176,177] with Alakpa *et al.* reporting that CS showed a less potent, but more selective osteogenic differentiation than dexamethasone on MSCs.[320] Being encouraged by the observed differentiation from 10 μM stimulation for the different small molecules, further studies were carried out to study cell behaviour. Given previous research on MSCs, and the group's interest in steroid scaffolds, cholesterol sulfate and fludrocortisone acetate were selected for further screening.

5.4.2 Effect of small molecule 10 µM treatment on MG-63

As previously described, MG-63 had reached cell confluence after 7 days in culture, forming overgrown monolayers, with disorganised actin filaments observed. Protein localisation and expression, for osteogenic markers, were studied via immunofluorescence. First the osteogenesis master regulator RUNX2 was imaged, with relatively abundant expression, and perinuclear localisation observed (Figure 5.4). This was in line with previous observations from nanovibration studies, described in chapter 3. CS and TAU appeared to drive an increase in RUNX2 expression. Upward trends in RUNX2 expression were observed during the dose response experiment (Figure 5.3), which were also visually observed from immunofluorescence for CS and TAU, while RUNX2 seemed less abundant in the FA treated cells. OSX expression was also studied, though the protein was not abundant in MG-63 cells, as previously discussed.

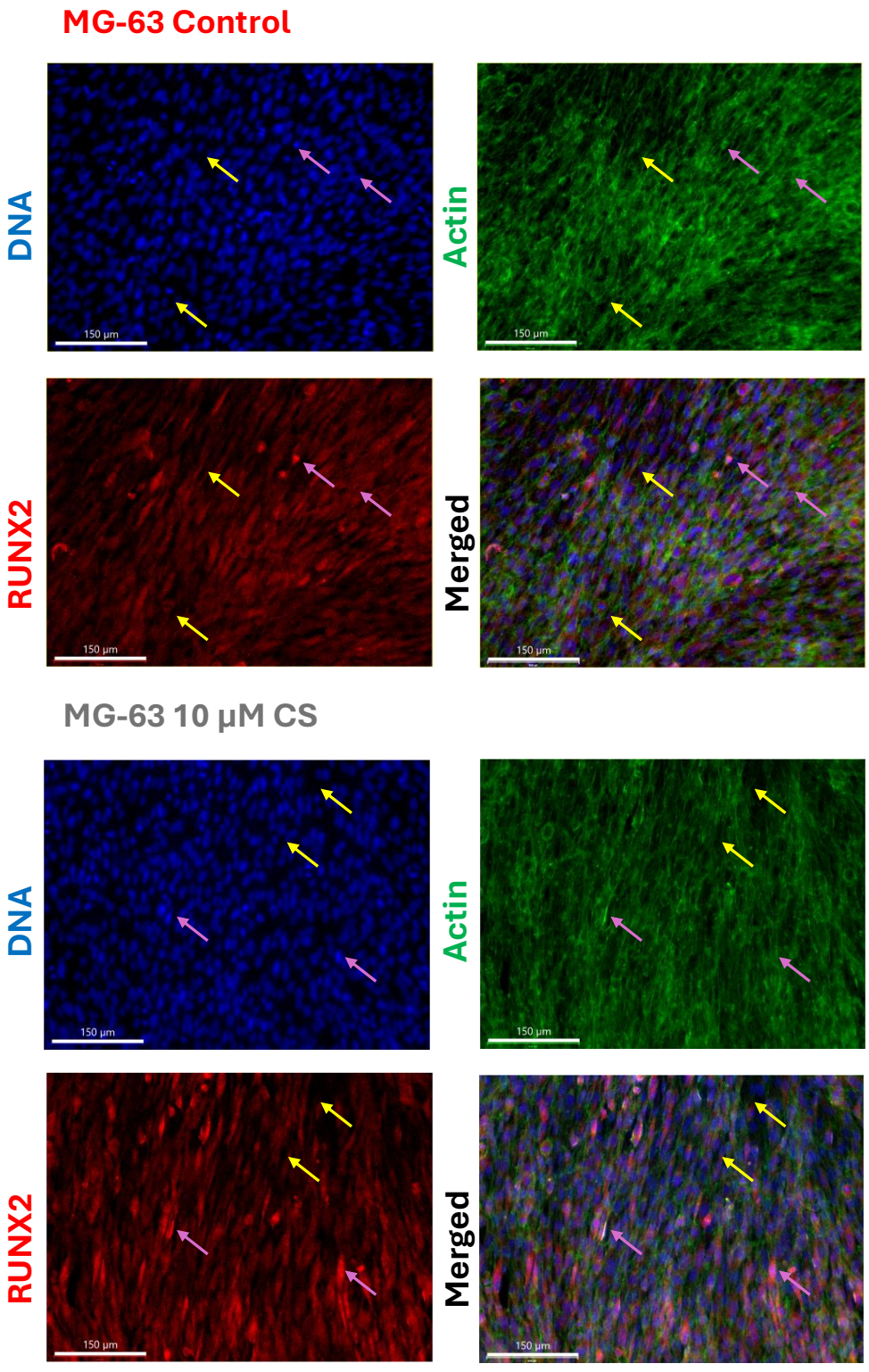
MG-63 Control
DNA
Actin
RUNX2
Merged
150 µm
MG-63 10 µM CS
DNA
Actin
RUNX2
Merged
150 µm

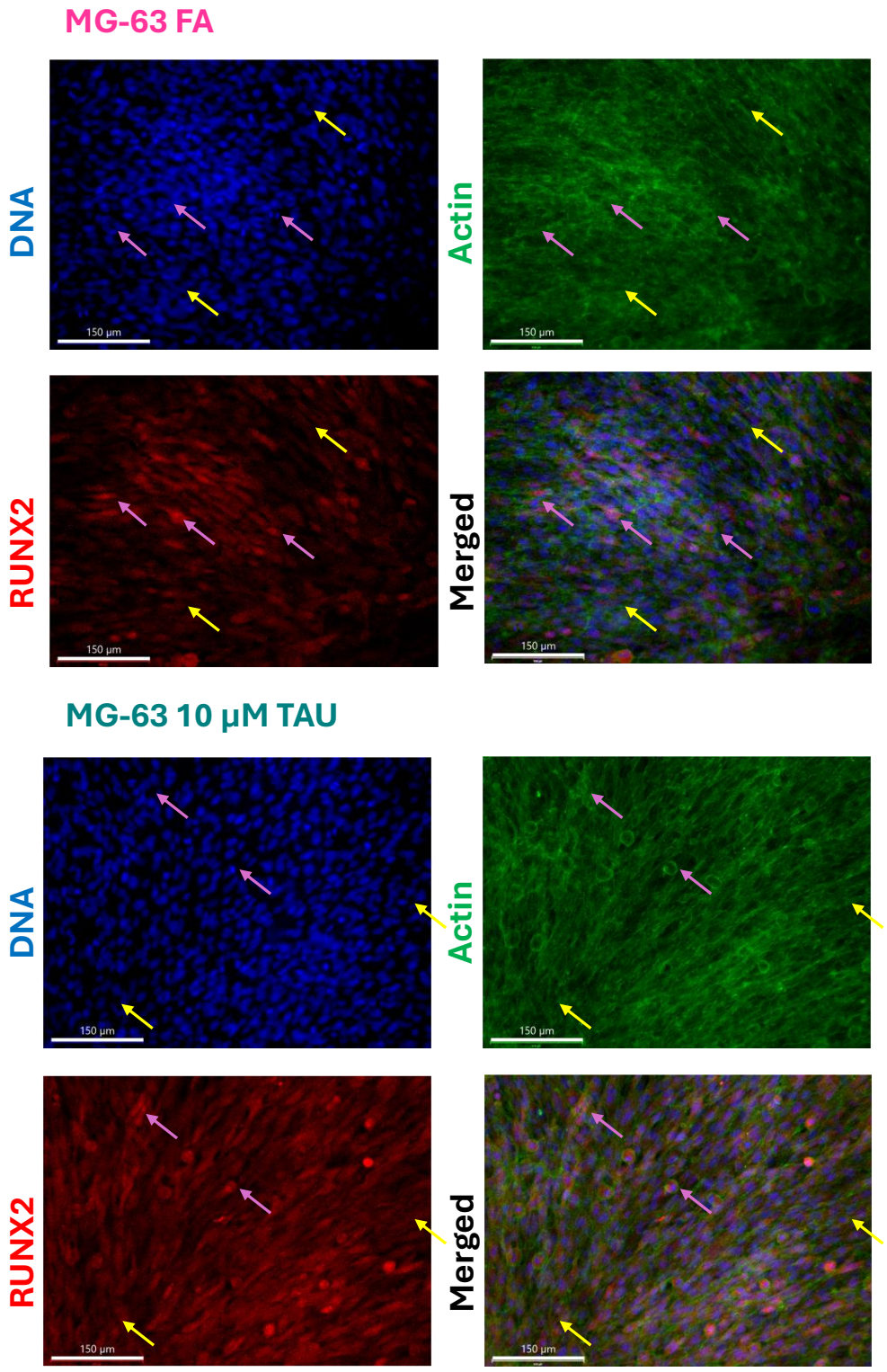

Figure 5.4: Immunofluorescence staining: MG-63 cells were treated with 10 µM CS, FA or TAU for 7 days. Cells were stained with DAPI (blue), phalloidin (green), and RUNX2 (red), and imaged on EVOS at 20x magnification. imaged on EVOS microscope at 20x magnification. Images processed with Imaris Viewer. Scale bars: 150 µm. Yellow arrows point to areas of decreased RUNX2 expression, and pink arrows point to areas of increased RUNX2 expression. N=1 biological replicate, N=2 experimental replicates.

As was previously described in chapter 3 ONN expression was found to be perinuclear in MG-63 cells (Figure 5.5). Not all cells were ONN positive, and the protein was expressed in lower levels than RUNX2. FA and TAU treated cells visually showed a small increase in protein expression, as indicated by pink arrows, though protein expression was not quantified at this stage.

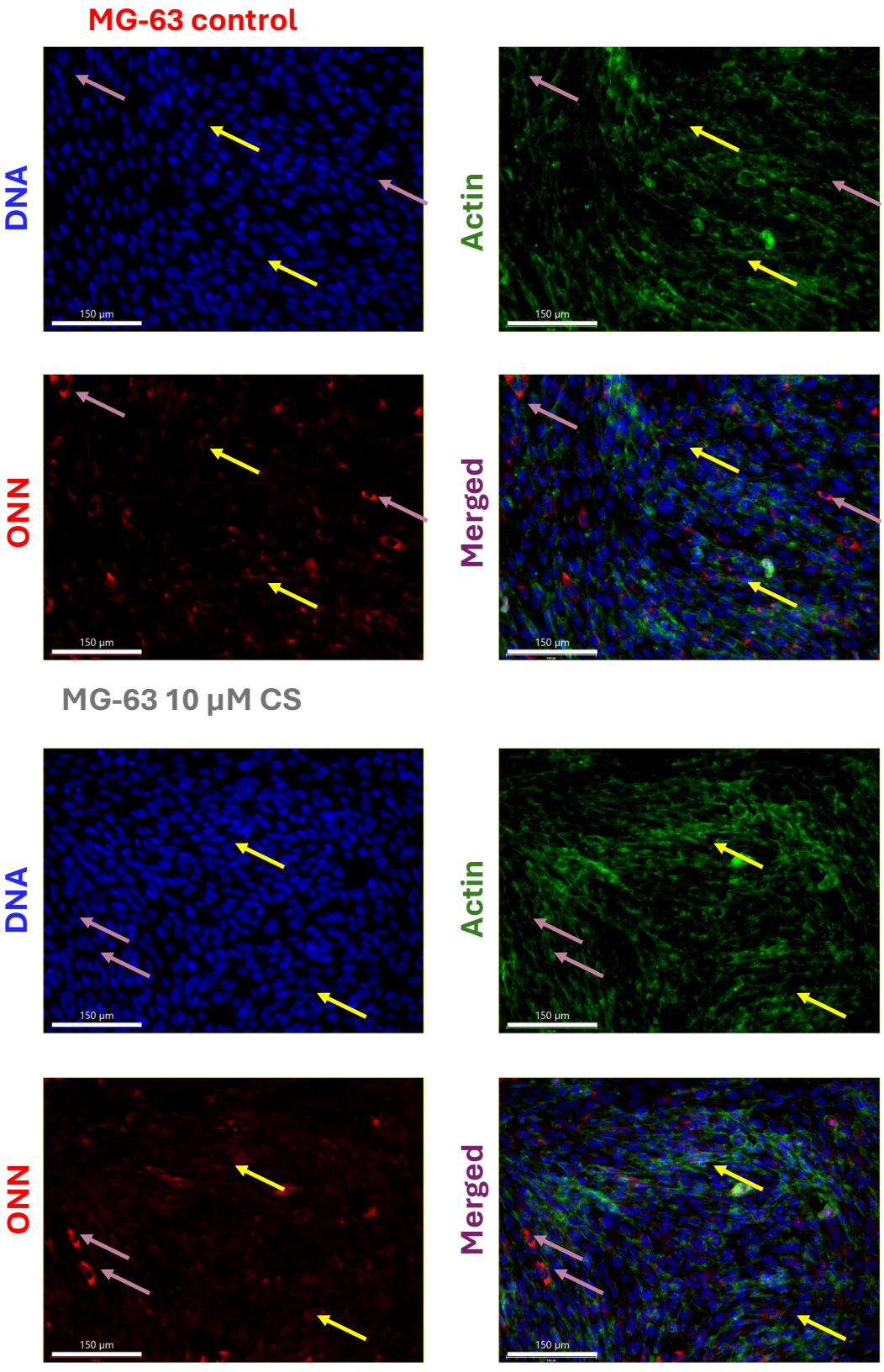

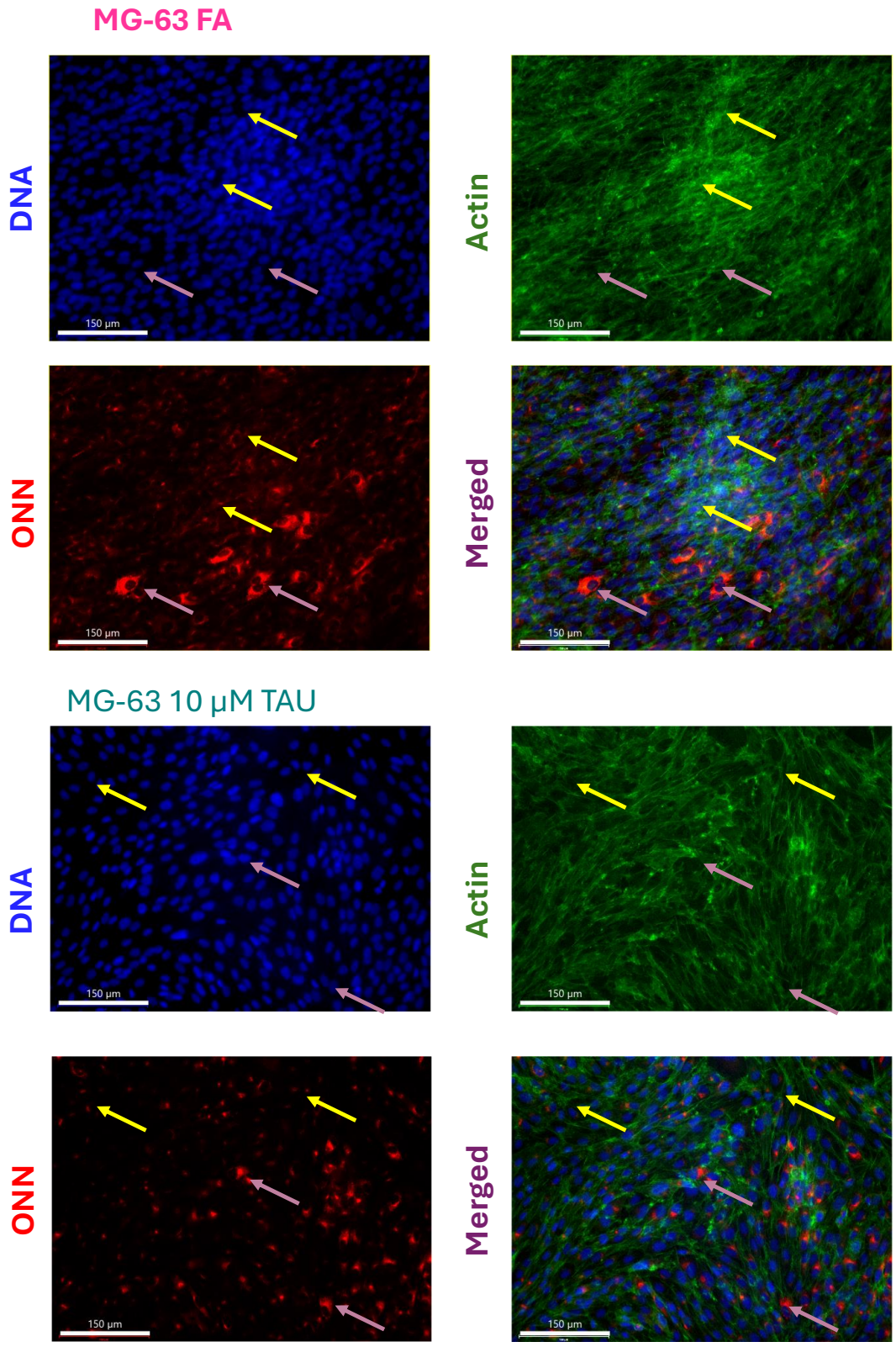

Figure 5.5: Immunofluorescence staining: MG-63 cells were treated with 10 µM CS, FA or TAU for 7 days. Cells were stained with DAPI (blue), phalloidin (green), and ONN (red), and imaged on EVOS at 20x magnification. imaged on EVOS microscope at 20x magnification. Images processed with Imaris Viewer. Scale bars: 150 µm. Yellow arrows point to areas of decreased ONN expression, and pink arrows point to areas of increased ONN expression. N=1 biological replicate, N=2 experimental replicates.

Perinuclear and cytoplasmic localisation of the matricellular protein OPN was observed for different conditions. (Figure 5.6). Qualitative observations revealed increased OPN in certain cells within the population for FA and TAU treated cells (pink arrows). This increase in OPN may suggest differentiation, and potentially mineralisation from small molecule induction, though immunofluorescence was solely used as a qualitative tool.

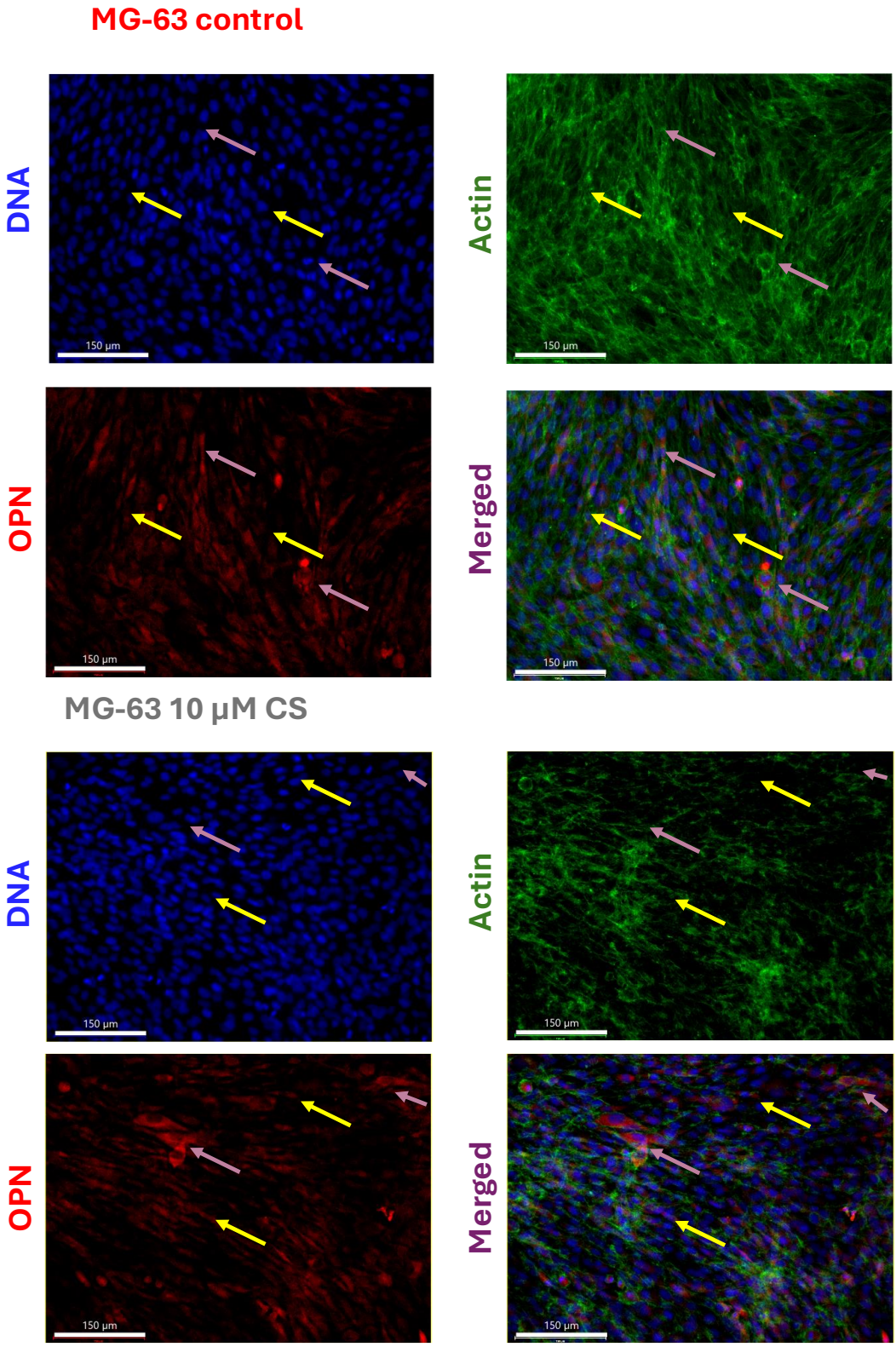

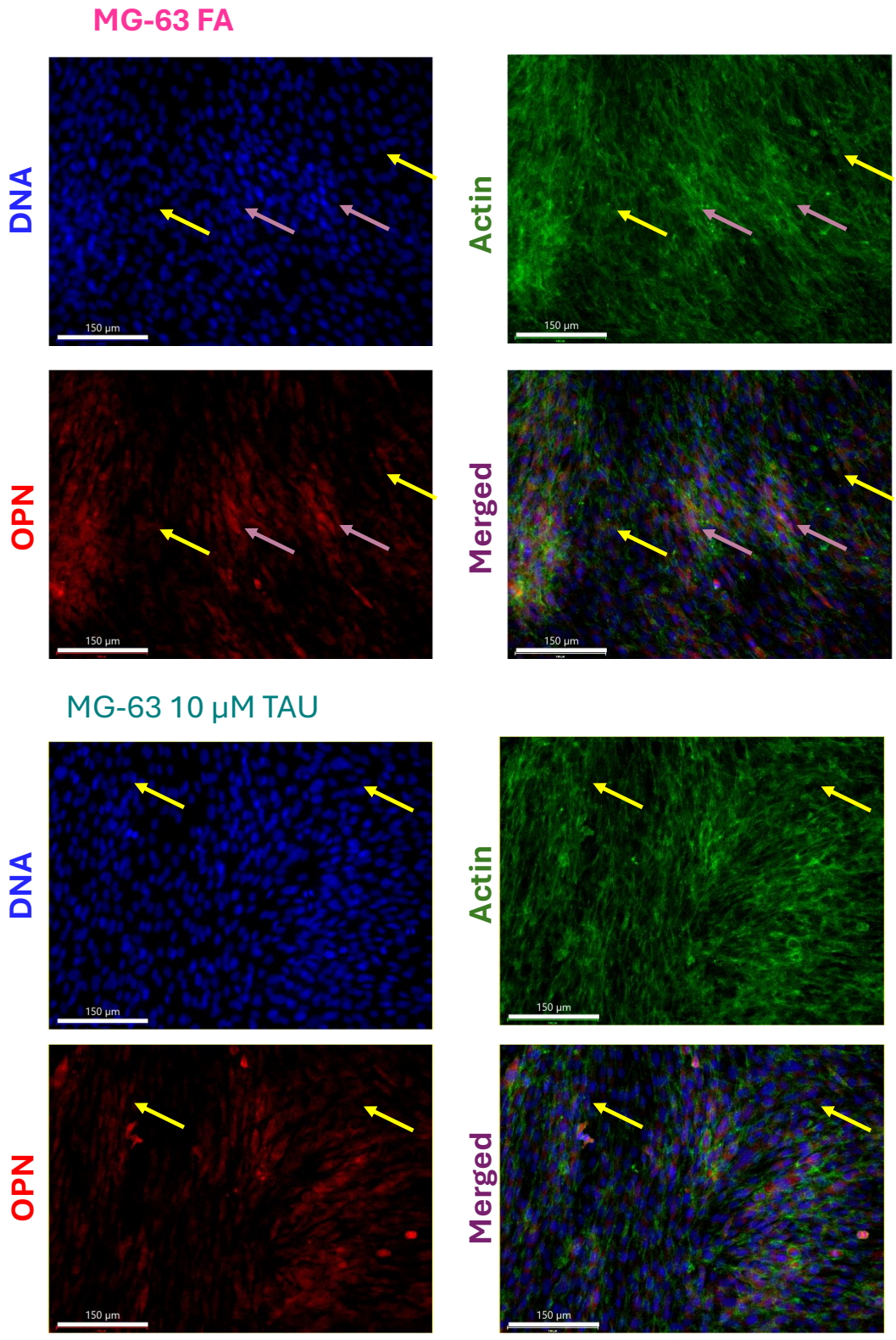

Figure 5.6: Immunofluorescence staining: MG-63 cells were treated with 10 µM CS, FA or TAU for 7 days. Cells were stained with DAPI (blue), phalloidin (green), and OPN (red), and imaged on EVOS at 20x magnification. Images processed with Imaris Viewer. Scale bars: 150 µm. Yellow arrows point to areas of decreased OPN expression, and pink arrows point to areas of increased OPN expression. N=1 biological replicate, N=2 experimental replicates.

Cells were treated with 10 μM CS, FA or TAU or with OGM for 7 days, and protein expression was quantified via ICW analysis. Cells appeared to differentiate under CS treatment, as seen by the upward trend in RUNX2 and OSX expression (Figure 5.7, (A)), despite the lack of statistical significance. FA treatment on the other hand showed the most statistically significant upregulation of RUNX2, with comparable action to OGM treatment. An upward trend in OSX was observed, with the caveat of a lack of statistical significance. TAU also drove differentiation in MG-63 cells, as observed by the statistically significant increase in RUNX2 protein expression, and the insignificant increase in OSX. Overall, all the tested conditions showed an increase in differentiation, with FA showing the most pronounced effect. These were exciting findings, as they indicated that the small molecules identified through metabolomics indeed presented the desired activity and drove differentiation. Fludrocortisone acetate was reported by Hodgkinson *et al*,[141] to drive enhanced, selective differentiation in MSCs, so it was interesting to observe that enhanced differentiation in the OS cells. Lack of upregulation was observed in certain biological repeats, so it was considered that studying a wider panel of proteins, over an extended period, may provide further information on cell phenotype, and differentiation trends. Having obtained information on protein expression during differentiation, gene expression was then studied via qPCR.

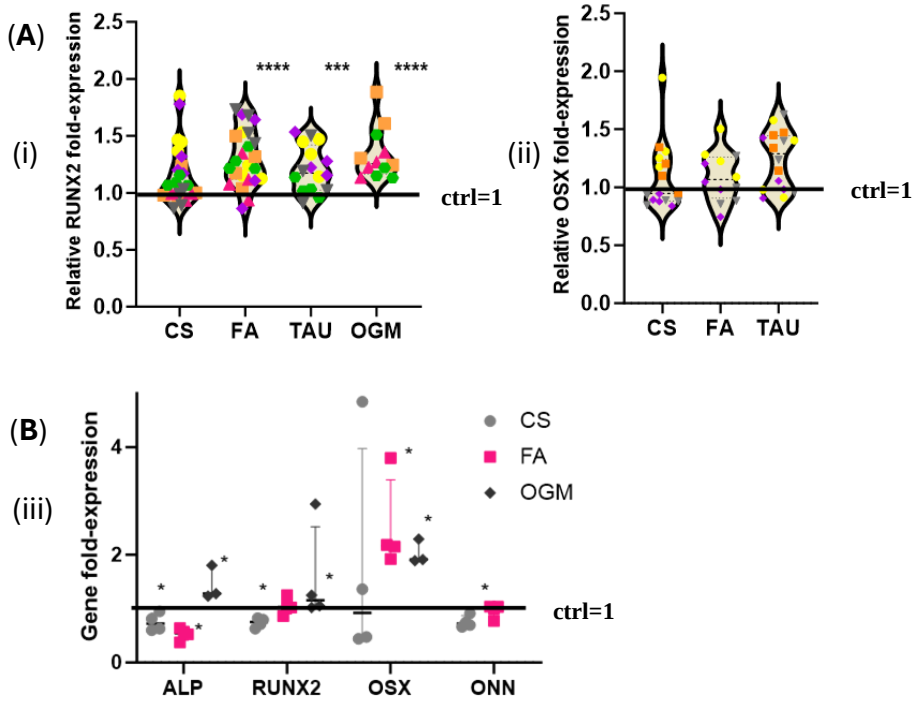

*Figure 5.7: MG-63 cells were treated with 10 μM CS, 10 μM FA, 10 μM TAU or OGM for 7 days. (A) Protein fold-expression was quantified against untreated D7 SAOS-2 control, via ICW analysis. (i) RUNX2 protein expression. Data collected from 6 separate experiments (ii) OSX protein expression. Data collected from 4 separate experiments. (B) Gene expression was quantified via qPCR. N=1 biological replicate. N=3-4 experimental replicates. Statistical analysis: Mann Whitney u test used to statistically compare treatments' protein or gene fold-expression vs control=1 (ns=blank=p>0.05, *=p<00.5, **=p<0.01, ***=p<0.001, ****=p<0.0001).*

More subtle changes were observed for the gene expression, compared to the protein expression (Figure 5.7 (B)). ALP levels were downregulated in the small molecule groups and upregulated in the OGM group. RUNX2 fold-expression was statistically significantly downregulated for the CS group, while protein expression was increased. For FA there were no changes in RUNX2 gene expression (B), but protein levels were found to be significantly upregulated (A). Protein expression is longer-lasting and downstream to gene expression,[321] which may explain in part the observed differences. OGM treatment was included as a positive control, and displayed increase in ALP, RUNX2 and OSX, which verified differentiation. Fludrocortisone acetate treatment drove significant upregulation of OSX expression, which is an indication of osteogenesis. Cells cultured in osteogenic medium too, as a positive control, showed more significant upregulation of osteogenic genes. Osteogenic medium contains the glucocorticoid dexamethasone, but also contains β-glycerophosphate, and ascorbic acid, which play an active role in differentiation and mineralisation.

Cell cycle distribution was then studied in MG-63 cells, to see how small molecules alter cell cycle. Modal analysis of the histograms revealed minimal shifting between the control and the treatments, while changes in distribution were evident (Figure 5.8 (i)). Analysis based on cell counts revealed that more cells were present in the control group population, compared to the treatments (ii). In the control group 73.2% of cells were in the G0/G1 phase, 4.84% of cells were in the S phase, and 18.67% of cells were in the G2/M phase (iii). MG-63 cells are partially differentiated, so the higher percentage of cells in the G0/G1 phase reflects that osteoblastic commitment. For CS treated cells there was an insignificant decrease in cells in the G1 phase, while there was a small increase of cells in the S and G2 phases. On the other hand, in FA treated cells there was an increase of cells in the G1 phase and decrease of cells in the S and G2 phase. FA supplementation previously showed the most consistent differentiation in MG-63 cells, amongst other small molecule treatments. These findings were in line with previous observations of cell cycle distribution in differentiated cells, where an increase of cells in G1 may signify osteogenic commitment. For TAU there was a decrease of cells in the G1 phase, and an increase of cells in the S and G2 phase. Overall, it was observed that small molecule driven differentiation drove some subtle changes in cell cycle distribution. Cell cycle dysregulation is widely documented in OS, with mutations in checkpoint kinases and cyclin kinases aiding cells to undergo uncontrolled proliferation.[322] This may in part explain the more discreet changes in OS cell cycle, as well as provide a link to cancer cells' resistance to terminal differentiation. Having studied the effect of 10 μM treatment on MG-63 cells, cells were then treated with CS, FA or TAU over a span of 28 days, and osteogenic protein expression patterns were studied at different timepoints.

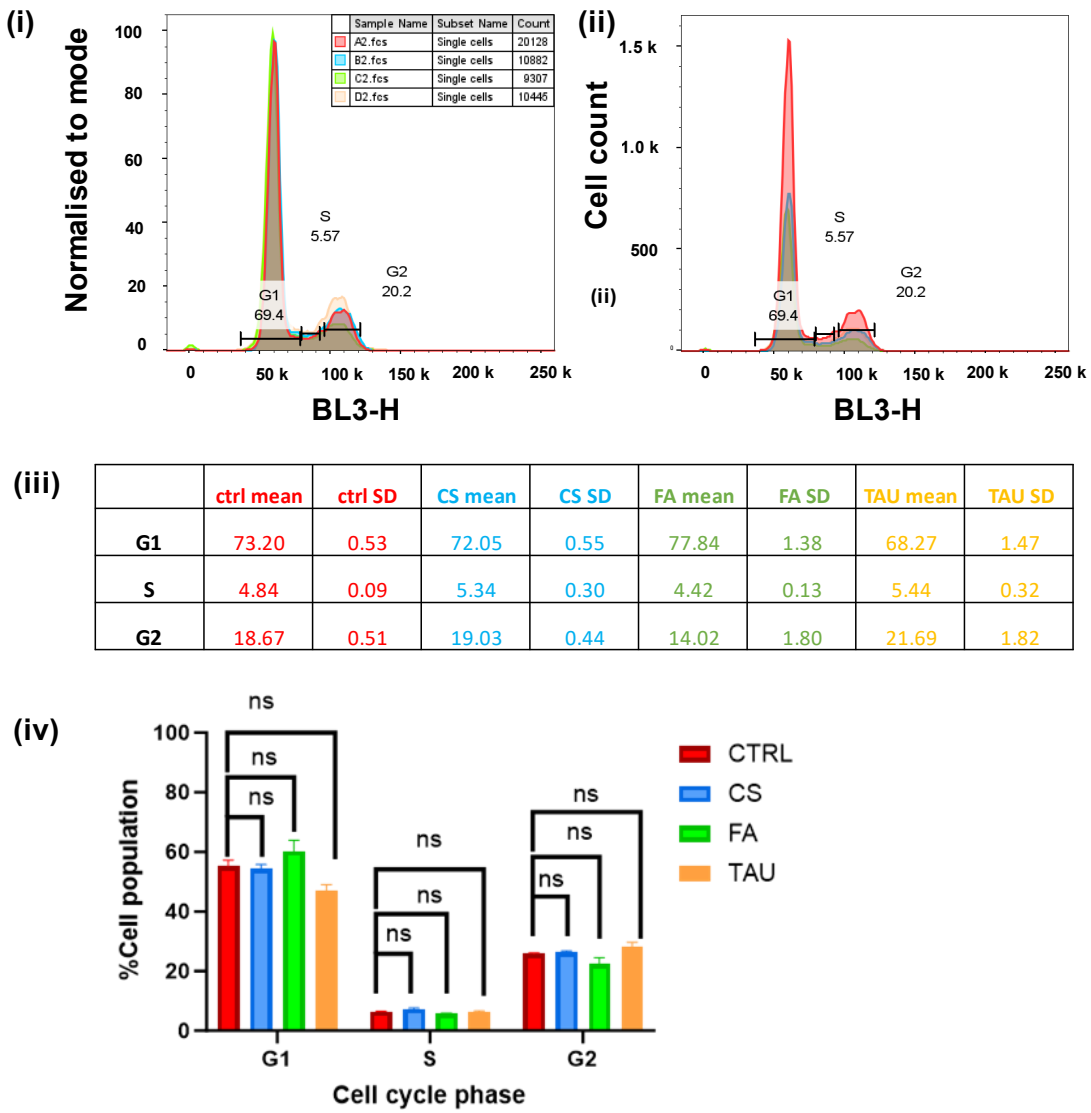

	ctrl mean	ctrl SD	CS mean	CS SD	FA mean	FA SD	TAU mean	TAU SD
G1	73.20	0.53	72.05	0.55	77.84	1.38	68.27	1.47
S	4.84	0.09	5.34	0.30	4.42	0.13	5.44	0.32
G2	18.67	0.51	19.03	0.44	14.02	1.80	21.69	1.82

Figure 5.8: PI cell cycle analysis via flow cytometry for MG-63 cells. (i) modal analysis (ii) cell count based analysis of histograms of BL3-H function of control (red), CS (blue), FA (green), and TAU (orange) were overlapped. (iii) table showing cell cycle distribution. (iv) bar chart of cell cycle distribution. N=1 biological replicate. N=2 experimental replicates, N=3 analytical replicates, Mann Whitney stats (ns)

5.4.3 Changes in osteogenic protein expression, after CS, FA or TAU treatment of MG-63 cells for 28 days

Having studied the effect of small molecule concentration on differentiation, a temporal protein expression study was then carried out. The aim was to study protein expression patterns over time for the different treatments and see how osteogenic regulator RUNX2 affected the expression of downstream proteins. OS cells are highly proliferative and tend to form confluent monolayers within a week of seeding. To limit variables, and differing stimuli that can affect the degree of differentiation, cells were allowed to form monolayers,

prior to small molecule treatment. This should in theory limit competing effects between cell proliferation and cell differentiation. RUNX2 and ONN were studied at more timepoints, while OSX, OPN and OCN were also tested, but with fewer datapoints, due to sample availability.

Previous studies on mechanical vs chemical stimulation on OS cells had shown that a 3-day treatment with OGM or NK was insufficient to drive differentiation, as discussed in chapter 3. In this instance OGM, CS and FA initiated differentiation after 3 days (Figure 5.9 (i)), with TAU displaying no increase in RUNX2. CS drove a gradual increase in RUNX2, with a dip at 7 days of treatment, and a peak in protein expression after 28 days. This earlier increase of RUNX2 after 3 days of treatment, followed by more limited upregulation after 7 days may explain previous observations of more limited protein increase after 7 days of CS treatment. ONN expression was also increased in a time-dependent manner in the CS group, with significant upregulation after 14 and 28 days. This was a strong indicator of maturation, which was confirmed by the slight upregulation of OPN and OCN, despite a lack of statistical significance. In the future it would be interesting to study protein expression of OPN, and OCN over more timepoints. FA treatment induced a gradual increase in RUNX2 protein expression, in a time-dependent manner. RUNX2 expression peaked at 14 days, and was then decreased after 28 days, albeit being higher than the control. Statistically significant increases were observed across the different timepoints, which further confirm the RUNX2 initiated differentiation. While ONN expression was upregulated in the CS, and TAU and OGM groups to a lesser degree, in a time dependent manner, ONN expression was downregulated in the FA group. OPN levels were slightly elevated, while OCN levels were downregulated after 28 days. Taurine was previously found to drive differentiation at a 10 μM concentration, after 7 days of treatment (Figure 5.3), but in this instance it was found that differentiation initiated after 14 days of treatment (Figure 5.9). RUNX2 expression was solely found to be upregulated at this later timepoint, while no increase in RUNX2 was detected after 3, 7 or 28 days. A statistically insignificant upregulation of OPN and OCN was observed after 28 days of stimulation, indicating that taurine drove cells to further mature, but did not drive terminal differentiation in OS cells. It was interesting to observe that while all treatments appear to drive differentiation, each condition displays its own expression pattern over time.

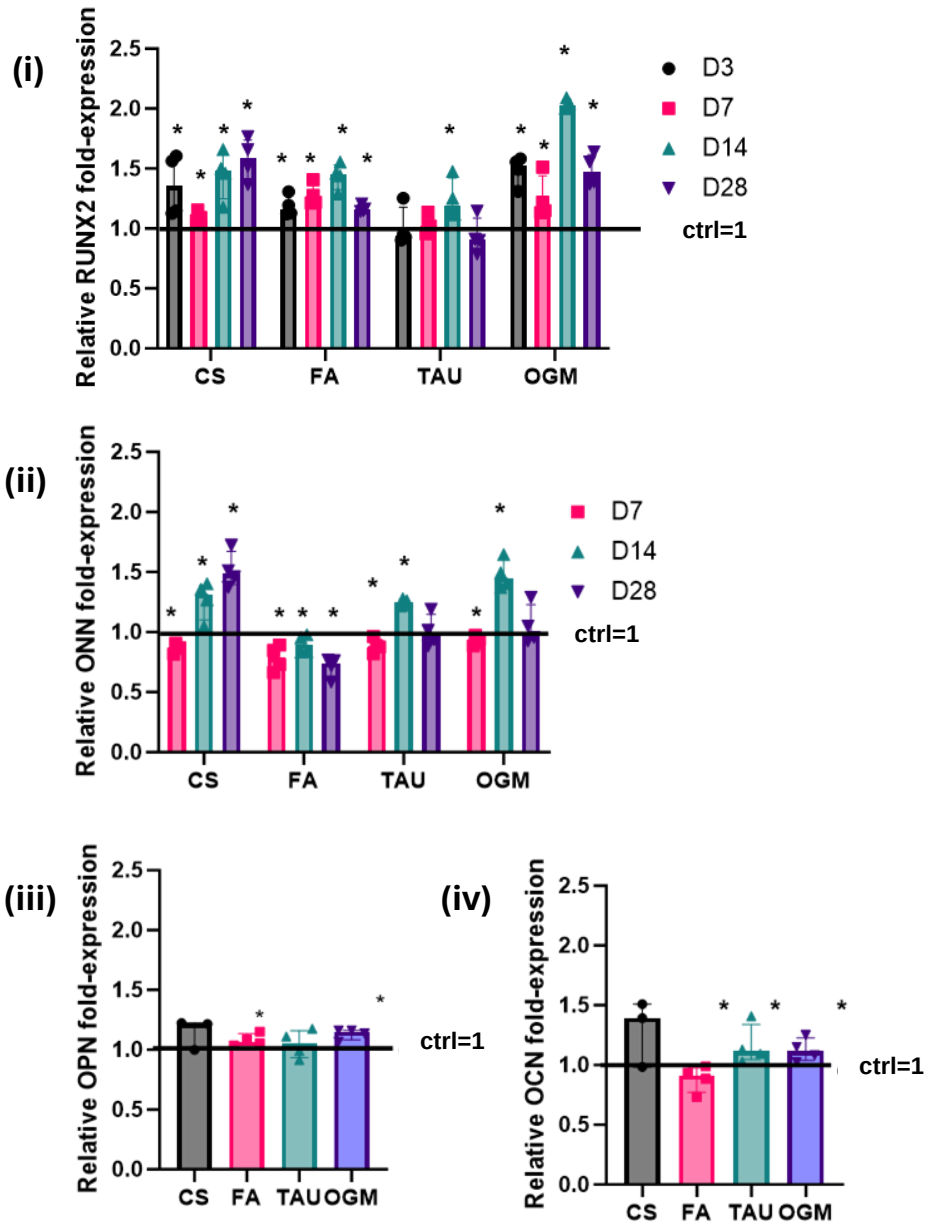

*Figure 5.9: ICW protein expression: MG-63 cells were grown into a monolayer and treated with 10 µM CS, FA or TAU over a month. Protein fold-expression assessed vs untreated MG-63 control of the respective timepoint. (i) RUNX2 expression was assessed after 3,7, 14 and 28 days. (ii) ONN expression was assessed after 7, 14, and 28 days. (iii) OCN expression was assessed after 28 days. (iv) OPN expression was assessed after 28 days. N=1 biological replicate, N=4 experimental replicates. Mann Whitney u test used to statistically compare treatments' protein fold-expression vs control=1 (blank=ns=p>0.05, *=p<0.05)*

5.4.4 Dose response experiment for SAOS-2

After observing that CS, FA and TAU induced osteogenic differentiation on MG-63 cells, in a concentration, and time-dependent manner, the same assays were applied for SAOS-2 cells. First the small molecules were tested at 0.1, 1 and 10 μM on SAOS-2 cells, and viability was assessed via the alamar blue assay, after 3 and 7 days. Cells were also trypsinised, and counted, and imaged via immunofluorescence, for the highest tolerated concentration, from the range that was tested. Small molecule treatment at the tested range of concentrations did not induce cytotoxicity. For CS viability was comparable to the control, after 3 days of treatment (Figure 5.10, (A)), and after 7 days there was a small decrease in alamar reduction after 0.1 μM of CS treatment. For FA treatment there was an increase in resazurin reduction, with increase in FA concentration, which may suggest increased proliferation. TAU did not appear to significantly alter cell viability, with comparable alamar reduction between the control and TAU observed after 3, and 7 days, except for downregulation from 0.1 μM treatment, after 7 days. High cell numbers were present across all the conditions, as evident by fluorescence staining, with confluence observed across all conditions (C). It was interesting to observe that while treatment with osteogenic medium drove extensive cell death in SAOS-2 cells, chemical stimulation using CS, FA or TAU did not induce the same cytotoxicity. Further assays were carried out after 7 days of treatment with 10 μM CS, FA and TAU, since cells tolerated small molecule induction. Cell counts showed that more cells were collected for the different treatments vs the control (Figure 5.10 (B)), with the limitation of small number of replicates, and cell detachment. Fluorescent imaging confirmed that high cell numbers were present across all groups, including the control (Figure 5.10 (C)). Monolayers were formed after 7 days, so cell crowding was observed for the different treatments. Overall, it was evident that the small molecules did not induce cytotoxicity in SAOS-2 cells, which was also observed for the less mature MG-63 cells.

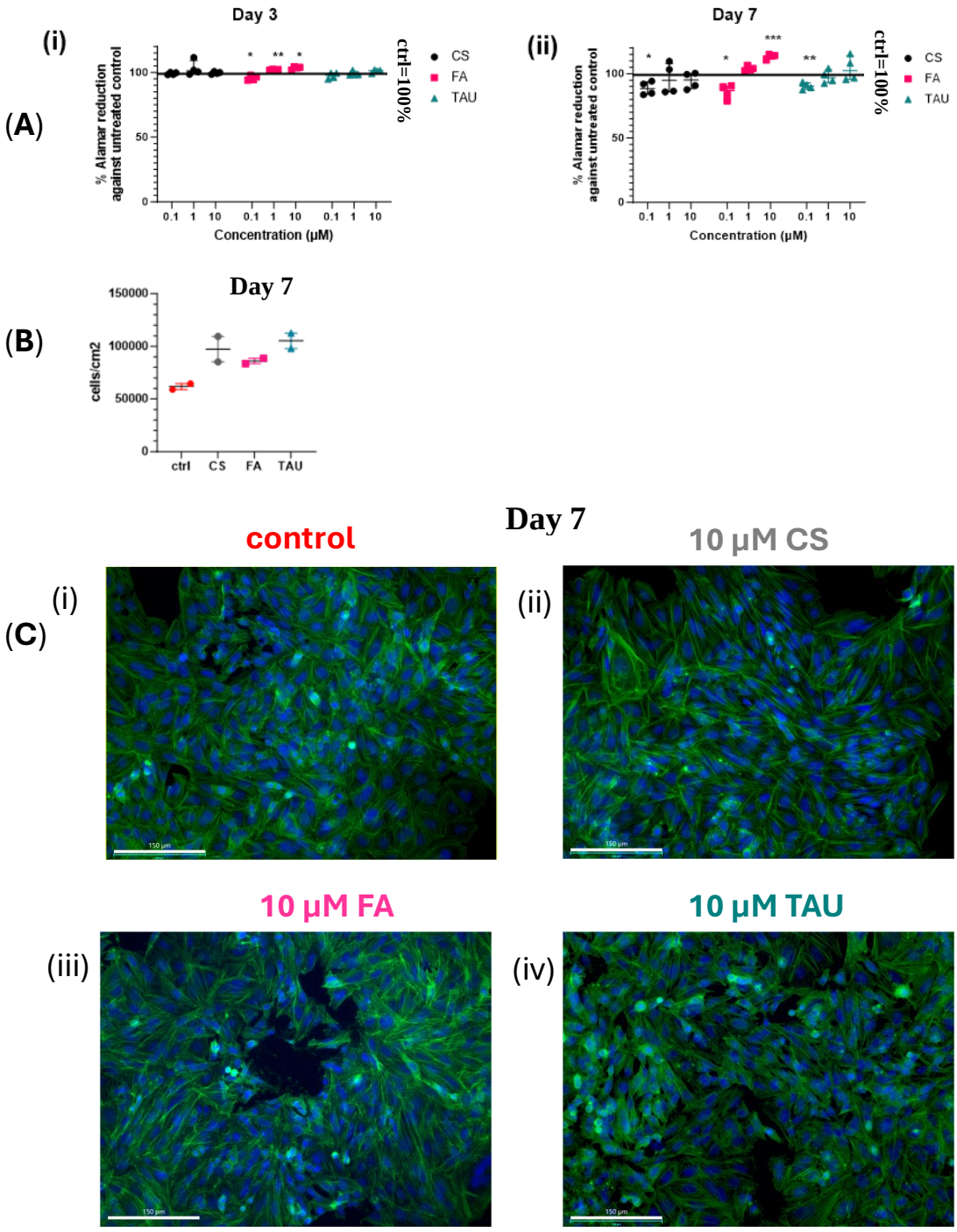

Figure 5.10: Concentration effect of CS, FA and TAU on SAOS-2 viability: ***A)*** *%Alamar reduction of CS, FA and TAU against untreated SAOS-2 control, of (i) D3 and (ii) D7 timepoints. N=2 experimental replicates, N=2 analytical replicates, Welch's adjusted t-test used to statistically compare treatments' alamar reduction vs control=100% (p>0.05=blank=ns, p<0.05=*, p<0.01=**, p<0.001=***). (B) Cell numbers after trypsinisation. Cells were treated for 7 days with 10 µM of CS, FA or TAU, trypsinised and counted., N=1 biological replicate, N=2 experimental replicates (C) Fluorescent images showing cell distribution during differentiation. Cells were (i) untreated or treated with 10 µM of (ii) CS, (iii) FA or (iv) TAU for 7 days. DAPI (blue) stained nuclei, and phalloidin (green) stained actin cytoskeleton. Scale bar= 150 µm. N=1 biological replicate, N=6 experimental replicates.*

After confirming cell viability at the tested range of concentrations, differentiation was assessed by quantifying RUNX2 and OSX protein expression via ICW. CS treatment appeared to drive differentiation in SAOS-2 cells (Figure 5.11). 0.1 µM treatment did not adequately promote differentiation, as apart from a small increase in RUNX2, protein expression was comparable between the control and the small molecule. At 1 µM there was a statistically significant increase in RUNX2, and a small increase in OSX. At 10 µM a statistically significant increase in both RUNX2, and OSX was observed, so the 10 µM concentration was chosen for future experiments. Overall concentration dependent osteogenesis was observed for CS treatment.

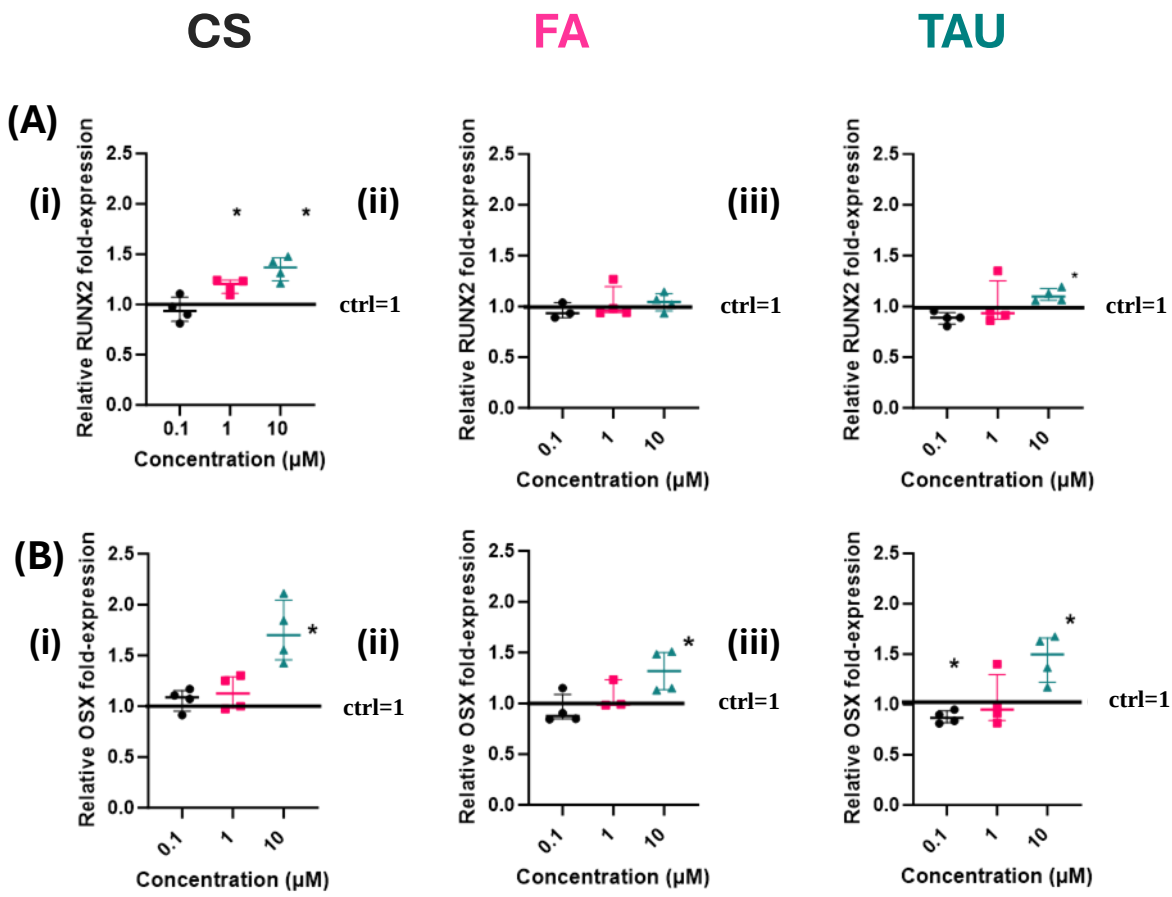

Figure 5.11: ICW protein expression. Protein fold-expression of (A) RUNX2 and (B) OSX was normalised against untreated SAOS-2 control treatment after 7 days. SAOS-2 cells were treated with 0.1, 1 or 10 µM of (i) CS, (ii) FA or (iii) TAU. Mann Whitney u test used to statistically compare treatments' protein fold-expression vs control=1 (=p<0.05, blank=ns=p>0.05), N=1 biological replicate, N=4 experimental replicates*

FA supplementation did not trigger upregulation of RUNX2 or OSX at 0.1 and 1 µM. Therefore, these lower concentrations were ineffective in driving further maturation. At 10 µM a statistically significant increase in OSX was observed, therefore FA treatment was shown to cause differentiation. High doses of glucocorticoids can have osteolytic effects,[323] so a maximum concentration of 10 µM was tested for differentiation for cholesterol sulfate and fludrocortisone acetate.

For TAU there was no increase of osteogenic markers at lower concentrations, but RUNX2 and OSX were significantly upregulated, at the highest concentration. Curiously while differentiation was observed at the highest tested concentration, a small decrease in OSX was observed in 0.1 µM treated SAOS-2 cells, which may indicate dedifferentiation. It was therefore considered that the identified metabolites from the metabolomic screen, and related structures, played an active role in osteogenesis of OS cells, in a concentration dependent manner. Moreover, FA was also found to drive differentiation. These observations were in line, with results on MG-63 cells, which also strongly indicated differentiation occurred in a concentration dependent manner, with 10 µM being the optimal concentration evaluated.

Overall, a dose dependent increase in osteogenic markers was observed for the different treatments, with a concentration of 10 µM showing the most statistically significant increase of osteogenic proteins. CS appeared to show a larger increase in RUNX2 and OSX at the highest concentration, compared to FA and Taurine. Moreover, OSX was increased for all 3 of the small molecules, at the highest concentration, which would indicate differentiation. OSX is required to initiate differentiation in stem cells, so the activation of this osteogenesis regulator was a good indicator of osteogenesis. RUNX2 is required, to activate OSX expression during osteoblastogenesis,[324] so the smaller increase in RUNX2, compared to OSX is understandable.

5.4.4 Effect of small molecule 10 µM treatment on SAOS-2 cells

Having decided that a 10 µM concentration was the most effective at driving differentiation, further assays were then used to characterise cell response, to the small molecules. Immunofluorescence was used to study protein expression, observe whether the marker was abundantly expressed, and visualise localisation. While preliminary observations on relative abundance, compared to the control were made, immunofluorescence was solely used qualitatively. qPCR and ICW later quantified osteogenic genes and proteins respectively.

As discussed in chapter 3, the osteogenesis regulator RUNX2 is highly expressed in SAOS-2 cells and located in their nucleus. This nuclear localisation relates to SAOS-2's more mature phenotype, compared to MG-63 cells, where RUNX2 localisation was perinuclear or cytoplasmic. Arrows were used to point areas of higher protein expression. The untreated control highly expressed RUNX2, with some cells within the population showing upregulation (Figure 5.12). Steroid treatment with CS and FA showed signs of increased RUNX2 expression, which is an indicator of maturity. Taurine treatment also seemed to drive differentiation in the cells, as evident by the qualitative observation of RUNX2 increase. Though no quantitative measurements were made, overall RUNX2 was found to be abundant across all conditions, with some increase in RUNX2 observed, as previously seen through ICW (Figure 5.11).

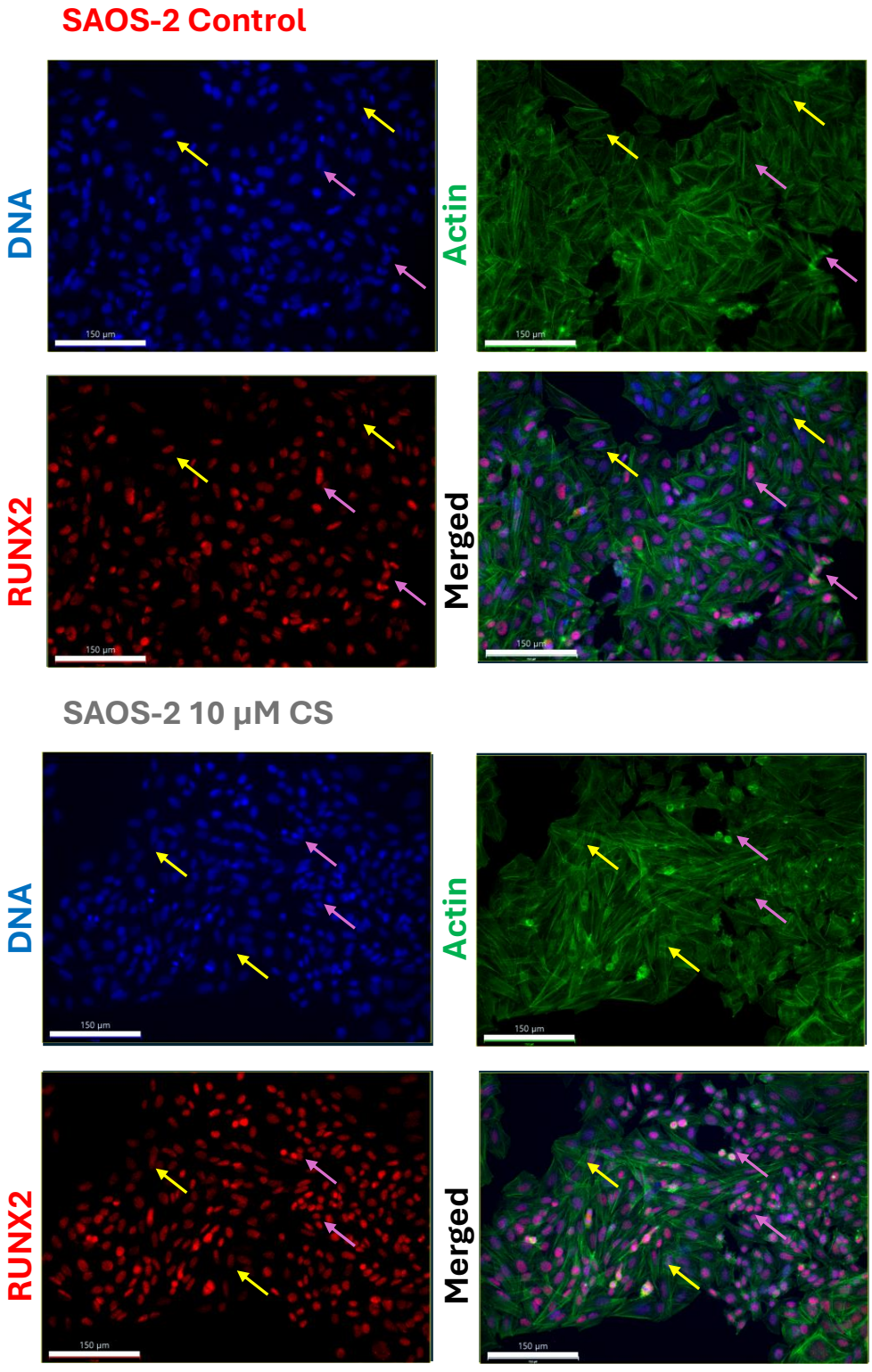
SAOS-2 Control
DNA
Actin
RUNX2
Merged
SAOS-2 10 µM CS
DNA
Actin
RUNX2
Merged

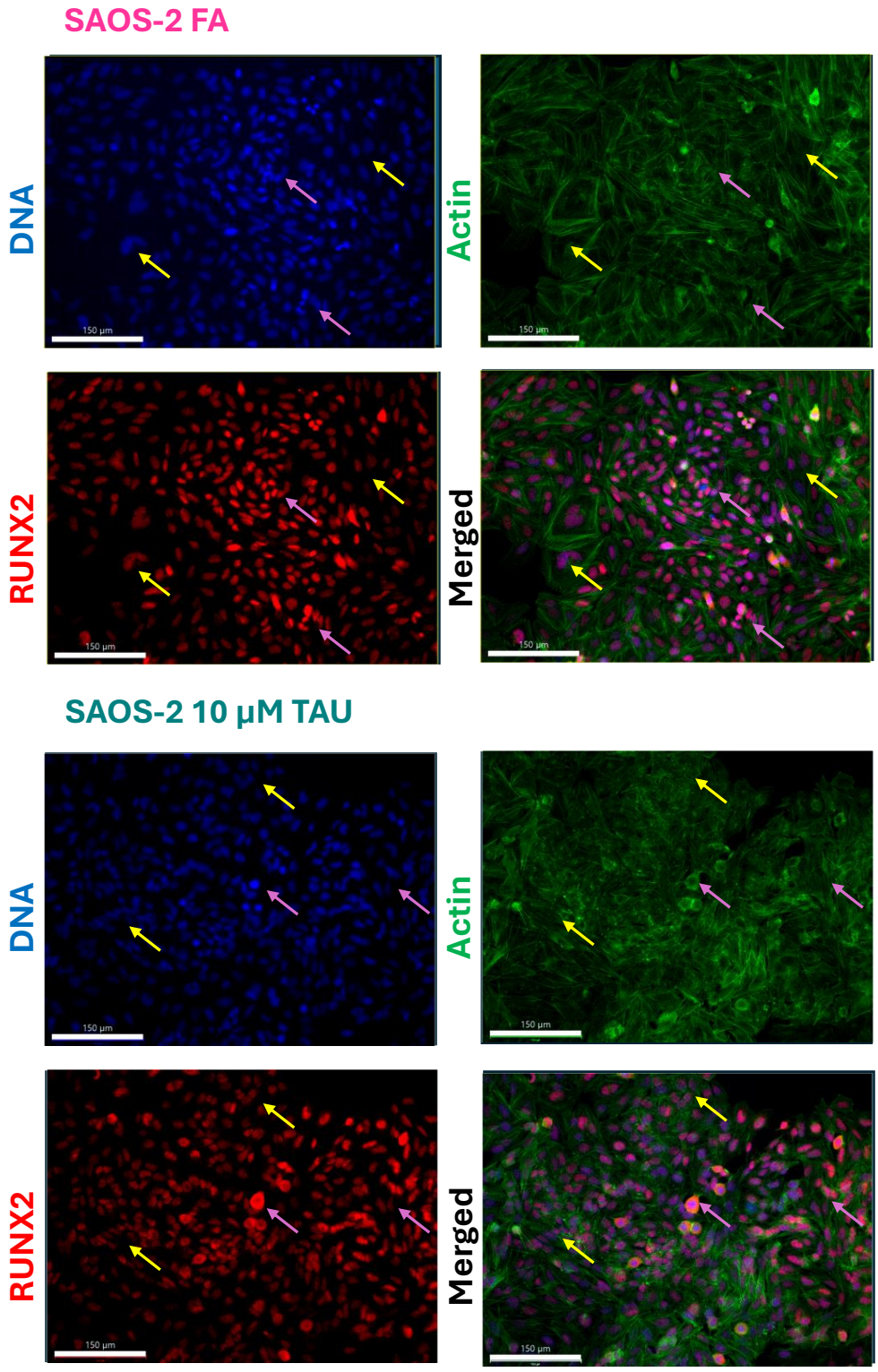

Figure 5.12:Immunofluorescence staining: SAOS-2 cells were treated with 10 µM CS, FA or TAU for 7 days. (n=2) Cells were stained with DAPI (blue), phalloidin (green), and RUNX2 (red), and imaged on EVOS at 20x magnification. imaged on EVOS microscope at 20x magnification. Images processed with Imaris Viewer. Scale bars: 150 µm. Yellow arrows point to areas of decreased RUNX2 expression, and pink arrows point to areas of increased RUNX2 expression. N=1 biological replicate, N=2 experimental replicates.

OSX was also found to be situated in the nucleus of SAOS-2 cells both in treated and untreated groups (Figure 5.13), as previously discussed in chapter 3. The protein was expressed abundantly, though general observations suggested that not all cells within the population expressed OSX. Again, a visual observation of OSX upregulation from the different treatments was made, but this would have to be corroborated by different quantitative assays. It is however in line with preliminary observations from ICW.

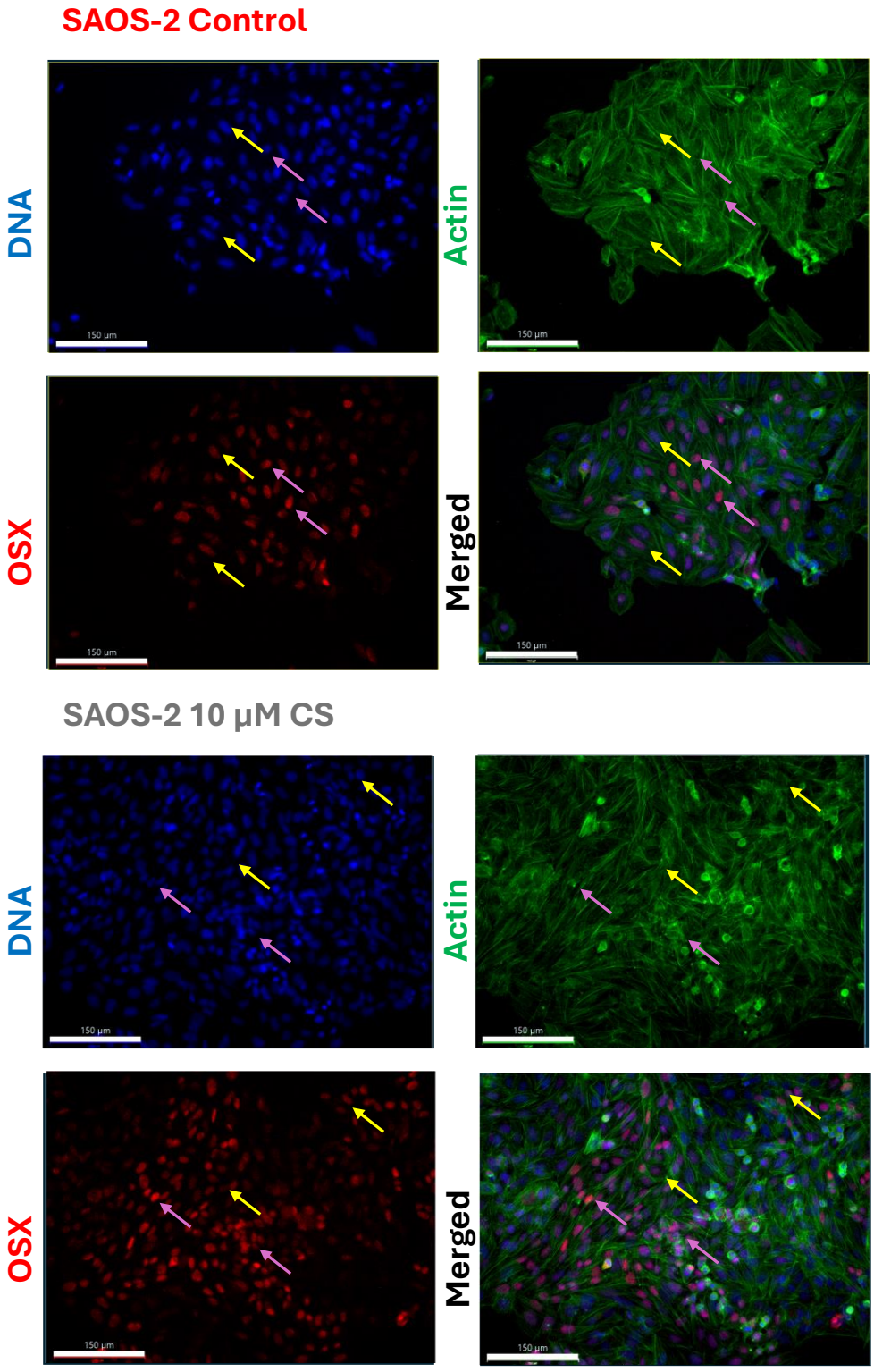
SAOS-2 Control
DNA
Actin
OSX
Merged
150 µm
SAOS-2 10 µM CS
DNA
Actin
OSX
Merged
150 µm

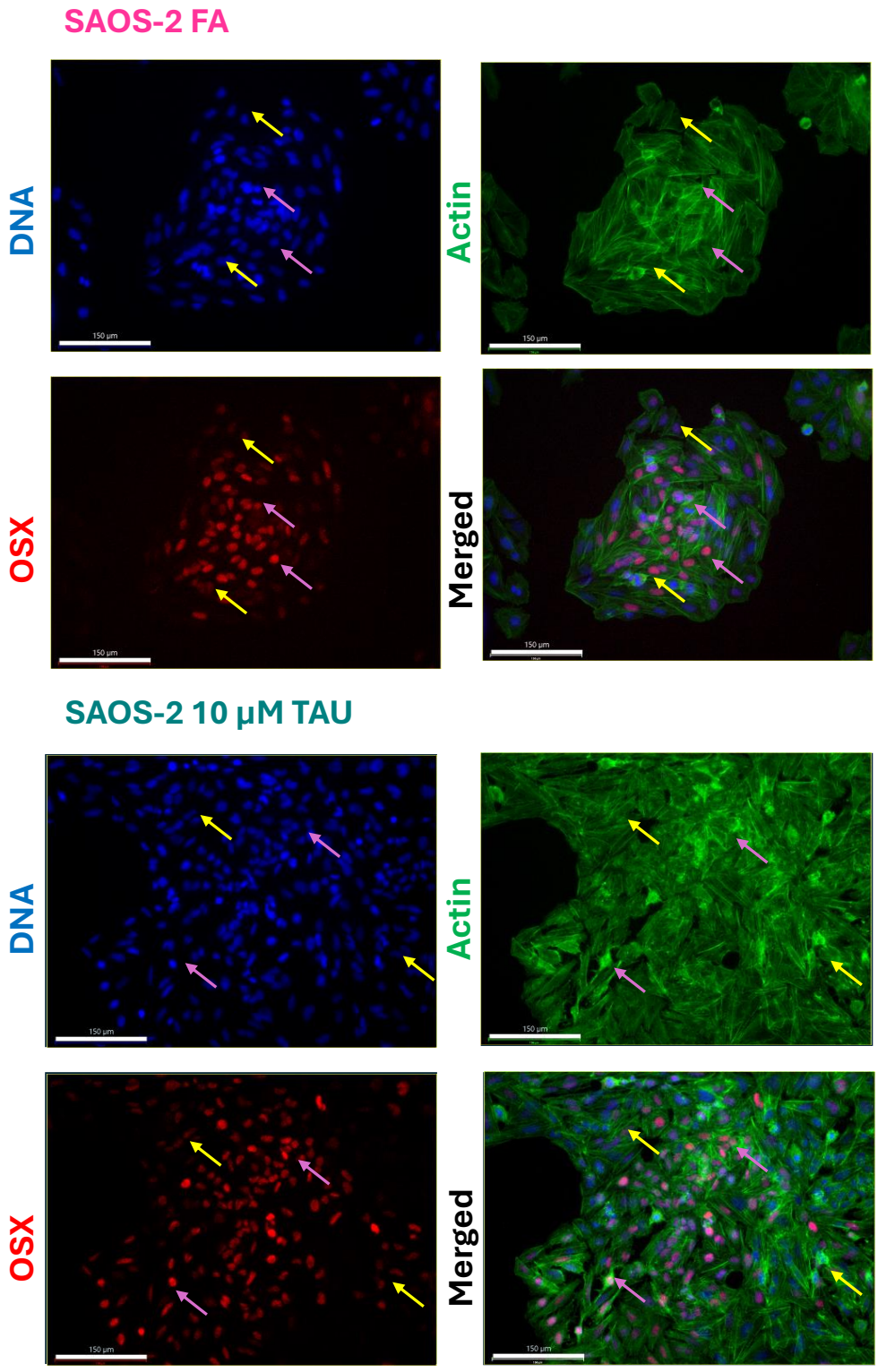

Figure 5.13: Immunofluorescence staining: SAOS-2 cells were treated with 10 µM CS, FA or TAU for 7 days. Cells were stained with DAPI (blue), phalloidin (green), and RUNX2 (red), and imaged on EVOS at 20x magnification. imaged on EVOS microscope at 20x magnification. Images processed with Imaris Viewer. Scale bars: 150 µm. Yellow arrows point to areas of decreased OSX expression, and pink arrows point to areas of increased OSX expression. N=1 biological replicate, N=2 experimental replicates.

OPN localisation was either perinuclear or cytoplasmic (Figure 5.14). Expression of this mature marker, that is an indicator of mineralisation and maturation, appeared to be less abundant than RUNX2 or OSX. CS treatment and FA treatment appeared to drive upregulation of OPN compared to the control, with areas of cluster formation, also displaying increased expression.

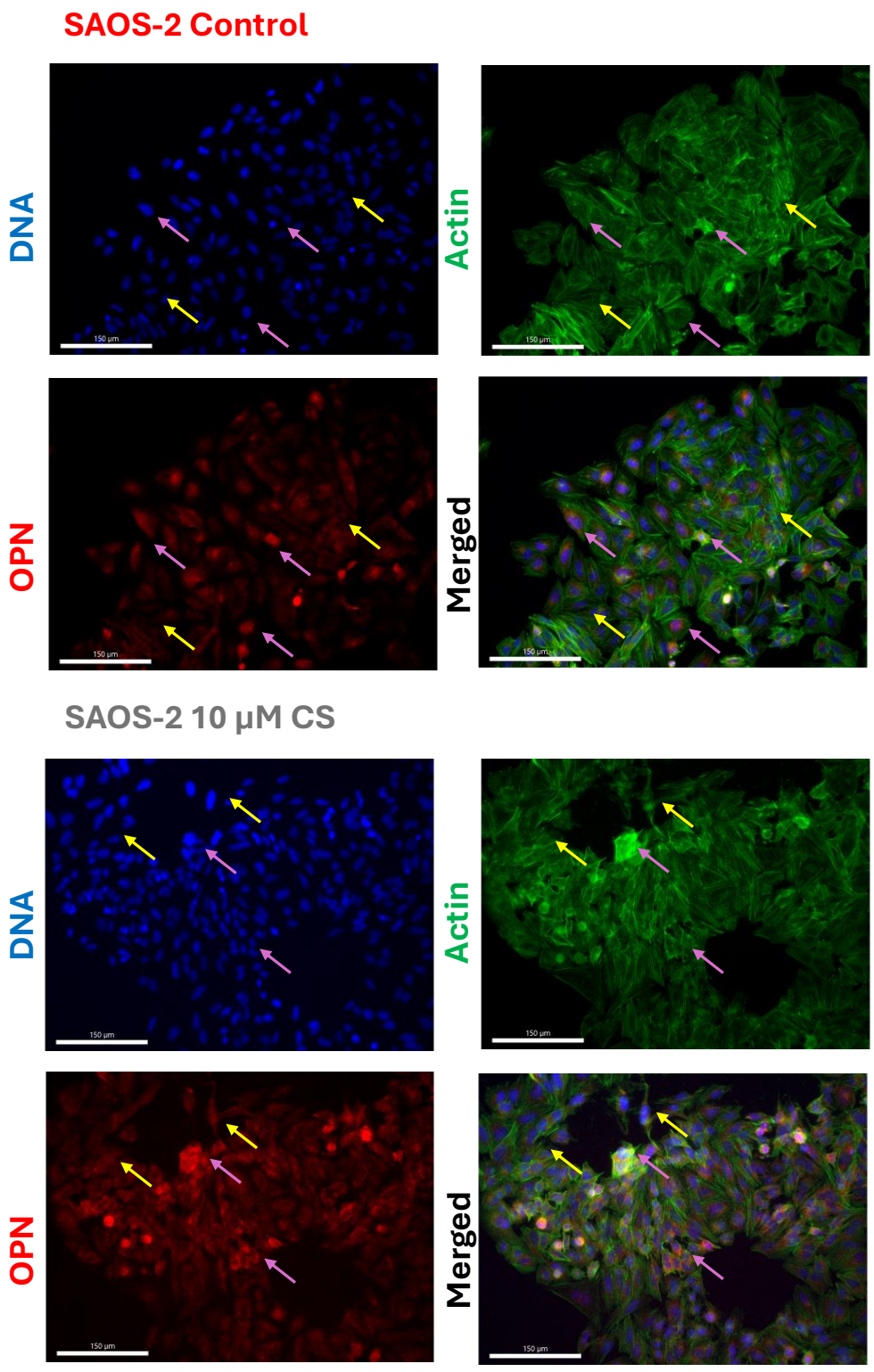
SAOS-2 Control
DNA
Actin
OPN
Merged
SAOS-2 10 µM CS
DNA
Actin
OPN
Merged

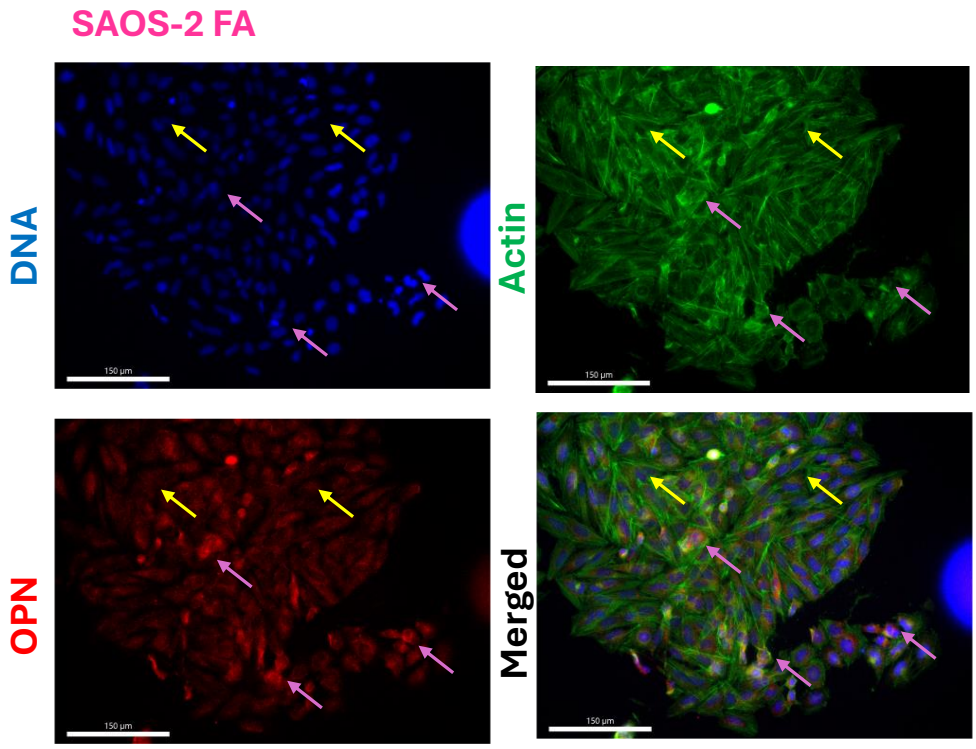

Figure 5.14: Immunofluorescence staining: SAOS-2 cells were treated with 10 µM CS or FA for 7 days. Cells were stained with DAPI (blue), phalloidin (green), and OPN (red), and imaged on EVOS at 20x magnification. imaged on EVOS microscope at 20x magnification. Images processed with Imaris Viewer. Scale bars: 150 µm. Yellow arrows point to areas of decreased OPN expression, and pink arrows point to areas of increased OPN expression. N=1 biological replicate, N=2 experimental replicates.

Protein expression was variable within cell populations, which would indicate cells were differentiated to varying degrees. RUNX2 and OSX were situated in the nucleus, which was contrary to observations in MG-63 cells, which represent a more immature phenotype. OPN and ONN localisation was perinuclear or diffuse cytoplasmic, and expression increased in areas of cluster formation, potentially due to macromolecular interactions, and mineralisation/matrix influence.[213]

After assessing protein localisation and abundance via immunofluorescence, ICW was carried out, to quantify protein expression, and qPCR was carried out to quantify gene expression. There was a greater focus on CS, and FA, due to particular interest in steroid driven differentiation. 10 µM CS induced statistically significant upregulation of RUNX2, while there was a trend towards increased OSX expression, which would confirm differentiation. 10 µM FA showed the most statistically significant upregulation of RUNX2, and statistically significant upregulation of OSX. TAU also drove a significant increase in RUNX2, and even more statistically significant upregulation of OSX. These findings were exciting, as they confirmed that SAOS-2 cells were maturing under those conditions and

combined with MG-63 results confirmed that the identified metabolites, and FA were bioactive and involved in differentiation. FA showed the most significant upregulation at this timepoint, which corroborated were findings in MG-63 cells, and Hodgkinson's finding in MSCs.[141]

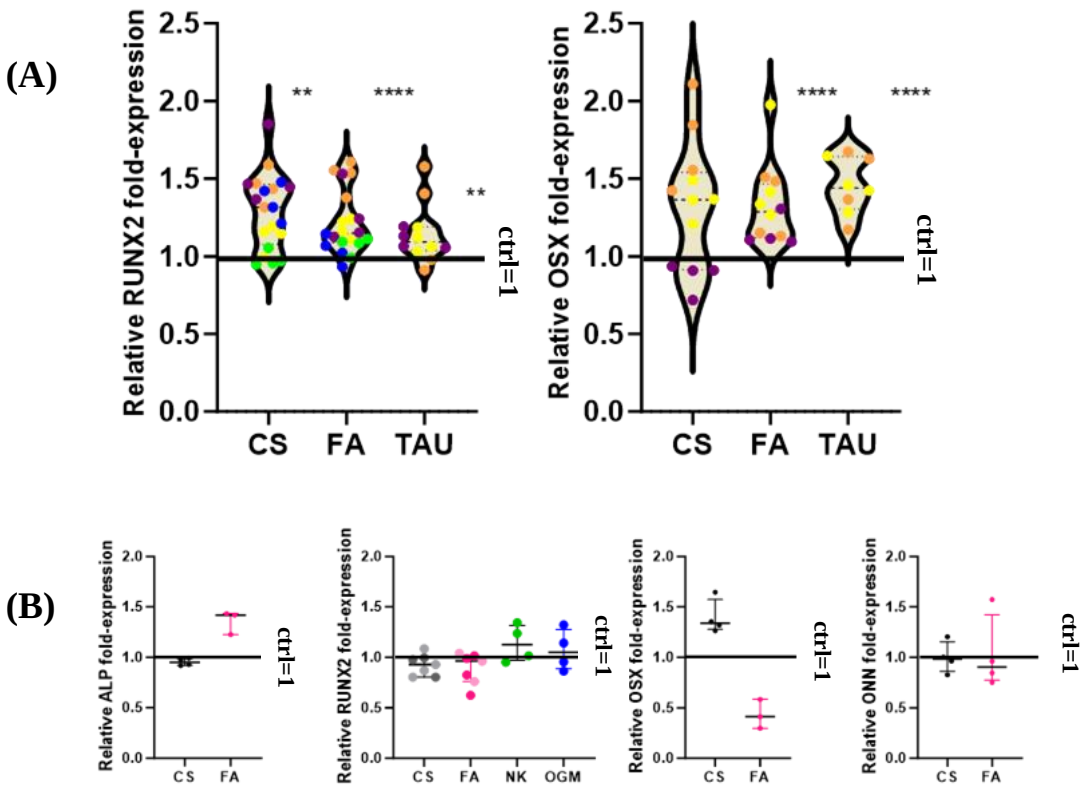

Figure 5.15: SAOS-2 cells were treated with 10 μM CS, 10 μM FA, 10 μM TAU or OGM for 7 days. ***(A)*** *Protein fold-expression vs untreated SAOS-2 D7 control was assessed via ICW analysis.* ***(i)*** *RUNX2 protein expression. n=5 biological replicates, n=4 experimental replicates* ***(ii)*** *OSX protein expression. n=3 biological replicates, n=4 experimental replicates* ***(B)*** *Gene expression was quantified via QPCR. N=3-4 experimental replicates, 2 analytical replicates. For ICW and qPCR Statistical analysis: Mann Whitney u test used to statistically compare treatments' protein or gene fold-expression vs control=1 (p<0.05=*, p<0.01=**, p<0.001=***, p<0.0001=****, blank: p>00.5=ns)*

Some upward trends in osteogenic genes were observed from qPCR analysis, indicating differentiation, though results were not statistically significant, according to the Mann Whitney test. An increase in alkaline phosphatase (ALP) fold-expression was observed for cells treated with 10 μM FA, despite a lack of statistical significance (Figure 5.15 (B)). ALP is highly expressed in SAOS-2 cells and is typically upregulated after 14 days of osteogenic differentiation of MSCs, so ALP increase is an indicator of relatively later differentiation. For CS, ALP levels remained unchanged. For RUNX2 it is interesting to note that significant upregulation in protein expression was induced across all treatments, but gene levels

remained comparable to the control. This was also observed for CS, and FA in MG-63 cells. The osteogenesis regulator OSX was upregulated in CS treated cells, which would suggest differentiation. OSX was downregulated in FA treated cells. Both treatments had shown trends of upregulation of OSX protein expression, but FA had shown most significant upregulation, so it is possible that gene expression had occurred earlier. ONN expression was similar for the control and the treatments. A more thorough investigation into a wider panel of osteogenic genes could offer more information on the phenotype of the small molecule treated cells, in the future. As previously discussed for MG-63 cells, discrepancy between protein and gene data is common, with the more short-lived gene transcription requiring the right timing, to observe the changes.[321] Overall, though changes in gene expression were more subtle, small molecule treatment appears to drive osteogenic differentiation in SAOS-2 cells, and MG-63 cells.

Upon observing that 7 days of 10 μM CS, FA and TAU treatment drove differentiation in SAOS-2 cells, cell cycle distribution was then studied via propidium iodide (PI) based flow cytometry. As seen in Figure 5.10 (B) cells were counted before cell cycle analysis. Collected cell numbers for the small molecules were higher than the control, so cell numbers were adjusted, to obtain comparable cell populations for flow cytometry. As observed for MG-63 cells, the highest portion of SAOS-2 cells were in the G0/G1 phase, illustrating the differentiation state of the cancer cells (Figure 5.16). Modal analysis (i) revealed an overlap between conditions, with limited shifting in the G1 phase, which was contrary to observations from nanokicking SAOS-2, though subtle change in G2 distribution was observed. Analysis based on number of cells (height of histogram) (ii) showed differences in height for the different cell cycle phases, depending on the treatment. In the control group 63.3% of cells were in the G0/G1 phase, 8.19% of cells were in the S phase, and 24.05% of cells were in the G2/M phase (iii). Small molecule treatment induced very subtle changes in cell cycle distribution, with a small decrease of cells in the G2 phase for CS, a decrease of cells in the G1 phase for FA, and a small increase of cells in the G1 phase and decrease of cells in the G2 phase for TAU. Overall limited observations could be made for the different treatments in terms of cell cycle distribution, but cells did appear to differentiate under those conditions. As previously stated, cell cycle is dysregulated in OS cells, which may also be linked to observed aberrant differentiation.

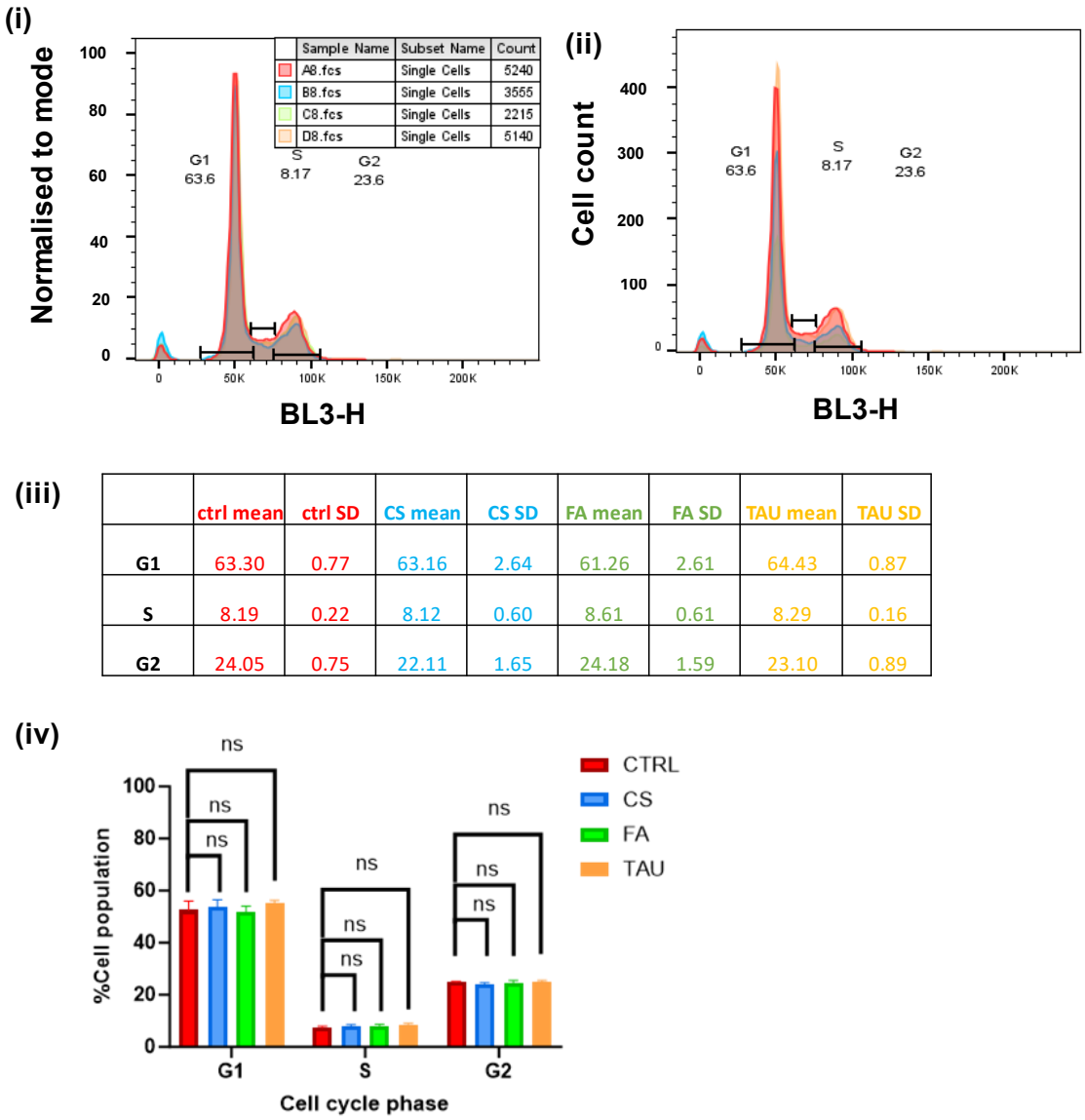

	ctrl mean	ctrl SD	CS mean	CS SD	FA mean	FA SD	TAU mean	TAU SD
G1	63.30	0.77	63.16	2.64	61.26	2.61	64.43	0.87
S	8.19	0.22	8.12	0.60	8.61	0.61	8.29	0.16
G2	24.05	0.75	22.11	1.65	24.18	1.59	23.10	0.89

Figure 5.16: PI cell cycle analysis via flow cytometry. Histograms (i) modal mode, (ii) height mode, of BL3-H function of control (red), CS (blue), FA (green), and TAU (orange) were overlapped. (iii) table showing cell cycle distribution for treatments. (iv) bar chart of cell cycle distribution. No statistical significance from Mann-Whitney stats.

5.4.5 Changes in osteogenic protein expression, after CS, FA or TAU treatment of SAOS-2 cells for 28 days

After deducing that differentiation occurred in a dose-dependent manner for different small molecule treatments, and further studying cell response at a 10 µM concentration, the temporal influence on differentiation was assessed. SAOS-2 cells were grown into monolayers, to allow for more uniform differentiation, and treated with 10 µM CS, FA or

TAU for 3, 7, 14 or 28 days. Protein response was assessed for different osteogenic markers, via the ICW assay.

Overall, differentiation appeared to occur in a time-dependent manner, though upregulation of osteogenic proteins was not as consistent in SAOS-2 cells, as it was in MG-63 cells. In agreement with previous observations on NK and OGM treated cells, 3 days appeared to be insufficient to drive osteogenic differentiation in SAOS-2 cells. CS treatment drove a small increase in RUNX2 after 7 days, which indicates differentiation, while protein expression was comparable to the control for the other timepoints (Figure 5.17). CS treatment also triggered statistically significant OSX upregulation after 14 days of treatment, which is a strong indicator of differentiation. No increase in downstream protein expression was observed, with unchanged levels of ONN, OPN and OCN, which may indicate a lack of terminal differentiation. 10 μM FA treatment of SAOS-2 cells had shown to effectively drive differentiation in the SAOS-2 cell line, and in this instance a gradual increase in RUNX2, with a peak after 28 days was observed (Figure 5.17). FA treatment caused the largest fold-increase of RUNX2, though this didn't appear to trigger an increase in expression of downstream proteins, including OSX, ONN, OCN and OPN. TAU triggered statistically significant upregulation from day 7 onwards, but fold-increase was not as large as for FA. A small increase in OSX was also observed after 14 days. Previous findings have corroborated that CS, FA and TAU can drive osteogenesis in SAOS-2, as evident by upregulation of RUNX2, and OSX so this response was more limited than previous observations. Changes in osteogenic proteins were also more limited than what was seen for MG-63 cells, where more significant increases in RUNX2 and ONN were observed, but it was still apparent that protein expression changed over time for SAOS-2.

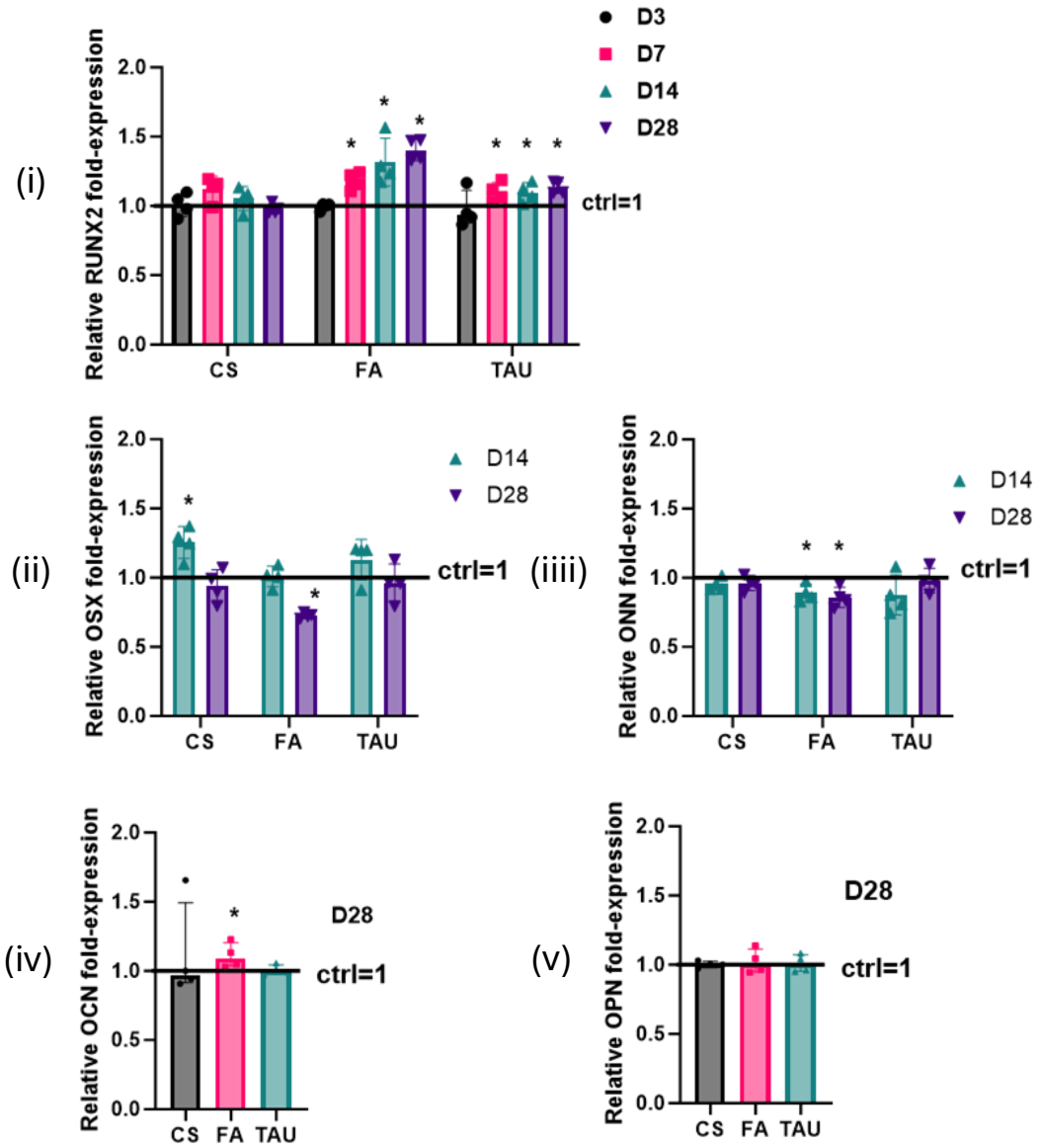

*Figure 5.17: SAOS-2 cells were grown into a monolayer and treated with 10 µM CS, FA or TAU. Osteogenic markers were analysed over 28 days via ICW analysis. Protein expression was normalised against CellTag, and the fold-expression is reported against untreated SAOS-2 control, for the respective protein and timepoint. (i) RUNX2 expression was assessed after 3,7, 14 and 28 days. (ii) OSX expression was assessed after 14 and 28 days. (iii) ONN expression was assessed after 14, and 28 days. (iv) OCN expression was assessed after 28 days. (v) OPN expression was assessed after 28 days. N=1 biological replicate, N=4 experimental replicates. Mann Whitney u test used to statistically compare treatments' protein fold-expression vs control=1 (blank=ns=p>0.05, *=p<0.05).*

Overall CS, FA and TAU appeared to promote a more osteoblastic phenotype in faster-proliferating MG-63 cells, and the more mature SAOS-2 cells, in a concentration and temporal dependent manner. The small molecules did not appear to induce cytotoxicity in the OS cells, at the tested concentrations, while both cell lines had typically reached

confluence, within 7 days. At the day 7 timepoint there was an upward trend in RUNX2 protein expression, for CS treated MG-63 cells. A timepoint study revealed that CS caused most significant differentiation, between the different treatments, with initial upregulation at day 3, a dip at day 7, and increased RUNX2, at day 14, and 28. SAOS-2 cells present a more mature phenotype that MG-63 cells, and thus innately express osteogenic markers more abundantly, which may explain the limited observations in later osteogenic markers. This timepoint experiment was carried out once, both for MG-63 and SAOS-2 cells, so repeating this experiment, and including more osteogenic proteins, across all timepoints would be worth investigating in the future.

5.5 General discussion

The aim of this chapter was to assess whether the identified small molecules from the metabolomic screen, including metabolites, and related compounds, presented bioactivity, and to study the cell behaviour under treatment. The fact that metabolomics indicated TAU and CS may be involved in mechanically induced osteogenic differentiation, and drove an increase in osteogenic proteins, indicates that they are bioactive metabolites, with a role in differentiation. Moreover, seeing that conditions that have been proven to drive differentiation of MSCs, including CS, and FA drove differentiation on OS cells, further proved the original aim of the thesis. Though increased differentiation has been observed, it must be noted that the effect is not as potent, as it has been described in MSCs, with fold-increase in osteogenic genes and proteins not being as large as is reported in literature for MSCs.[141]

Differentiation was observed for small molecule treatments in a dose and time dependent manner, for SAOS-2 and MG-63 cells. Earlier differentiation marker RUNX2 was most consistently upregulated across cell lines and conditions. Treatment with NK or OGM was seen to drive upregulation of ONN and OPN, depending on the cell line (chapter 3), but small molecule treatment did not appear to drive as significant an increase in mineralisation markers.

An increase in RUNX2 protein was observed across different condition for both OS cell lines, but changes in osteogenic genes were more limited than previously observed for NK and OGM treated cells in chapter 3. FA treated MG-63 cells and CS treated SAOS-2 cells showed an upregulation in OSX gene levels, while FA treated SAOS-2 cells showed an upregulation of ALP. The observation of protein and gene expression not directly correlating is plausible, as correlation between protein and gene expression is low in mammals.[325] In

fact, Schwanhäusser *et al*. characterised 1000s of proteins, and discovered that there is limited correspondence between protein and mRNA expression.[321] Protein expression was found to be more stable, lasting a few days typically, while mRNA expression typically lasted a few hours, and was more unstable. Protein levels were found to be 2,800 times more abundant, than mRNA copies. Potentially including more timepoints and expanding the panel of genes in the future may aid in obtaining further information. Moreover, osteogenic differentiation has been reported to be regulated via post-translational modifications, including MAPK initiated RUNX2 phosphorylation, and BMP2 induced Histone acetyltransferase (HAT) acetylation of RUNX2.[326] Therefore potentially assessing how protein expression may be modulated by post-translational modifications in OS, would be of particular interest in the future. Some data exists on nuclear receptor agonists inducing osteogenic through PPAR-γ,[128] so it would be interesting to see if differentiation is modulated through alternative pathways for CS, FA and TAU.

Taurine (TAU) has previously been reported to drive apoptosis in different cancer cells. Zhang *et al.* reported pro-apoptic effects on colon cancer, by upregulating PUMA, Bax and caspases. Cells were treated with 40-160 mM TAU,[327] compared to 10 μM testing, described in this chapter, which may partially explain the lack of apoptosis. Okano *et al.* also reported apoptotic effects of 36 mM TAU on nasopharyngeal cancer cells, through upregulation of p53,[307] which was also a significantly higher than the tested concentrations. Potentially testing the effect of increased concentration of taurine on OS cells may be of interest in the future, though this high concentration may be an indicator of a lack of potency. Taurine was found to promote differentiation both in SAOS-2 and MG-63 cells in a dose and time dependent manner, without a significant effect on viability. No previous information on the effect of taurine on OS cells was uncovered but has previously been reported to drive osteogenic differentiation through ERK signalling.[328]

Glucocorticoid receptor (GR) is clearly involved in osteogenesis, but there are differing opinions, and contrasting research as to its role. More research exists on the effect of synthetic glucocorticoid dexamethasone (DEX) on osteogenesis of MSCs, compared to studies on the effect of endogenous metabolite CS.[141] Glucocorticoids have historically played a major role in osteogenesis, with differentiation protocols for MSCs often including dexamethasone, to initiate maturation.[176,177] Rauch *et al.* reported that knockdown of the glucocorticoid receptor in mice, led to inhibition of osteogenesis, with statistically significant downregulation of RUNX2 and OCN, as well as decreased mineralisation.[329] They found that the glucocorticoid receptor plays a complex role in osteogenesis, with

absence of GR dimerization leading to inhibition of osteoblastogenesis, while loss of bone mass was also reported, in higher doses of dexamethasone. The role of glucocorticoids however is complicated, with higher doses of dexamethasone leading to osteoporosis.[330] Ciao *et al.* also reported osteoporosis and glucocorticoid induced senescence at high doses of dexamethasone.[331] Treatment with 50 μM of dexamethasone was found to downregulate osteogenic genes, compared to the control group. Glucocorticoids have been reported to suppress osteoblast differentiation, by decreasing Sema3A expression via the PIK3/Akt pathway, with semaphorins rescuing loss of differentiation.[332] While the glucocorticoid receptor is essential for differentiation,[333] a more targeted approach, which would lead to selective delivery, and lower doses being administered, would be beneficial.

Cholesterol can undergo biotransformation in the presence of sulfotransferases and a sulfate donor, to produce cholesterol sulfate (CS). Sulfated steroids have traditionally been considered inactive reservoirs of their parent compound,[334] and while CS does contribute to the generation of cholesterol, through desulfation, it has its own biological function too. Jimenez-Perez *et al*. reported that by inactivating steroid sulfatase in mice, ageing could be reversed, in the context of Alzheimer's disease.[335] They hypothesised that since in the absence of steroid sulfatase, sulfated derivatives of steroids were more abundant, and more active, they must possess a more active biological role, than previously thought of. They also observed that steroid sulfatase inhibitor STX64 was almost as effective at inactivating STS, as knockdown of the receptor in mice. CS has also been found to be involved in signal transduction, lipid metabolism, glucose regulation and gluconeogenesis,[310] and differentiation of keratinocytes.[336] Overall it appears that while sulfated steroids do else act as reservoirs for their desulfated precursors, CS possesses its own biological activity. To confirm the effect of CS on OS cells in the future, and pathways involved in differentiation, it may be of interest to assess the effect of CS in the presence of a steroid sulfatase inhibitor, such as STX64.

Previous research in the group had documented the effect of the glucocorticoid vs mineralocorticoid receptor on osteogenic differentiation of MSCs.[141] Inhibitor studies had shown that fludrocortisone acetate induced osteogenic differentiation through the mineralocorticoid pathway. When MR antagonist, canrenone was administered to the cells alongside fludrocortisone acetate, differentiation was found to be inhibited. For cholesterol sulfate, inhibition of the glucocorticoid receptor, using mifepristone was reported to also inhibit differentiation, which would indicate differentiation occurred more through the glucocorticoid receptor (GR). Zhou *et al.* reported that treatment of OS cells with

glucocorticoids can slow proliferation, and trigger apoptosis,[337] however this was not something that was observed when treating cells OS with CS. Gross *et al.* reported that OS cells that stably express the α-isoform of GR, evaded apoptosis induced by glucocorticoids.[338] Gundisch *et al*. reported that treatment of tumour cells with glucocorticoids such as dexamethasone can induce proliferation, via Akt, and p38 MAPK activation.[339] They therefore suggested limited use of glucocorticoids in cancer patients, while also highlighting that glucocorticoids do not typically trigger apoptosis in cancer cells. On the other hand, while some steroid receptors are cancer promoters, including estrogen receptor for breast cancer, and androgen receptor for prostate cancer, glucocorticoids are not considered oncogenes.[340] Clearly further research needs to be carried out on glucocorticoids and their effect on differentiation, proliferation, and invasion in cancer cells. Given the pleiotropic effect of the glucocorticoid receptor, chapter 6 explored the conjugation of dexamethasone to a cancer targeting group, to promote enhanced dexamethasone in cancer cells.

5.6 Conclusions

SAOS-2 and MG-63 cells were treated with previously identified metabolites taurine (TAU) and cholesterol sulfate (CS), as well as corticosteroid fludrocortisone acetate (FA) for 7 days. CS, FA and TAU were found to drive differentiation in a dose dependent manner, as evident by the gradual upregulation of RUNX2 and/or OSX, in MG-63 and SAOS-2 cells. A 10 μM concentration was found to drive most consistent differentiation for the small molecules, so further assays were carried out at this concentration. Immunofluorescent microscopy was used to qualitatively study protein localisation and abundance, with some initial indications of osteogenic marker upregulation for different treatments, across both cell lines. For MG-63 cells qPCR analysis showed an upregulation of OSX for FA and OGM treatment, but changes in gene expression were not observed for CS stimulated cells. On the other hand, for SAOS-2 CS treatment drove an upregulation of OSX, and FA drove an upregulation of ALP gene expression, indicating maturity. The gene expression data did not directly correlate to protein expression data, which is a commonly described cell behaviour, as previously discussed.[321] More extensive studies of the effect of small molecules on RUNX2 and OSX protein expression was carried out via ICW, and trends in increased protein expression were evident for the different small molecules. Protein expression was then studied over a period of 28 days, and small molecules were found to drive osteogenesis in a time-dependent manner, both in SAOS-2 and MG-63. CS treatment showed more significant

stimulation of osteogenic genes over time in MG-63 cells, while FA treatment showed the most significant upregulation of RUNX2 over the span of 28 days in SAOS-2 cells. The tested steroids showed osteogenic response in OS, however GR is known to be involved in multiple signalling pathways. Conjugating a glucocorticoid to a cancer targeting group was considered a promising approach to promote selective administration of the differentiation agent to the cancer cells. This strategy will be explored in chapter 6.

5.7 Future work

Studying the effect of signalling pathway inhibition, on OS differentiation may help further understand the mode of action of the small molecules, as well as elucidate the biochemistry of osteogenesis in OS. As Jnk, ERK1/2 and the Akt signalling pathways were predicted to play a role in differentiation, through metabolomics, studying their role in differentiation of OS cells would be of special interest. Studying the effect of the glucocorticoid vs mineralocorticoid receptor on OS cells could help elucidate the mode of action of CS and FA. The balance between proliferation, and differentiation is fine, so obtaining further information on signalling pathways, differentiation and cancer progression could lead to a deeper understanding of OS. Omics studies of the treated cells would be particularly interesting, in understanding the effect of glucocorticoids and mineralocorticoids on OS cells. Moreover, comparing omics data for the steroid treatments to the previously described nanokicked and osteogenic medium treated cells could offer broader understanding. Coupling metabolomics data with RNA-sequencing data or transcriptomics can provide interesting information, on how changes in gene expression can alter changes in metabolism.

As previously mentioned, taurine plays an important role in lipid metabolism and liver detoxification, by forming bile acid-taurine conjugates. Bile acids are end-products of cholesterol metabolism,[341] so there is a link between tested conditions in chapters 3 and 5. It was found that taurine, and cholesterol sulfate both drove osteogenic differentiation in OS cells. Given both molecules' role in osteogenesis it would be interesting to synthesise and test the effect of steroid-taurine conjugates, on the osteogenesis of MSCs and OS cells. Given taurine's role in bioconjugation with bile acids, which are cholesterol derivatives, it would be of interest to carry out further metabolic studies in the future, on the link between cholesterol and taurine metabolism in OS.

Chapter 6: targeted delivery of dexamethasone to osteosarcoma cells

6.1 Introduction

Dexamethasone (Figure 6.1) is a synthetic glucocorticoid used to treat chronic eczema, auto-immune diseases, such as lupus and rheumatoid arthritis,[342] as well as COVID-19.[343] Dexamethasone is also commonly administered alongside chemotherapy regimens, to manage inflammation and nausea.[344] As previously discussed, dexamethasone is a common osteogenic differentiation supplement,[176,177] which is of special interest for this project. While glucocorticoids are some of the most potent anti-inflammatory drugs, they are also known for their pleiotropic effect, thus altering multiple signalling pathways.[345] This pleiotropic effect leads to glucocorticoids presenting broad activity, thus treating multiple ailments, but also inducing side-effects in patients.[140] Conjugating existing therapeutic agents to cancer targeting groups can reduce side-effects and improve selectivity and pharmacological properties of drugs, by increasing therapeutic payload at the cancer site and decreasing drug distribution at other sites.[346]

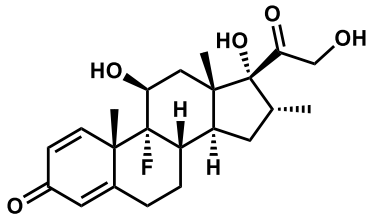

Dexamethasone: 6.1

*Figure 6.1: Structure of dexamethasone (**6.1**)*

As discussed in chapter 1, commonly employed targeting strategies in OS have included the use of antibody-drug conjugates, nanomedicine, and macromolecules,[52] with more limited research on small molecule-drug conjugates. Improved pharmacological and toxicological properties of a drug can be attained by forming prodrug derivatives of cancer drugs.**Error! Bookmark not defined.** A therapeutic payload can be attached to a cancer targeting group, through a cleavable linker designed to release the active drug at the site of interest, in response to stimuli from the tumour microenvironment, or exogenous stimuli.[347] This strategy typically involves forming a bond that is stable in blood plasma, but undergoes cleavage at the site of

interest due to a shift in the environment,[348] such as changes in pH, temperature, oxygen, or due to enzymatic activity. Examples of such cleavable linkages include esters, which are typically cleaved at the delivery site by esterases, and disulfide linkers, which are cleaved by glutathione.[349] Oximes and hydrazones are examples of cleavable linkers, that are considered stable at physiological pH, but undergo hydrolysis at an acidic environment, to release the drug.[350] Multiple drugs have been conjugated to various targeting groups, including micelles, glucose, and polymers, using oxime-based cleavable linkers, which have demonstrated a more controlled release of the therapeutic agent at the site of interest.[351]

Hydrazone derivatives of drugs have proven effective in minimising off-target effects and modulating controlled release of the drug in cancer cells.[352] An example of anti-cancer, hydrazone-based drug derivatives is zorubicin (Figure 6.2), which is a benzoyl hydrazone derivative of the DNA intercalating drug doxorubicin.[353] Zorubicin may be administered to patients who present resistance to anthracyclines.[354] Different cancer targeting groups have been used for targeted release of doxorubicin to cancer cells, via cleavable hydrazone linkers. This includes the use of a doxorubicin-micelle conjugate in liver cancer cells,[355] different 2-hydroxypropyl methacrylate (HPMA) based targeted delivery platforms,[356,357] and nanoconjugates.[358] In most cases, doxorubicin was not released at physiological pH, as it was still conjugated to the targeting group via the hydrazone bond. At around pH 5, the hydrazone bond was hydrolysed within lysosomes[358] and in some cases within endosomes,[357] which led to controlled release of the chemotherapeutic agent.

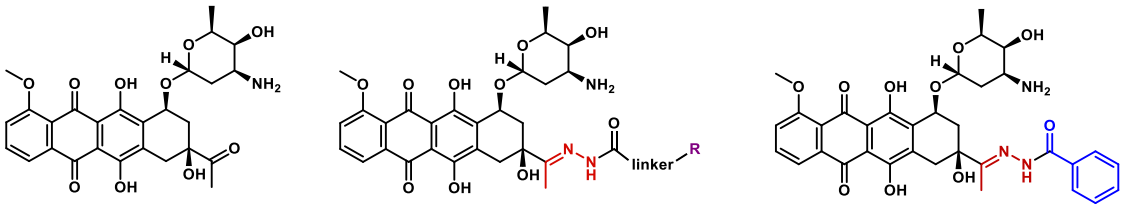

Figure 6.2: Targeted delivery of doxorubicin to cancer cells can be achieved via the conjugation of doxorubicin to micelles,[355] macromolecules,[356] or small molecules,[354] via hydrazone based cleavable linkers.

Hydrazone condensation can be carried out for dexamethasone at carbonyls C3 and C20 (Figure 6.3).[359] C20 functionalisation was previously reported in dexamethasone hydrazone conjugates to peptide nanofibers,[360] nanobodies,[361] while C20 hydrazone formation was also reported for a prednisolone polypseudorotaxane.[362] Linkage of dexamethasone to micelles,[363] sialic acid,[364] HPMA[365] and ANANAS[366] was also previously reported to be carried out at the C3 position via a hydrazone cleavable linker. From the literature, similar

conditions have been reported to lead to functionalisation C3 and C20 hydrazones, leading to conflicting findings.

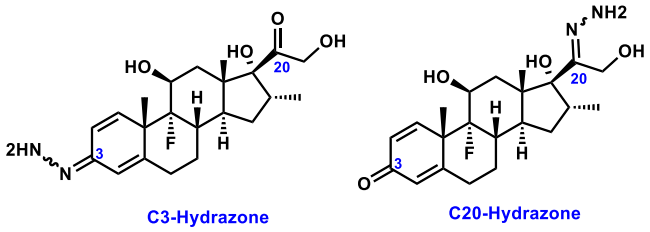

Figure 6.3: Functionalisation can occur in C3 or C20 of dexamethasone, to afford a hydrazone.

A variety of cancer targeting groups have been investigated, to achieve increased therapeutic concentration in cancer cells, compared to healthy cells.[367] Folate is commonly targeted in cancer. Folate receptor was found to be overexpressed in OS, according to a study that analysed 100 OS patient samples.[368] Folate receptor targeting strategies have widely been explored in the context of cancer and have shown some promising results.[369]

Altered cancer metabolism sustains cancer's uncontrolled proliferation,[69] but also offers a promising therapeutic avenue, with the cancer cells' increased glucose uptake. Glucose transporter-1 (GLUT1) is a membrane protein, that facilitates glucose transport into the cytoplasm through diffusion.[370] GLUT1 is an abundant glucose transporter in human tissues, with cancer cells typically showing increased ^{18}F-fluorodeoxyglucose uptake, and overexpression of GLUT1.[371] Most pertinently GLUT1 was previously reported to be overexpressed in 75% of tested OS patient samples, with higher GLUT1 expression connected to worse outcomes typically.[372] Multiple studies have exploited cancer cells' increased glucose uptake, by conjugating drugs to glucose, to achieve increased drug delivery to the cancer cells.[373,374,375] An example of this strategy is glufosfamide, which is a glucose based derivative of alkylating agent ifosfamide, found to circumvent side-effects of this highly cytotoxic drug, by targeting delivery to cancer cells.[376] Glufosfamide was found to display comparable anti-tumour effects to ifosfamide, in a GLUT1 dependent manner, as no bioactivity was present, in the presence of a GLUT1 inhibitor phloretin. Calvaresi *et al.* have carried out an excellent review of glucose conjugation strategies for cancer, that was consulted during experimental design.[374] Liu *et al.* theorised that modifying glucose in the anomeric C1 or modifying C2 is less likely to interfere, with recognition of glucose in GLUT1, thus facilitating small molecule transport into cells[377]

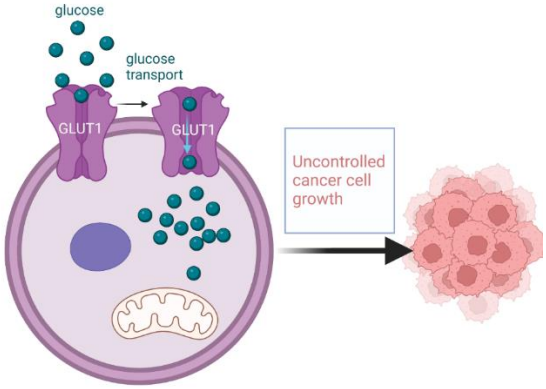

Figure 6.4: GLUT1 is overexpressed in cancer, leading to cancer growth. GLUT1 facilitates glucose transfer. (created with biorender.com)

6.2 Aim

The aim for this chapter was to exploit GLUT1 overexpression in OS, by conjugating dexamethasone to glucose, via a cleavable linker. The objectives were to design a synthetic route for the molecule of interest, synthesise it, purify it, and verify its complex structure. A further aim was to investigate the activity of the molecule, by comparing the effect of dexamethasone, and the hydrazone derivative on poorly differentiated MG-63 OS cells, and more mature SAOS-2 OS cells. An essential aspect of this research was to assess the differentiation potential of the synthesised small molecule compared to dexamethasone, as well as the GLUT1 expression. The aim was to achieve targeted delivery to the cancer cells, and controlled release at the tumour microenvironment.

6.3 Materials and methods

6.3.1 Chemistry

General methods

Reagents were purchased from commercial suppliers, unless otherwise stated. For conditions using dry solvents, flasks were dried in a 150 ^{o}C oven overnight and kept under N_2. Dry DCM was dispensed through a dry solvent purification system, and dry DMF was obtained commercially. Reactions were monitored by thin-layer chromatography (TLC), liquid chromatography-mass spectrometry (LC-MS) and/or nuclear magnetic resonance (NMR) spectroscopy. TLC analysis was conducted on Merck silica gel 60 coated alumina plates. TLC plates were visualised using an acidic ethanolic anisaldehyde stain, and subsequent heating.

NMR spectra were recorded on a Bruker DPX-400 spectrometer (1H NMR at 400 MHz, 13C NMR at 101 MHz), for most samples. NMR spectra for compound **6.12** were collected on a 600 MHz Bruker Ascend Aeon 2 channel HD spectrometer, with a 5 mm CPDCH CryoProbe,^{TM} courtesy of James McIver, and Prof Lee Cronin. 1D gradient NOE experiments, using method described by Huy *et al*,[378] were carried out with the help of Alec Mungall. NMR spectra were recorded in CD_3OD or $CDCl_3$. Chemical shift values are reported in ppm, relative to residual chloroform (δ=7.26) or methanol (δ=3.31), for ^{1}H NMR, and relative to the central resonance of $CDCl_3$ (δ=77.2) or CD_3OD (δ=49.0), for ^{13}C NMR. Signals are reported as singlet (s), doublet (d), doublet of doublets (dd), triplet (t), quartet (q), or multiplet (m), for the multiplicity. Splitting constants are reported in Hertz (Hz). Two-dimensional NMR spectroscopy (COSY, HSQC, HMBC, NOESY) was employed to assign spectra. Spectra were analysed using MestreNova software.

HPLC grade solvents were used for LC-MS analysis, and HPLC purification, which included H_2O and CH_3CN, with 0.1% optima formic acid. LC-MS analysis was carried out on a nominal mass Agilent 6125B Single Quad LC-MS mass spectrometer, coupled with an Agilent 1290 Infinity UHPLC chromatography system, and an electrospray (ESI) source, and a diode array detector measuring wavelengths from 190 to 640 nm. A Dr Maisch GmbH Reprosil Gold 120 C18 (3 μm 150×4 mm) column was used. LC-MS analysis was carried out using gradients ranging from 10-95% to 40-95% CH_3CN in H_2O depending on the sample, over 15 minutes Accurate mass measurements for samples were obtained on the Agilent 6546 Q-TOF-MS High Resolution Accurate Mass Spectrometer, by Dr Giovanni Enrico Rossi, using sample appropriate analytical methods.

Semi-preparative HPLC purification was carried out on a Gilson HPLC instrument, equipped with Gilson 306 pumps, a Phenomenex Synergi C18 (80 Å, 10 μm, 250×21.2 mm) column at a flow rate of 10 mL/min, with a Gilson 155 UV/VIS detector. UV traces were detected at 214 and 254 nm. Gradient optimisation was carried out for different samples, based on solubility, purity and peak resolution. Samples were dissolved in appropriate solvent, sonicated, centrifuged at 10,000 rpm, and filtered, before injecting 1 mL of sample into the instrument. HPLC grade solvents were used for HPLC purification, which included H_2O and CH_3CN, supplemented with 0.1% optima formic acid. Collected fractions were analysed via LC-MS and lyophilised using a Christ Alpha 2-4 LDplus lyophiliser.

Bromination of glucose pentaacetate[379]

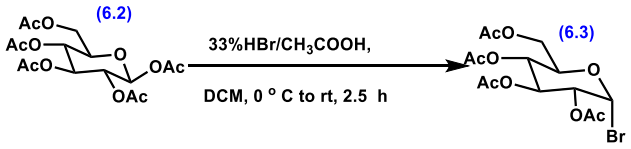

HBr (33% in CH_3COOH, 15 mL) was added dropwise to a solution of *β*-D-glucose pentaacetate **6.2** (3.00 g, 7.6 mmol) in anhydrous DCM (30 mL) at 0 °C under N_2. The reaction was allowed to reach room temperature, and stirred for 2.5 h. The reaction mixture was poured onto ice-water and the aqueous layer was extracted 3 times with DCM. The combined organic layers were washed with saturated aqueous sodium bicarbonate, until the acid was neutralised. The organic layer was then washed with brine, dried with anhydrous $MgSO_4$, filtered, and concentrated *in vacuo*. The crude product **6.3** was obtained as an oil (2.60 g) and used in the next step without further purification.

Glucose linker bromide substitution[380]

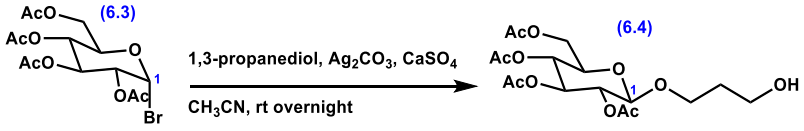

The bromide derivative **6.3** (1.00 g, 2.6 mmol), 1,3 propane-diol (0.95 g, 12.5 mmol), Ag_2CO_3 (0.41 g, 1.5 mmol), $CaSO_4$ (0.13 g, 0.95 mmol), and CH_3CN (1.25 mL) were stirred at rt, under N_2 overnight. The crude mixture was filtered through celite, and the celite pad was washed with EtOAc, followed by addition of water to filtrate. The supernatant was collected, and the aqueous layer was extracted 3 times with EtOAc. The combined organic layers were dried over anhydrous $MgSO_4$, and solvent was removed *in vacuo*. The product was purified via column chromatography, with a 50–85% gradient of EtOAc in petroleum ether. Compound **6.4** was isolated as an off-white solid, 452.8 mg, 45.2% yield.

^{1}H NMR (400 MHz, $CDCl_3$) δ 5.21 (t, *J* = 9.5 Hz, 1H), 5.08 (t, *J* = 9.7 Hz, 1H), 4.99 (dd, *J* = 9.6, 8.0 Hz, 1H), 4.53 (d, *J* = 7.9 Hz, 1H), 4.32 – 4.12 (m, 2H), 4.01 (ddd, *J* = 9.7, 6.7, 5.2 Hz, 1H), 3.80 – 3.61 (m, 4H), 2.15 – 1.96 (m, 12H), 1.82 (m, 2H).

^{13}C NMR (101 MHz, $CDCl_3$) δ 170.9 (q C, **OAc**), 170.4 (q C, **OAc**), 169.6 (q C, **OAc**), 169.6 (q C, **OAc**), 100.9 (CH, **C1**), 72.9 (CH), 72.0 (CH), 71.4 (CH), 68.6 (CH), 67.9, 62.1 (CH_2), 60.3, 32.2, 20.9 (CH_3), 20.8 (CH_3), 20.8 (CH_3), 20.8 (CH_3)

Acid linker TEMPO BAIB oxidation

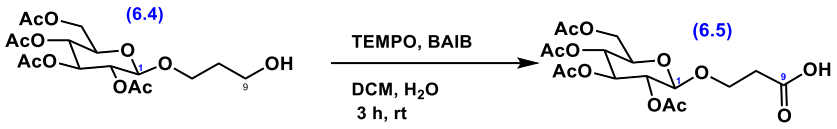

Glucose derivative **6.4** (500 mg, 1.2 mmol) was dissolved in DCM (6.15 mL, 0.2 M) and water (3 mL, 0.4 M). TEMPO (39 mg, 0.25 mmol) and Bis-acetoxy-iodobenzene (BAIB) (1.18 g, 3.65 mmol) were then added to the reaction mixture, and the reaction was stirred for 3 hours at room temperature. The reaction was quenched with saturated aqueous $NaHSO_3$ and extracted with DCM 3 times. The combined organic layers were washed with brine, dried over anhydrous $MgSO_4$, and solvent was removed *in vacuo*. Purification: by silica gel column chromatography (Petroleum ether/Ethyl acetate = ¼). This gave product **6.5** as a white solid, in 61% yield.

^{1}H NMR (400 MHz, $CDCl_3$) δ 5.20 (t, *J* = 9.5 Hz, 1H), 5.08 (t, *J* = 9.7 Hz, 1H), 4.97 (dd, *J* = 9.6, 8.0 Hz, 1H), 4.56 (d, *J* = 8.0 Hz, 1H, **C1**), 4.27 (dd, *J* = 12.3, 4.6 Hz, 1H), 4.18 – 4.05 (m, 2H), 3.86 (ddd, *J* = 10.2, 7.6, 5.6 Hz, 1H), 3.70 (ddd, *J* = 9.9, 4.6, 2.5 Hz, 1H), 2.75 – 2.54 (m, 2H, C8), 2.14 – 1.98 (m, 12H).

^{13}C NMR (101 MHz, $CDCl_3$) δ 174.6 (q C, **C9**), 170.9 (q C, OAc), 170.4 (q C, OAc), 169.6 (q C, OAc), 101.2 (CH, **C1**), 72.8 (CH), 72.0 (CH), 71.2 (CH), 68.5 (CH), 65.4 (CH_2), 62.1 (CH_2), 34.5 (CH_2), 20.9 (CH_3), 20.8 (CH_3), 20.8 (CH_3), 20.7 (CH_3).

Synthesis of Hydrazone derivative of dexamethasone

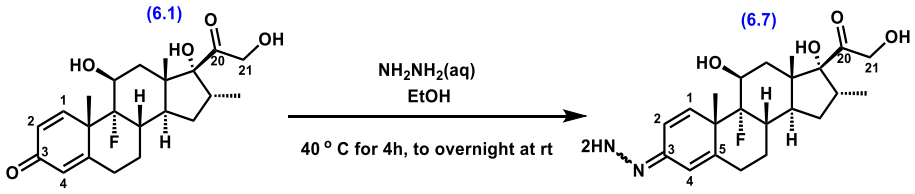

55% aqueous hydrazine hydrate (0.11 mL, 1.5 mmol) was dissolved in EtOH (1.8 mL), under N_2, in a round bottomed flask. Dexamethasone **6.1** (450 mg, 1.2 mmol) was dissolved in EtOH (7.8 mL) and added dropwise to the hydrazine mixture. The reaction was stirred at 40 ^{o}C for 4 h, and then was left to stir overnight at room temperature. The crude mixture was then poured into a mixture of ice and water (40 mL). The aqueous layer was extracted 3 times with ethyl acetate. Anhydrous $MgSO_4$ was added to the combined organic layers, filtered off, and solvent was removed *in vacuo*, yielding a yellow crystalline solid. The solid

was purified in 18 injections, via semi preparative RP-HPLC, using a 10-95% CH_3CN in H_2O gradient, with the product eluting at a retention time of 25.63-28.76 minutes, and 62% CH_3CN. Solvent was removed in the lyophiliser, to afford product **6.7**, as a mixture of **6,7A**, and **peak B** (98 mg, 0.24 mmol, 21% yield), as a white fluffy powder, in high purity according to LC-MS. Product was collected as a *cis-trans* mixture, with **6.7.A** referring to the 1st isomer eluted via HPLC, and **6.7.B** referring to the second isomer eluted via HPLC.

Isolation of pure peak A was not achieved, and a mixture of the 2 isomers was collected and used in the following step, as a 7:3 mixture of **6.7A:6.7B**, according to ^{1}H NMR. Two peaks of the same mass according to LCMS, of high purity, with changes around the A ring, confirmed *cis-trans* isomers around the hydrazone bond. NMR. NMR data is reported for one isomer, but ^{1}H NMR spectrum of the mixture has been attached on the appendix.

Peak B (6.7.B) characterisation data:

LC-MS retention time: 4.04 (20-95% CH_3CN in H_2O gradient gradient)

LC-MS (ESI+): calculated M+H=407.2, Measured M+H=407.2

Molecular formula: $C_{22}H_{31}FN_2O_4$

Calculated $(M+Cl)^-$: 441.1966, **Measured $(M+Cl)^-$**: 441.1962

^{1}H NMR: (400 MHz, $CDCl_3$) δ 6.35 (s, 0.9 H, **C4**), 6.28 (dd, *J*= 10.1, 1.6 Hz, 0.9 H, **C2**), 6.15 (d, *J*= 10.1 Hz, 0.9 H, **C1**), 4.60 (d, *J* = 20.0 Hz, 1H, **C21**), 4.42-4.34 (m, 1H, **C11**), 4.27 (d, *J* = 20.0 Hz, 1H, **C21**), 3.13-3.02 (m, 1H, **C16**), 2.69 – 2.57 (m, 1H), 2.43 – 2.13 (m, 4H), 1.82 – 1.70 (m, 2H), 1.59 – 1.44 (m, 4H), 1.35 (d, *J* = 14.2, 1H), 1.30-1.20 (d, 1H), 1.03 (s, 3H, **C18**), 0.92 (d, *J* = 7.3 Hz, 3H, **C22**).

^{13}C NMR: (101 MHz, $CDCl_3$) δ 212.3 (q C, **C20**), 154.4 (q C, **C5**), 144.7 (q C, **C3**), 134.5 (CH, **C1**), 127.5 (CH, **C2**), 109.8 (CH, **C4**), 99.8 (d, $^1J_{CF}$=174 Hz, C-F, **C9**), 90.3 (CH), 71.2 (d, $^2J_{CF}$=38.9 Hz, CH, **C11**), 68.0 (CH_2, **C21**), 48.9 (q C), 46.7 (d, $^2J_{CF}$=22.8 Hz, q C, **C10**), 44.4 (CH), 37.0 (CH_2), 36.3 (CH), 34.4 (d, $^2J_{CF}$=19.7 Hz, CF-CH, **C9**), 32.5 (CH_2), 31.6 (CH_2), 27.7 (CH_2), 24.7 (d, $^3J_{CF}$=5.1 Hz, CF-CH_3), 17.4 (CH_3), 14.9 (CH_3).

Acyl hydrazone formation

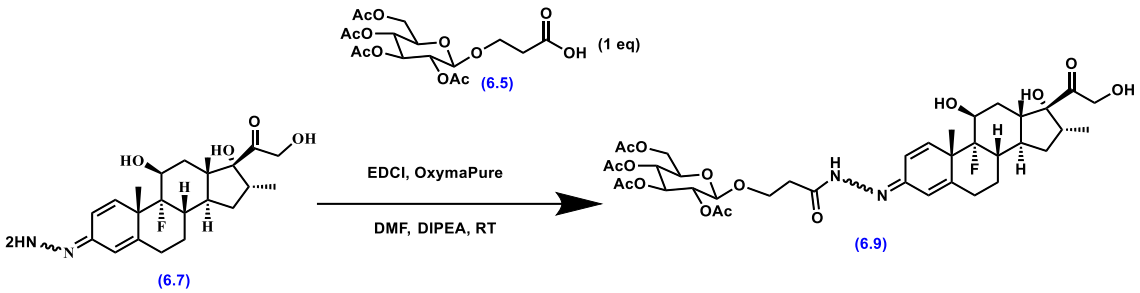

Carboxylic acid **6.5** (91 mg, 0.21 mmol), EDC.Cl (48.3 mg, 0.25 mmol), OxymaPure (35.8 mg, 0.25 mmol) were premixed in DMF (0.4 mL) for 10 mins, to preactivate the acid. Hydrazone **6.7** (98 mg, 0.21 mmol) was premixed in DIPEA (0.11 mL, 0.63 mmol), and DMF (0.6 mL). Premixed acid was added to hydrazone dropwise. Reaction was monitored via LC-MS and left to stir overnight at room temperature. EtOAc was added to the reaction mixture, and the organic layer was washed 2 times with 5% LiCl. Anhydrous MgSO4 was added to the organic layer, filtered off, and solvent was removed *in vacuo*, to afford a yellow solid. The product was purified via RP-HPLC, using a 30-95% CH_3CN in H_2O gradient, over 60 minutes. Solvent was removed on the lyophiliser. The *cis* and *trans* isomers were isolated, and each isolated isomer had rotamers.

Compound 6.9.A: first eluted isomer peak from HPLC

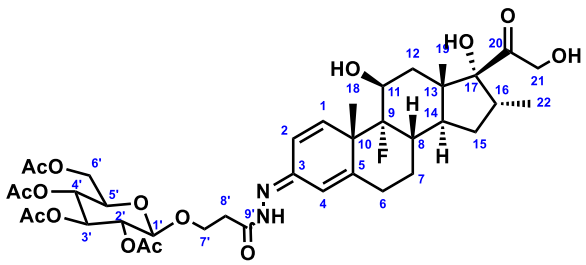

white solid, 31.8 mg. 18.7% yield

LC-MS retention time: 9.11 minutes (20-95% CH_3CN to H_2O), M+H=809.3

Molecular formula: $C_{39}H_{53}FN_2O_{15}$

Calculated M+H= 809.3503, **measured M+H**=809.3517 via high resolution mass spec

^{1}H NMR (400 MHz, CD_3OD) δ 6.62 (s, 1H, **C4**), 6.58 (d, *J*= 10.2 Hz, 1H, **C1**), 6.38 (dd, *J* = 10.2, 2.0 Hz, 1H, **C2**), 5.23 (t, *J* = 9.5 Hz, 1H, **C3'**), 5.00 (t, *J*= 9.7 Hz, 1 H, **C4'**), 4.90-4.80 (m, 1 H, **C2'**), 4.68 (d, *J* = 8.0 Hz, 1H, **C1'**), 4.59 (d, *J* = 19.1 Hz, 1H, **C21**), 4.32 – 4.19

(m, 3H, **C21, C6', C11**), 4.18 – 4.07 (m, 2H), 3.93 (dd, *J*= 9.5, 4.1 Hz, 1H), 3.90 – 3.83 (m, 1H), 3.08 (ddd, *J*= 11.2, 7.3, 4.1 Hz, 1H), 2.78 – 2.62 (m, 2H), 2.58-2.49 (m, 1H), 2.49 – 2.30 (m, 2H), 2.32-2.18 (m, 2H), 2.08 – 1.89 (m, 12H, **acetates**), 1.90 – 1.79 (m, 1H), 1.79 – 1.66 (m, 1H), 1.61-1.54 (m, 1H), 1.52 (s, 3H), 1.44 (d, *J* = 13.8 Hz, 1H), 1.25 – 1.13 (m, 1H), 0.99 (s, 3H), 0.86 (d, *J* = 7.3 Hz, 3H).

^{13}C NMR (101 MHz, CD_3OD) 212.7 (q C, **C20**), (172.3, 171.6, 171.3, 171.3 (4x q C, **acetyl C**)) 170.2 (q C, **C9'**), 161.3 (q C), 150.0 (q C, **C3**), 142.5 (CH, **C1**), 127.1 (CH, **C2**), 112.4 (CH, **C4**), 102.2 (CH, **C1'**), 101.9 (q C, d, $^1J_{CF}$=174.1 Hz, **C9**), 92.1 (CH_2), 74.2 (CH, **C3'**), 72.8 (CH, **C2'**), 72.7 (CH, **C5'**), 72.1 (CH, d, $^2J_{CF}$=35.4 Hz, **C11**), 69.8 (CH, **C4'**), 68.1 (CH_2), 67.4 (CH_2, **C7'**), 63.0 (CH_2, **C6'**), 49.9-48.2 (2x q C in CD_3OD), 45.2 (CH), 37.5 (CH_2), 37.0 (CH), 36.1 (CH_2), 35.7 (CH, d, $^2J_{CF}$=19.6), 33.4 (CH_2), 32.6 (CH_2, **C8'**), 28.9 (CH_2), 24.8 (CH_3, d, $^3J_{CF}$=5.1), 20.6 (CH_3), 20.6 (CH_3), 20.6 (CH_3), 20.5 (CH_3), 17.5 (CH_3), 15.4 (CH_3).

Acetate deprotection

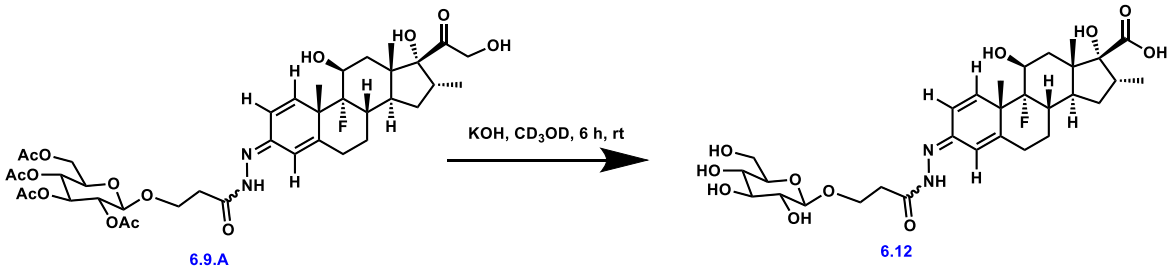

KOH (12.62 mg, 0.23 mmol) was dissolved in CD_3OD (0.75 mL, 0.02 M) and cooled to 0 ^oC. The solution was then added slowly to the glucose-dexamethasone conjugate 9.A. The reaction mixture was allowed to reach room temperature and stirred for 6 hours. Resin IRA-120[381] was then added to the mixture until neutralisation. Resin was removed by filtration, and the filtrate was washed with cold methanol. Solvent was removed *in vacuo*, to yield a complex crude mixture, as a yellow oil. The compound was purified via RP- HPLC, using a 10-95 gradient, and the compound was eluted after 19.2 minutes. Solvent was removed on the lyophiliser, to afford compound **6.12**, as a white solid, in a 1.4 mg, 10% yield.

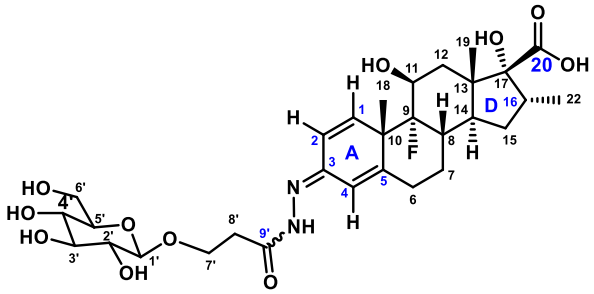

LC-MS retention time: 3.99 minutes (gradient 30-95% CH_3CN in H_2O)

Molecular formula: $C_{30}H_{43}FN_2O_{11}$

Calculated M^-=626.2835, **measured M^-** =626.2856 via high resolution mass spec

^{1}H NMR (600 MHz, CD_3OD) δ 6.64 – 6.58 (m, 2H, **C1, C4**), 6.39 (dd, *J* = 10.2, 2.1 Hz, 1H, **C2**), 4.90-4.80 (in HDO), 4.31 (d, *J* = 7.7 Hz, 1H, **C1'**), 4.24-4.18 (m, 1H) 4.16 – 4.11 (m, 1H), 3.98 – 3.93 (m, 1H), 3.89 – 3.83 (m, 1H), 3.65-3.60 (m, 1H), 3.37-3.33 (m, 1H), 3.26-3.23 (m, 1H) 3.21 – 3.15 (m, 1H), 3.00 (ddd, *J* = 11.3, 7.3, 4.2 Hz, 1H, **C16**), 2.76 – 2.69 (m, 1H), 2.68 – 2.61 (m, 1H), 2.45 – 2.29 (m, 2H), 2.15 – 2.06 (m, 2H), 1.88 – 1.80 (m, 1H), 1.68-1.76 (m, 1H), 1.51 – 1.47 (m, 5H), 1.20-1.16 (m, 1H), 1.16 (s, 3H), 0.90 (d, *J* = 7.2 Hz, 3H).

^{13}C NMR (151 MHz, CD_3OD) δ 170.7 (q C, **C9'**), 163.3 (q C, **C20**), 161.8 (q C), 150.6 (q C, **C3**), 143.0 (CH, **C1**), 126.9 (CH), 112.3 (CH), 104.7 (CH, **C1'**), 102.1 (q C-F, d, $^1J_{CF}$ = 174.5 Hz, **C9**), 88.5 (q C, **C17**), 78.1 (CH, **C4'**), 78.1 (CH, **C3'**), 75.1 (CH, **C2'**), 72.4 (CH, d, $^2J_{CF}$ = 37.6 Hz, **C11**), 71.7 (CH, **C5'**), 67.1 (CH_2, **C7'**), 62.8 (CH_2, **C6'**), 49.9-48.1, 44.9 (CH_2, **C15**), 37.2 (CH **C16**), 37.2 (CH_2) 35.9 (CH, d, $^2J_{CF}$ = 19.7 Hz), 33.8, 32.8 (CH_2), 29.0 (CH_2), 24.8 (CH_3, d, $^3J_{CF}$= 5.2 Hz), 18.0 (CH_3), 15.6 (CH_3).

6.3.2 Biological testing

Cell culture

Cells were cultured in Dulbecco's modified essential medium (DMEM) (Sigma) supplemented with 5% Foetal Bovine Serum (FBS; Sigma), 1% (v/v) L-glutamine (200 mM, Gibco) and 2% antibiotics (6.74 U/mL penicillin-streptomycin, 0.2 µg/mL fungizone) (Sigma). 2,000 cells/cm^2 MG-63, and 4,000 cells/cm^2 SAOS-2 cells were seeded in 48 well plates, in DMEM. Cells were left to attach overnight, and medium was switched the following day to low glucose (**1** g/L) DMEM, substituted with Glutamax, and 2% antibiotics

(6.74 U/mL penicillin-streptomycin, 0.2 µg/mL fungizone) (Sigma), for the cells to acclimatise to the low glucose conditions for 2 days. 10 mM DMSO stocks of dexamethasone, and the final compound (**6.12**) were prepared. Cells were treated with 0.01, 0.1, 1, 10 or 20 µM of dexamethasone (**6.1)** or the final compound (**6.12**), in the low glucose Glutamax medium. Cells were washed with PBS, and fixed after 7 days, with 4% formaldehyde at 37 ºC for 20 minutes and stored in PBS.

Alamar blue

Cell viability was assessed after 1,3 and 7 days (n=4 experimental replicates, n=3 analytical replicates), by using the alamar blue assay, as was described in chapter 2. %Alamar reduction was quantified against the untreated cell control for the individual cell line and timepoint, using equation 3 from Bio-Rad.[145]

In-cell Western staining (ICW)

ICW staining was carried out following the protocol described in chapter 2. In brief, cells were treated with dexamethasone or the final compound, at a range of concentrations (n=4 experimental replicates) and fixed after 7 days. Monoclonal antibodies against the proteins GLUT1, ONN and RUNX2 were used. (1:200 dilution in 1% Milk in PBS). Samples were imaged on the LICOR Odyssey SA, and protein expression was normalised to CellTag, and the untreated control.

Immunofluorescence

Immunofluorescence staining and imaging was carried out following the general protocol from chapter 2. In brief, cells were seeded, treated with 10 µM of dexamethasone or the steroid-glucose conjugate **6.12** (n=2 experimental replicates), fixed and stained. Monoclonal antibodies against the proteins GLUT1 and RUNX2 were used. Cells were imaged on EVOS M7000 microscope, at a 20x magnification. Images were processed using ImarisViewer.

6.4 Results and discussion

6.4.1 Small molecule synthesis

Experimental design

As previously discussed, cancer cells exhibit higher glucose uptake, to support their increased energy demands.[69] GLUT1, which is the most abundant glucose transporter, was previously found to be overexpressed in OS,[372] making it an attractive target in cancer. To exploit cancer's affinity for glucose and drive targeted delivery to OS, dexamethasone (the "therapeutic payload"), was tethered to glucose (the targeting group), via an acid-cleavable acyl hydrazone linker.

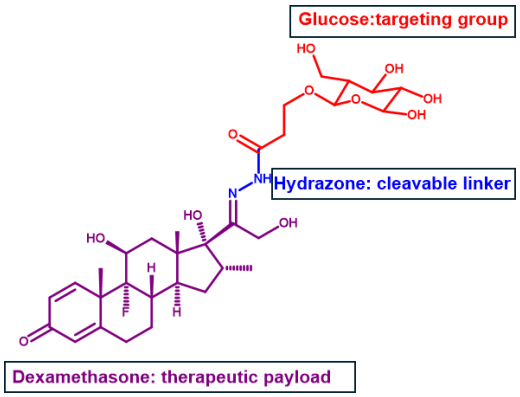

Figure 6.5:Dexamethasone glucose conjugate (6.13) design

The first step was to prepare the glucose linker, by bromination of β-D-glucose-pentaacetate on the anomeric carbon, followed by substitution with 1,3-propane-diol, and subsequent oxidation of the alcohol, to prepare carboxylic acid derivative **6.5 (**Figure 6.6**)**. This would be followed by the synthesis of the C20 hydrazone derivative of dexamethasone **6.6**, in the presence of aqueous hydrazine, following literature precedent by Pishesha *et al*.[361] The next step was to carry out an amide coupling between the glucose linker carboxylic acid, with dexamethasone's hydrazone group, to afford an acyl hydrazone linkage. The final step of this synthetic route was the deprotection of the glucose acetate groups to produce the dexamethasone-conjugate **6.13.**

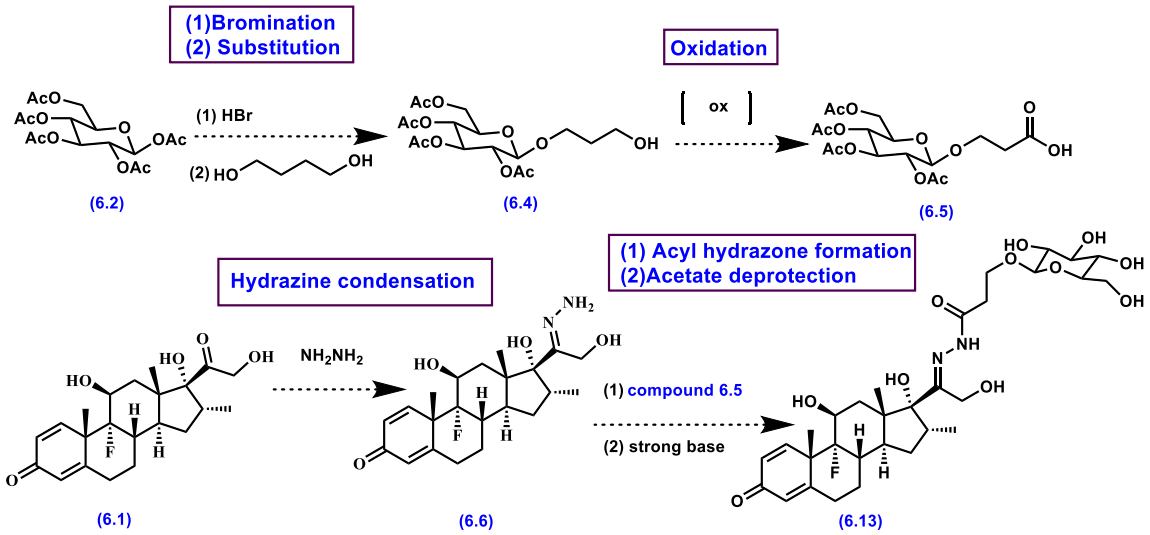

*Figure 6.6:Synthetic plan for glucose-dexamethasone conjugate (**6.13**), via a hydrazone cleavable linker.*

The glycoconjugate was designed to be recognised by GLUT1, and transported to the cancer cells, where upon reaching the slightly more acidic tumour environment, the hydrazone would be hydrolysed, to release dexamethasone (Figure 6.7). Increased uptake of the small molecule conjugate would be expected in cancer cells, compared to healthy cells, due to the glucose moiety. Biological testing would include assessing the effect of the small molecule vs dexamethasone on OS cells, at a range of concentrations. Initial screening would involve assessing viability, differentiation and GLUT1 expression after treatment.

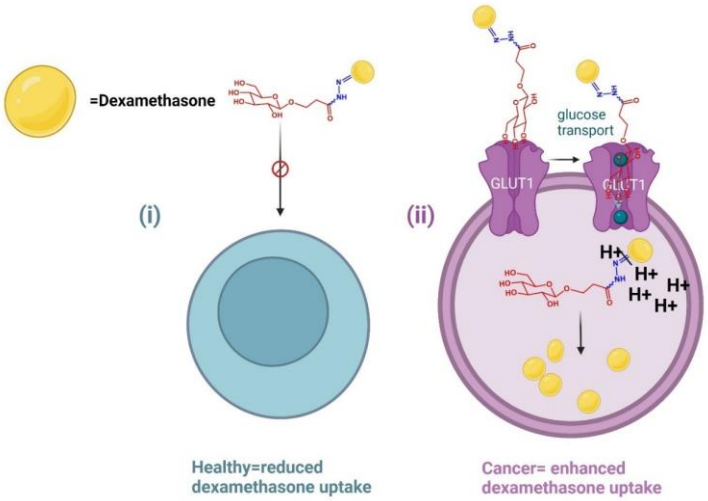

Figure 6.7: GLUT1 is overexpressed in cancer. The glucose moiety of the conjugate would be recognised by GLUT1 and transported in the cancer cell through diffusion. This should be followed by hydrazone hydrolysis in the cancer acidic environment, to release dexamethasone. Increased uptake would be expected in cancer than healthy cells.

Synthesis of glucose-based linker

The glucose ether linker was prepared in 3 steps. First, bromination of β-glucose pentaacetate **6.2** was carried out on the anomeric carbon (Figure 6.8), which is widely reported to form the α-glucose bromide **6.3**.[379] This intermediate is reactive, so the bromide was not isolated and characterised and was instead carried through to the next step. Substitution of the bromide **6.3** with 1,3 propane-diol, in the presence of Ag_2CO_3 catalyst,[380] afforded compound **6.4**. Radical chemistry was employed for the oxidation of the propanol group, to obtain the carboxylic acid **6.5**, via the TEMPO BAIB oxidation. The radical reagent TEMPO was used in catalytic amounts, while the BAIB reagent was used in excess, to regenerate the catalyst. A yield of 60% was achieved, which was sufficient to produce an excess amount than what was required for the glucose linker.

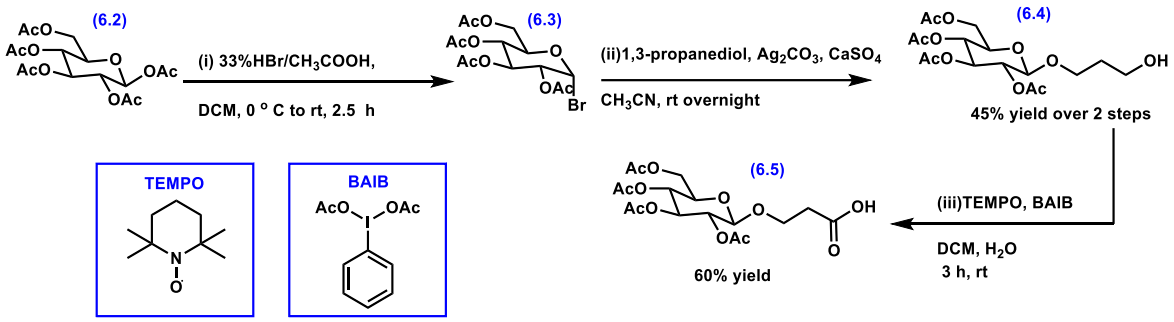

*Figure 6.8: Synthesis of acid **6.5** (i) Bromination of glucose pentaacetate, (ii) Substitution of bromide, (iii) Oxidation of alcohol.*

Synthesis of dexamethasone hydrazone

Hydrazones can be synthesised via condensation of a ketone or aldehyde, with a hydrazine derivative, in the presence of heat or a catalytic amount of acid.[382] Dexamethasone (**6.1**) can react with hydrazine, to afford a mono-substituted hydrazone at C20 position (**6.6**), at the C3 position (**6.7**) or to form a disubstituted species (**6.8**). Pishesha *et al.'s* protocol was adapted first, due to the reported biological activity of the synthesised molecule, so it was initially presumed that C20 functionalisation would occur.[361] As will be discussed later, spectroscopic studies revealed that C3-functionalised **6.7**, hydrazone was formed, instead of the expected C20-functionalised **6.6**. The reaction was first carried out by stirring overnight at room temperature dexamethasone with 4 equivalents of aqueous hydrazine (Table 6.1, entry 1), in the presence of catalytic trifluoroacetic acid (TFA). LC-MS indicated that extensive di-substitution occurred. Milder conditions were employed, to limit di-substitution (entry 2), by reducing hydrazine equivalents, and reaction times. While di-substitution

appeared to be less substantial, the reaction appeared to plateau, and after 4h there was still 35% dexamethasone **6.1** present according to LC-MS. Normal phase chromatography proved unsuccessful at separating the mono-substituted compound **6.7**, from dexamethasone **6.5** and the di-substituted byproduct **6.8**. Bílková *et al.* reported the synthesis of a prednisolone-hydrazone at the C20 position, but also reported purification issues via normal-phase chromatography, and synthesis of *cis*, *trans* mixtures around the hydrazone bond.[362] These conditions were adapted (entry 3), but the reaction plateaued again. Coupling the hydrazone to the glucose linker, without prior purification was attempted, but due to complex mixtures, and low yields, it was considered essential to obtain the pure hydrazone.

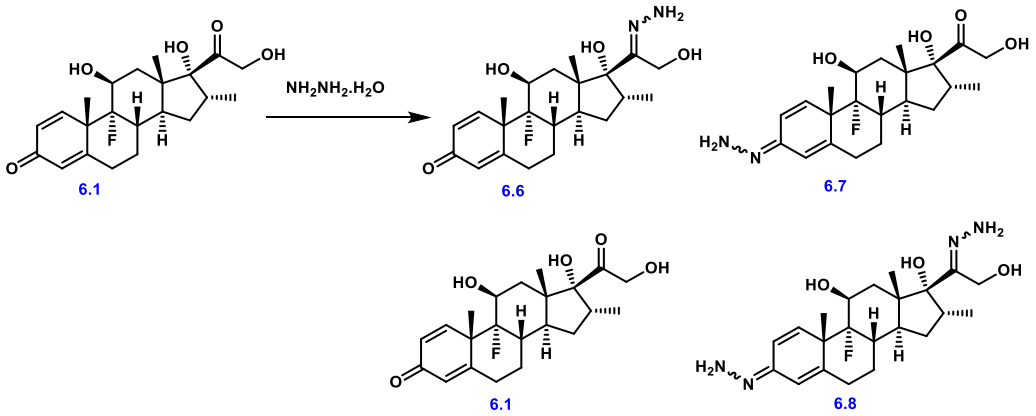

Entry	NH_2NH_2 equivalents	Solvent	TFA	Temperature	Reaction time	LC-MS observations
1	4	MeOH	cat	RT	20 hours	Extensive disubstitution (**6.8**)
2	2	MeOH	cat	RT	6 hours	~40% (**6.7**), 12% (**6.8**), 35% (**6.1**)
3	1	EtOH	-	40 °C to RT	24 hours	~43% (**6.7**), 24.2% (**6.8**), 28.5% (**6.1**)

Table 6.1: Figure shows that hydrazone condensation with dexamethasone (6.1), can form a mixture of C20-mono-substitution (6.6), C3-mono-substitution (6.7) and di-substitution (6.8). Table shows reaction conditions for hydrazone condensation of dexamethasone.

As seen in Figure 6.9, di-substituted species **6.8**, and mono-substituted species **6.7** presented close retention times, which introduced monitoring and separation challenges. Dexamethasone **6.1** and mono-substituted species **6.7** presented close RFs on normal phase chromatography but could easily be separated via reverse phase (RP) chromatography. Moreover, a mixture of mono-substituted species was formed (Figure 6.9), which had close retention times, and the same mass (peaks A,B), which were later confirmed as *cis-trans* isomers of the hydrazone. The first eluting mono-substituted species will be referred to as peak A, or compound **6.7.A**, and the second eluting species peak B, or compound **6.7.B**.

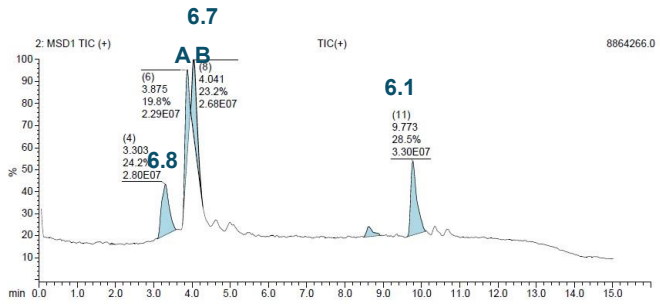

*Figure 6.9: Example of LC-MS chromatogram of crude hydrazone condensation mixtures. Di-substituted hydrazone **6.8** eluted first. Mono-substituted hydrazone **6.7** appeared as 2 peaks on the chromatogram (A, B), due to the presence of distinctive cis-trans isomers. Dexamethasone (**6.1**) eluted last.*

Semi-preparative RP-HPLC was used to purify the compound. The mobile system gradient is critical to successful separation, so optimisation was required. A 30-95% CH_3CN in H_2O gradient was first employed (Figure 6. 10 (i)), and while the compound with the mass of interest was isolated, in small quantities, the product co-eluted with the disubstituted species, making separation sub-optimal. Subsequent chromatographic optimisation studies were carried out to find optimal separation conditions. A 10-95% gradient (ii), with a slower increase in CH_3CN allowed for better separation from the di-substituted species. **6.7B** was successfully separated, isolated, and fully characterised. The purification was repeated multiple times, with a final 98 mg of clean product being obtained from 450 mg of the crude mixture. However, due to close retention times between mono and di substituted species, impure crude mixture, and instrument limitations, 18 HPLC injections were required, to isolate that amount. This is sub-optimal, and led to lengthy purification protocols, but the product was isolated in good purity. Purity of the compound was confirmed via LC-MS, ^{1}H NMR and ^{13}C NMR, while the accurate mass was confirmed via high resolution mass spectroscopy.

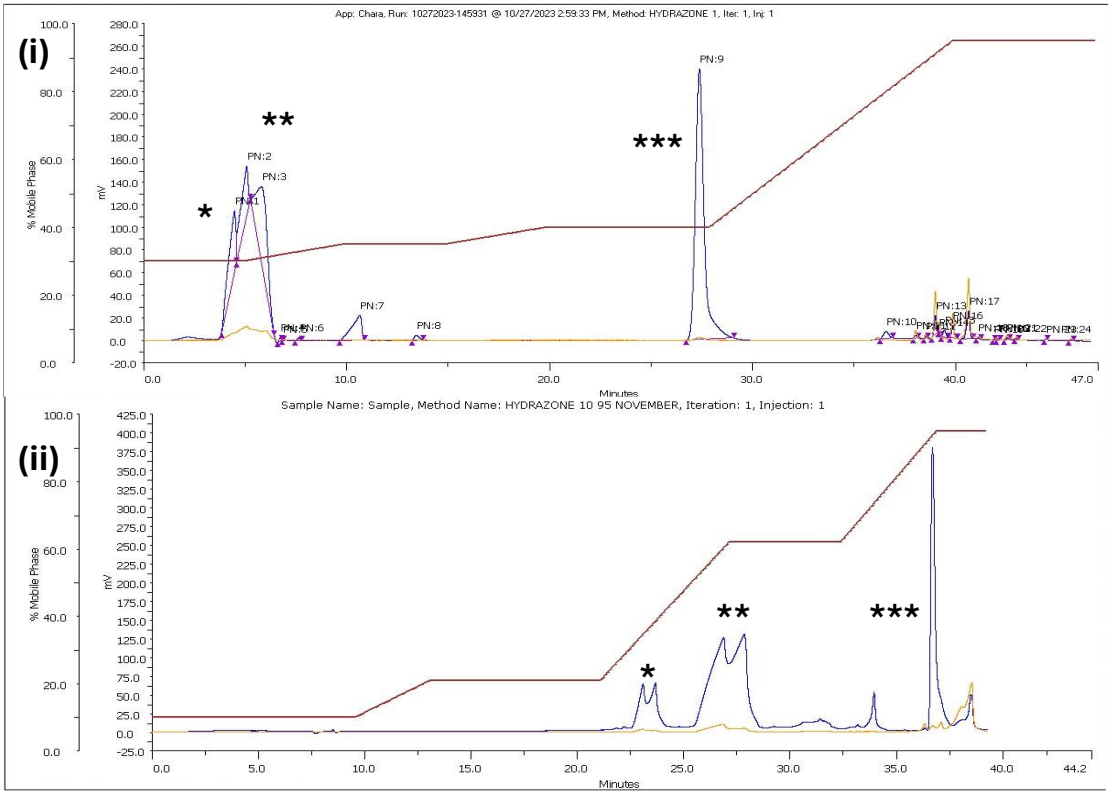

Figure 6. 10: RP-HPLC was employed to purify compound 6.7: (i) 30-95% CH_3CN gradient, (ii) 20-95% CH_3CN gradient, (iii) 10-95% CH_3CN gradient. (*) =6.8, (**)=6.7A, 6.7B, (***)=6.1.

A mixture of *cis-trans* isomers was present on the LC-MS, and isolated via HPLC, as hydrazones can interconvert *in situ*. While the peak A isomer **6.7.A** was not successfully isolated on its own, the peak B isomer **6.7.B** was isolated in a 9:1 ratio, in small amounts. ^{1}H NMR data were collected both for the mixture (Figure S.7), and for the peak B (6.7.B) isomer (Figure S.5), but full spectroscopic data has been reported solely for the peak B isomer.

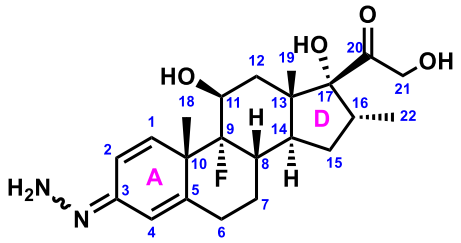

	^{1}H NMR (ppm)	Multiplicity	J (Hz)	C-type	^{13}C NMR (ppm)
C1*	6.15	d	10.1	CH	134.5
C2*	6.28	d	10.1	CH	127.5
C3	-	-	-	q	144.7
C4*	6.35	s	10.1 Hz	CH	109.8
C5	-	-	-	q	154.4
C6	2.13-2.43 ,2.57-2.69	m	-	CH2	31.5
C7	1.42-1.58, 1.70-1.82	m	-	CH2	27.7
C8	2.13-2.43	m	-	CH	34.4 (d, J=19.7)
C9	-	-	-	q	99.8 (d, J=174.0)
C10	-	-	-	q	46.7 (d, J=22.8)
C11	4.34-4.42	m	-	CH	71.2 (d, J=39.0)
C12	1.31-1.40, 2.13-2.40	m	14.2	CH2	37.0
C13	-	-	-	q	48.9
C14	2.13-2.43	m	-	CH	44.4
C15	1.20-1.30, 1.70-1.82	m	-	CH2	32.5
C16	3.02-3.13	m		CH	36.2
C17	-	-	-	q	90.3
C18	1.03	s	-	CH3	22.7, (d, J=5.0 Hz)
C19	1.47	s	-	CH3	27.7
C20*	-	-	-	q	212.3
C21*	4.27, 4.60	d	20.0 Hz	CH2	68.0
C22	0.92	d	7.3 Hz	CH3	14.9

*Table 6.2: NMR spectral assignment of compound **6.7B.** Condensation of dexamethasone with hydrazine led to mono substitution at the C3 position, forming compound **6.7.B** *Key resonances. **Assigned through multiple 2D NMR techniques.*

While originally expecting C20 functionalisation, as reported by protocols by Pishesha,[361] Webber,[360] and Bilkova,[362] spectroscopic analysis revealed changes in the A ring instead.^{13}C NMR confirmed that hydrazone formation occurred at C3, rather than C20 (Table 6.2), as the quaternary (q) C corresponding to the C20 carbonyl was still at 212.3, while C3 signal shifted to 147.7. Moreover, the 2 doublets corresponding to the diastereotopic protons of C21 did not significantly shift, compared to dexamethasone, as may have been expected if a C20 hydrazone was formed. Changes were observed in the A ring of dexamethasone with new doublets observed for C1 and C2, and a new singlet observed for C4. A smaller set of peaks was also observed via ^{1}H NMR in the A ring region, belonging to the peak A isomer, as was confirmed by comparing the spectra of the mixture (Figure S7.), with peak B (Figure S5). C-F carbons were also identified, with coupling constants reported. The doublet at 99.8, corresponding to C9, displayed a coupling constant of 174.0 Hz, which was within the

expected range of a carbon directly bonded to F. The presence of overlapping signals up-field, due to the steroid scaffold made characterisation challenging, but by comparing the spectrum to dexamethasone, and using HSQC, HMBC and COSY 2D NMR, to assign each signal, full characterisation was achieved.

It was clear from the NMR data of the purified compounds that hydrazone formation had occurred in the A ring of dexamethasone at the C3 position. Further investigation revealed that some papers reporting C20 functionalisation, that had employed similar conditions, had not purified the compound, and reported it as a mixture of dexamethasone, mono and di-substituted species.[362] Others identified product formation via mass spectrometry,[360,361] which would not confirm the position of functionalisation. The dexamethasone conjugates had still presented biological activity since the linker was designed to be cleavable. Through literature review it was revealed that C3-functionalisation was also reported,[363,364,365,366] which would corroborate modification of the A ring. Full characterisation data has been reported in literature for the TBS protected species of dexamethasone. No spectrum for the unprotected species **6.7** was identified, which makes this the first characterisation of compound **6.7**.

Synthesis of acetate protected glucose-dexamethasone conjugate.

Having successfully synthesised and characterised compound **6.7**, the next step was to couple hydrazone **6.7** to the glucose linker **6.5**. Carbodiimide coupling chemistry was employed to form an amide bond between the acid of the glucose-based linker and the free amine of the dexamethasone hydrazone derivative (Figure 6.11). OxymaPure or HOBT were used as coupling additives, to avoid side reactions, and improve reaction efficiency.

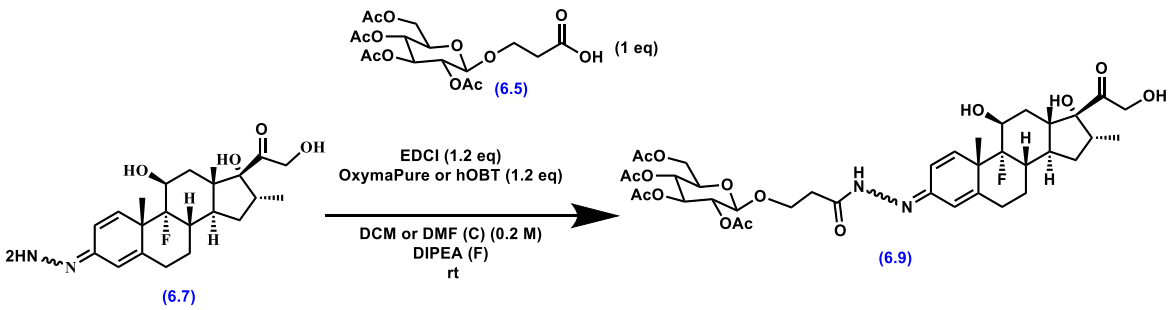

*Figure 6.11: Amide coupling between compounds **4** and **7**.*

Overall, the different reaction conditions, documented in Table 6.3, led to successful conversion into compound **6.9**, with consumption of both starting materials confirmed by LC-MS. As was observed for the hydrazone precursor, a mixture of 2 isomers with the same mass were present (Figure 6.12), which was expected, since a *cis-trans* mixture of compound **6.7** was used in the reaction. Overall, similar conversion occurred with the different reaction conditions, according to the LC-MS chromatograms. The reaction was carried out in dry DCM or DMF, and while conversion was similar under both solvents, fewer impurities were present in DMF (iv), which may be attributed to the LiCl workup. From the tested conditions, EDCI, OxymaPure and DIPEA, in DMF was considered superior.

Coupling agents	Solvent and base	Observations from LC-MS
EDCI, HOBT	DCM, DIPEA	Figure 6.12 (i)
EDCI, OxymaPure	DMF, no DIPEA	Figure 6.12 (ii)
EDCI, OxymaPure	DCM, DIPEA	Figure 6.12 (iii)
EDCI, OxymaPure	DMF, DIPEA	Figure 6.12 (iv)

*Table 6.3: Coupling conditions employed to afford acyl hydrazone **6.9***

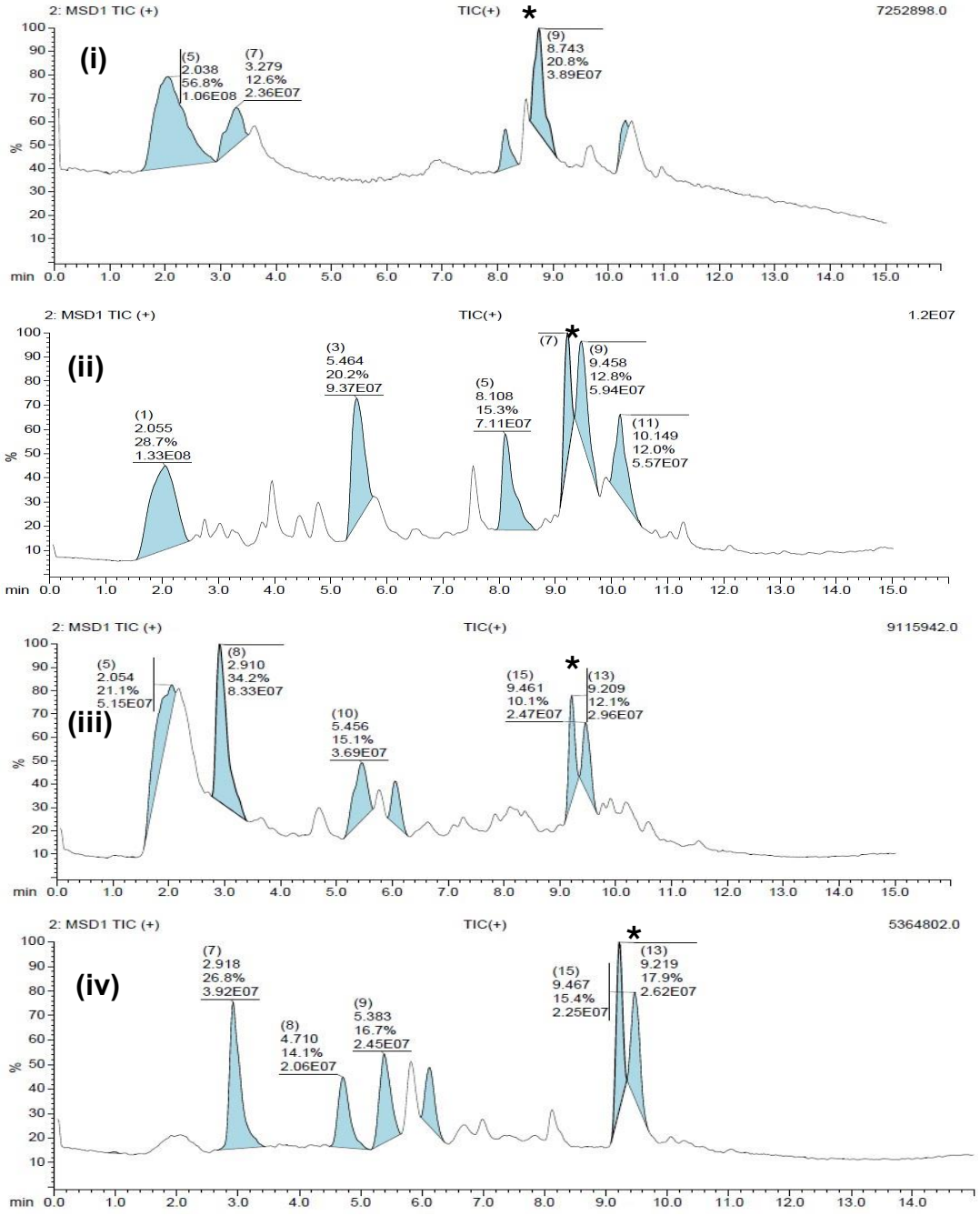

*Figure 6.12: LC-MS chromatograms for different coupling conditions between compounds **6.5** and **6.7**. * =compound **6.9,** which appeared as 2 peaks on the chromatogram, due to the presence of distinctive cis-trans isomers. Table 6.3 shows corresponding conditions for the different chromatograms.*

Purification proved to be daunting, due to the formation of a complex mixture, and normal phase silica chromatography proved ineffective at separating compound **6.9**, as was seen for compound **6.7**. Hydrazones are sensitive compounds, that are easily hydrolysed at an acidic pH.[383] Hence, RP-HPLC was employed to purify compound **6.9**. The first eluted compound **6.9.A** and the second eluted compound **6.9.B** had very close retention times, so co-elution along with further impurities, was observed at a 40-95% CH_3CN gradient (Figure 6.13, (i)).

The purification protocol was optimised with a slower gradual increase in CH_3CN from 30-95% (ii) led to successful isolation of compounds **6.9.A** and **6.9.B**. As was described for compound **6.7**, product was purified in multiple batches, to obtain enough product for characterisation, and for further reactions. Both isolated compounds appeared clean via LC-MS, while they had the same M+H (Figure 6.13 (iii), (iv)), further highlighting they were isomers of each other.

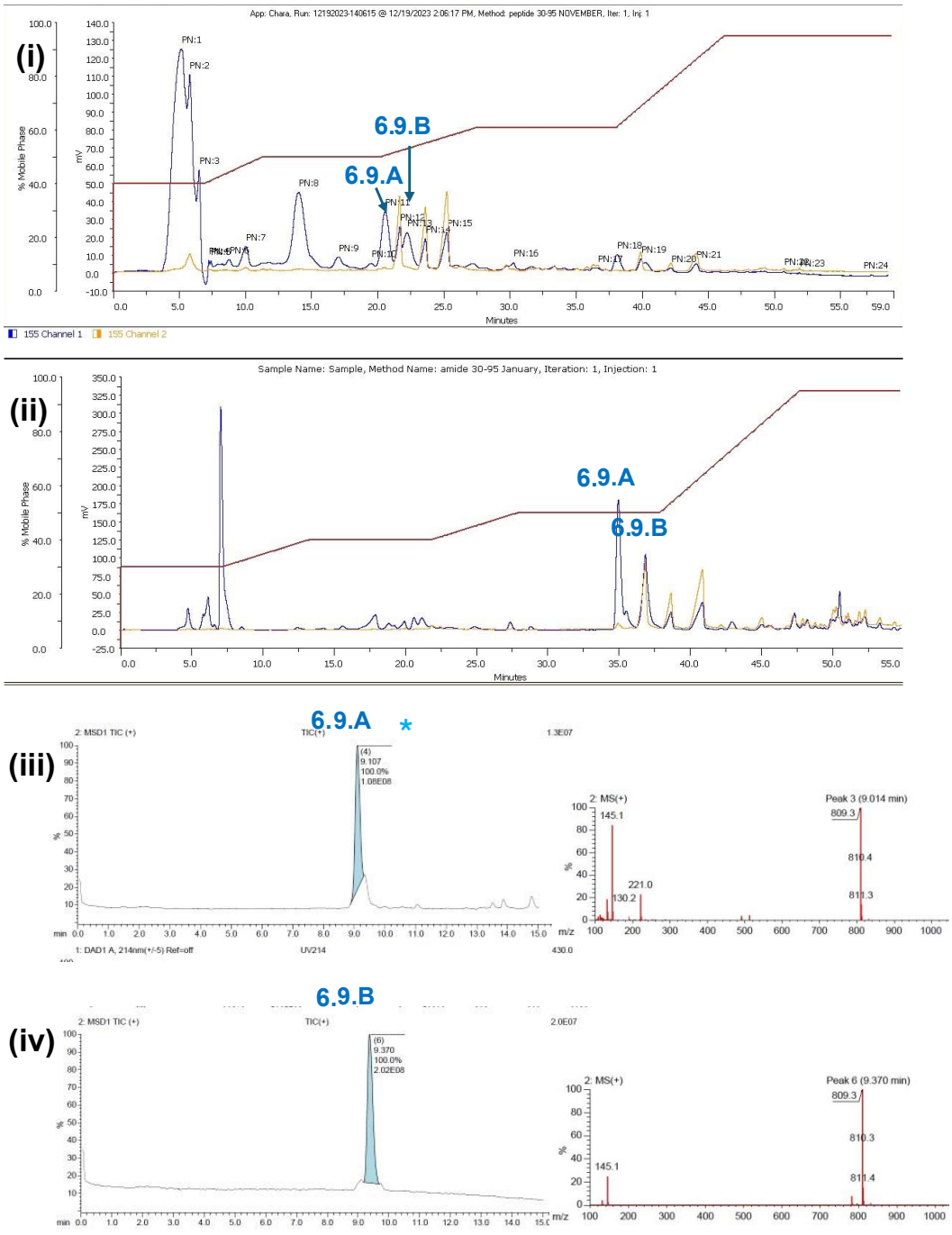

*Figure 6.13: Tested HPLC conditions included a (i)40-95% CH_3CN in H_2O gradient, (ii)30-95% CH_3CN in H_2O gradient. LC-MS traces of compound **6.9.A** (iii) and compound **6.9.B** (iv): **6.9A** and **6.9B** were isomers, according to MS, as they had the same M+H=809.3.*

Structural elucidation using NMR proved challenging due to the presence of complex mixtures. The presence of *cis-trans* isomers, as well as conformational isomers and rotamers have been reported for acyl hydrazones.[384] Despite close retention times, separation of *cis* and *trans* isomers was achieved via HPLC, which was encouraging. This was confirmed by the separation of compounds of the same mass, which showed their own distinct sets of signals, when comparing their ^{1}H NMR spectra (Figure 6.14). Each compound had 2 sets of peaks around the A ring, which did not overlap, suggesting complete separation of the 2 isomers. It was theorised that the smaller sets of peaks, within the 9.A and 9.B isomers, belonged to rotational isomers around the O=C-N bond, so a 1D NOE experiment was carried out.

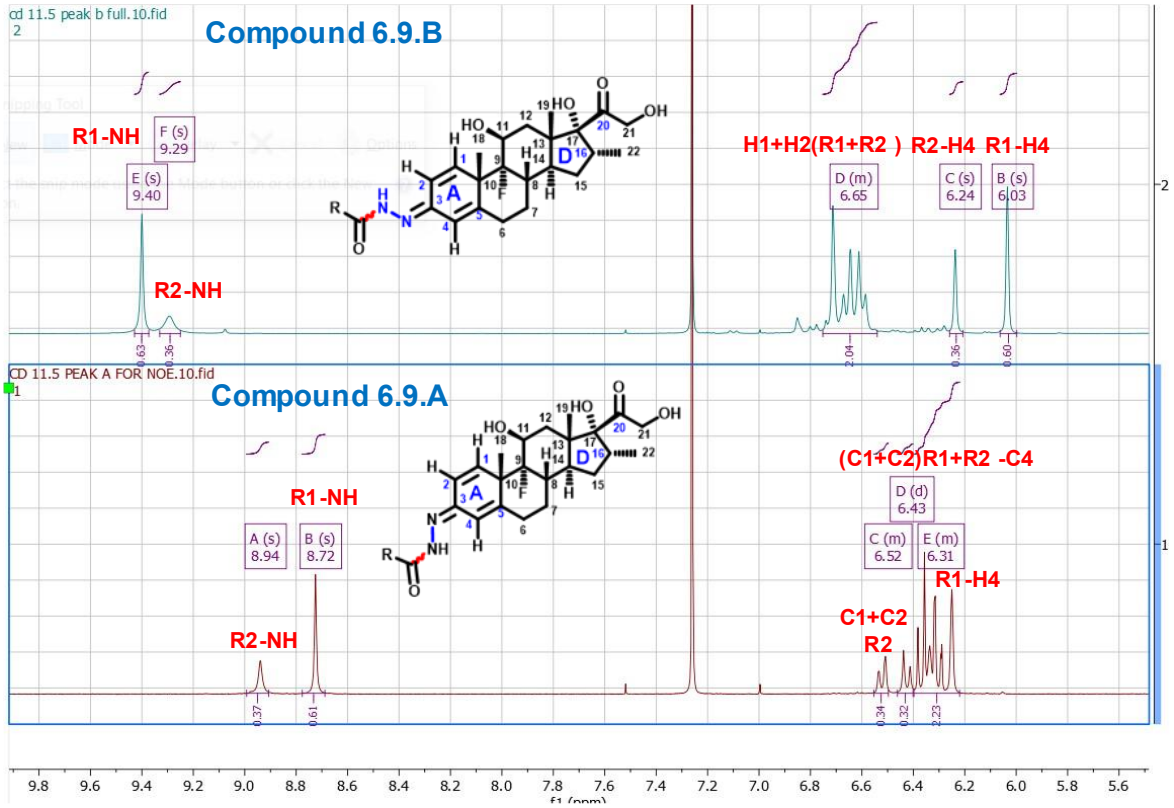

*Figure 6.14: Overlapped 1H NMR spectra (in $CDCl_3$) of isomers of compounds **6.9.A** and **6.9.B** showed distinctive sets of peaks around ring A of dexamethasone, confirming isolation of cis-trans isomers. Each isomer had 2 sets of rotamers.*

Hu, Ley *et al.* have previously described the use of a 1D gradient NOESY ^{1}H NMR based experiment, to assess the presence of rotamers, vs diastereomers.[378] For isomer B two distinctive singlets, with different peak integrations were observed, so the peak at 5.97 was irradiated, to study through space interactions. Both singlets at 5.97 and 6.17 were on the same phase upon irradiation, which would indicate the presence of rotamers. No other

interactions were observed. This absence of correlations also provided some further information, as no interaction with the NH peak was present. While 2 easily separable singlets were observed for H4, the same was not the case for H1 and H2, with a multiplet containing those protons observed. This multiplet integrated as 2 protons compared to a known peak with a singlet proton, which further proved the hypothesis. NOESY 2D NMR showed an interaction between the NH and the multiplet, which includes the C2 peak. The absence of a correlation between the H4 singlet and the NH from 1D NOE, and the observation of interaction between the multiplet containing H2 and the NH, from 2D NOESY, provided final confirmation of the **6.9.B** structure.

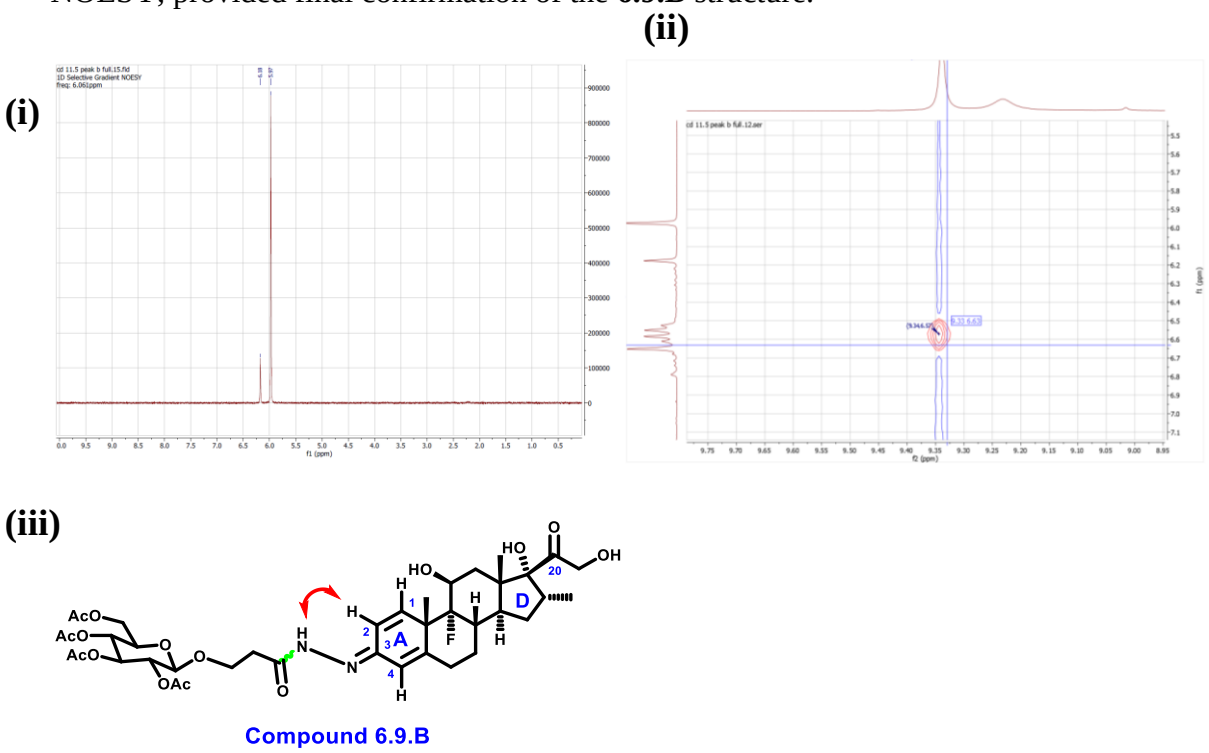

*Figure 6.15: NMR spectroscopy data in $CDCl_3$, confirming the structure compound **6.9.B**: (i) 1D NOE experiment illustrating the 2 H4 singlets belong to rotamers. (ii) 2D NOESY experiment showed an interaction between NH, and doublet belonging to H2. (iii) structure of isomer B*

The 1D NOE experiment for compound for compound **6.9.A** provided further information on conformation, however there were overlapping signals within the multiplet at 6.30-6.50 ppm (Figure 6.14). The H4 singlet was irradiated for compound **6.9.A** and showed an interaction through space with the major NH peak, which was seen on in the inverse phase of the spectrum. The presence of rotamers was presumed for **6.9.A,** due to confirmed rotamers for isomer **6.9.B**. Initial trial of the acetate deprotection showed that the final compound was poorly soluble in $CDCl_3$, so full spectral assignment was carried out in CD_3OD. Full structural elucidation of the acetate protected compound from peak A was carried out in CD_3OD, to be able to directly compare spectral changes between the acetate

protected, and the deprotected species. 2D NMR data was employed, to carry out the assignment, including COSY, NOESY, HSQC and HMBC.

As previously described, 2 sets of peaks were present for H1, H2 and H4, which was attributed to rotamers. A 1D NOE experiment had shown interaction between NH and the singlet at C4, suggesting that the *cis*-isomer was isolated. The major isomer's peaks were reported in Table 6.4, but as can be seen in the ^{1}H NMR in the appendix, a mixture of approximately 4:1 of rotational isomers was formed, with variation on the ratio observed in different sample concentrations and solvents. The quaternary (q) carbon for C3, belonging to the acyl hydrazone's C=N bond, was identified at 150.0 ppm, through HMBC interaction with H1, confirming the hydrazone bond was not cleaved. The H21 doublets (d) were masked within a multiplet (m), with glucose, but were still present, as identified through HSQC, and HMBC interaction with the C20 carbonyl. Multiplets, containing Hs from multiple Cs were analysed via the use of HSQC, which helped show how many carbons corresponded to each peak. All carbons in the molecule were assigned, apart from C10 and C13, which were masked within the CD_3OD peak, according to previous analyses in $CDCl_3$, and 2D NMR. C-F carbons were also identified, with coupling constants reported. The doublet at 108.8, corresponding to C9, displayed a coupling constant of 174.4 Hz, which was within the expected range of an α-C- F. Moreover, C doublets (d) were identified for C7, C8 and C11, with the expected coupling constants for ^{19}F coupling. Despite characterisation challenges, the glucose-dexamethasone acetate protected linker was synthesised, isolated, and fully characterised. This compound has not previously been reported in literature, making it a novel compound.

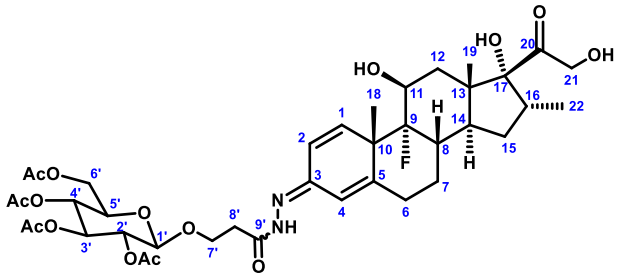

	^{1}H NMR shift (ppm)	Multiplicity	J (Hz)	C-type	^{13}C NMR
C1*	6.58	d	10.17	CH	142.3
C2*	6.38	dd	10.2, 2.0	CH	127.1
C3	-	-	-	q	150.0
C4*	6.62	s	-	CH	112.4
C5	-	-	-	q	161.3
C6	2.49-2.58, 2.62-2.78?	m	-	CH_2	36.1
C7	1.54-1.61, 1.79-1.9	m		CH_2	28.9
C8	2.3-2.49	m	-	CH	35.7 (d, J=19.6)
C9	-	-	-	q C-F	101.9 (d, J=174.1)
C10	-	-	-	q	In CD_3OD**
C11	4.19-4.32	m	-	CH	72.1 (d, J=35.4)
C12	1.44, 2.18-2.32	m		CH_2	37.2
C13	-	-	-	q	In CD_3OD
C14	2.18-2.32	m		CH	43.7
C15	1.13-1.25, 1.66-1.79	m	-	CH_2	33.4
C16	3.0	m	-	CH	37.0
C17	-	-	-	q	92.1
C18	1.52	s	-	CH_3	24.8 (d, J=5.1)
C19	0.99	s	-	CH_3	17.5
C20*	-	-	-	-	212.7
C21*	4.19-4.32, 4.59	m		CH_2	68.1
C22	0.86	d	7.3	CH_3	15.4
C1'	4.68	d	8.0	CH	102.2
C2'	In HDO** (4.80-4.90)			CH	72.8
C3'	5.23	t	9.5	CH	74.2
C4'	5.00	t	9.7	CH	69.8
C5'	3.83-3.9	m	-	CH	72.7
C6'	4.08-4.16, 4.19-4.32	m	-	CH_2	63.0
C7'	3.9-3.97, 4.08-4.16	m		CH_2	67.4
C8'	2.3-2.49, 2.62-2.78	m	-	CH_2	32.6
C9'*	-			q	170.2
Acetyl	-	-	-	q	171.3, 171.3, 171.6, 172.3
Acetyl methyl	1.89-2.08	m	-	4xCH_3	20.5, 20.6, 20.6, 20.6

*Table 6. 4: NMR assignment of compound **6.9.A** in CD_3OD: * Denotes key resonances. **According to 2D NMR data.*

Acetate deprotection

Due to the acid sensitive nature of acyl hydrazones, base catalysed acetate deprotection was carried out. A protocol by Guilherme, *et al.* was followed, that employed excess strong base to promote full deprotection of the glucose acetates, without cleaving the hydrazone bond.[381] The conditions were first trialled on the glucose linker (Figure 6.16), and loss of acetates was confirmed by ^{1}H NMR, ^{13}C NMR, and mass spec. Moreover, a shift up-field was observed for the glucose peaks on the ^{1}H NMR. The conditions were then tested on compound **6.9.A**, with caution, due to sample availability.

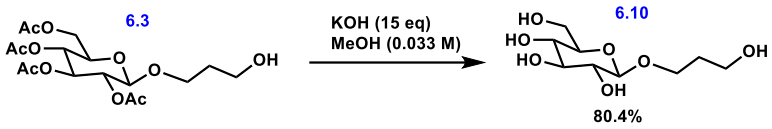

*Figure 6.16: Acetate deprotection of glucose linker **6.3**.*

The aim was to first test the deprotection conditions on compound **6.9.A**, and upon confirming bioactivity of the small molecule, to then obtain the deprotected derivative of compound **6.9.B.** The conditions shown on Figure 6.16 were used, and the reaction was monitored via LC-MS and stopped after 6 hours. Acetates were removed upon workup on the K ion exchange resin IR-120.[381] The resin was considered a favourable way to remove excess KOH, without requiring an aqueous workup, which may have caused product loss, due to the aqueous solubility of glucose. Loss of acetates was confirmed via ^{1}H NMR and ^{13}C NMR. LC-MS showed several peaks of unknown mass, with the predominant peak showing a mass of 627.4.

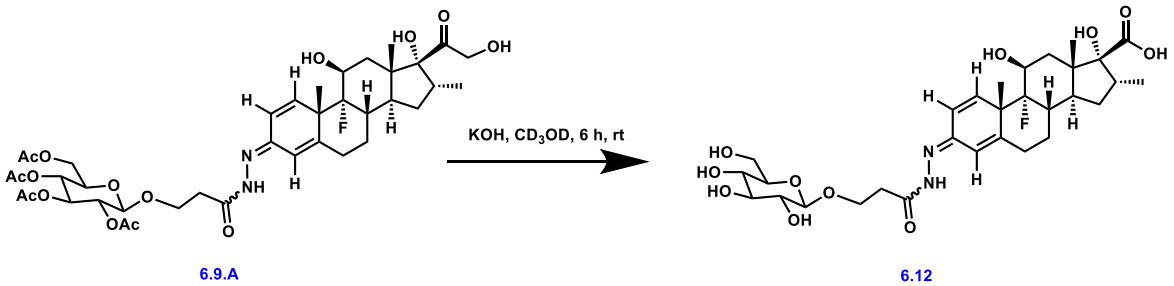

*Figure 6.17: Acetate deprotection of compound **6.9.A***

RP-HPLC purification was carried out on this crude material, with some solubility issues faced. Despite adapting the gradient to the LC-MS conditions, which had showed separation, both the peak of interest, and the byproducts showed close retention times (Figure 6.18, (i)). Nonetheless, the predominant peak was successfully isolated, in a relatively low recovery of

1.4 mg. LC-MS analysis of the compound revealed high purity (ii), however the mass did not correspond to the expected product.

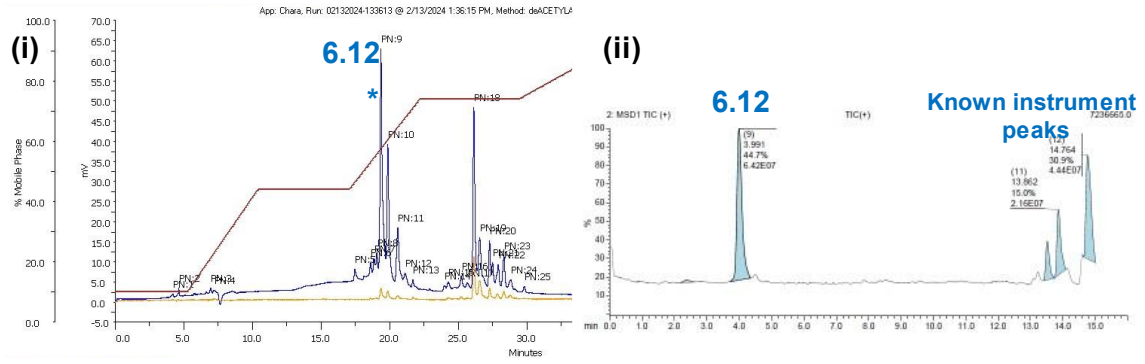

*Figure 6.18: Compound **6.12** was purified using a 10-95% CH_3CN in H_2O gradient, via RP-HPLC. (i)HPLC chromatogram, (ii) LC-MS chromatogram (gradient 30-95% CH_3CN in H_2O)*

Structural elucidation was then carried out via previously mentioned 2D NMR techniques, with challenges of overlapping peaks being faced again, as well as a need for special NMR protocols, due to low sample availability. The loss of mass led to considering that degradation had potentially occurred, under the strongly basic conditions, but it was not immediately clear what had occurred. The mass loss was calculated to either correspond to a loss of N, or CH_2, which initially seemed unlikely.

Hydrazone hydrolysis had not occurred in the isolated compound, as the glucose linker was still attached, and the doublet of doublets (dd) corresponding to C2, and multiplet containing C1 and C4, that belong to the A ring, were still present (Table 6.5). Moreover, the C9', corresponding to the acyl-hydrazone, amide bond, was still present in the ^{13}C NMR, at 170.7 ppm. A set of smaller peaks were also observed on the ^{1}H NMR, but LC-MS showed that the product was clean. More extensive analysis on the acetate protected conjugate **6.9** had revealed the presence of rotamers, so it was considered that the same behaviour would also be present in the final compound.

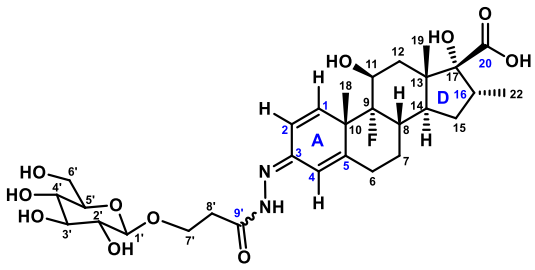

	H NMR (ppm)	multiplicity	J (Hz)	C-type	^{13}C NMR (ppm)
C1*	6.58-6.64	m	-	CH	143.0
C2*	6.39	dd	10.2, 2.1	CH	126.9
C3	-	-	-	q	150.6
C4*	6.58-6.64	m	-	CH	112.3
C5	-	-	-	q	161.8
C6	2.29-2.45, 2.69-2.76	m	-	CH_2	32.8
C7	1.47-1.51, 1.80-1.88	m	-	CH_2	29.0
C8	2.29-2.45	m	-	CH	35.9 (d, J=19.7)
C9	-	-	-	q C-F	102.1 (d, J=174.5 Hz)
C10	-	-	-	-	IN CD_3OD
C11	4.18-4.24	m		CH	72.4 (d, J=3j7.6)
C12	1.47-1.51, 2.06-2.15	m	-	CH_2	37.1
C13	-	-	-	q	IN CD_3OD
C14	2.06-2.15	m	-	CH	44.9
C15	1.16-1.20, 1.68-1.76	m	-	CH_2	33.8
C16	3.00	ddd	11.3, 7.3, 4.2	CH	37.2
C17	-	-	-	q	88.5
C18	1.53	s	-	CH3	24.8 (d, J=5.2)
C19	1.16	s	-	CH3	18.0
C20*	163.33 moved from 212	-	-	q	163.3
C21*	**Lost**	-	-	-	-
C22	0.90	d	7.22	CH3	15.6
C1'	4.31	d		CH	104.7
C2'	3.17	t	9.17. 6.52	CH	75.1
C3'	3.33-3.37	m		CH	78.1
C4'	In CD_3OD				78.1
C5'	3.23-3.26	m		CH	71.7
C6'	3.60-3.65, 3.83.-3.89	m		CH_2	62.8
C7'	3.93-3.98, 4.11-4.16	m		CH_2	67.1
C8'	2.60-2.68,	m		CH_2	36.6
C9'*	-	-	-	q	170.7
Acetyls*	Lost				Lost

*Table 6.5: NMR assignment of deprotected steroid-glucose conjugate **6.12**. *=key resonances*

Despite C21 peaks previously being masked in a multiplet with glucose, they were positively identified in the acetylated precursor compound **6.9.A**. Both the Hs and the C were clearly removed in the final compound, according to NMR. Moreover, a quaternary C, belonging to the C20 ketone, previously located at 212.7 was no longer visible in the final compound. This led to the hypothesis that degradation on the 20-keto-21-hydroxyl side chain of the D ring occurred, due to excess KOH, leading to the formation of a reactive enolate. Li *et al.* had reported that treatment of betamethasone, which is an isomer of dexamethasone, with

excess base could lead to extensive degradation on the C20 side-chain.[385] One of the compounds identified was carboxylic acid **6.12**, whose mass would match the mass observed by LC-MS and would also explain the apparent loss of a methylene unit. HMBC analysis was not fully diagnostic, due to a weak signal, which led to difficulties assigning quaternary Cs. However, having previously assigned the spectrum for the acetylated precursor, it was possible to extrapolate the results. C3, C5 and C9' were within the same region as previously observed, while the quaternary Cs, belonging to the acetates were lost. C10 and C13 were previously identified upfield, in the region of the CD_3OD peak. Therefore, having fully assigned the remainder of the peaks, it was concluded that while deprotection did occur, degradation on the C20 side chain also occurred. Future work would include scaling up, to obtain further characterisation data, as well as attempting different deprotection conditions.

As can be seen in Figure 6.19, in the presence of excess base deprotonation can occur at the α-carbon of the C20 carbonyl, to generate a reactive enolate (I-1). This enolate can then react to generate by-products (Figure 6.18). Given a carboxylic acid was successfully isolated, it is important to identify the mechanism involved in the formation of conjugate **6.12**. According to Li *et al.* a Baeyer-Villiger-type oxidation occurred in the presence of air, which generated a carboxylic acid derivative of betamethasone, akin to the degradation observed for conjugate **6.12**.[385] A plausible mechanism involved enolate formation (I-1) in the presence of excess base, which then reacted with atmospheric oxygen, to generate a peroxide intermediate (I-2).[385] This was followed by a proton transfer and a Baeyer-Villiger type-rearrangement, which generated a formic anhydride intermediate (I-3). This intermediate was then hydrolysed in the presence of excess KOH, which led to formate loss, and afforded the K salt of the final product (I-4). Protonation finally occurred with an ion-exchange resin, which generated conjugate **6.12**.

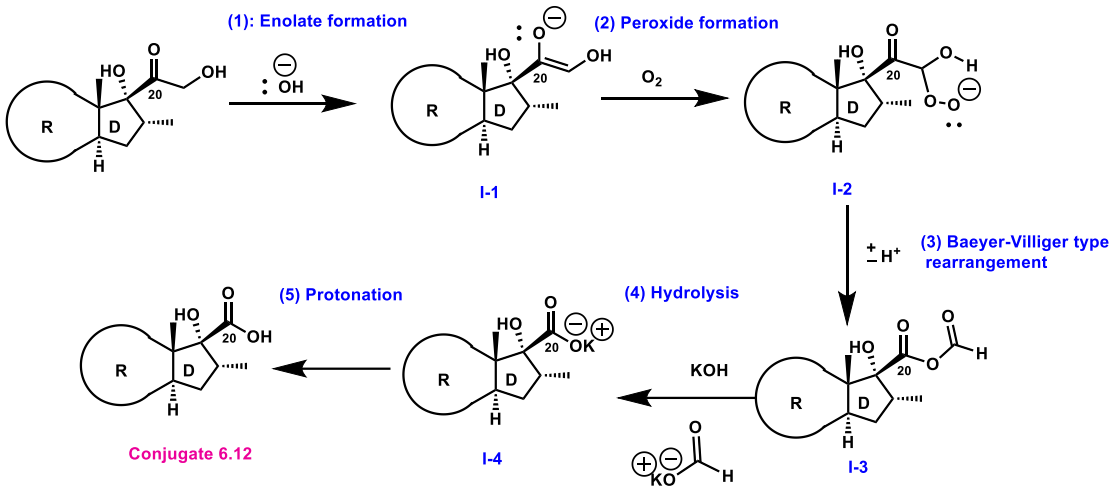

*Figure 6.19: Plausible reaction mechanism of degradation, and intermediates involved: (1) An enolate intermediate (I-1) was generated in the presence of excess KOH. (2) This was followed by a peroxide formation (I-2) in the presence of O_2. (3) Baeyer-Villiger type rearrangement (I-3). (4) Hydrolysis (I-4). (5): Protonation with an ion exchange led to the formation of conjugate **6.12**. Adapted from betamethasone degradation mechanism reported by Li et al.*[385]

6.4.2 Biological testing of steroid-glucose conjugate 6.12.

Although the planned target was not generated, evaluation of the biological properties of compound **6.12** was undertaken. This small molecule still contains the GLUT1 targeting group, hydrazone linker, and glucocorticoid scaffold. Poorly differentiated MG-63 cells, and more mature SAOS-2 OS cells were treated with control medium, dexamethasone, or the small molecule conjugate **6.12**. In previous experiments a high glucose DMEM medium was used, as a basal medium. However, since in this chapter the aim was to study the effect of the steroid-glucose conjugate on GLUT1 expression, a low glucose Glutamax-supplemented version of DMEM was used. Glucose starvation is often employed for GLUT1 studies, in order to study protein expression and localisation,[386] but given the longer differentiation experiments employed in OS studies, extensive starvation was deemed unsuitable.

Effect of steroid glucose conjugate 6.12 on MG-63 cells.

The first objective was to observe whether treatment with the conjugate would alter viability, via the alamar blue assay. SAOS-2 and MG-63 cells were treated with a wider range of concentrations of 0.01, 0.1, 1, 10 and 20 μM of dexamethasone or the conjugate **6.12**. Viability was studied over the course of a week, while cell growth was assessed at regular intervals via microscopy. After 1 day of treatment viability was comparable between the untreated control and the treatments (Figure 6.20). After 3 days of treatment, fewer metabolically active cells were present in the conjugate treated group, though cells were still

viable, while an increase was observed for MG-63. After 7 days of treatment comparable cell numbers were observed between the control and the 2 treatments, having formed confluent monolayers for all the conditions. It was exciting to observe that while the glucose-steroid conjugate was not cytotoxic, it led to a small decrease in cell numbers, which may potentially translate to a decrease in OS proliferation.

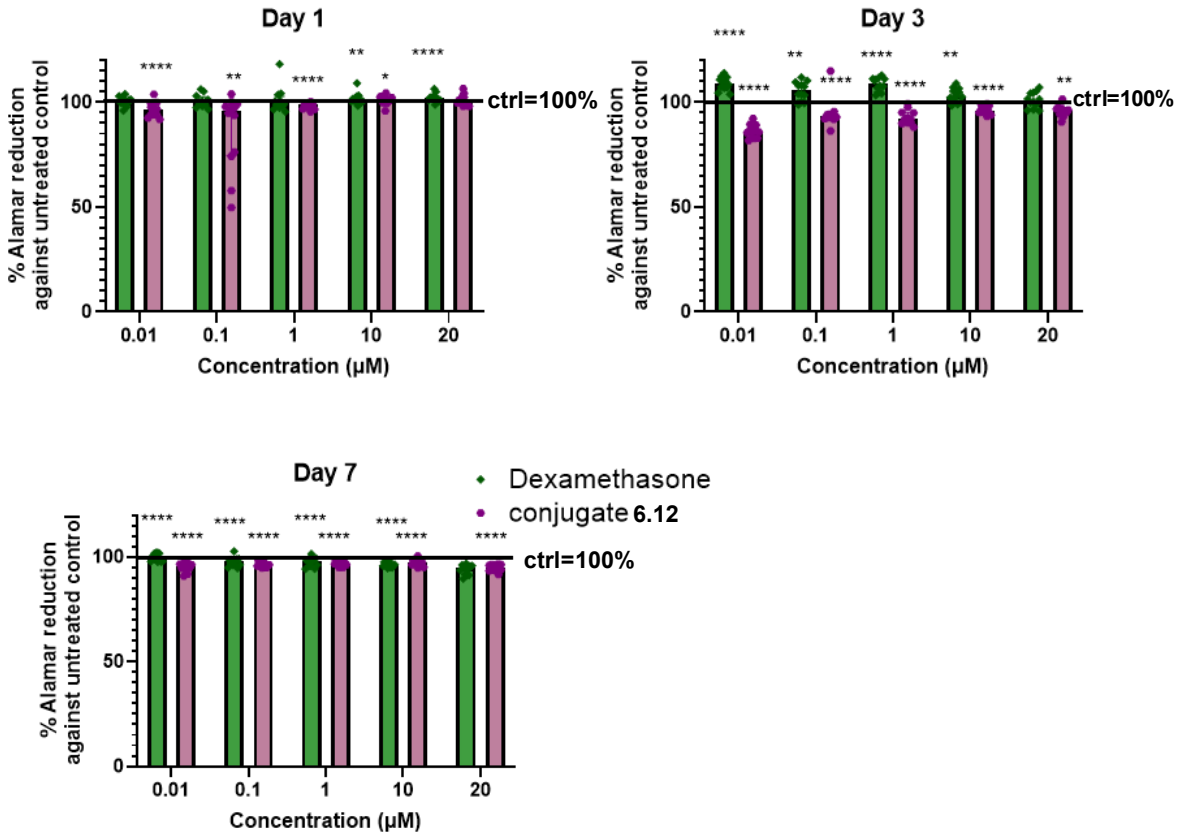

*Figure 6.20: Cell viability was assessed via the alamar blue assay: MG-63 cells were treated with 0.01, 0.1, 1, 10 or 20 μM of dexamethasone or conjugate **6.12.** %Alamar reduction was measured against the untreated control, after 1, 3 and 7 days of treatment. Mann Whitney test used for statistical comparison between treatments and control=100% (blank=ns=p>0.05, *=p<0.05, **=p<0.01)*

Having confirmed cell viability, the effect of small molecule treatment on differentiation was studied via ICW analysis. Changes in protein expression were quantified across the different concentrations. Having modified the structure of dexamethasone, the aim was to observe whether the synthesised steroid-glucose conjugate could induce biological response in the OS cells. The response of MG-63 cells to dexamethasone was more limited than expected (Figure 6.21). A small, yet statistically significant increase in RUNX2 was observed at the highest tested concentration, at 20 μM, while some insignificant upregulation of ONN was observed at 0.01 and 0.1 μM. On the other hand, the synthesised small molecule presented clear biological response and appeared to drive differentiation in MG-63 cells (Fig

6.20 B). It was highly encouraging that RUNX2 was upregulated in a dose dependent manner, as evident by the gradual increase in RUNX2 fold-expression, with the highest fold-upregulation observed at a 20 μM concentration. Moreover, the conjugate **6.12** drove an upregulation of ONN, with statistically significant increase in ONN expression at a 20 μM concentration of conjugate **6.12**, further corroborating findings of differentiation.

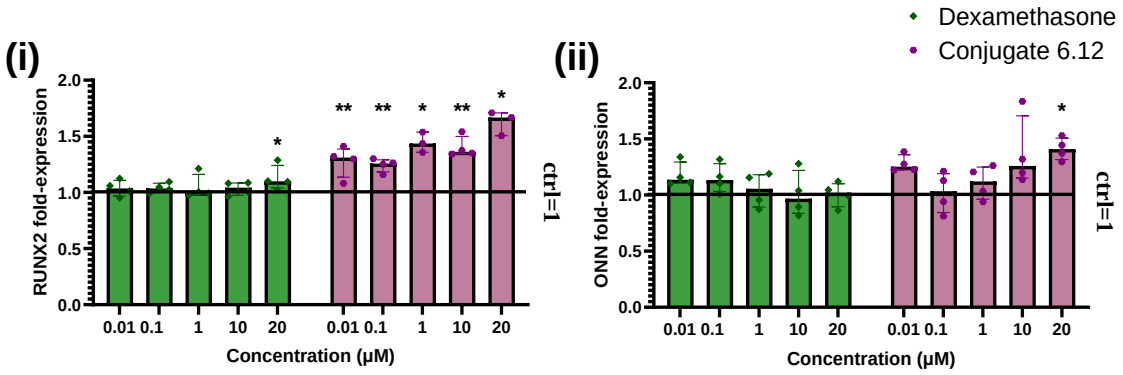

*Figure 6.21: Protein fold-expression measured by ICW: Differentiation was assessed in MG-63, after 7 days of treatment with dexamethasone (green) or conjugate 6.12 (pink): (i) RUNX2, (ii) ONN protein fold-expression was quantified against untreated MG-63 D7 control. The Mann Whitney u-test was used to statistically compare treatments' protein fold-expression compared to control=1. (blank=ns=p>0.05, *=p<0.05, **=p<0.01)*

Immunofluorescence staining was subsequently carried out, in order to further study RUNX2 protein expression and localisation. As was previously seen in chapters 3 and 5 RUNX2 present perinuclear and cytoplasmic localisation in MG-63 cells (Figure 6.22). Inhomogeneous protein expression was observed with arrows pointing to areas of increased protein expression. Dexamethasone treated cells showed reduced protein expression compared to the control group, with areas of high protein expression. Conjugate **6.12** on the other hand showed increased protein expression compared to the control group, validating ICW findings, and confirming differentiation being driven.

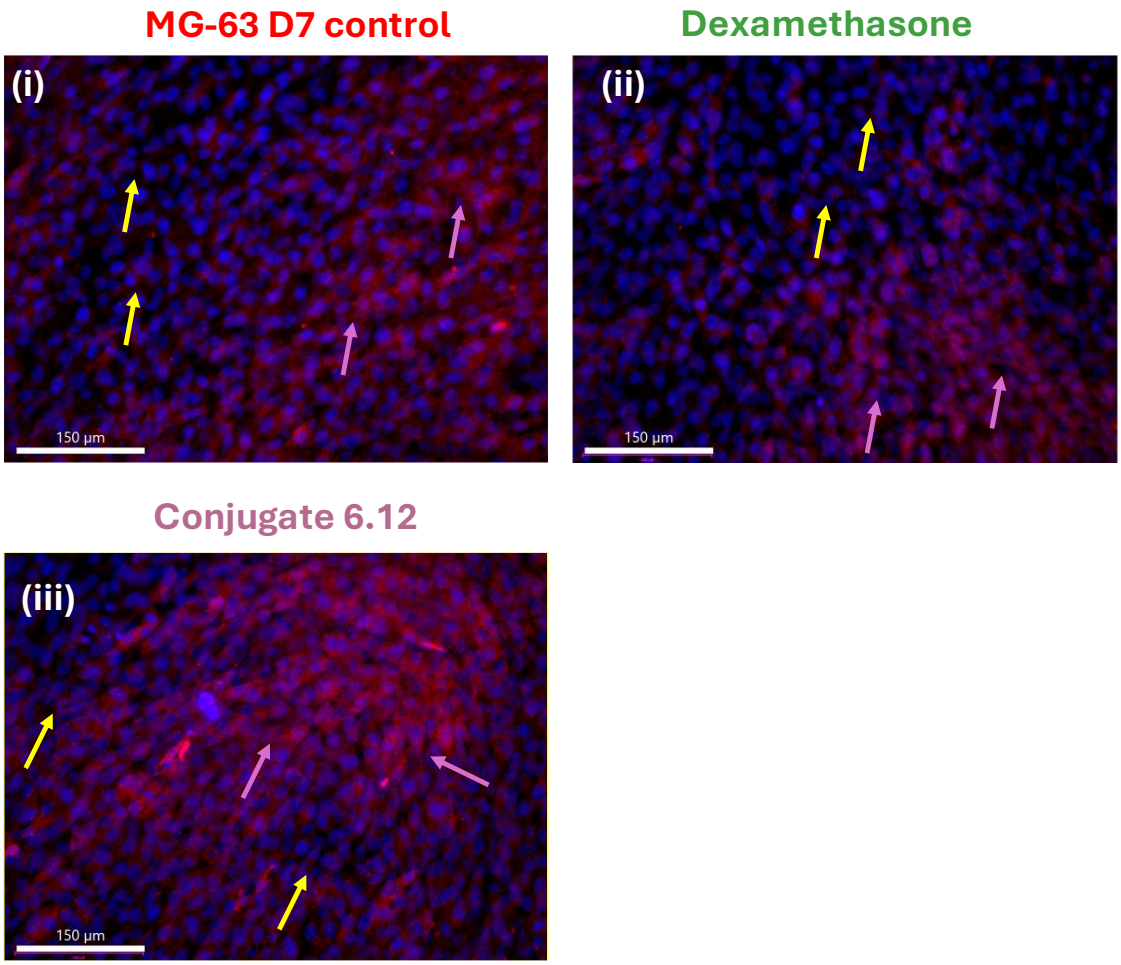

Figure 6.22: RUNX2 expression assessed by immunofluorescence: MG-63 cells were treated with 10 µM of dexamethasone (ii) and conjugate 6.12 (iii) for 7 days, while an untreated MG-63 D7 control (i) was also included. Cells were stained with RUNX2 (red) and DAPI (blue) and imaged on EVOS microscope at 20x magnification. Images processed with Imaris Viewer. Scale bars: 150 µm. Yellow arrows point to areas of decreased RUNX2 expression, and pink arrows point to areas of increased RUNX2 expression. N=1 biological replicate, N=2 experimental replicates.

Despite degradation on the C20 side chain, conjugate **6.12** was still able to drive differentiation in MG-63 cells, and showed enhanced biological response, compared to dexamethasone. It was theorised that conjugation of dexamethasone to glucose would drive more selective differentiation in OS cells, via GLUT1. GLUT1 levels were also assessed via ICW. Dexamethasone induced statistically significant downregulation of GLUT1 in MG-63 cells at all tested concentrations, that ranged from 0.01-10 µM (Figure 6.23, (iv)). MG-63 treatment with **6.12** did not trigger increased GLUT1 expression at lower concentrations, while at a 10 µM concentration, an insignificant upregulation was observed. However, GLUT1 expression was higher than what was observed for dexamethasone, potentially indicating a role of GLUT1 in small molecule uptake in OS cells. Significant increase in

GLUT1 was expected, so future work would include further testing, to identify pathways of delivery and differentiation. Having previously observed most consistent differentiation after 10 μM treatment with steroids cholesterol sulfate, and fludrocortisone acetate, some preliminary immunofluorescence imaging was carried out for that concentration. GLUT1 was abundantly expressed in MG-63 cells, and presented mostly diffuse cytoplasmic expression, though GLUT1 is also localised on the cell membrane (i, ii, iii). As previously seen for different markers GLUT1 was inhomogeneously expressed, with arrows pointing to areas of higher protein expression. Dexamethasone treated cells presented lower protein expression (ii), compared to the control (i), matching observations from ICW. On the other hand, conjugate **6.12** treated cells abundantly expressed GLUT1 (iii), with some areas presenting higher protein expression than the control group.

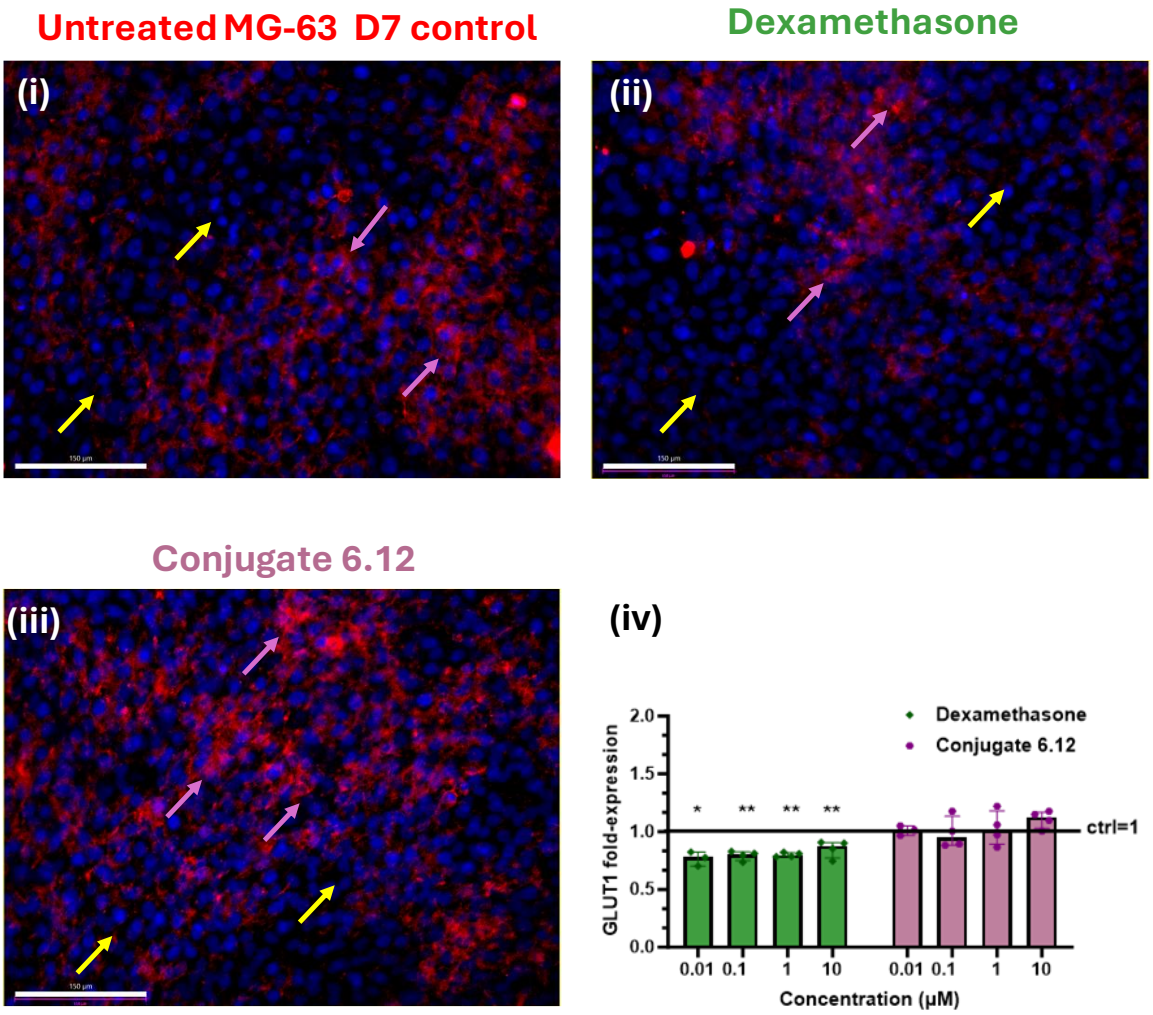

*Figure 6.23: GLUT1 fold-expression was assessed via IF and ICW: MG-63 cells were treated with 10 µM of dexamethasone (ii) and conjugate 6.12 (iii) for 7 days, while an untreated MG-63 D7 control (i) was also included. Cells were stained with GLUT1 (red) and DAPI (blue) and imaged via immunofluorescence. N=1 biological replicate, N=2 experimental replicates. Images processed with Imaris Viewer. Scale bars: 150 µm. Yellow arrows point to areas of decreased GLUT1 expression, and pink arrows point to areas of increased GLUT1 expression. N=1 biological replicate, N=2 experimental replicates. (iv) GLUT1 fold-expression was measured vs untreated MG-63 D7 control via ICW. Cells were treated with 0.01-10 µM of dexamethasone and conjugate 6.12. Mann Whitney stats. (blank=ns=p>0.05, *=p<0.05, **=p<0.01). Statistical comparison of treatments' protein fold-expression against untreated MG-63 control=1. N=1 biological replicate, N=4 experimental replicates.*

Effect of steroid glucose conjugate 6.12 on SAOS-2 cells

After 1 day of treatment dexamethasone presented a small increase in cell viability, while conjugate **6.12** showed a small decrease in alamar reduction, suggesting fewer cell numbers (Figure 6.24). After 3 days comparable viability was observed between dexamethasone and the control, while significantly reduced cell numbers were observed for the conjugate. Cell viability was further increased in MG-63 cells after 7 days of dexamethasone treatment,

while viability was further decreased in the conjugate group. It was promising to see that cells tolerated the synthesised small molecule at a range of concentrations but showed decrease in proliferation. The same effect was observed in MG-63 cells but was more pronounced for the more mature SAOS-2.

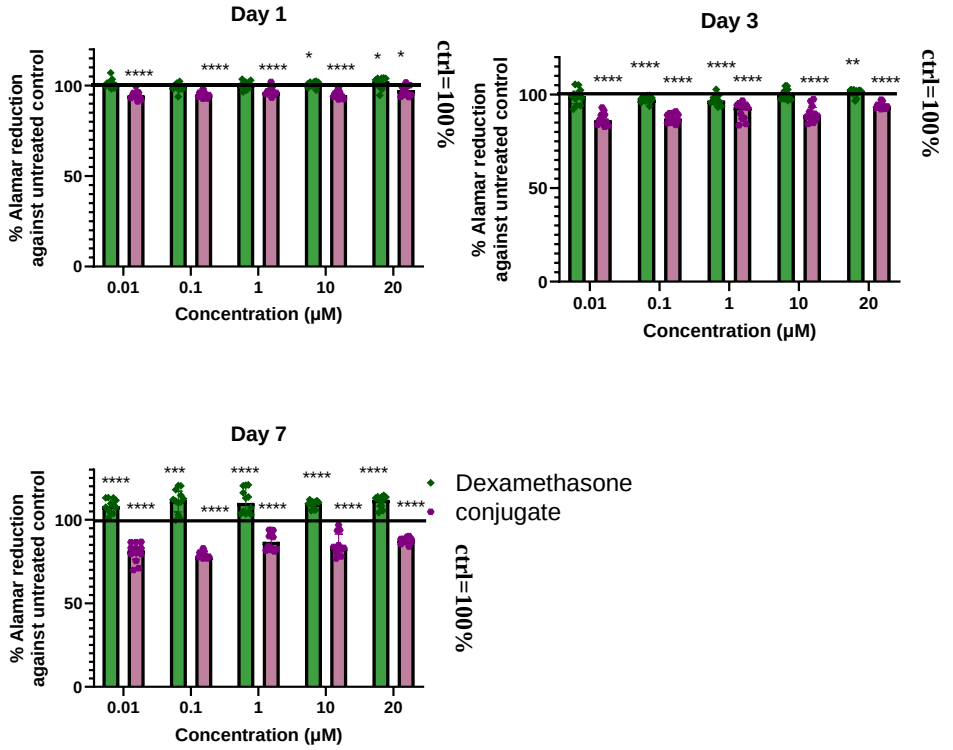

Figure 6.24: Cell viability was assessed via the alamar blue assay: SAOS-2 cells were treated with 0.01-20 μM of dexamethasone or conjugate ***6.12.*** *%Alamar reduction was measured against the untreated SAOS-2 control, after 1, 3 and 7 days of treatment. (blank=ns=p>0.05, *=p<0.05, **=p<0.01, ***=p<0.001, ****=p<0.0001). Mann-Whitney statistical comparison between treatments' alamar reduction and untreated SAOS-2 control=100%. N=1 biological replicate, N=4 experimental replicates.*

Insignificant increase in RUNX2 was observed for the conjugate with 20 μM treatment showing the largest increase, which was similar to what was observed for dexamethasone (Figure 6.25). Dose-dependent decrease in ONN expression was observed for dexamethasone treated cells, while decreased levels were also observed for conjugate **6.12**. While significant dose-dependent differentiation was observed for MG-63 cells, when treated with the conjugate, effects on differentiation were more limited in SAOS-2 cells.

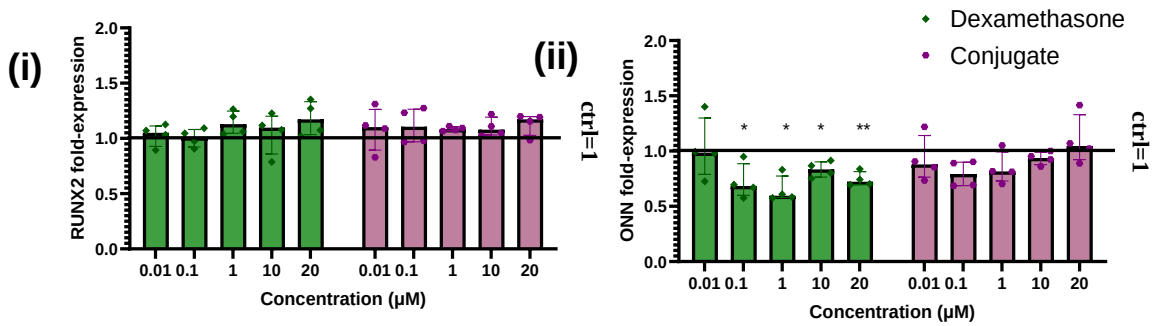

*Figure 6.25: Protein fold-expression measured by ICW: Differentiation was assessed in SAOS-2, after 7 days of 0.01-20 μM treatment with dexamethasone **6.1** or the synthesised conjugate **6.12**: (i) RUNX2 and (ii) ONN protein fold-expression was compared against untreated SAOS-2 D7 control. Mann Whitney stats (blank=ns=p>0.05, *=p<0.05, **=p<0.01). Statistical comparison between treatments' protein fold-expression and untreated SAOS-2 D7 control=1. N=1 biological replicate, N=4 experimental replicates.*

RUNX2 protein expression was further assessed via immunofluorescence, with nuclear, abundant localisation being evident (Figure 6.26), as previously seen in chapters 3 and 5. RUNX2 was highly expressed across the different conditions, with no dramatic changes observed, as was noted from ICW staining. Overall, both dexamethasone and conjugate **6.12** had a limited effect in the differentiation of SAOS-2 cells, which was contrary to what was previously observed in MG-63 cells.

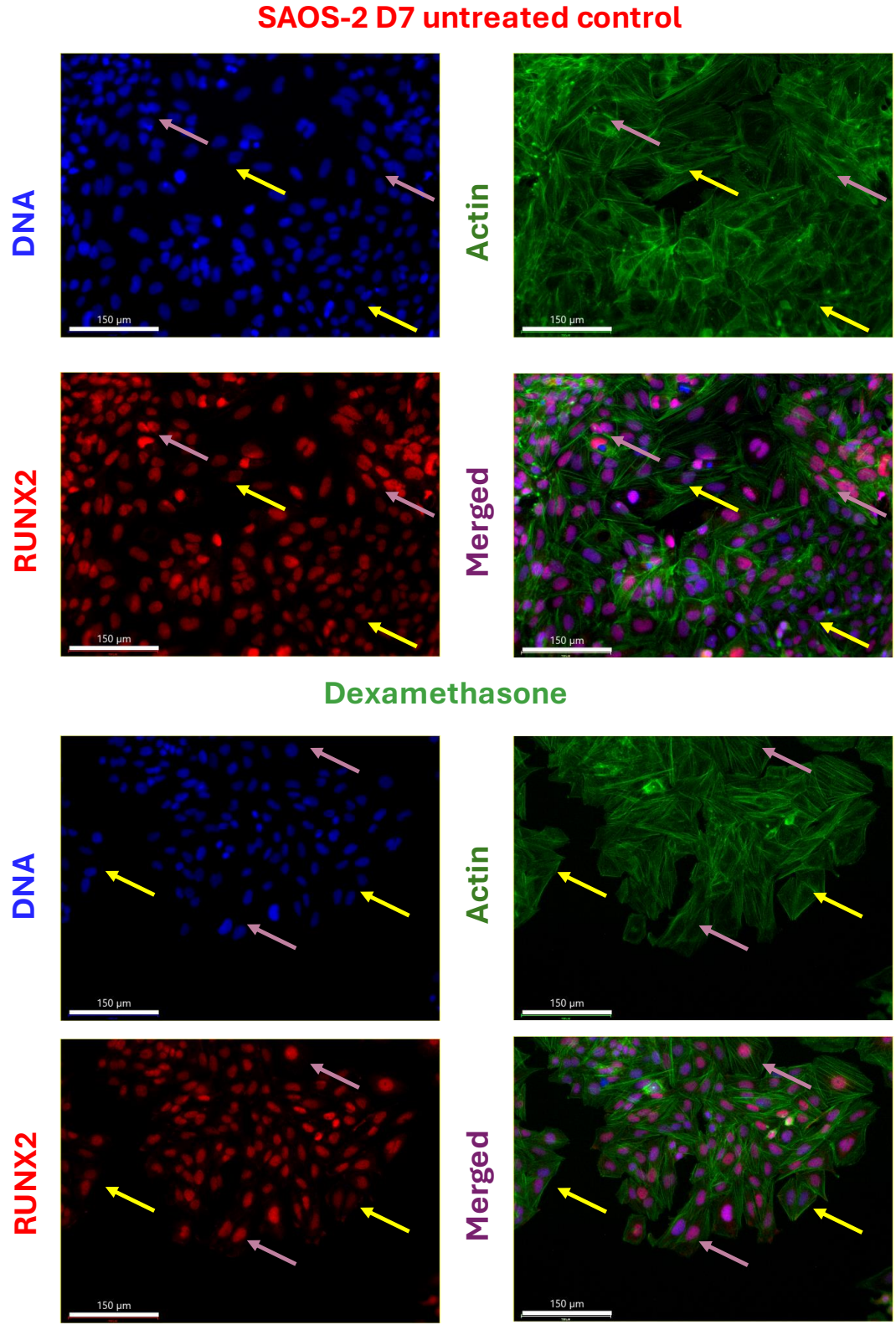
SAOS-2 D7 untreated control
DNA
Actin
RUNX2
Merged
150 µm
Dexamethasone
DNA
Actin
RUNX2
Merged
150 µm

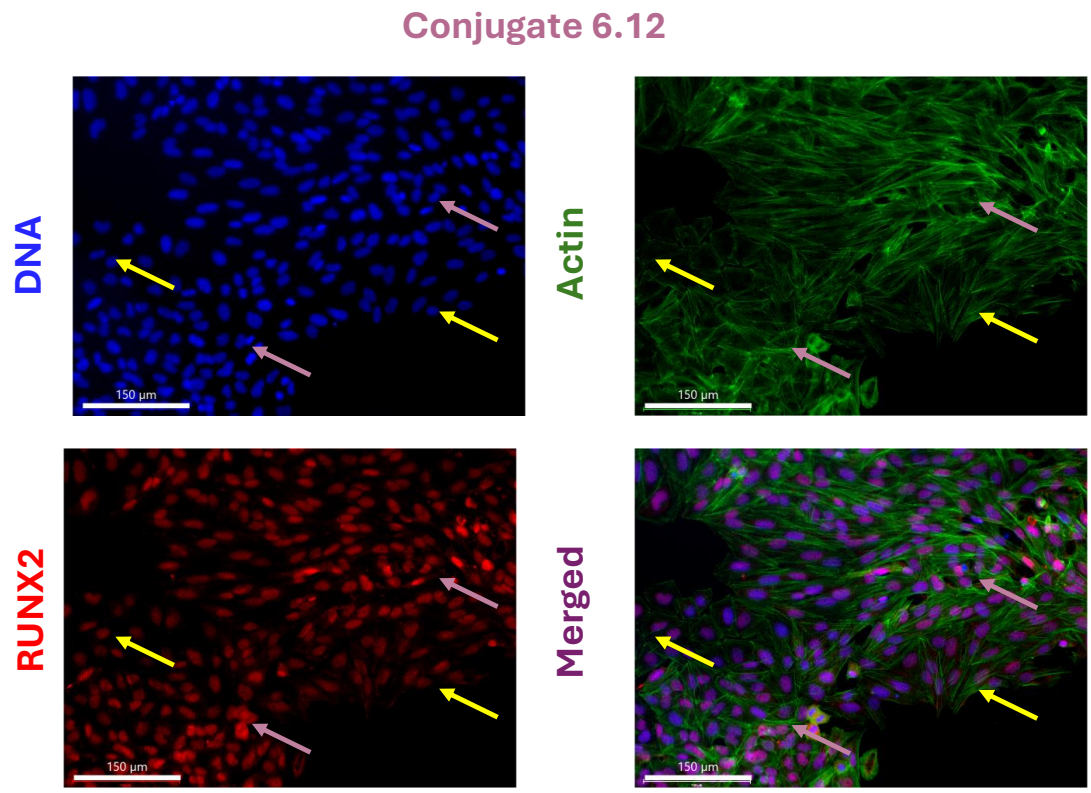

Figure 6.26: Immunofluorescence staining: SAOS-2 cells were treated with 10 µM of dexamethasone or conjugate 6.12 for 7 days. Cells were stained with DAPI (blue), phalloidin (green), and RUNX2 (red), and imaged on EVOS at 20x magnification. Images processed with Imaris Viewer. Scale bars: 150 µm. Yellow arrows point to areas of decreased RUNX2 expression, and pink arrows point to areas of increased RUNX2 expression. N=1 biological replicate, N=2 experimental replicates.

GLUT1 expression was assessed via ICW, by normalising protein expression in treated cells relative to the control. GLUT1 expression was found to be decreased after both treatment with dexamethasone and conjugate **6.12 (**Figure 6.27**,** iv**).** A trend towards dose-dependent decrease in GLUT1 was observed for the small molecule **6.12**, which would need further investigating in the future. Perinuclear granular localisation of GLUT1 was observed in SAOS-2 cells (arrows), according to immunofluorescence imaging (i, ii, iii). Abundant GLUT1 expression was observed for the control (i), while high protein expression was also observed for dexamethasone (ii) and conjugate 6.12 (iii).

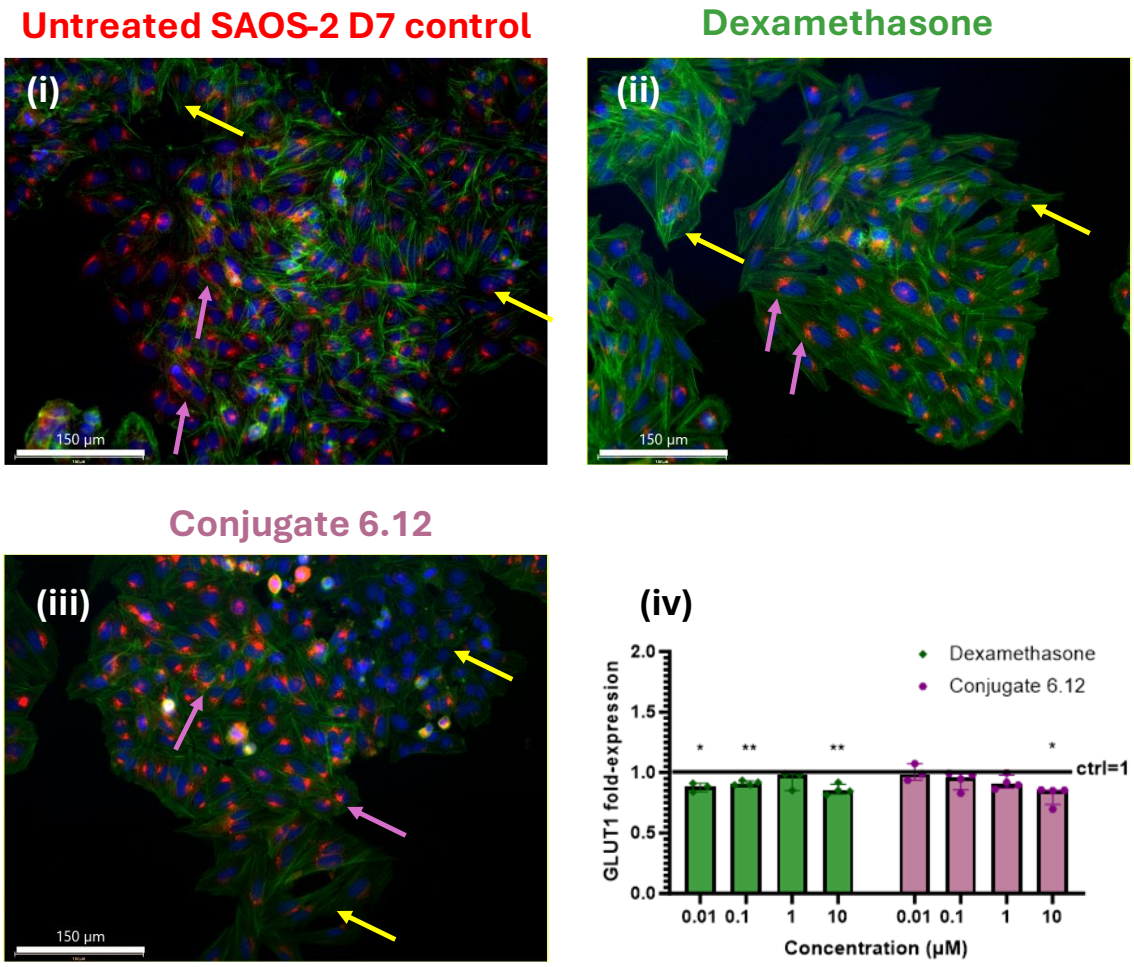

*Figure 6.27: GLUT1 fold-expression was assessed via IF and ICW: SAOS-2 cells were treated with 10 µM of dexamethasone (ii) and conjugate 6.12 (iii) for 7 days, while an untreated SAOS-2 D7 control was also included. Cells were stained with GLUT1 (red) and DAPI (blue) and imaged via immunofluorescence. Images processed with Imaris Viewer. Scale bars: 150 µm. Yellow arrows point to areas of decreased GLUT1 expression, and pink arrows point to areas of increased GLUT`1 expression. N=1 biological replicate, N=2 biological replicates. (iv) GLUT1 fold-expression was measured vs untreated SAOS-2 D7 control via ICW. Cells were treated with 0.01-10 µM of dexamethasone and conjugate 6.12. Welch t-test was used to statistically compare treatments' protein fold-expression against control=1. (blank=ns=p>0.05, *=p<0.05, **=p<0.01)*

6.5 General discussion

The role of hormone steroid receptors is complicated in cancer. Several receptors including the estrogen receptor (ER), and the androgen receptor (AR) are overexpressed in cancers including breast cancer,[387] and prostate cancer[388] respectively. On the other hand, the glucocorticoid receptor (GR) is not an oncogene, and glucocorticoids are included in cancer treatment, to help manage side effects.[340] glucocorticoids including dexamethasone and prednisolone are used to treat various cancers including different types of lymphoma and

leukaemia, with glucocorticoid induced apoptotic effects being observed in combination with chemotherapy.[389] Achieving enhanced delivery of glucocorticoids to cancer cells is a promising strategy for enhanced action and reduced side-effects of the drugs.

As previously mentioned, altered metabolism is a hallmark of cancer, as instead of employing oxidative phosphorylation to produce ATP, cancer cells favour aerobic glycolysis.[69] Glucose conjugation strategies seek to exploit the enhanced glucose consumption in cancer cells, compared to healthy cells, as well as the overexpression of the glucose transporter GLUT1, at the tumour site.[371] 5-fluorodeoxyglucose is employed as a radiotracer for PET scans, leading to labelling of cancer cells, due to cancer cells' increased glucose uptake.[390] This selectivity has been exploited to circumvent toxicity issues of chemotherapeutic agents, by using inactive prodrugs, that are metabolised to selectively release the active drug at the cancer site, and present reduced side-effects in patients.[376] It was considered that given the widespread use of dexamethasone in cancer treatment, as well as its use as a differentiation supplement, it would be beneficial promote targeted delivery in OS cells, by conjugating glucose to dexamethasone.

A synthetic route was devised for conjugation of glucose to dexamethasone via a hydrazone linker. The glucose linker was prepared in sufficient yields and purity, via bromination of β-glucose pentaacetate, subsequent alkylation of the bromide, and TEMPO BAIB oxidation of the alcohol. Hydrazone formation proved to be more challenging, with purification issues, selectivity issues, overlapping signals, and formation of *cis-trans* isomers and rotamers for the acyl-hydrazone. Condensation of hydrazine with dexamethasone afforded a mixture of *cis-trans* hydrazone isomers at the C3 position, which conflicted with the findings in some of the literature.[361,360,362] RP-HPLC protocols were optimised, to allow separation from dexamethasone, and the di-substituted species, and the C3 mono-substituted compound **6.7** was successfully isolated and characterised. The following step involved the coupling of the glucose carboxylic acid linker, with compound **6.7**, using EDCI and OxymaPure as coupling agents. A complex mixture was formed, but 2 isomers of the same mass, which resulted from *cis-trans* isomers around C=N-NH were successfully isolated. Presence of rotamers was confirmed and the 2 peaks were assigned as individual *cis* and *trans* isomer. Compound **6.9A**, resulting from peak A, was fully assigned in CD_3OD, to compare to the final compound. Deprotection of the glucose acetates under strongly basic conditions, led to degradation of the C20 side chain, leading to a loss of CH_2, and subsequent formation of an acid. The final compound was deemed clean via LC-MS, though rotamers were still present. Compound **6.12** was then tested on MG-63 and SAOS-2 OS cells, alongside dexamethasone,

to assess whether the small molecule could drive differentiation, and whether increased GLUT1 expression would be induced by **6.12**.

Some preliminary biological testing was carried out, to observe whether the OS cells would tolerate the synthesised conjugate **6.12**. MG-63 cells and SAOS-2 cells showed decrease in proliferation after treatment with small molecule **6.12**, which was encouraging. Conjugate **6.12** promoted enhanced differentiation in MG-63 cells, while for limited differentiation was observed for SAOS-2, highlighting the effect of cell phenotype on response to glucocorticoid treatment. As was discussed in chapter 5, the role of dexamethasone in osteogenesis is complicated. Some reports suggest that glucocorticoids may inhibit bone formation, while dexamethasone is a common osteogenic differentiation supplement, and loss of bone mass has been reported in GR_{null} mice.[329] Furthermore, as was shown in chapter 3, a differentiation medium containing water-soluble dexamethasone drove differentiation in MG-63 cells. The same small molecule cocktail that drove cell death in SAOS-2 cells but was found to drive differentiation in MG-63 cells. In chapter 5, cholesterol sulfate, which presents glucocorticoid action, also drove differentiation in a dose dependent manner on MG-63 and SAOS-2 cells. So, it would be interesting to assess differentiation using the synthesised small molecule conjugate **6.12**, and previously tested conditions including nanokicking, and metabolites and related structures.

The original hypothesis was that conjugating glucose to dexamethasone, via a cleavable linker would lead to increased uptake in cancer cells via the GLUT1 transporter. Given the experimental design and precedent of recognition of small molecule conjugates by GLUT1, when functionalisation happened in the anomeric C1 of glucose,[374] it was thought that forming a conjugate at that position would lead increase in GLUT1 expression in OS cells. So, it was expected that with increased concentration of the conjugate an increase in glucose uptake via the GLUT1 would be observed. Since RUNX2 has been reported to regulate GLUT1 and glucose uptake during osteogenesis, it may have been assumed that differentiation may trigger upregulation of GLUT1.[391] Future work may include ^{13}C labelling the conjugate and tracing via targeted metabolomics. The environment in the tested conditions was not fully representative of the tumour, which may explain why the hydrazone bond may not have been cleaved. The rationale behind the use of a cleavable acyl-hydrazone linker was that the bond is stable in plasma, but should be hydrolysed at the slightly more acidic environment of the tumour. So more closely mimicking the tumour OS microenvironment in future biological testing, may provide further insight into the

mechanism of action of conjugate 6.12 on cancer cells, and clarify whether the steroid scaffold would be released in the OS cells.

As described in chapter 4, increased glucose consumption was observed for MSCs and OS cells (from metabolomics dataset), after 7 days of osteogenic differentiation, which highlights the role of glucose in differentiation. Glucose is predominantly transported in the cells, using the GLUT1 transporter, which is overexpressed in OS, but has also been described to regulate RUNX2 function.[391] Since GLUT1 expression was not significantly increased from treatment with steroid-glucose conjugate, future work may include assessing whether the small molecule may be transported to cancer cells, using alternate glucose carriers, including SLCA1 and GLUT4. Moreover, testing conditions that more closely mimic the tumour microenvironment and pH, may give further physiologically relevant information, as to whether the hydrazone bond may be cleaved, upon reaching cancer cells. Comparing the effect of conjugation on the A ring position vs the initially intended D ring functionalisation would be interesting in the future.

6.6 Conclusions

A dexamethasone derivative was conjugated to glucose via a cleavable acyl hydrazone linker, at the A ring's C3 position. The initial experimental plan involved hydrazine condensation with dexamethasone, at the C20 position. However, extensive purification optimisation and structural elucidation revealed that hydrazone condensation preferably occurs at the C3 position. A mixture of *cis*-*trans* isomers around the hydrazone bond were generated. An acetate protected, glucose linker was prepared in 3 steps, and conjugated to the hydrazone, using EDCI and OxymaPure, to form an acyl hydrazone. The *cis* and *trans* isomers were successfully separated via RP-HPLC, and fully characterised. Analysis of the spectra proved challenging, due to overlapping signals, and the presence of rotamers, but structures were eventually assignment. Acetate deprotection was carried out under strongly basic conditions, which led to degradation of the C20 side chain, but biological activity was still assessed, as the molecule possessed the key functionality of the hydrazone, and the glucose. The small molecule was tested and while cells were still metabolically active after treatment, the conjugate also appeared to drive decrease in proliferation in MG-63 and SAOS-2 cells. concentration dependent increase in RUNX2 was observed for MG-63, which strongly suggested osteogenesis could be induced using compound **6.12**.

6.7 Future work

To limit degradation at the side chain of the D ring, it would be worth investigating different hydrolysis conditions, as well as different protecting groups. It would be interesting to synthesise hydrazone conjugates both for the C3 and the C20 position of dexamethasone and see how this would affect reactivity. Overall, the design of the small molecule was based on the principle of hydrazone being an acid cleavable group, that would release the active dexamethasone into the cancer cells, after the small molecule reached the acidic environment of the cancer cells. Carrying out optimisation, to limit degradation of the side-chain of the D ring may be beneficial in the future, so that the originally planned dexamethasone conjugate, could be compared to the "degraded" dexamethasone conjugate we obtained. Given the glucose, and hydrazone bond was still intact, and connected to the steroid scaffold, the small molecule was preliminarily tested. Limited sample availability was a constrictive factor, as to the analyses that could be carried out. Further characterisation would involve measuring solubility vs dexamethasone. Stability of **6.12** can be tested by carrying out a timepoint HPLC study, in buffers of different ph. In vivo studies were not within the scope of this project, but assessing delivery of the glucose conjugate, on the tumour, vs heatlhy tissue, would provide better information on off-target effects. In the future carrying out more extensive studies on glucose uptake, GLUT1 expression, and assessing hydrazone bond hydrolysis in the cells, would provide further information as to compound **6.12**'s mode of action.

Chapter 7: Discussion and conclusions

7.1 Scope of research

This thesis focused on identifying conditions that could promote differentiation in osteosarcoma cells, with a special focus on small molecules. As discussed in chapter 1, OS is a very rare, and aggressive bone cancer, which unfortunately largely affects children.[16] Current chemotherapeutic treatments are particularly aggressive, causing severe adverse effects, and affecting quality of life, while many patients also face resistance to chemotherapy, recurrence of OS, and/or metastasis.[17] Clinical trials on tyrosine kinase therapies and immune system modulation, have been unsuccessful at identifying a widely applicable treatment, that presents a curative effect in advanced OS.[42] Thus, it is imperative to identify treatments that are applicable to different subsets of OS, present reduced side-effects, and reduce chemoresistance in OS cells.

Lack of terminal differentiation is a hallmark of cancer (Figure 7.1), yielding immature, fast-proliferating cancer cells, with cancer's degree of differentiation largely dictating the degree of malignancy.[71] Differentiation therapy seeks to restore differentiation potential in cancer cells, thus slowing their growth, and sensitising them to chemotherapy.[83] Differentiation therapy has found application in haematological cancers, where patients with APL, showed improved prognosis, and reduced chemoresistance, when treated with differentiation therapy, along chemotherapy.[392] Employing conditions that promote stem cell differentiation in healthy cells, may restore differentiation potential in the cancer cells.

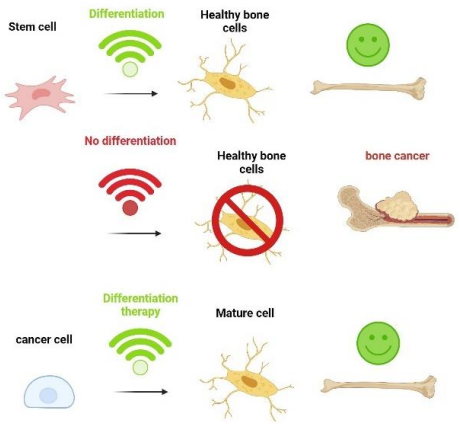

Figure 7.1: Differentiation is interrupted in osteosarcoma. Differentiation therapy aims to restore differentiation potential. (created with biorender.com)

The effect of differentiation was studied on poorly differentiated, fast-proliferating MG-63 cells, and more osteoblastic, slower proliferating SAOS-2 cells. First, conditions that drive osteogenesis in MSCs, were tested on OS cells, to observed how the different stimuli may induce differentiation in the cancer cells, and whether they would be cytotoxic. The effect osteogenic medium, containing, dexamethasone, ascorbic acid, and β-glycerophosphate, as means of chemical stimulation, and nanokicking at 30 nm, 1000 Hz, as a means of mechanical stimulation on OS cells (chapters 3,4). Altered cell metabolism is a hallmark of cancer, so it was considered of interest to observe whether differentiation would induce metabolic reprogramming in OS, and to identify metabolites involved in osteogenesis (chapter 4). Metabolites, and related structures, which included cholesterol sulfate (CS), fludrocortisone acetate (FA), and taurine (TAU) were then tested on the OS cells, to observe whether they were active drivers of differentiation (chapter 5). Due to the wide use of glucocorticoids, as differentiation supplements, and their wide activity on different cell types, it was considered that tethering dexamethasone to glucose, would drive more selective differentiation in OS cells (chapter 6).

7.2 Summary of thesis findings, and discussion.

7.2.1Mechanical stimulation vs chemical stimulation in OS (chapter 3)

As discussed in chapter 3, modulating the mechanical environment is an established method for driving differentiation in MSCs.[198] Different researchers have employed nanotopographies,[191] electrical stimulation, magnetic stimulation, gels, and mechanical stimulation techniques, to induce an osteogenic phenotype in MSCs.[186] Studies on the mechanical environment of OS cells has been more limited to observing mechanical properties of the cancer cells, with fewer studies on directly stimulating the cells.[219,222] Nanokicking was applied to OS cells, which is a technique co-developed at the University of Glasgow, which harnesses the reverse piezoelectric effect, to mechanically stimulate MSCs, in order to drive osteogenesis.[198,199.200]

An osteogenic medium, containing, dexamethasone, ascorbic acid, and β-glycerophosphate was employed as means of chemical stimulation of OS cells. Nanokicking at 30 nm, 1000 Hz, was employed as means of mechanical stimulation on OS cells. Mechanical and chemical stimulation appeared to drive osteogenic differentiation in OS cells, as evident by the upregulation of osteogenic markers. Differentiation did not significantly decrease proliferation in OS cells, apart from observed cell death in OGM-treated SAOS-2 cells.

Literature has previously reported osteogenic medium containing ascorbic acid either driving differentiation or apoptosis on SAOS-2 cells, in different instances.[225] Both the differentiation state of the cell line, and the treatment appeared to play a role on the rate of osteogenesis. After observing that mechanical and chemical stimulation could drive differentiation, metabolomics studies were carried out on the OS cell lines, and the MSCs, to further understand cell behaviour, and identify small molecules that could drive differentiation.

7.2.2 Effects of mechanical vs chemical stimulation on OS metabolism (chapter 4)

As discussed in chapter 4, altered cell metabolism is a hallmark of cancer.[69] Research on OS metabolome is limited, with a larger focus on identification of disease biomarkers, and characterisation of disease progression.[70] There is little information on the differentiation, mechanotransduction and OS metabolome,[272] so it was considered valuable to obtain further insights into bioenergetics of OS, and metabolic reprogramming during differentiation (Figure 7.2). Moreover, little literature precedent on the links between mechanically induced stimulation[272] and metabolism in OS was identified, though preliminary data on patient tumours exist in the group (manuscript in preparation, Tsimbouri *et al.*). HILIC-MS was employed to study changes in the metabolome of SAOS-2, MG-63 and MSC cells, during mechanical and chemical stimulation. Lv *et al*. had previously suggested that lipid and carbohydrate pathways were impaired in OS, while others have suggested impaired TCA cycle.[372] However, metabolomic analysis revealed significant changes in carbohydrate metabolism, when OS cells were differentiated. TCA metabolites were significantly altered, and increased citrate uptake was observed in OGM treated cells. Observations of increased mineralisation markers in OGM treated cells for MG-63 was corroborated by metabolomics, which revealed increased citrate uptake, which has previously been linked to increase in mineralisation.[277] Overall, significant metabolic alterations were observed under mechanical, and chemical stimulation, thus suggesting differentiation may induce metabolic reprogramming in OS. Cholesterol sulfate (CS) and taurine (TAU) were identified to be altered during differentiation of OS cells, and MSCs. CS was previously described to be involved in osteogenic differentiation of MSCs, through a metabolomic screen, while the structural relevant corticosteroid FA was reported to promote enhanced osteogenesis.[141]

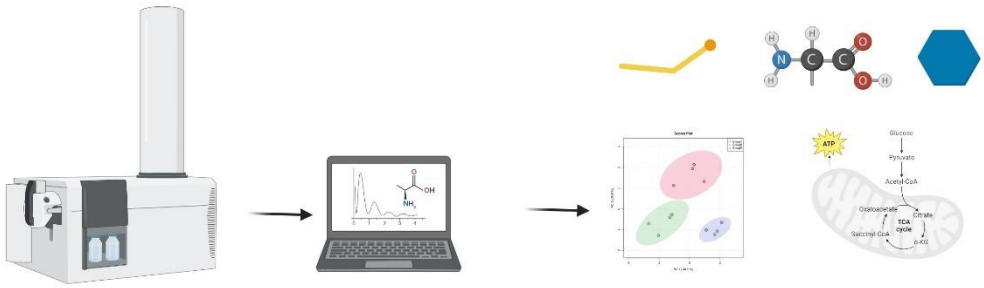

Figure 7.2: Metabolomics was employed to study the effects of NK and OGM on metabolism (created with biorender.com)

7.2.3 Effects of metabolites, and related structures on OS cells. (chapter 5)

CS, FA and TAU (Figure 7.3) all drove dose-dependent increase in differentiation, as evident by the increase in RUNX2, or OSX, with an increase in small molecule concentration, in MG-63 and SAOS-2 cells. Limited observations were made on gene expression, with osteogenic gene and protein data, showing poor correlation, which is a widely reported effect.[321] Future work would include repeating experiments, to further confirm findings. A temporal protein expression experiment was carried out and it was observed that 10 µM CS drove most significant differentiation in MG-63 over the course of a month. 10 µM treatment of SAOS-2 cells with FA showing the most significant response. CS and FA both possess the steroid scaffold but have been reported to present biological activity via different pathways in MSCs.[141] While CS is an endogenous metabolite, that has been reported to activate glucocorticoid receptor, FA is a synthetic steroid that presents enhanced mineralocorticoid activity.[141] Both small molecules induced differentiation on OS cells and may be of interest in the future to carry out glucocorticoid and mineralocorticoid receptor studies, to observe how that may affect biological response in OS. Sulfated steroids have traditionally been considered inactive reservoirs of the steroid hormones, but later research has indicated they may present separate biological activity, to their desulfated precursor.[334] Treating OS cells with CS and inhibiting steroid sulfatase in the future would help gain better understanding of the sulfated steroid's bioactivity, compared to cholesterol. Given the reported involvement of the glucocorticoid receptor on osteogenesis, and the wide activity in multiple cell types, and pathways,[141] it was considered beneficial to investigate a targeted delivery approach to OS cells.

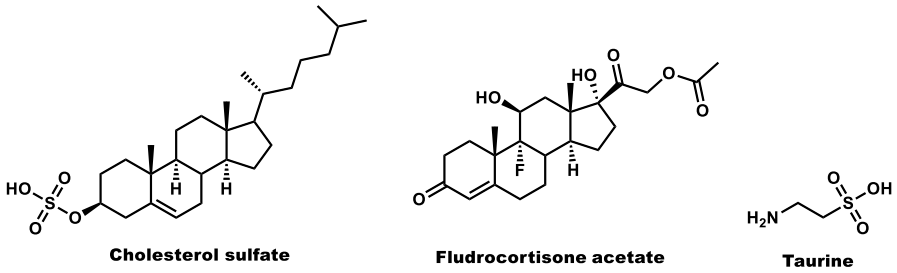

Figure 7.3: Small molecules studied in chapter 5 included cholesterol sulfate, fludrocortisone acetate and taurine.

7.2.4 Targeted delivery in OS (chapter 6)

Increased glucose uptake is a hallmark of cancer, with GLUT1, which is the main glucose transporter, being overexpressed in OS.[372] Glycoconjugates have been investigated as cancer prodrugs, with the aim of exploiting cancer's increased affinity to glucose, to drive increased drug uptake in cancer, and minimising accumulation in healthy cells.[371] After extensive optimisation of purification protocols, and structural elucidation, a steroid-glucose conjugate was synthesised, which was linked via an acyl hydrazone based cleavable linker (Figure 7.4). Despite degradation having occurred, in the final step of the synthesis, conjugate **6.12** presented biological activity in OS cells. Preliminary testing showed that the small molecule was tolerated at different concentrations by the cells, though small increase in viability was observed. For SAOS-2 cells more limited differentiation was observed, while more promising results from MG-63 cells, displayed a dose-dependent increase in differentiation from treatment with conjugate **6.12**. It was originally postulated that GLUT1 mediated transport would promote enhanced uptake in OS, but limited upregulation was observed. Further information should be obtained in the future, on differentiation assays, uptake in cancer vs healthy cells, as well as to the mechanism of action.

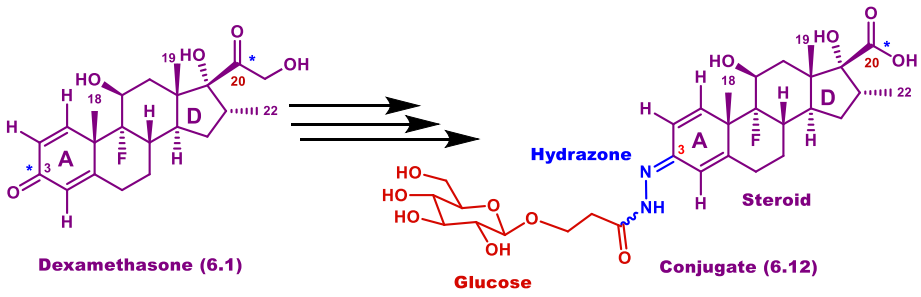

Figure 7. 4: Conjugate 6.12 was synthesised via linkage of dexamethasone to glucose, via a hydrazone linker.

7.2.5 Summary of effect of small molecules and nanokicking on OS cells

Immunofluorescence was employed to study cell morphology, confluence, and to qualitatively study osteogenic protein expression, and localisation, as discussed in chapter 3, 5, and 6. In SAOS-2 cells RUNX2 was abundant, and localised in the nucleus, while for MG-63 cells perinuclear, and cytoplasmic expression was observed, according to immunofluorescence studies for the different conditions. RUNX2 is reported to translocate during osteoblastic differentiation, via ERK signalling, during mechanical stimulation, according to Li *et al*.[393] OSX was also found to be in the nucleus for SAOS-2, though not all cells within the population appeared to be OSX positive, with MG-63 cells presenting low expression of OSX, as has previously been described in the literature. ONN and OPN are matricellular proteins that were also found to be cytoplasmically, and perinuclearly located, in both cell lines, and were more abundant in areas of high confluence, potentially due to macromolecular interactions.[213] Immunofluorescence studies for different conditions showed that CS, FA, TAU, NK, OGM, and compound **6.12**, could drive upregulation of osteogenic proteins in both cell lines. More limited observations being made on OGM treated SAOS-2, due to cell death. More consistent observations on RUNX2 upregulation were made, while osteogenesis was not always uniform, as evident by inhomogeneous expression of osteogenic markers. Protein expression was quantified for different treatments, using a quantitative immunofluorescence technique called in-cell western (ICW). Earlier differentiation marker RUNX2 was most consistently upregulated across cell lines and conditions, while later mineralisation markers were more significantly upregulated from NK than small molecule treatments.

Cells in early stages of osteogenesis are fast-proliferating, to promote cell growth, and increase bone mass.[72] Once cells start further differentiating, and committing to osteoblastogenesis, and mineralisation, the cells shift from a more proliferative state (phenotype) to a more mature, slower-proliferating state.[72] Bearing more resemblance to immature osteoprogenitors, MG-63 cells' rapid growth hence reflects on their poorer degree of differentiation. Different treatments, including NK, OGM, CS, FA, TAU and the synthesised steroid-conjugate **6.12** were found to promote osteogenic differentiation in MG-63 cells, to varying degrees. Treatments, including NK, OGM and compound **6.12**, were shown to drive differentiation, and induce a small decrease in metabolically active cells, confluent monolayers were still formed within 7 days, for all tested treatments. On the other hand, SAOS-2 cells present an example of OS cells with a more differentiated phenotype,

which are more susceptible to decrease in cell numbers from treatment. This reflects on how cells' pre-existing phenotype significantly affects their response to differentiation agents.

As discussed in chapter 1, BMP2 and the TGF-β superfamily have been reported to play an active role in driving osteogenesis in OS cells.[117] Future directions may include studying whether identified conditions may drive osteogenesis through this pathway. Moreover, ERK, and MAPK in general are known to play a role in osteogenesis[279] but have also been found to be involved in osteosarcomagenesis,[278] so it would be worth investigating whether mechanical and chemical stimulation drive differentiation in ERK-dependent manner. ERK was also predicted to be involved in differentiation of MG-63 cells but was predicted to be inhibited during differentiation of SAOS-2 cells, through the IPA algorithm. This would further highlight how cell phenotype affects cell response in OS. Sciandra, Manara *et al.* reported that CD99 was able to drive terminal differentiation on multiple OS cell lines via the ERK1/2 pathway.[135]

Cell cycle distribution was studied in MG-63 and SAOS-2 cells, after 7 days of differentiation, with NK and OGM (chapter 3), as well as CS, FA, and TAU (chapter 5). Both for MG-63 cells, and SAOS-2 cells, most cells were in the G0/G1 phase, and fewest of the cells were in the S phase. An elongated G0/G1 phase has been linked to commitment of stem cells to differentiation,[394] which further highlights the partially differentiated phenotype of OS cells. While a small increase of cells in the G0/G1 phase was observed for some of the conditions, no statistically significant changes were induced during differentiation, across the different cell lines and treatments. An exception was the observation of SAOS-2 cells treated with OGM residing in the sub-G1 phase, which confirmed previous observations of cell death. Cell cycle dysregulation is widely documented in OS, with mutations in checkpoint kinases and cyclin kinases aiding cells to undergo uncontrolled proliferation.[322]

Conditions that could promote osteogenic differentiation in OS cells were identified, but differentiation did not appear to significantly slow proliferation in these cells, which was one of the original hypotheses. The more poorly differentiated, faster-proliferating MG-63 cell line had formed monolayers within a week, regardless of the treatment. It must be noted that there was a statistically significant increase in osteogenic markers, but the fold-expression increase is not as high, as is described in MSCs undergoing differentiation.[141] These cancer cells are known to already express proteins of interest, so the increase in markers is not always dramatic, while there are also known abnormalities in osteogenic

genes, which lead to bone defects and OS initiation. While conditions did enhance differentiation, they did not appear to induce terminal differentiation, which would mean that cells would exit the proliferative phase, and produce high levels of mature markers, more uniform mineralisation.

As stated in chapter 3, the role of RUNX2 is complicated in OS. RUNX2 is required for terminal osteogenic differentiation, as there is ample evidence of inhibition of bone formation when RUNX2 is inhibited, which inhibits downstream expression of osteogenic markers.[148] Given defects in differentiation for OS cells, osteogenic markers are expressed in lower levels and can have abnormal function.[151] As lack of terminal differentiation is a hallmark of cancer, some research is focused on either reprogramming cell behaviour, or reactivating the faulty genes. Therapeutic effects were reported in mice by Green *et al*, where RUNX2 was knocked down.[395] RUNX2 is a commonly employed marker for differentiation. Gupta *et al.* theorised that dysregulation in *RUNX2* could be a contributing factor to abnormal differentiation and OS malignancy.[90] While various conditions that may drive further differentiation in OS have been reported, via the use of biomaterials, small molecules, or biological factors, there is limited proof of terminal differentiation.[52] Treatments may induce a more osteogenic phenotype, but the tested conditions did not significantly alter the proliferative capacity of OS cells. After identifying conditions that could promote osteogenesis on OS cells

7.3 Conclusions

To conclude, conditions that promote osteogenic differentiation in OS cells were identified. Treating OS cells with various differentiation conditions did not prove to be cytotoxic, in general. Nanokicking proved to be particularly effective at promoting differentiation in OS cells, as evident by mineralisation marker upregulation. RUNX2 was most consistently upregulated for the different osteogenic conditions, though this did not always appear to translate to downregulation of downstream proteins, which may be linked to abnormal RUNX2 expression in OS. Metabolomics analysis revealed that differentiation under mechanical and chemical stimulation induced metabolic reprogramming in OS cells. Small molecules cholesterol sulfate, fludrocortisone acetate and taurine were identified from metabolomic analysis, and previous research and tested on OS cells. The different small molecules drove differentiation in a dose dependent manner. To achieve targeted delivery in cancer cells, a steroid was conjugated to glucose, via a cleavable hydrazone linker. Despite synthetic challenges, and degradation at the C20 side chain of dexamethasone, a small

molecule **6.12** was successfully synthesised, characterised, and tested on OS cells. **6.12** appeared to promote differentiation in a concentration dependent manner in OS cells, which was an encouraging finding.

7.4 Future directions

The study of nanokicking on OS cells was predominantly focused on the osteogenesis aspect of the treatment, so future work would include characterisation the of mechanical properties. This may include studying focal adhesions, mechanical signalling pathways, as well as mechanosensitive ion channels. Coupling observations on the effect of mechanical vs chemical stimulation on OS cells from the metabolomics analysis to proteomics or RNA-sequencing may lead to valuable insights on cell behaviour and pathways in the future. Studying pathways that have been reported to be involved in osteogenesis, and/or carcinogenesis, include ERK, JNK, Akt, and TGF-β, so future work may include pathway analyses for the different treatments. This would provide more information on how individual treatments may promote differentiation via different means.

Potential alternative approaches to achieving enhanced differentiation may involve carrying structural activity relation studies on the tested small molecules, and synthesising small molecules with different functionalities, that may promote enhanced response. Moreover, nanokicking showed enhanced osteogenic differentiation, so combining nanokicking, and small molecule treatment may offer enhanced osteogenesis in the future.

Steroid-dexamethasone conjugate **6.12** presented some initial biological activity, so future work would involve further characterisation of cell behaviour. Metabolic studies of the OS cells treated with **6.12**, may provide further information on small molecule uptake, and explain whether hydrazone hydrolysis occurred in the cancer microenvironment. Moreover, since the C3-functionalised hydrazone was synthesised, it would be of interest to synthesise the C20-functionalised hydrazone and compare their biological response.

References

[1] R. Grimer, N. Athanasou, C. Gerrand, I. Judson, I. Lewis, B. Morland, D. Peake, B. Seddon and J. Whelan, *Sarc*, 2010, **2010**, 317462–317462.

[2] S. A. Savage and L. Mirabello, *Sarc*, 2011, **2011**, 548151.

[3] S. J. Taran, R. Taran and N. B. Malipatil, *Ind J Med Paediatr Oncol*, 2017, **38**, 33–43.

[4] L. R. Sadykova, A. I. Ntekim, M. Muyangwa-Semenova, C. S. Rutland, J. N. Jeyapalan, N. Blatt and A. A. Rizvanov, *Cancer Investig*, 2020, **38**, 259–269.

[5] T. Quist, H. Jin, J.-F. Zhu, K. Smith-Fry, M. R. Capecchi and K. B. Jones, *Oncogene*, 2015, **34**, 4278–4284.

[6] R. A. Durfee, M. Mohammed and H. H. Luu, *Rheumatol Ther*, 2016, **3**, 221–243.

[7] J. Jiang, H. Pan, M. Li, B. Qian, X. Lin and S. Fan, *Sci Rep*, 2021, **11**, 5542.

[8] M. P. Link, A. M. Goorin, A. W. Miser, A. A. Green, C. B. Pratt, J. B. Belasco, J. Pritchard, J. S. Malpas, A. R. Baker and J. A. Kirkpatrick, *N Engl J Med*, 1986, **314**, 1600–1606.

[9] X. Huang, J. Zhao, J. Bai, H. Shen, B. Zhang, L. Deng, C. Sun, Y. Liu, J. Zhang and J. Zheng, *J Bone Oncol*, 2019, **16**, 100230.

[10] R. Belayneh, M. S. Fourman, S. Bhogal and K. R. Weiss, *Curr Oncol Rep*, 2021, **23**, 71.

[11] G. T. Calvert, R. L. Randall, K. B. Jones, L. Cannon-Albright, S. Lessnick and J. D. Schiffman, *Sarc*, 2012, **2012**, e152382.

[12] B. J. Aubrey, G. L. Kelly, A. Janic, M. J. Herold and A. Strasser, *Cell Death Diff*, 2018, **25**, 104–113.

[13] T. Velletri, N. Xie, Y. Wang, Y. Huang, Q. Yang, X. Chen, Q. Chen, P. Shou, Y. Gan, G. Cao, G. Melino and Y. Shi, *Cell Death Dis*, 2016, **7**, e2015–e2015.

[14] A. MacCarthy, A. M. Bayne, G. J. Draper, E. M. Eatock, M. E. Kroll, C. A. Stiller, T. J. Vincent, M. M. Hawkins, H. C. Jenkinson, J. E. Kingston, R. Neale and M. F. G. Murphy, *Brit J Ophthalmol*, 2009, **93**, 1159–1162.

[15] J. W. V. de Azevedo, T. A. A. de Medeiros Fernandes, J. V. Fernandes, J. C. V. de Azevedo, D. C. F. Lanza, C. M. Bezerra, V. S. Andrade, J. M. G. de Araújo and J. V. Fernandes, *Oncol Lett*, 2020, **19**, 1099–1116.

[16] F. Jafari, S. Javdansirat, S. Sanaie, A. Naseri, A. Shamekh, D. Rostamzadeh and S. Dolati, *Ann Diagn Pathol*, 2020, **49**, 151654.

[17] Y. Zhang, J. Yang, N. Zhao, C. Wang, S. Kamar, Y. Zhou, Z. He, J. Yang, B. Sun, X. Shi, L. Han and Z. Yang, *Oncol Lett*, 2018, **16**, 6228–6237.

[18] P. Koźmiński, P. K. Halik, R. Chesori and E. Gniazdowska, *Int J Mol Sci*, 2020, **21**, 3483.

[19] C. F. Thorn, C. Oshiro, S. Marsh, T. Hernandez-Boussard, H. McLeod, T. E. Klein and R. B. Altman, *Pharmacogenet Genom*, 2011, **21**, 440–446.

[20] T. Boulikas and M. Vougiouka, *Oncol Rep*, 2003, **10**, 1663–1682.

[21] M. Löhr, P. Müller, P. Karle, J. Stange, S. Mitzner, R. Jesnowski, H. Nizze, B. Nebe, S. Liebe, B. Salmons and W. H. Günzburg, *Gene Ther*, 1998, **5**, 1070–1078.

[22] X. Xiao, W. Wang and Z. Wang, *Pediatr Drugs*, 2014, **16**, 503–512.

[23] A. Montecucco, F. Zanetta and G. Biamonti, *EXCLI J*, 2015, **14**, 95–108.

[24] M. S. Isakoff, S. S. Bielack, P. Meltzer and R. Gorlick, *JCO*, 2015, **33**, 3029–3035.

[25] M. Xu, S. F. Xu and X. C. Yu, *Curr Oncol*, 2014, **21**, e678–e684.

[26] A. J. Chou and R. Gorlick, *Exp Rev Anticanc Ther*, 2006, **6**, 1075–1085.

[27] W. S. Ferguson and A. M. Goorin, *Cancer Investig*, 2001, **19**, 292–315.

[28] L. C. Sayles, M. R. Breese, A. L. Koehne, S. G. Leung, A. G. Lee, H.-Y. Liu, A. Spillinger, A. T. Shah, B. Tanasa, K. Straessler, F. K. Hazard, S. L. Spunt, N. Marina, G. E. Kim, S.-J. Cho, R. S. Avedian, D. G. Mohler, M.-O. Kim, S. G. DuBois, D. S. Hawkins and E. A. Sweet-Cordero, *Cancer Discov*, 2019, **9**, 46–63.

[29] S. B. Whittle, K. Offer, R. D. Roberts, A. LeBlanc, C. London, R. G. Majzner, A. Y. Huang, P. Houghton, E. A. S. Cordero, P. J. Grohar, M. Isakoff, M. W. Bishop, E. Stewart, E. K. Slotkin, E. Greengard, S. C. Borinstein, F. Navid, R. Gorlick, K. A. Janeway, D. R. Reed and P. Hingorani, *Pediatr Blood Cancer*, 2021, **68**, e29188.

[30] V. V. Veselov, A. E. Nosyrev, L. Jicsinszky, R. N. Alyautdin and G. Cravotto, *Cancers (Basel)*, 2022, **14**, 622.

[31] V. Sampson, R. Gorlick, D. Kamara and E. A. Kolb, *Front. Oncol*, 2013, **13**, 00132

[32] D. Bradley and P. Beltrao, *PLoS Biol*, 2019, **17**, e3000341.

[33] L. J. Wilson, A. Linley, D. E. Hammond, F. E. Hood, J. M. Coulson, D. J. MacEwan, S. J. Ross, J. R. Slupsky, P. D. Smith, P. A. Eyers and I. A. Prior, *Cancer Res*, 2018, **78**, 15–29.

[34] F. M. Carcano, L. V. dos Santos, D. O. Vidal, L. F. Lopes and J. P. da Silveira Nogueira Lima, *JCO*, 2015, **33**, e21504–e21504.

[35] C. Zhang, L. Wang, C. Xiong, R. Zhao, H. Liang and X. Luo, *J Orthop Surg Res*, 2021, **16**, 738.

[36] E. D. G. Fleuren, Y. M. H. Versleijen-Jonkers, O. C. Boerman and W. T. A. van der Graaf, *Biochim Biophys Acta Rev Cancer*, 2014, **1845**, 266–276.

[37] C. Chen, Q. Shi, J. Xu, T. Ren, Y. Huang and W. Guo, *Cell Death Discov.*, 2022, **8**, 1–9.

[38] F. Duffaud, O. Mir, P. Boudou-Rouquette, S. Piperno-Neumann, N. Penel, E. Bompas, C. Delcambre, E. Kalbacher, A. Italiano, O. Collard, C. Chevreau, E. Saada, N. Isambert, J. Delaye, C. Schiffler, C. Bouvier, V. Vidal, S. Chabaud and J.-Y. Blay, *Lancet Oncol*, 2019, **20**, 120–133.

[39] A. Raciborska and K. Bilska, *Med Oncol*, 2018, **35**, 126.

[40] N. Paksoy, I. Dogan, M. Ekenel and M. Basaran, *JCO*, 2021, **39**, e23511–e23511.

[41] L. Xie, J. Xu, X. Sun, X. Li, K. Liu, X. Liang, Z. Zhou, H. Zhuang, K. Sun, Y. Wu, J. Gu and W. Guo, *Oncol Lett*, 2021, **22**, 552.

[42] A. Assi, M. Farhat, M. C. R. Hachem, Z. Zalaquett, M. Aoun, M. Daher, A. Sebaaly and H.-R. Kourie, *J Bone Oncol*, 2023, **43**, 100511.

[43] F. M. Burnet, *Lancet*, 1967, **1**, 1171–1174.

[44] Z. Yao, Z. Lin and W. Wu, *Hum Vaccines Immunother*, 2023, **2**, 2219191.

[45] M. Al-Haideri, S. B. Tondok, S. H. Safa, A. H. maleki, S. Rostami, A. T. Jalil, M. E. Al-Gazally, F. Alsaikhan, J. A. Rizaev, T. A. M. Mohammad and S. Tahmasebi, *Cancer Cell Int*, 2022, **22**, 365.

[46] E. Goleva, T. Lyubchenko, L. Kraehenbuehl, M. E. LaCouture, D. Y. M. Leung and J. A. Kern, *Ann Allergy Asthma Immunol*, 2021, **126**, 630–638.

[47] B. Zheng, T. Ren, Y. Huang, K. Sun, S. Wang, X. Bao, K. Liu and W. Guo, *J Hematol Oncol*, 2018, **11**, 16.

[48] A. Le Cesne, P. Marec-Berard, J.-Y. Blay, N. Gaspar, F. Bertucci, N. Penel, E. Bompas, S. Cousin, M. Toulmonde, A. Bessede, W. H. Fridman, C. Sautes-Fridman, M. Kind, F. Le Loarer, M. Pulido and A. Italiano, *Eur J Cancer*, 2019, **119**, 151–157.

[49] M. Li, Q. Bao, Z. Zhang, B. Wang, Z. Liu, J. Wen, R. Wan, Y. Shen and W. Zhang, *J Immunother Cancer*, 2022, **10**, e004673.

[50] D. Sun, W. Gao, H. Hu and S. Zhou, *Acta Pharm Sin B*, 2022, **12**, 3049–3062.

[51] M. Chehelgerdi, M. Chehelgerdi, O. Q. B. Allela, R. D. C. Pecho, N. Jayasankar, D. P. Rao, T. Thamaraikani, M. Vasanthan, P. Viktor, N. Lakshmaiya, M. J. Saadh, A. Amajd, M. A. Abo-Zaid, R. Y. Castillo-Acobo, A. H. Ismail, A. H. Amin and R. Akhavan-Sigari, *Mol Cancer*, 2023, **22**, 169.

[52] D. Xie, Z. Wang, J. Li, D. Guo, A. Lu and C. Liang, *Front Oncol*, 2022, **12**, 843345.

[53] J. Gill and R. Gorlick, *Nat Rev Clin Oncol*, 2021, **18**, 609–624.

[54] P. Hingorani, M. E. Roth, Y. Wang, W. Zhang, J. B. Gill, D. J. Harrison, B. Teicher, S. Erickson, G. Gatto, M. A. Smith, E. A. Kolb and R. Gorlick, *Mol Cancer Ther*, 2021, **20**, 535–540.

[55] C. H. Chau, P. S. Steeg and W. D. Figg, *Lancet*, 2019, **394**, 793–804.

[56] X. Shan, X. Gong, J. Li, J. Wen, Y. Li and Z. Zhang, *Acta Pharm Sin B*, 2022, **12**, 3028–3048.

[57] L. Kager, U. Pötschger and S. Bielack, *Ther Clin Risk Manag*, 2010, **6**, 279–286.

[58] H. Wei, J. Chen, S. Wang, F. Fu, X. Zhu, C. Wu, Z. Liu, G. Zhong and J. Lin, *Int J Nanomed*, 2019, **14**, 8603–8610.

[59] W. Meng, C. He, Y. Hao, L. Wang, L. Li and G. Zhu, *Drug Deliv*, 2020, **27**, 585–598.

[60] S. Senapati, A. K. Mahanta, S. Kumar and P. Maiti, *Sig Transduct Target Ther*, 2018, **3**, 1–19.

[61] J. Li and D. J. Mooney, *Nat Rev Mater*, 2016, **1**, 16071.

[62] Z. Yang, S. Yu, D. Li, Y. Gong, J. Zang, J. Liu and X. Chen, *Colloids Surf B Biointerfaces*, 2018, **172**, 387–394.

[63] K. Li, D. Zhao, H. Chen, W. Zhang, W. Zhao and Z. Zhang, *Materials & Design*, 2022, **224**, 111365.

[64] Y. Yang, S. Wang, P. Ma, Y. Jiang, K. Cheng, Y. Yu, N. Jiang, H. Miao, Q. Tang, F. Liu, Y. Zha and N. Li, *Cancer Letters*, 2023, **552**, 215969.

[65] I. Giang, E. L. Boland and G. M. K. Poon, *AAPS J*, 2014, **16**, 899–913.

[66] R. K. Upadhyay, *Biomed Res Int*, 2014, **2014**, 869269.

[67] H.-H. Han, H.-M. Wang, P. Jangili, M. Li, L. Wu, Y. Zang, A. C. Sedgwick, J. Li, X.-P. He, T. D. James and J. S. Kim, *Chem Soc Rev*, 2023, **52**, 879–920.

[68] D. Hanahan and R. A. Weinberg, *Cell*, 2000, **100**, 57–70.

[69] D. Hanahan and R. A. Weinberg, *Cell*, 2011, **144**, 646–674.

[70] Y. Shi, X. Yue and Q. Luo, *Pediatr Discov*, 2023, **1**, e18.

[71] D. Hanahan, *Cancer Discovery*, 2022, **12**, 31–46.

[72] A. Rutkovskiy, K.-O. Stensløkken and I. J. Vaage, *Med Sci Monit Basic Res*, 2016, **22**, 95–106.

[73] G. Chamberlain, J. Fox, B. Ashton and J. Middleton, *Stem Cells*, 2007, **25**, 2739–2749.

[74] W. Huang, S. Yang, J. Shao and Y.-P. Li, *Front Biosci*, 2007, **12**, 3068–3092.

[75] C. Pautke, M. Schieker, T. Tischer, A. Kolk, P. Neth, W. Mutschler and S. Milz, *Anticanc Res.*, 2004, **24**, 3743–3748.

[76] N. Rucci, *Clin Cases Miner Bone Metab*, 2008, **5**, 49–56.

[77] A. Abarrategi, J. Tornin, L. Martinez-Cruzado, A. Hamilton, E. Martinez-Campos, J. P. Rodrigo, M. V. González, N. Baldini, J. Garcia-Castro and R. Rodriguez, *Stem Cells Int*, 2016, **2016**, 3631764.

[78] C. P. Gibbs, P. P. Levings and S. C. Ghivizzani, *Curr Orthop Pract*, 2011, **22**, 322–326.

[79] B.-C. He, L. Chen, G.-W. Zuo, W. Zhang, Y. Bi, J. Huang, Y. Wang, W. Jiang, Q. Luo, Q. Shi, B.-Q. Zhang, B. Liu, X. Lei, J. Luo, X. Luo, E. R. Wagner, S. H. Kim, C. J. He, Y. Hu, J. Shen, Q. Zhou, F. Rastegar, Z.-L. Deng, H. H. Luu, T.-C. He and R. C. Haydon, *Clin Cancer Res*, 2010, **16**, 2235–2245.

[80] N. Tang, W.-X. Song, J. Luo, R. C. Haydon and T.-C. He, *Clin Orthop Relat Res*, 2008, **466**, 2114–2130.

[81] N. Bar-Hai and D. Ishay-Ronen, *Front Pharmacol, 2022*, ***13***, 944773.

[82] X. Zhang, F. D. Cruz, M. Terry, F. Remotti and I. Matushansky, *Oncogene*, 2013, **32**, 2249–2260.

[83] M. Yan and Q. Liu, *Chin J Canc*, 2016, **35**, 3.

[84] T. R. Breitman, S. J. Collins and B. R. Keene, *Blood*, 1981, **57**, 1000–1004.

[85] Y. Zhang, D. Guan, J. Shi, H. Gao, J. Li, J. Zhao, L. Qiu, J. Liu, N. Li, W. Guo, J. Xue, F. Zhou, M. Wu, H. Wang, D. Xie and S. Cheng, *J Hepatol*, 2013, **59**, 1255–1263.

[86] J. K. Rane, D. Pellacani and N. J. Maitland, *Nat. Rev. Urol.*, 2012, **9**, 595–602.

[87] Y. Chen, J. Cao, N. Zhang, B. Yang, Q. He, X. Shao and M. Ying, *Drug Discov. Today*, 2020, **25**, 497–504.

[88] H. de Thé, *Nat Rev Cancer*, 2018, **18**, 117–127.

[89] C. Adamopoulos, A. N. Gargalionis, E. K. Basdra and A. G. Papavassiliou, *Exper Biol Med*, 2016, **241**, 1296.

[90] S. Gupta, T. Ito, D. Alex, C. M. Vanderbilt, J. C. Chang, N. Islamdoust, Y. Zhang, K. Nafa, J. Healey, M. Ladanyi and M. R. Hameed, *Hum Pathol*, 2019, **94**, 23–28.

[91] Y. Arima, H. Nobusue and H. Saya, *Cancer Sci*, 2020, **111**, 2689–2695.

[92] J. Liskova, O. Babchenko, M. Varga, A. Kromka, D. Hadraba, Z. Svindrych, Z. Burdikova and L. Bacakova, *Int J Nanomed*, 2015, **10**, 869–884.

[93] E. Filova, M. Vandrovcova, M. Jelinek, J. Zemek, J. Houdkova, Jan Remsa, T. Kocourek, L. Stankova and L. Bacakova, *J Mater Sci: Mater Med*, 2016, **28**, 17.

[94] L. Lin, R. Hao, W. Xiong and J. Zhong, *J Biosci Bioeng*, 2015, **119**, 591–595.

[95] N. Ayobian-Markazi, T. Fourootan and M. J. Kharazifar, *Dent Res J (Isfahan)*, 2012, **9**, 86–92.

[96] L. Postiglione, G. Di Domenico, L. Ramaglia, S. Montagnani, S. Salzano, F. Di Meglio, L. Sbordone, M. Vitale and G. Rossi, *J Dent Res*, 2003, **82**, 692–696.

[97] Q. Huang, X. Li, T. Liu, H. Wu, X. Liu, Q. Feng and Y. Liu, *Appl Surf Sci*, 2018, **447**, 767–776.

[98] B. Voltrova, V. Hybasek, V. Blahnova, J. Sepitka, V. Lukasova, K. Vocetkova, V. Sovkova, R. Matejka, J. Fojt, L. Joska, M. Daniel and E. Filova, *RSC Advances*, 2019, **9**, 11341–11355.

[99] V. Hefka Blahnova, J. Dankova, M. Rampichova and E. Filova, *Bone Joint Res*, 2020, **9**, 412–420.

[100] B. Lucendo-Villarin, H. Rashidi, K. Cameron and D. C. Hay, *J Mater Chem B*, 2016, **4**, 3433–3442.

[101] M. Wabitsch, H. Hauner, E. Heinze and W. M. Teller, *Metabol*, 1995, **44**, 45–49.

[102] M. Beederman, J. D. Lamplot, G. Nan, J. Wang, X. Liu, L. Yin, R. Li, W. Shui, H. Zhang, S. H. Kim, W. Zhang, J. Zhang, Y. Kong, S. Denduluri, M. R. Rogers, A. Pratt, R. C. Haydon, H. H. Luu, J. Angeles, L. L. Shi and T.-C. He, *J Biomed Sci Eng*, 2013, **6**, 32–52.

[103] T. W. Axelrad and T. A. Einhorn, *Cytokine & Growth Factor Reviews*, 2009, **20**, 481–488.

[104] J. Kendal, A. Singla, A. Affan, K. Hildebrand, A. Al-Ani, D. Itani and M. Ungrin, *Orthop Proc*, 2020, **102-B**, 30–30.

[105] H. Tian, T. Zhou, H. Chen, C. Li, Z. Jiang, L. Lao, S. A. Kahn, M. E. L. Duarte, J. Zhao, M. D. Daubs, Z. Buser, E. J. Brochmann, J. C. Wang and S. S. Murray, *J Orthop Res*, 2019, **37**, 1638–1648.

[106] R. E. Mutha, A. U. Tatiya and S. J. Surana, *Fut J Pharm Sci*, 2021, **7**, 25.

[107] D. Tungmunnithum, A. Thongboonyou, A. Pholboon and A. Yangsabai, *Med*, 2018, **5**, 93.

[108]R. B. de Andrade Teles, T. C. Diniz, T. C. Costa Pinto, R. G. de Oliveira Júnior, M. Gama e Silva, É. M. de Lavor, A. W. C. Fernandes, A. P. de Oliveira, F. P. R. de Almeida Ribeiro, A. A. M. da Silva, T. C. F. Cavalcante, L. J. Quintans Júnior and J. R. G. da Silva Almeida, *Oxid Med Cellul Longev*, 2018, **2018**, 7043213.

[109] A. N. Panche, A. D. Diwan and S. R. Chandra, *J Nut Sci*, 2016, **5**, e47.

[110] J. S. Heo, S. G. Lee and H. O. Kim, *Stem Cells Intl*, 2017, **2017**, 6921703.

[111] N. Zhang, M.-D. Ying, Y.-P. Wu, Z.-H. Zhou, Z.-M. Ye, H. Li and D.-S. Lin, *PLoS ONE*, 2014, **9**, e98973.

[112] H. Lan, W. Hong, P. Fan, D. Qian, J. Zhu and B. Bai, *Cell Physiol Biochem*, 2017, **43**, 553–567.

[113] Y. Pang, L. Liu, H. Mu and V. Priya Veeraraghavan, *Saudi J Biol Sci*, 2021, **28**, 4916–4920.

[114] C. Liu, M. Ma, J. Zhang, S. Gui, X. Zhang and S. Xue, *Biomed Pharmacother*, 2017, **89**, 1415–1421.

[115] C. Morris, J. Thorpe, L. Ambrosio and M. Santin, *J Nut*, 2006, **136**, 1166–1170.

[116] A. R. Sharma and J.-S. Nam, *J Nut Biochem*, 2019, **74**, 108228.

[117] S. Zhou, *J Cell Biochem*, 2011, **112**, 1651–1660.

[118] F. Verrecchia and F. Rédini, *Front Oncol*, 2018, **8**, 133.

[119] L. Wang, P. Park, F. La Marca, K. Than, S. Rahman and C.-Y. Lin, *Int J Oncol*, 2013, **43**, 1095–1102.

[120] J. Bisson, J.B. McAlpine, J.B. Friesen, S.N. Chen, J Graham and G.F. Pauli, *J Med Chem*, 2015, **59**, 1671–1690.

[121] C. Aldrich, C. Bertozzi, G. I. Georg, L. Kiessling, C, Lindsley, D. Liotta, K. M. Merz, A. Schepartz, and S. Wang, *ACS Cent. Sci.*, 2017, **3**, 143–147.

[122] P. Luo, X. Yang, M. Ying, P. Chaudhry, A. Wang, H. Shimada, W. A. May, G. B. Adams, D. Mock, T. J. Triche, Q. He and L. Wu, *Oncogene*, 2010, **29**, 2772–2783.

[123] K. Lavudi, S. M. Nuguri, Z. Olverson, A. K. Dhanabalan, S. Patnaik, and R. R. Kokkanti, *Front Cell Dev Biol*, 2023, **11**, 1254612.

[124] L. J. Gudas and J. A. Wagner, *J Cell Physiol*, 2011, **226**, 322–330.

[125] E. R. Wagner, B.-C. He, L. Chen, G.-W. Zuo, W. Zhang, Q. Shi, Q. Luo, X. Luo, B. Liu, J. Luo, F. Rastegar, C. J. He, Y. Hu, B. Boody, H. H. Luu, T.-C. He, Z.-L. Deng and R. C. Haydon, *PPAR Res*, 2010, **2010**, 956427.

[126] Q. Zhou, L. Zhang, Z. Chen, P. Zhao, Y. Ma, B. Yang, Q. He and M. Ying, *FEBS J*, 2014, **281**, 3032–3047.

[127] B. Yuan, K. Shi, J. Zha, Y. Cai, Y. Gu, K. Huang, W. Yue, Q. Zhai, N. Ding, W. Ren, W. He, Y. Xu and T. Wang, *Cell Death Dis*, 2023, **14**, 1–12.

[128] R. C. Haydon, L. Zhou, T. Feng, B. Breyer, H. Cheng, W. Jiang, A. Ishikawa, T. Peabody, A. Montag, M. A. Simon and T.-C. He, *Clin Cancer Res*, 2002, **8**, 1288–1294.

[129] R. C. Haydon, H. H. Luu and T.-C. He, *Clin Orthopaed Relat Res*, 2007, **454**, 237.

[130] T. Higuchi, J. Yamamoto, N. Sugisawa, Y. Tashiro, H. Nishino, N. Yamamoto, K. Hayashi, H. Kimura, S. Miwa, K. Igarashi, M. Bouvet, S. R. Singh, H. Tsuchiya and R. M. Hoffman, *Canc Genom Proteom*, 2020, **17**, 35–40.

[131] P. V. Bharatam and S. Khanna, *J. Phys. Chem. A*, 2004, **108**, 3784–3788.

[132] S. Patel, M. von Mehren, D. R. Reed, P. Kaiser, J. Charlson, C. W. Ryan, D. Rushing, M. Livingston, A. Singh, R. Seth, C. Forscher, G. D'Amato, S. P. Chawla, S. McCarthy, G. Wang, T. Parekh, R. Knoblauch, M. L. Hensley, R. G. Maki and G. D. Demetri, *Cancer*, 2019, **125**, 2610–2620.

[133] C. Ratti, L. Botti, V. Cancila, S. Galvan, I. Torselli, C. Garofalo, M. C. Manara, L. Bongiovanni, C. F. Valenti, A. Burocchi, M. Parenza, B. Cappetti, S. Sangaletti, C. Tripodo, K. Scotlandi, M. P. Colombo and C. Chiodoni, *Clinic Cancer Res*, 2017, **23**, 5149–5161.

[134] C. Cascini, C. Ratti, L. Botti, B. Parma, V. Cancila, A. Salvaggio, C. Meazza, C. Tripodo, M. P. Colombo and C. Chiodoni, *J Exp Clinic Cancer Res*, 2023, **42**, 154.

[135] M. Sciandra, M. T. Marino, M. C. Manara, C. Guerzoni, M. Grano, A. Oranger, E. Lucarelli, P.-L. Lollini, B. Dozza, L. Pratelli, M. F. Di Renzo, M. P. Colombo, P. Picci and K. Scotlandi, *Journal of Bone and Mineral Research*, 2014, **29**, 1295–1309.

[136] R. Newton, *Thorax*, 2000, **55**, 603–613.

[137] N. Bordag, S. Klie, K. Jürchott, J. Vierheller, H. Schiewe, V. Albrecht, J.-C. Tonn, C. Schwartz, C. Schichor and J. Selbig, *Sci Rep*, 2015, **5**, 15954–15954.

[138] L. N. Song, *Oncol Res*, 1994, **6**, 111–118.

[139] S. Russinoff, S. Miran, A. L. Gowda and P. A. Lucas, *Clin Orthop Relat Res*, 2011, **469**, 2895–2904.

[140] R. H. Oakley and J. A. Cidlowski, *J Allergy Clin Immunol*, 2013, **132**, 1033–1044.

[141] T. Hodgkinson, P. M. Tsimbouri, V. Llopis-Hernandez, P. Campsie, D. Scurr, P. G. Childs, D. Phillips, S. Donnelly, J. A. Wells, F. J. O'Brien, M. Salmeron-Sanchez, K. Burgess, M. Alexander, M. Vassalli, R. O. C. Oreffo, S. Reid, D. J. France and M. J. Dalby, *Sci Adv*, 2021, **7**, eabb7921.

[142] H.-S. Chae and S.-T. Hong, *Int J Mol Sci*, 2022, **24**, 12.

[143] S. Lin, S. Yin, J. Shi, G. Yang, X. Wen, W. Zhang, M. Zhou and X. Jiang, *Bioact Mater*, 2022, **18**, 116–127.

[144] C. B. Clish, *Cold Spring Harb Mol Case Stud*, 2015, **1**, a000588.

[145] Bio-Rad, Measuring cytotoxicity or proliferation - alamarBlue Assay Protocol, https://www.bio-rad-antibodies.com/measuring-cytotoxicity-proliferation-spectrophotometry-fluorescence-alamarblue.html, (accessed 27 May 2024).

[146] K. J. Livak and T. D. Schmittgen, *Methods*, 2001, **25**, 402–408.

[147] P. Mishra, C. M. Pandey, U. Singh, A. Gupta, C. Sahu and A. Keshri, *Ann Card Anaesth*, 2019, **22**, 67–72.

[148] J. W. Martin, M. Zielenska, G. S. Stein, A. J. van Wijnen and J. A. Squire, *Sarc*, 2011, **2011**, 282745.

[149] C. M. J. Lucero, O. A. Vega, M. M. Osorio, J. C. Tapia, M. Antonelli, G. S. Stein, A. J. van Wijnen and M. A. Galindo, *J Cell Physiol*, 2013, **228**, 714–723.

[150] A. Roos, L. Satterfield, S. Zhao, D. Fuja, R. Shuck, M. J. Hicks, L. A. Donehower and J. T. Yustein, *Brit J Canc*, 2015, **113**, 1289–1297.

[151] D. M. Thomas, S. A. Johnson, N. A. Sims, M. K. Trivett, J. L. Slavin, B. P. Rubin, P. Waring, G. A. McArthur, C. R. Walkley, A. J. Holloway, D. Diyagama, J. E. Grim, B. E. Clurman, D. D. L. Bowtell, J.-S. Lee, G. M. Gutierrez, D. M. Piscopo, S. A. Carty and P. W. Hinds, *J Cell Biol*, 2004, **167**, 925–934.

[152] K. Nakashima, X. Zhou, G. Kunkel, Z. Zhang, J. M. Deng, R. R. Behringer and B. de Crombrugghe, *Cell*, 2002, **108**, 17–29.

[153] Y. Cao, Z. Zhou, B. de Crombrugghe, K. Nakashima, H. Guan, X. Duan, S.-F. Jia and E. S. Kleinerman, *Cancer Res*, 2005, **65**, 1124–1128.

[154] X. Luo, J. Chen, W.-X. Song, N. Tang, J. Luo, Z.-L. Deng, K. A. Sharff, G. He, Y. Bi, B.-C. He, E. Bennett, J. Huang, Q. Kang, W. Jiang, Y. Su, G.-H. Zhu, H. Yin, Y. He, Y. Wang, J. S. Souris, L. Chen, G.-W. Zuo, A. G. Montag, R. R. Reid, R. C. Haydon, H. H. Luu and T.-C. He, *Lab Investig*, 2008, **88**, 1264–1277.

[155] H. Sage, R. B. Vernon, J. Decker, S. Funk and M. L. Iruela-Arispe, *J Histochem Cytochem*, 1989, **37**, 819–829.

[156] K. Kapinas, C. B. Kessler and A. M. Delany, *J Cell Biochem*, 2009, **108**, 216–224.

[157] A. Durkin, C. DeVile, P. Arundel, M. Bull, J. Walsh, N. J. Bishop, E. Hupin, S. Parekh, R. Nadarajah, A. C. Offiah, A. Calder, J. Brock, D. Baker and M. Balasubramanian, *J Med Genet*, 2022, **59**, 810–816.

[158] J. Si, C. Wang, D. Zhang, B. Wang, W. Hou and Y. Zhou, *Med Sci Monit*, 2020, **26**, e919159-1-e919159-9.

[159] Y.-S. Li, Z.-H. Deng, C. Zeng and G.-H. Lei, *Med Oncol*, 2015, **32**, 449.

[160] X. Han, W. Wang, J. He, L. Jiang and X. Li, *Oncol Lett*, 2019, **17**, 2592–2598.

[161] C. R. Schott, A. L. Koehne, L. C. Sayles, E. P. Young, C. Luck, K. Yu, A. G. Lee, M. R. Breese, S. G. Leung, H. Xu, A. T. Shah, H.-Y. Liu, A. Spillinger, I. H. Behroozfard, K. D. Marini, P. T. Dinh, M. V. Pons Ventura, E. N. Vanderboon, F. K. Hazard, S.-J. Cho, R. S. Avedian, D. G. Mohler, M. Zimel, R. Wustrack, C. Curtis, M. Sirota and E. A. Sweet-Cordero, *Clin Cancer Res*, 2024, **30**, 849–864.

[162] E. C. González Díaz, A. G. Lee, L. C. Sayles, C. Feria, E. A. Sweet-Cordero and F. Yang, *Adv Healthc Mater*, 2022, **11**, e2200768.

[163] J. Beck, L. Ren, S. Huang, E. Berger, K. Bardales, J. Mannheimer, C. Mazcko and A. LeBlanc, *Vet Pathol*, 2022, **59**, 399–414.

[164] J. Dvorakova, L. Wiesnerova, P. Chocholata, V. Kulda, L. Landsmann, M. Cedikova, M. Kripnerova, L. Eberlova and V. Babuska, *Biomed Eng Online*, 2023, **22**, 33.

[165] H. Wilson-Robles, K. Franks, R. Pool and T. Miller, *BMC Vet Res*, 2019, **15**, 357.

[166] A. B. Mohseny, I. Machado, Y. Cai, K.-L. Schaefer, M. Serra, P. C. W. Hogendoorn, A. Llombart-Bosch and A.-M. Cleton-Jansen, *Lab Investig*, 2011, **91**, 1195–1205.

[167] T. Ikeda, Y. Futaesaku and N. Tsuchida, *Virchows Archiv B Cell Pathol*, 1992, **62**, 199–206.

[168] A. Billiau, V. G. Edy, H. Heremans, J. Van Damme, J. Desmyter, J. A. Georgiades and P. De Somer, *Antimicrob Ag Chemother*, 1977, **12**, 11–15.

[169] S. U. Lauvrak, E. Munthe, S. H. Kresse, E. W. Stratford, H. M. Namløs, L. A. Meza-Zepeda and O. Myklebost, *Brit J Canc*, 2013, **109**, 2228–2236.

[170] I.-S. Hsieh, R.-S. Yang and W.-M. Fu, *PLoS One*, 2014; 9(**10)**: e109550..

[171] J. Fogh and G. Trempe, in *Hum Tum Cells in Vitro*, ed. J. Fogh, Springer US, Boston, MA, 1975, pp. 115–159.

[172] H. Adwan, T. J. Bäuerle and M. R. Berger, *Canc Gene Ther*, 2004, **11**, 109–120.

[173] M. J. Ortuño, S. Ruiz-Gaspà, E. Rodríguez-Carballo, A. R. G. Susperregui, R. Bartrons, J. L. Rosa and F. Ventura, *J Biol Chem*, 2010, **285**, 31985–31994.

[174] C. Maucort, A. Di Giorgio, S. Azoulay and M. Duca, *ChemMedChem*, 2021, **16**, 14–29.

[175] J. A. Efe and S. Ding, *Philos Trans R Soc Lond B Biol Sci*, 2011, **366**, 2208–2221.

[176] H. Hanna, L. M. Mir and F. M. Andre, *Stem Cell Res Ther*, 2018, **9**, 203.

[177] N. Jaiswal, S. E. Haynesworth, A. I. Caplan and S. P. Bruder, *J Cell Biochem*, 1997, **64**, 295–312.

[178] V. Sottile, A. Thomson and J. McWhir, *Cloning Stem Cells*, 2003, **5**, 149–155.

[179] F. E. Freeman, H. Y. Stevens, P. Owens, R. E. Guldberg and L. M. McNamara, *Tissue Eng Part A*, 2016, **22**, 1176–1190.

[180] L. Thiagarajan, H. A.-D. M. Abu-Awwad and J. E. Dixon, *Stem Cells Transl Med*, 2017, **6**, 2146–2159.

[181] M. Yuasa, T. Yamada, T. Taniyama, T. Masaoka, W. Xuetao, T. Yoshii, M. Horie, H. Yasuda, T. Uemura, A. Okawa and S. Sotome, *PLoS One*, 2015, **10(2)**, e0116462.

[182] F. Martino, A. R. Perestrelo, V. Vinarský, S. Pagliari and G. Forte, *Front Physiol*, 2018, **9**, 824.

[183] H. Krahl, U. Michaelis, H.-G. Pieper, G. Quack and M. Montag, *Am J Sports Med*, 1994, **22**, 751–757.

[184] P. P. Provenzano and P. J. Keely, *J Cell Sci*, 2011, **124**, 1195–1205.

[185] A. M. Handorf, Y. Zhou, M. A. Halanski and W.-J. Li, *Organogen*, 2015, **11**, 1–15.

[186] C. Shuai, W. Yang, S. Peng, C. Gao, W. Guo, Y. Lai and P. Feng, *Int J Bioprint*, 2018, **4**, 138.

[187] J. Cao, Y. Man and L. LI, *Biomed Rep*, 2013, **1**, 428–432.

[188]J. G. Hardy, R. C. Sukhavasi, D. Aguilar, M. K. Villancio-Wolter, D. J. Mouser, S. A. Geissler, L. Nguy, J. K. Chow, D. L. Kaplan and C. E. Schmidt, *J. Mater. Chem. B*, 2015, **3**, 8059–8064.

[189] Z. Liu, L. Dong, L. Wang, X. Wang, K. Cheng, Z. Luo and W. Weng, *Sci Rep*, 2017, **7**, 17926.

[190]A. S. G. Curtis and M. Varde, *JNCI: J Nation Cancer Inst*, 1964, **33**, 15–26.

[191] A. S. G. Curtis, S. Reid, I. Martin, R. Vaidyanathan, C.-A. Smith, H. Nikukar and M. J. Dalby, *IEEE Trans Nanobiosci*, 2013, **12**, 247–254.

[192]M. J. Dalby, N. Gadegaard, R. Tare, A. Andar, M. O. Riehle, P. Herzyk, C. D. W. Wilkinson and R. O. C. Oreffo, *Nature Mater*, 2007, **6**, 997–1003.

[193] A. K. Luu and A. M. Viloria-Petit, *Int J Mol Sci*, 2020, **21**, 7595.

[194] X. Wang, Y. Yang, X. Hu, N. Kawazoe, Y. Yang and G. Chen, *ANAL. SCI.*, 2016, **32**, 1177–1182.

[195] D. Docheva, D. Padula, C. Popov, W. Mutschler, H. Clausen-Schaumann and M. Schieker, *J Cell Mol Med*, 2008, **12**, 537–552.

[196] S. Li, H. Bai, X. Chen, S. Gong, J. Xiao, D. Li, L. Li, Y. Jiang, T. Li, X. Qin, H. Yang, C. Wu, F. You and Y. Liu, *ACS Biomater Sci Eng*, 2020, **6**, 5588–5598.

[197] A. Singh, P. Singh and A. K. Dubey, *Open Ceram*, 2022, **9**, 100234.

[198] P. M. Tsimbouri, P. G. Childs, G. D. Pemberton, J. Yang, V. Jayawarna, W. Orapiriyakul, K. Burgess, C. González-García, G. Blackburn, D. Thomas, C. Vallejo-Giraldo, M. J. P. Biggs, A. S. G. Curtis, M. Salmerón-Sánchez, S. Reid and M. J. Dalby, *Nature Biomedl Eng*, 2017, **1**, 758–770.

[199] H. Nikukar, S. Reid, P. M. Tsimbouri, M. O. Riehle, A. S. G. Curtis and M. J. Dalby, *ACS Nano*, 2013, **7**, 2758–2767.

[200] W. Orapiriyakul, M. P. Tsimbouri, P. Childs, P. Campsie, J. Wells, M. A. Fernandez-Yague, K. Burgess, K. E. Tanner, M. Tassieri, D. Meek, M. Vassalli, M. J. P. Biggs, M. Salmeron-Sanchez, R. O. C. Oreffo, S. Reid and M. J. Dalby, *ACS Nano*, 2020, **14**, 10027–10044.

[201] S. N. Robertson, P. Campsie, P. G. Childs, F. Madsen, H. Donnelly, F. L. Henriquez, W. G. Mackay, M. Salmerón-Sánchez, M. P. Tsimbouri, C. Williams, M. J. Dalby and S. Reid, Phil Trans R Soc*: Math Phys Eng Sci*, 2018, **376**, 20170290.

[202] G. E. Neurohr and A. Amon, *Trends Cell Biol*, 2020, **30**, 213–225.

[203] S. N. Rampersad, *Sensors (Basel)*, 2012, **12**, 12347–12360.

[204] I. G. Reddin, T. R. Fenton, M. N. Wass and M. Michaelis, *Pharmacol Res*, 2023, **188**, 106671.

[205] F. Prinz, T. Schlange and K. Asadullah, *Nat Rev Drug Discov*, 2011, **10**, 712–712.

[206] S. J. Lord, K. B. Velle, R. D. Mullins and L. K. Fritz-Laylin, *J Cell Biol*, 2020, **219**, e202001064.

[207] P. Ghahremani, Y. Li, A. Kaufman, R. Vanguri, N. Greenwald, M. Angelo, T. J. Hollmann and S. Nadeem, *Nat Mach Intell*, 2022, **4**, 401–412.

[208] V. Boveia and A. Schutz-Geschwender, *Methods Mol Biol*, 2015, **1314**, 115–130.

[209] L. D. Lu and J. M. Salvino, *Methods Enzymol*, 2023, **681**, 115–153.

[210] M. J. Cecchini, M. Amiri and F. A. Dick, *J Vis Exp*, 2012, 3491.

[211] J. Muhr and D. W. Hagey, *BioEssays*, 2021, **43**, 2000285.

[212] G. Tai, I. Christodoulou, A. E. Bishop and J. M. Polak, *Biochem Biophys Res Commun*, 2005, **333**, 1116–1122.

[213] M. Marinkovic, O. N. Tran, T. J. Block, R. Rakian, A. O. Gonzalez, D. D. Dean, C.-K. Yeh and X.-D. Chen, *Matrix Biol Plus*, 2020, **8**, 100044

[214] D. Plesca, S. Mazumder and A. Almasan, *Methods Enzymol*, 2008, **446**, 107–122.

[215] A. De Becker, R. Heestermans, W. De Brouwer, K. Bockstaele, K. Maes and I. Van Riet, *Front Bioeng Biotechnol*, 2022, **10**, 1008271.

[216] D. G. Phinney, G. Kopen, W. Righter, S. Webster, N. Tremain and D. J. Prockop, *J Cell Biochem*, 1999, **75**, 424–436.

[217] K. Nagayama, F. Kodama, N. Wataya, A. Sato and T. Matsumoto, *Journal of the Mechanical Behavior of Biomed Mater*, 2023, **138**, 105630.

[218] M. Griffin, A. Sebastian, J. Colthurst and A. Bayat, *PLOS ONE*, 2013, **8**, e72978.

[219] G. Alloisio, D. B. Rodriguez, M. Luce, C. Ciaccio, S. Marini, A. Cricenti and M. Gioia, *Int J Mol Sci*, 2023, **24**, 7686.

[220] H. J. Choi, J. J. Lee, J. B. Lee, H.-J. Sung, J.-W. Shin, J. W. Shin, Y. Wu and J. K. Kim, *Biomater Res*, 2016, **20**, 32.

[221] Y.-J. Chen, M.-C. Chang, C.-C. Jane Yao, H.-H. Lai, J. Z.-C. Chang and J.-H. Jeng, *J Formosan Med Associat*, 2014, **113**, 447–453.

[222] P.-Y. Wang, D. T. Bennetsen, M. Foss, H. Thissen and P. Kingshott, *Biointerphases*, 2015, **10**, 04A306.

[223] R. S. Carvalho, J. E. Scott and E. H. Yen, *Arch Oral Biol*, 1995, **40**, 257–264.

[224] M. Yang, L.-W. Xiao, E.-Y. Liao, Q.-J. Wang, B.-B. Wang and J.-X. Lei, *Int J Clin Exp Pathol*, 2014, **7**, 7451–7459.

[225] O. S. Yevlashevskaya, B. A. Scheven, A. D. Walmsley and R. M. Shelton, *Sci Rep*, 2023, **13**, 14472.

[226] H. Orimo and T. Shimada, *Mol Cell Biochem*, 2006, **282**, 101–108.

[227] A. G. Ayala, J. Y. Ro, A. K. Raymond, N. Jaffe, S. Chawla, H. Carrasco, M. Link, J. Jimenez, J. Edeiken, S. Wallace, J. A. Murray and R. Benjamin, *Cancer*, 1989, **64**, 2162–2173.

[228] U. E. Martinez-Outschoorn, M. Peiris-Pagés, R. G. Pestell, F. Sotgia and M. P. Lisanti, *Nat Rev Clin Oncol*, 2017, **14**, 11–31.

[229] O. Warburg, *Naturwissenschaften*, 1924, **12**, 1131–1137.

[230] C. F. Cori and G. T. Cori, *J Biol Chem*, 1925, **65**, 397–405.

[231] M. Potter, E. Newport and K. J. Morten, *Biochem Soc Trans*, 2016, **44**, 1499–1505.

[232] O. Warburg, *Sci*, 1956, **123**, 309–314.

[233] P. Vaupel and G. Multhoff, *J Physiol*, 2021, **599**, 1745–1757.

[234] C. S. Ahn and C. M. Metallo, *Cancer Metabol*, 2015, **3**, 1.

[235] R. J. DeBerardinis and N. S. Chandel, *Nat Metab*, 2020, **2**, 127–129.

[236] J. Chen, L. Cui, S. Lu and S. Xu, *Cell Death Dis*, 2024, **15**, 1–18.

[237] A. Suzuki and J. Iwata, *Bone*, 2021, **146**, 115881.

[238] L. Shen, Y. Yu, Y. Zhou, S. M. Pruett-Miller, G.-F. Zhang and C. M. Karner, *eLife*, 2022, **11**, e76963.

[239] W. Xue, K. Wu, X. Guo, C. Chen, T. Huang, L. Li, B. Liu, H. Chang and J. Zhao, *Biochim Biophys Acta Mol Basis Dis*, 2024, **1870**, 166982.

[240] Z. Zhang, Y. Qiu, Y. Hua, Y. Wang, T. Chen, A. Zhao, Y. Chi, L. Pan, S. Hu, J. Li, C. Yang, G. Li, W. Sun, Z. Cai and W. Jia, *J Proteome Res*, 2010, **9**, 4861–4868.

[241] R. Fritsche-Guenther, Y. Gloaguen, M. Kirchner, P. Mertins, P.-U. Tunn and J. A. Kirwan, *Cancers (Basel)*, 2020, **12**, 1371.

[242] A. Horn and J. K. Jaiswal, *Curr Top Membr*, 2019, **84**, 67–98.

[243] L. A. Broadfield, A. A. Pane, A. Talebi, J. V. Swinnen and S.-M. Fendt, *Dev Cell*, 2021, **56**, 1363–1393.

[244] A. Akhmetshina, D. Kratky and E. Rendina-Ruedy, *Metabol*, 2023, **13**, 578.

[245] H. Sunshine and M. L. Iruela-Arispe, *Curr Opin Lipidol*, 2017, **28**, 408–413.

[246] C. Schiliro and B. L. Firestein, *Cells*, 2021, **10**, 1056.

[247] R. Goodacre, S. Vaidyanathan, W. B. Dunn, G. G. Harrigan and D. B. Kell, *Trends Biotechnol.*, 2004, **22**, 245–252.

[248] F. Danzi, R. Pacchiana, A. Mafficini, M. T. Scupoli, A. Scarpa, M. Donadelli and A. Fiore, *Sig Transduct Target Ther*, 2023, **8**, 1–22.

[249] L. G. Gardinassi, J. Xia, S. E. Safo and S. Li, *Curr Pharmacol Rep*, 2017, **3**, 374–383.

[250] S. Qiu, Y. Cai, H. Yao, C. Lin, Y. Xie, S. Tang and A. Zhang, *Sig Transduct Target Ther*, 2023, **8**, 1–37.

[251] D. B. Kell and S. G. Oliver, *Metabolomics*, 2016, **12**, 148.

[252] J. Klingberg, B. Keen, A. Cawley, D. Pasin and S. Fu, *Arch Toxicol*, 2022, **96**, 949–967.

[253] J. K. Khanijou, H. Kulyk, C. Bergès, L. W. Khoo, P. Ng, H. C. Yeo, M. Helmy, F. Bellvert, W. Chew and K. Selvarajoo, *Metab Eng Commun*, 2022, **15**, e00209.

[254] J.-P. Trezzi, C. Jäger, S. Galozzi, K. Barkovits, K. Marcus, B. Mollenhauer and K. Hiller, *MethodsX*, 2017, **4**, 95–103.

[255] A. Sengupta and A. M. Weljie, *Curr Protoc Protein Sci*, 2019, **98**, e98.

[256] L. Perez de Souza, S. Alseekh, T. Naake and A. Fernie, *Curr Protoc Plant Biol*, 2019, **4**, e20100.

[257] K. Contrepois, L. Jiang and M. Snyder, *Mol Cell Proteomics*, 2015, **14**, 1684–1695.

[258] D. C. Dean, S. Shen, F. J. Hornicek and Z. Duan, *Cancer Metastasis Rev*, 2018, **37**, 719–731.

[259] J. Roy, P. Dibaeinia, T. M. Fan, S. Sinha and A. Das, *J Lipid Res*, 2019, **60**, 375–387.

[260] L. Ren, E. S. Hong, A. Mendoza, S. Issaq, C. T. Hoang, M. Lizardo, A. LeBlanc and C. Khanna, *Oncotarget*, 2017, **8**, 38541–38553.

[261] L. Li, L. Zhang, Y. Yuan, X. Lu, Y. Zhang, Y. Liu, J. Wen, M. A. Khader, T. Liu, J. Li and Y. Zhang, *Cancer Med*, 2021, **10**, 4493–4509.

[262] H. Zhang, T. Wang, H. Gong, R. Jiang, W. Zhou, H. Sun, R. Huang, Y. Wang, Z. Wu, W. Xu, Z. Li, Q. Huang, X. Cai, Z. Lin, J. Hu, Q. Jia, C. Ye, H. Wei and J. Xiao, *Bone Res*, 2023, **11**, 1–15.

[263] I. F. Duarte, I. Lamego, J. Marques, M. P. M. Marques, B. J. Blaise and A. M. Gil, *J. Proteome Res.*, 2010, **9**, 5877–5886.

[264] F. Wang, Z. Zhang, Q. Li, T. Yu and C. Ma, *Cancer Cell Int*, 2020, **20**, 269.

[265] M. T. Santini, R. Romano, G. Rainaldi, A. Ferrante, A. Motta and P. L. Indovina, *Radiation Res*, 2006, **165**, 131–141.

[266] Z. Zhong, S. Mao, H. Lin, H. Li, J. Lin and J.-M. Lin, *Talanta*, 2019, **204**, 6–12.

[267] M. Cortini, S. Avnet and N. Baldini, *Cancer Lett*, 2017, **405**, 90–99.

[268] G. Bonuccelli, S. Avnet, G. Grisendi, M. Salerno, D. Granchi, M. Dominici, K. Kusuzaki and N. Baldini, *Oncotarget*, 2014, **5**, 7575–7588.

[269] S. Yang, Z. Tian, Y. Feng, K. Zhang, Y. Pan, Y. Li, Z. Wang, W. Wei, X. Qiao, R. Zhou, L. Yan, Q. Li, H. Guo, J. Yuan, P. Li and Z. Lv, *BMC Med Genomics*, 2022, **15**, 265.

[270] M. N. U. Le, R. Chen, L. Xia, J. Zhou and Y. Ning, *Data Brief*, 2023, **50**, 109500.

[271] S. B. Sunjic, A. C. Gasparovic, M. Jaganjac, G. Rechberger, A. Meinitzer, T. Grune, S. D. Kohlwein, B. Mihaljevic and N. Zarkovic, *Cells*, 2021, **10**, 269.

[272] G. Fanelli, G. Alloisio, V. Lelli, S. Marini, S. Rinalducci and M. Gioia, *Front Mol Biosci*, 2024, **10**, 1297826.

[273] https://www.polyomics.gla.ac.uk/ms_metabolomics.html, (accessed 31 May 2024).

[274] D. J. Creek, A. Jankevics, K. E. V. Burgess, R. Breitling and M. P. Barrett, *Bioinformatics*, 2012, **28**, 1048–1049.

[275] Z. Pang, Y. Lu, G. Zhou, F. Hui, L. Xu, C. Viau, A. F. Spigelman, P. E. MacDonald, D. S. Wishart, S. Li and J. Xia, *Nucleic Acids Res*, 2024, gkae253.

[276] A. Krämer, J. Green, J. Pollard and S. Tugendreich, *Bioinform*, 2014, **30**, 523–530., (QIAGEN Inc., https://digitalinsights.qiagen.com/IPA).

[277] C. Ma, X. Tian, J. P. Kim, D. Xie, X. Ao, D. Shan, Q. Lin, M. R. Hudock, X. Bai and J. Yang, *PNAS*, 2018, **115**, E11741–E11750.

[278] C. Chandhanayingyong, Y. Kim, J. R. Staples, C. Hahn and F. Y. Lee, *Sarcoma*, 2012, **2012**, 404810.

[279] J.-M. Kim, Y.-S. Yang, K. H. Park, H. Oh, M. B. Greenblatt and J.-H. Shim, *Int J Mol Sci*, 2019, **20**, 1803.

[280] Y.-S. Li, Z.-H. Deng, C. Zeng and G.-H. Lei, *J Recept Signal Transduct Res*, 2016, **36**, 465–470.

[281] M. B. Greenblatt, J.-H. Shim, S. Bok and J.-M. Kim, *J Bone Metab*, 2022, **29**, 1–15.

[282] C. O. Smith and R. A. Eliseev, *Stem Cells Dev*, 2021, **30**, 149–162.

[283] J. Zhang, X.-H. Yu, Y.-G. Yan, C. Wang and W.-J. Wang, *Clin Chim Acta*, 2015, **444**, 182–192.

[284] N. M. Anderson, P. Mucka, J. G. Kern and H. Feng, *Protein Cell*, 2018, **9**, 216–237.

[285] J. Eniafe and S. Jiang, *Oncogene*, 2021, **40**, 3351–3363.

[286] A. S. Martins, A. L. M. Batista de Carvalho, M. P. M. Marques and A. M. Gil, *Mol*, 2021, **26**, 4805.

[287] X. Wang, G. He, K. Mai, W. Xu and H. Zhou, *Sci Rep*, 2016, **6**, 21231.

[288] S. W. Schaffer, C. Ju Jong, R. KC and J. Azuma, *J Biomed Sci*, 2010, **17**, S2.

[289] L. Ren, S.-H. Hong, Q.-R. Chen, J. Briggs, J. Cassavaugh, S. Srinivasan, M. M. Lizardo, A. Mendoza, A. Y. Xia, N. Avadhani, J. Khan and C. Khanna, *Cancer Res*, 2012, **72**, 1001-1012.

[290] C. Wu, J. Tan, H. Shen, C. Deng, C. Kleber, G. Osterhoff and N. Schopow, *J Biomed Sci*, 2024, **31**, 4.

[291] D. Lohnes and G. Jones, *J Biol Chem*, 1987, **262**, 14394–14401.

[292] M.-L. Siu-Caldera, H. Sekimoto, A. S. Brem, R. Bina and G. S. Reddy, *Pediatr Res*, 1999, **45**, 98–98.

[293] C. C. Flarakos, A. Weiskopf, M. Robinson, G. Wang, P. Vouros, G. J. Sasso, M. R. Uskokovic and G. S. Reddy, *Steroids*, 2017, **119**, 18–30.

[294] R. A. Egnatchik, A. K. Leamy, S. A. Sacco, Y. E. Cheah, M. Shiota and J. D. Young, *J Biol Chem*, 2019, **294**, 3081–3090.

[295] M. Holeček, *Metabolism*, 2023, **145**, 155614.

[296] F. J. Ballard and R. W. Hanson, *J Lipid Res*, 1967, **8**, 73–79.

[297] N. N. Pavlova, J. Zhu and C. B. Thompson, *Cell Metabol*, 2022, **34**, 355–377.

[298] F. J. Shirkoohi, M. Ghollasi, R. Halabian, E. Eftekhari and M. Ghiasi, *Mol Biol Rep*, 2024, **51**, 451.

[299] O. E. Owen, S. C. Kalhan and R. W. Hanson, *J Biol Chem*, 2002, **277**, 30409–30412.

[300] X. Fu, Y. Li, T. Huang, Z. Yu, K. Ma, M. Yang, Q. Liu, H. Pan, H. Wang, J. Wang and M. Guan, *Adv Sci*, 2018, **5**, 1700755.

[301] K. Vasan, M. Werner and N. S. Chandel, *Cell Metab*, 2020, **32**, 341–352.

[302] V. L. Albaugh, K. Mukherjee and A. Barbul, *J Nutr*, 2017, **147**, 2011–2017.

[303] D.-Q. Tang, L. Zou, X.-X. Yin and C. N. Ong, *Mass Spec Rev*, 2016, **35**, 574–600.

[304] C.-L. Liu, A. M. Watson, A. R. Place and R. Jagus, *Mar Drugs*, 2017, **15**, 147.

[305] J. Y. L. Chiang, *Compr Physiol*, 2013, **3**, 1191–1212.

[306] Q. Song, J. xia Guo, Y. xun Ma, T. Ou, J. Zhang, H. zi Li, S. quan Mi, Y. zhen Zhang, H. Oda and W. Chen, *Heliyon*, 2023, **9**, e16401.

[307] M. Okano, F. He, N. Ma, H. Kobayashi, S. Oikawa, K. Nishimura, I. Tawara and M. Murata, *Acta Histochem*, 2023, **125**, 151978.

[308] P. Singh, K. Gollapalli, S. Mangiola, D. Schranner, M. A. Yusuf, M. Chamoli, S. L. Shi, B. L. Bastos, T. Nair, A. Riermeier, E. M. Vayndorf, J. Z. Wu, A. Nilakhe, C. Q. Nguyen, M. Muir, M. G. Kiflezghi, A. Foulger, A. Junker, J. Devine, K. Sharan, S. J. Chinta, S. Rajput, A. Rane, P. Baumert, M. Schönfelder, F. Iavarone, G. di Lorenzo, S. Kumari, A. Gupta, R. Sarkar, C. Khyriem, A. S. Chawla, A. Sharma, N. Sarper, N. Chattopadhyay, B. K. Biswal, C. Settembre, P. Nagarajan, K. L. Targoff, M. Picard, S. Gupta, V. Velagapudi, A. T. Papenfuss, A. Kaya, M. G. Ferreira, B. K. Kennedy, J. K. Andersen, G. J. Lithgow, A. M. Ali, A. Mukhopadhyay, A. Palotie, G. Kastenmüller, M. Kaeberlein, H. Wackerhage, B. Pal and V. K. Yadav, *Sci*, 2023, **380**, eabn9257.

[309] J. Prah, A. Winters, K. Chaudhari, J. Hersh, R. Liu and S.-H. Yang, *Brain Res*, 2019, **1723**, 146378.

[310] X. Shi, Q. Cheng, L. Xu, J. Yan, M. Jiang, J. He, M. Xu, M. Stefanovic-Racic, I. Sipula, R. M. O'Doherty, S. Ren and W. Xie, *Mol Cell Biol*, 2014, **34**, 485–497.

[311] M. Vallée, *Front Neuroendocrinol*, 2024, **72**, 101113.

[312] S. Higashi, M. Oeda, K. Yamamoto and K. Miyazaki, *J Biol Chem*, 2008, **283**, 35735–35744.

[313] K. Yamamoto, K. Miyazaki and S. Higashi, *J Biol Chem*, 2010, **285**, 28862–28873.

[314] J. Kallen, J.-M. Schlaeppi, F. Bitsch, I. Delhon and B. Fournier, *J Biol Chem*, 2004, **279**, 14033–14038.

[315] N. Melo, O. V. Belyaeva, W. K. Berger, L. Halasz, J. Yu, N. Pilli, Z. Yang, A. V. Klyuyeva, C. A. Elmets, V. Atigadda, D. D. Muccio, M. A. Kane, L. Nagy, N. Y. Kedishvili and M. B. Renfrow, *J Biol Chem*, 2023, **299**, 102746.

[316] D. Hasan, K. W. Lindsay, E. F. Wijdicks, G. D. Murray, P. J. Brouwers, W. H. Bakker, J. van Gijn and M. Vermeulen, *Stroke*, 1989, **20**, 1156–1161.

[317] S. J. Winters, T. Vitaz, M. R. Nowacki, D. C. Craddock, C. Silverman and F. A. Lopez, *The Am J Med Sci*, 2015, **349**, 526–529.

[318] C. Otte, H. Jahn, A. Yassouridis, J. Arlt, N. Stober, P. Maass, K. Wiedemann and M. Kellner, *Life Sci*, 2003, **73**, 1835–1845.

[319] A.-S. C. A. M. Koning, J. C. Buurstede, L. T. C. M. van Weert and O. C. Meijer, *J Endocr Soc*, 2019, **3**, 1917–1930.

[320] Alakpa, Enateri V (2014) Cell metabolism in response to biomaterial mechanics. PhD thesis, University of Glasgow, http://theses.gla.ac.uk/4970/, (accessed 03-06-24)

[321] B. Schwanhäusser, D. Busse, N. Li, G. Dittmar, J. Schuchhardt, J. Wolf, W. Chen and M. Selbach, *Nature*, 2011, **473**, 337–342.

[322] L. Cheng, C. Wang and J. Jing, *Curr Pharm Des*, 2016, **22**, 4830–4834.

[323] M. S. Cooper, *Clin Med (Lond)*, 2012, **12**, 261–265.

[324] Y. Nishio, Y. Dong, M. Paris, R. J. O'Keefe, E. M. Schwarz and H. Drissi, *Gene*, 2006, **372**, 62–70.

[325] A. Koussounadis, S. P. Langdon, I. H. Um, D. J. Harrison and V. A. Smith, *Sci Rep*, 2015, **5**, 10775.

[326] H.-J. Kim, W.-J. Kim and H.-M. Ryoo, *Mol Cells*, 2020, **43**, 160–167.

[327] X. Zhang, S. Tu, Y. Wang, B. Xu and F. Wan, *Acta Bioch Biophys Sin*, 2014, **46**, 261–272.

[328] C. Zhou, X. Zhang, L. Xu, T. Wu, L. Cui and D. Xu, *Amino Acids*, 2014, **46**, 1673–1680.

[329] A. Rauch, S. Seitz, U. Baschant, A. F. Schilling, A. Illing, B. Stride, M. Kirilov, V. Mandic, A. Takacz, R. Schmidt-Ullrich, S. Ostermay, T. Schinke, R. Spanbroek, M. M. Zaiss, P. E. Angel, U. H. Lerner, J.-P. David, H. M. Reichardt, M. Amling, G. Schütz and J. P. Tuckermann, *Cell Metabol*, 2010, **11**, 517–531.

[330] B. Frenkel, W. White and J. Tuckermann, *Adv Exp Med Biol*, 2015, **872**, 179–215.

[331] N. Cao, Z. Wang, C. Huang, B. Chen, P. Zhao, Y. Xu and Y. Tian, *Arch Gerontol Geriatr*, 2023, **114**, 105080.

[332] Q. Xing, J. Feng and X. Zhang, *Exp Cell Res*, 2021, **403**, 112595.

[333] M. Eijken, M. Koedam, M. van Driel, C. J. Buurman, H. A. P. Pols and J. P. T. M. van Leeuwen, *Mol Cell Endocrinol*, 2006, **248**, 87–93.

[334] L. D. Sanchez, L. Pontini, M. Marinozzi, L. C. Sanchez-Aranguren, A. Reis and I. H. K. Dias, *Brit J Pharmacol*, 2021, **178**, 3327–3341.

[335] M. M. Pérez-Jiménez, J. M. Monje-Moreno, A. M. Brokate-Llanos, M. Venegas-Calerón, A. Sánchez-García, P. Sansigre, A. Valladares, S. Esteban-García, I. Suárez-Pereira, J. Vitorica, J. J. Ríos, M. Artal-Sanz, Á. M. Carrión and M. J. Muñoz, *Nat Commun*, 2021, **12**, 49.

[336] P. M. Elias, M. L. Williams, E.-H. Choi and K. R. Feingold, *Biochim Biophys Acta Mol Cell Bio Lipids*, 2014, **1841**, 353–361.

[337] Q. Zhou, L. Shen, C. Liu, C. Liu, H. Chen and J. Liu, *Anticancer Res*, 2016, **36**, 1683–1691.

[338] K. L. Gross, R. H. Oakley, A. B. Scoltock, C. M. Jewell and J. A. Cidlowski, *Mol Endocrinol*, 2011, **25**, 1087–1099.

[339] S. Gündisch, E. Boeckeler, U. Behrends, E. Amtmann, H. Ehrhardt and I. Jeremias, *Anticancer Res*, 2012, **32**, 4251–4261.

[340] M. A. Pufall, *Adv Exp Med Biol*, 2015, **872**, 315–333.

[341] M. Schwarz, E. G. Lund, K. D. R. Setchell, H. J. Kayden, J. E. Zerwekh, I. Björkhem, J. Herz and D. W. Russell, *J Biol Chem*, 1996, **271**, 18024–18031.

[342] J. Urbańska, A. Karewicz and M. Nowakowska, *Life Sci*, 2014, **96**, 1–6.

[343] P. Horby, W. S. Lim, J. R. Emberson, M. Mafham, J. L. Bell, L. Linsell, N. Staplin, C. Brightling, A. Ustianowski, E. Elmahi, B. Prudon, C. Green, T. Felton, D. Chadwick, K. Rege, C. Fegan, L. C. Chappell, S. N. Faust, T. Jaki, K. Jeffery, A. Montgomery, K. Rowan, E. Juszczak, J. K. Baillie, R. Haynes and M. J. Landray, *N. Engl. J. Med.*, 2021, **384**, 693–704.

[344] P. J. Hesketh, M. G. Kris, E. Basch, K. Bohlke, S. Y. Barbour, R. A. Clark-Snow, M. A. Danso, K. Dennis, L. L. Dupuis, S. B. Dusetzina, C. Eng, P. C. Feyer, K. Jordan, K. Noonan, D. Sparacio and G. H. Lyman, *J Clin Oncol*, 2020, **38**, 2782–2797.

[345] T. Rhen, and J. A. Cidlowski, *N Engl J. Med*, 2005, **353**, 1711-1723

[346] C. Zhuang, X. Guan, H. Ma, H. Cong, W. Zhang and Z. Miao, *Eur J Med Chem*, 2019, **163**, 883–895.

[347] Y. Jin, S. Edalatian Zakeri, R. Bahal and A. J. Wiemer, *Pharmacol Rev*, 2022, **74**, 680–713.

[348] Z. Su, D. Xiao, F. Xie, L. Liu, Y. Wang, S. Fan, X. Zhou and S. Li, *Acta Pharm Sin B*, 2021, **11**, 3889–3907.

[349] T. K. Patel, N. Adhikari, S. A. Amin, S. Biswas, T. Jha and B. Ghosh, *New J. Chem.*, 2021, **45**, 5291–5321.

[350] X. Yang, Z. Pan, M. R. Choudhury, Z. Yuan, A. Anifowose, B. Yu, W. Wang and B. Wang, *Med Res Rev*, 2020, **40**, 2682–2713.

[351] Y. Jin, L. Song, Y. Su, L. Zhu, Y. Pang, F. Qiu, G. Tong, D. Yan, B. Zhu and X. Zhu, *Biomacromol*, 2011, **12**, 3460–3468.

[352] S. Murugappan, S. Dastari, K. Jungare, N. M. Barve and N. Shankaraiah, *J Mol Struc*, 2024, **1307**, 138012.

[353] R. Mohi-ud-din, A. Chawla, P. Sharma, P. A. Mir, F. H. Potoo, Ž. Reiner, I. Reiner, D. A. Ateşşahin, J. Sharifi-Rad, R. H. Mir and D. Calina, *Eur J Med Res*, 2023, **28**, 345.

[354] G. Zagotto, B. Gatto, S. Moro, C. Sissi and M. Palumbo, *J Chromatogr B Biomed Sci Appl*, 2001, **764**, 161–171.

[355] Y. Wang, J. Du, Y. Wang, Q. Jin and J. Ji, *Chem. Commun.*, 2015, **51**, 2999–3002.

[356] T. Etrych, M. Jelínková, B. Říhová and K. Ulbrich, *J Control Release*, 2001, **73**, 89–102.

[357] B. Říhová, T. Etrych, M. Pechar, M. Jelínková, M. Šťastný, O. Hovorka, M. Kovář and K. Ulbrich, *J Control Release*, 2001, **74**, 225–232.

[358] R. Patil, J. Portilla-Arias, H. Ding, B. Konda, A. Rekechenetskiy, S. Inoue, K. L. Black, E. Holler and J. Y. Ljubimova, *Int J Mol Sci*, 2012, **13**, 11681–11693.

[359] E. Kicková, S. Salmaso, F. Mastrotto, P. Caliceti and A. Urtti, *Pharmaceut*, 2021, **13**, 791.

[360] M. J. Webber, J. B. Matson, V. K. Tamboli and S. I. Stupp, *Biomaterials*, 2012, **33**, 6823–6832.

[361] N. Pishesha, T. Harmand, C. Carpenet, X. Liu, A. Bhan, A. Islam, R. van den Doel, W. Pinney and H. L. Ploegh, *PNAS*, 2022, **119**, e2211065119.

[362] E. Bílková, M. Sedlák, A. Imramovský, P. Chárová, P. Knotek and L. Beneš, *Int J Pharm*, 2011, **414**, 42–47.

[363] Z. Jia, X. Wang, X. Wei, G. Zhao, K. W. Foster, F. Qiu, Y. Gao, F. Yuan, F. Yu, G. M. Thiele, T. K. Bronich, J. R. O'Dell and D. Wang, *ACS Nano*, 2018, **12**, 7663–7681.

[364] H. Liu, D. Liu, M. Ji, P. Xiao, Y. Qin, J. Zhao, N. Wang, J. Gou, T. Yin, H. He, G. Chen, Y. Zhang and X. Tang, *Int J Pharmaceut*, 2022, **622**, 121900.

[365] Z. Jia, G. Zhao, X. Wei, D. Kong, Y. Sun, Y. Zhou, S. M. Lele, E. V. Fehringer, K. L. Garvin, S. R. Goldring and D. Wang, *J Control Release*, 2020, **324**, 560–573

[366] A. Ongaro, M. B. Violatto, E. Casarin, I. Pellerani, G. Marchini, G. Ribaudo, M. Salmona, M. Carbone, A. Passoni, E. Gnodi, E. Schiavon, A. Mattarei, D. Barisani, P. Invernizzi, P. Bigini and M. Morpurgo, *Nanomed Nanotech Biol Med*, 2022, **40**, 102497.

[367] L. Zhong, Y. Li, L. Xiong, W. Wang, M. Wu, T. Yuan, W. Yang, C. Tian, Z. Miao, T. Wang and S. Yang, *Sig Transduct Target Ther*, 2021, **6**, 1–48.

[368] R. Yang, E. A. Kolb, J. Qin, A. Chou, R. Sowers, B. Hoang, J. H. Healey, A. G. Huvos, P. A. Meyers and R. Gorlick, *Clin Cancer Res*, 2007, **13**, 2557–2567.

[369] M. Fernández, F. Javaid and V. Chudasama, *Chem Sci*, 2017, **9**, 790–810.

[370] A. M. Navale and A. N. Paranjape, *Biophys Rev*, 2016, **8**, 5–9.

[371] M. I. Molejon, G. Weiz, J. D. Breccia and M. I. Vaccaro, *World J Clin Oncol*, 2020, **11**, 110–120.

[372] J. Fan, J. Mei, M.-Z. Zhang, F. Yuan, S.-Z. Li, G.-R. Yu, L.-H. Chen, Q. Tang and C. J. Xian, *Oncol Lett*, 2017, **14**, 2439–2445.

[373] J. Fu, J. Yang, P. H. Seeberger and J. Yin, *Carbohydr Res*, 2020, **498**, 108195.

[374] E. C. Calvaresi and P. J. Hergenrother, *Chem Sci*, 2013, **4**, 2319–2333.

[375] Q.-L. He, I. Minn, Q. Wang, P. Xu, S. A. Head, E. Datan, B. Yu, M. G. Pomper and J. O. Liu, *Angew Chem*, 2016, **128**, 12214–12218.

[376] M. Veyhl, K. Wagner, C. Volk, V. Gorboulev, K. Baumgarten, W.-M. Weber, M. Schaper, B. Bertram, M. Wiessler and H. Koepsell, *PNAS*, 1998, **95**, 2914–2919.

[377] Y. Liu, J. Huang, M. Wu, B. Liu, Q. Lin, J. Wu, Y. Ouyang, X. Guo, R. Huang, Y. Zhang and J. Xu, *Eur J Med Chem*, 2022, **238**, 114463.

[378] D. X. Hu, P. Grice and S. V. Ley, *J. Org. Chem.*, 2012, **77**, 5198–5202.

[379] B. J. Ayers, J. Hollinshead, A. W. Saville, S. Nakagawa, I. Adachi, A. Kato, K. Izumori, B. Bartholomew, G. W. J. Fleet and R. J. Nash, *Phytochem*, 2014, **100**, 126–131.

[380] J.-P. Praly, G. Descotes, M.-F. Grenier-Loustalot and F. Metras, *Carbohydr Res*, 1984, **128**, 21–35.

[381] F. D. Guilherme, J. É. Simonetti, L. R. S. Folquitto, A. C. C. Reis, J. C. Oliver, A. L. T. Dias, D. F. Dias, D. T. Carvalho, G. C. Brandão and T. B. de Souza, Journal of Molecular Structure, 2019, 1184, 349–356.

[382] M. A. Shah, A. Uddin, M. R. Shah, I. Ali, R. Ullah, P. A. Hannan and H. Hussain, *Mol*, 2022, **27**, 6770.

[383] D. K. Kölmel and E. T. Kool, *Chem Rev*, 2017, **117**, 10358–10376.

[384] I. Hamzi, T. M. Barhoumi-Slimi and R. Abidi, *Heteroatom Chem*, 2016, **27**, 139–148.

[385] M. Li, B. Chen, S. Monteiro and A. M. Rustum, *Tetrahedron Lett*, 2009, **50**, 4575–4581.

[386] I. M. el-Kebbi, S. Roser, R. J. Pollet, S. W. Cushman and C. M. Wilson, *Biochem J*, 1994, **301**, 35–40.

[387] P. Miziak, M. Baran, E. Błaszczak, A. Przybyszewska-Podstawka, J. Kałafut, J. Smok-Kalwat, M. Dmoszyńska-Graniczka, M. Kiełbus and A. Stepulak, *Cancers (Basel)*, 2023, **15**, 4689.

[388]K. Fujita and N. Nonomura, *World J Mens Health*, 2019, **37**, 288–295.

[389] K.-T. Lin and L.-H. Wang, *Steroids*, 2016, **111**, 84–88.

[390] F. Liu, Q. Zhang, D. Zhou and J. Dong, *BMC Cancer*, 2019, **19**, 323.

[391] J. Wei, J. Shimazu, M. P. Makinistoglu, A. Maurizi, D. Kajimura, H. Zong, T. Takarada, T. lezaki, J. E. Pessin, E. Hinoi and G. Karsenty, *Cell*, 2015, **161**, 1576–1591.

[392] R. J. Stubbins and A. Karsan, *Blood Cancer J*, 2021, **11**, 1–9.

[393] Y. Li, C. Ge, J. P. Long, D. L. Begun, J. A. Rodriguez, S. A. Goldstein and R. T. Franceschi, *J Bone Miner Res*, 2012, **27**, 1263–1274.

[394] M. ter Huurne and H. G. Stunnenberg, *Cell Mol Life Sci*, 2021, **78**, 4507–4519.

[395] D. Green, A. Singh, V. L. Tippett, L. Tattersall, K. M. Shah, C. Siachisumo, N. J. Ward, P. Thomas, S. Carter, L. Jeys, V. Sumathi, I. McNamara, D. J. Elliott, A. Gartland, T. Dalmay and W. D. Fraser, *J. Bone Oncol*, 2023, **39**, 100474.

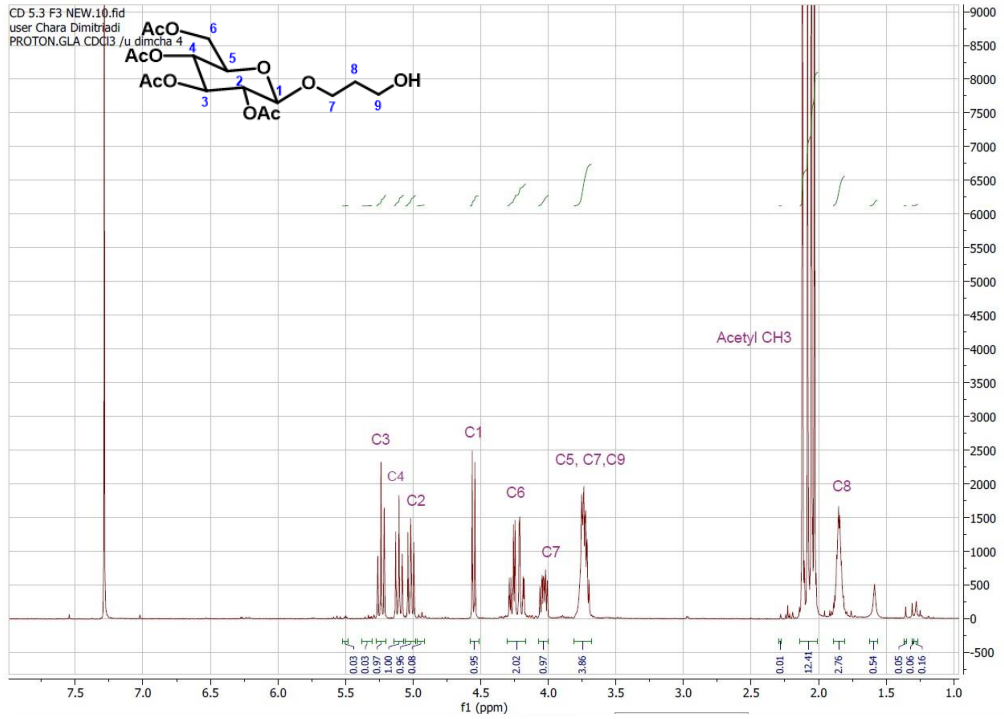

Figure S.1: ^{1}H NMR of Compound 6.4 in $CDCl_3$

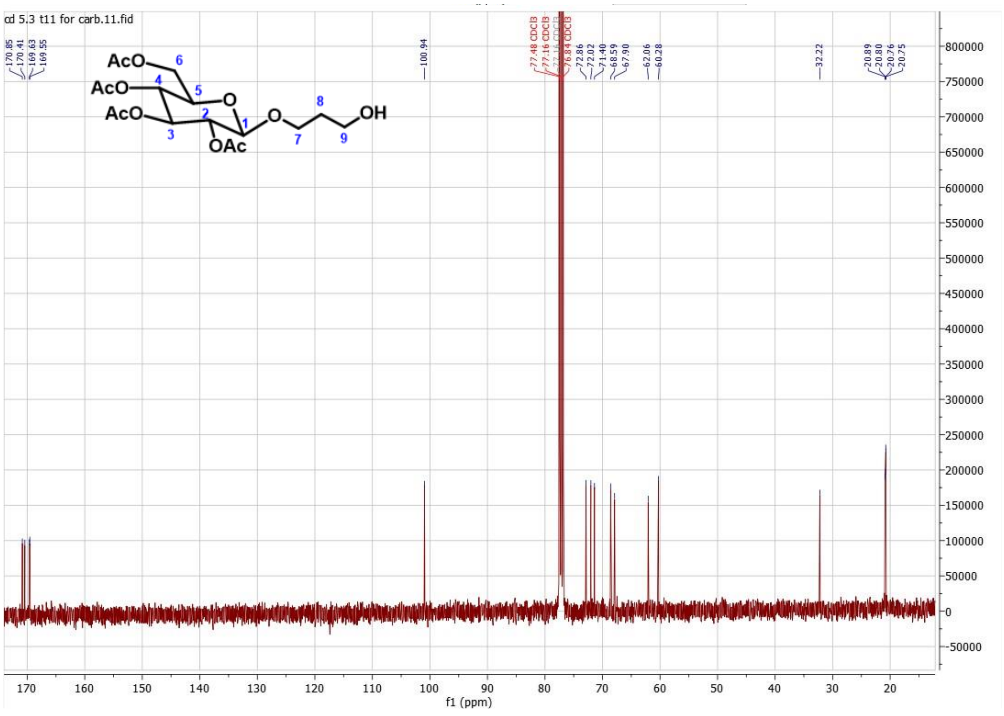

Figure S.2: ^{1}H NMR of Compound 6.4 in $CDCl_3$

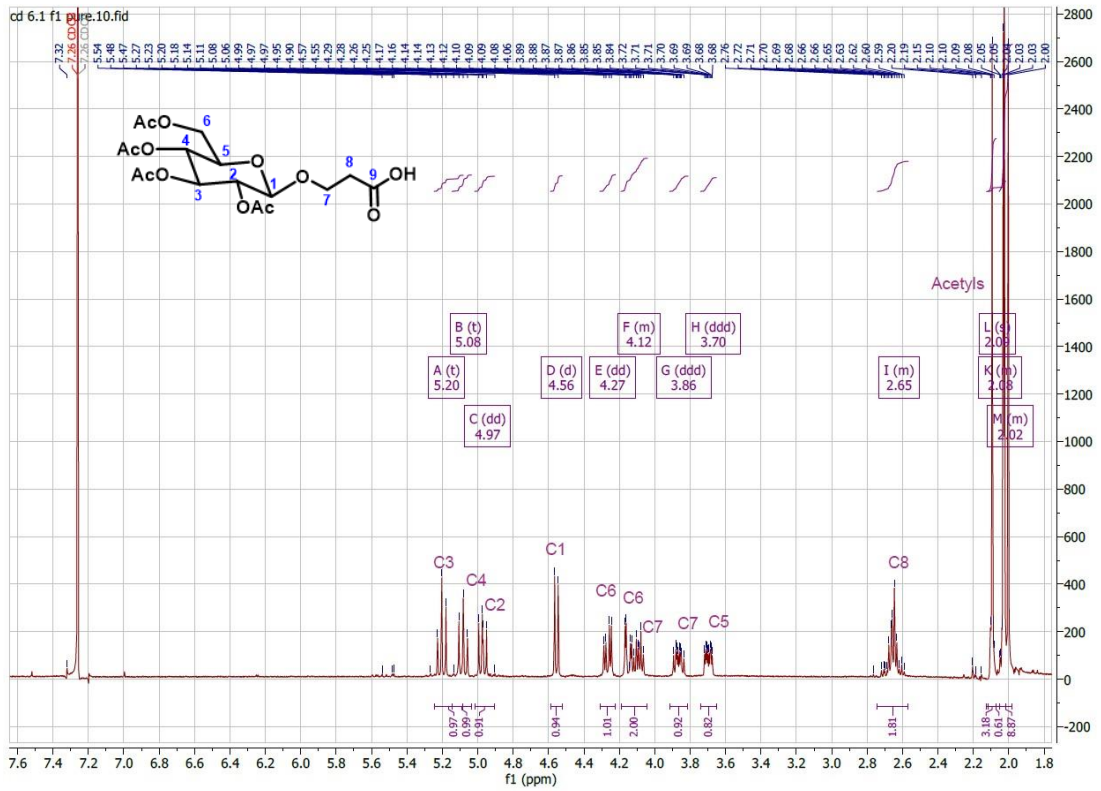

Figure S.3: ^{1}H NMR of Compound 6.5 in $CDCl_3$

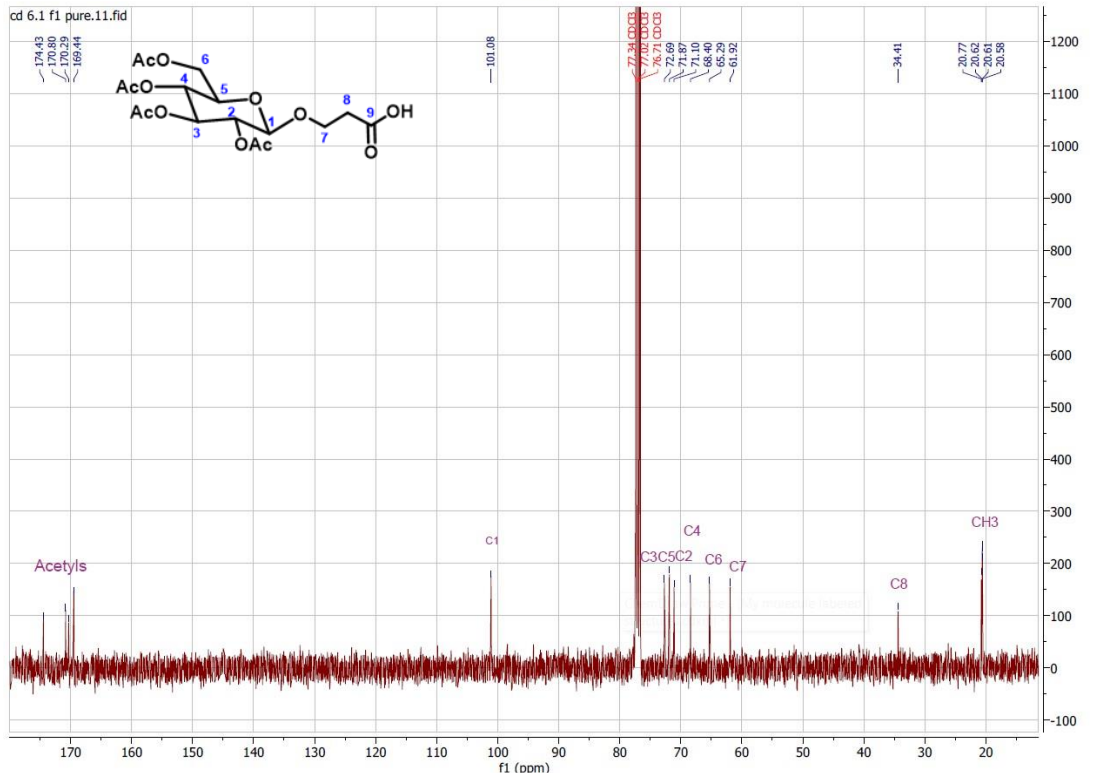

Figure S.4: ^{13}C NMR of Compound 6.5 in $CDCl_3$

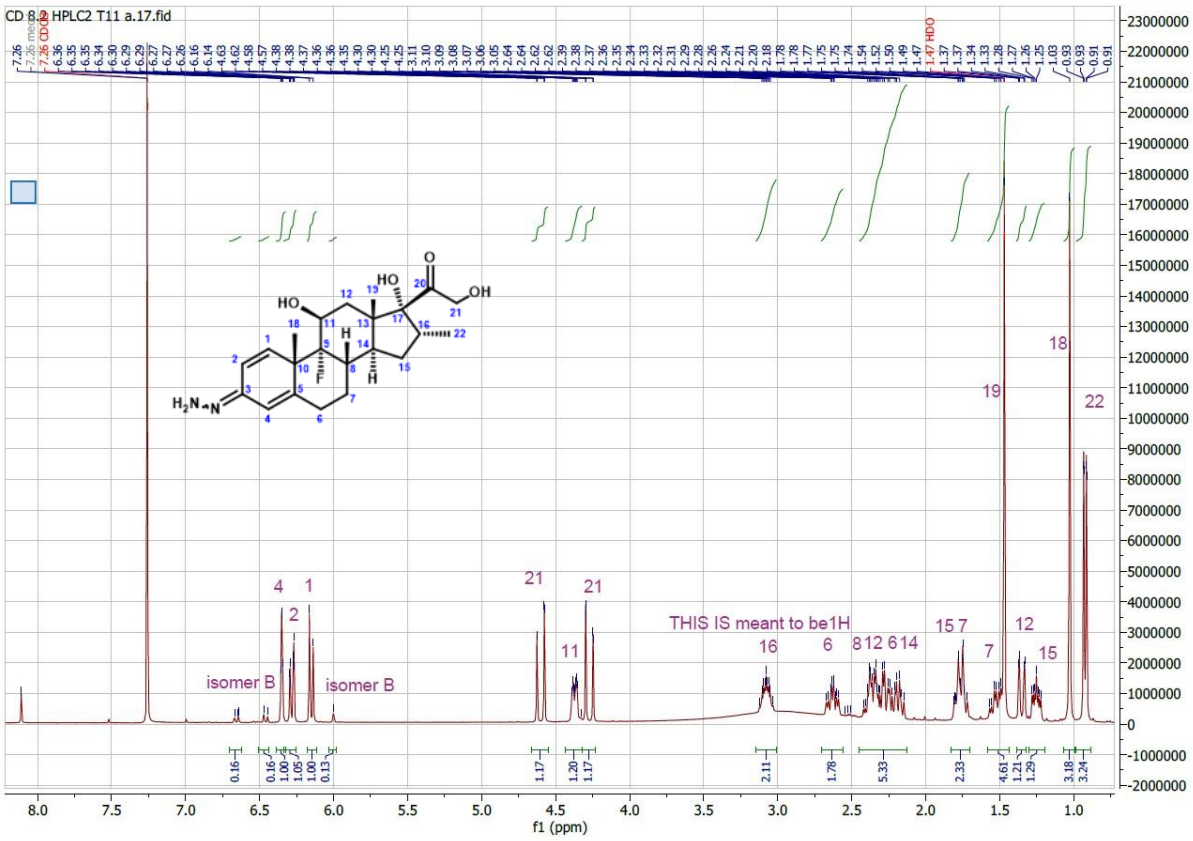

Figure S.5: Compound 6.7.B ^{1}H NMR in $CDCl_3$

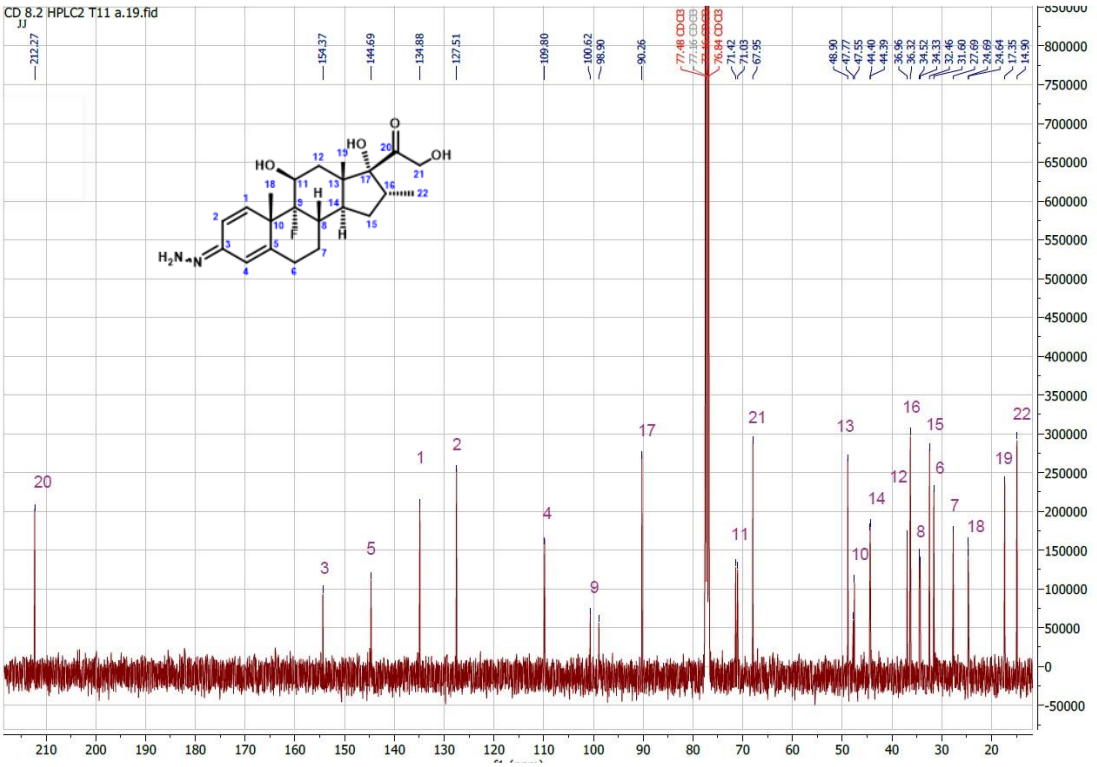

Figure S.6: Compound 6.7.B ^{13}C NMR in $CDCl_3$

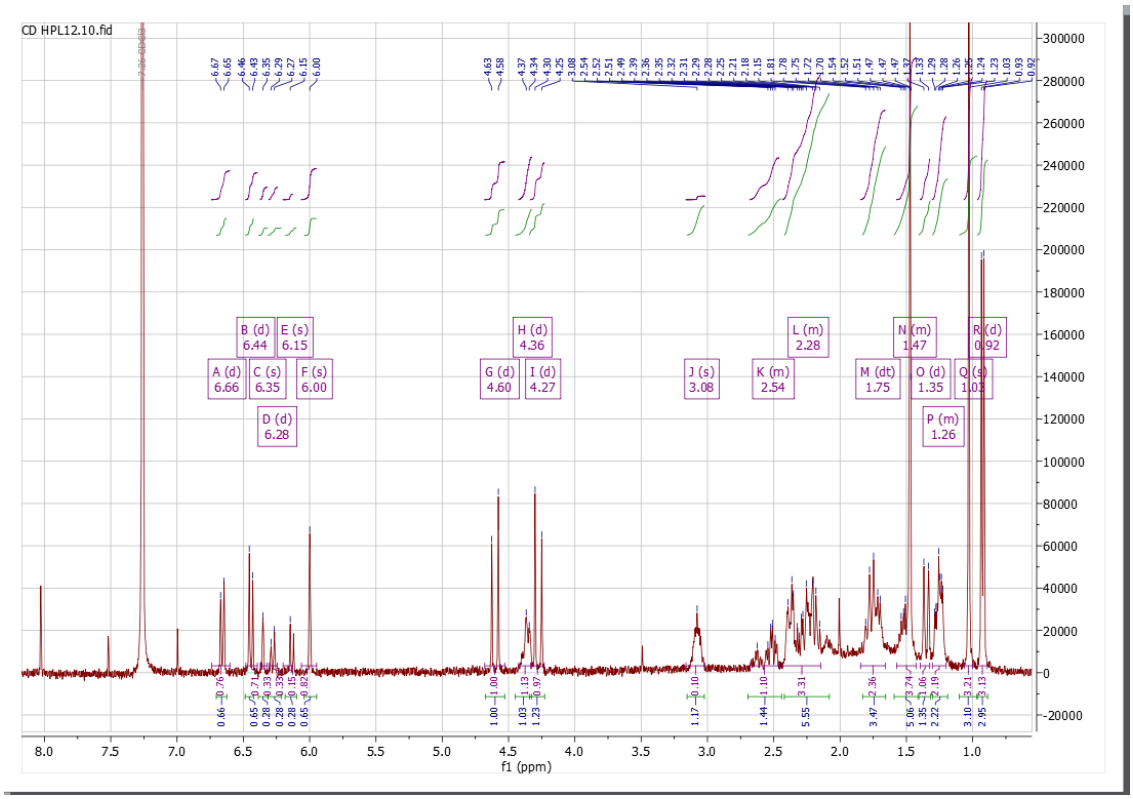

Figure S.7: Compounds 6.7A+6.7B mixture. ^{1}H NMR in $CDCl_3$

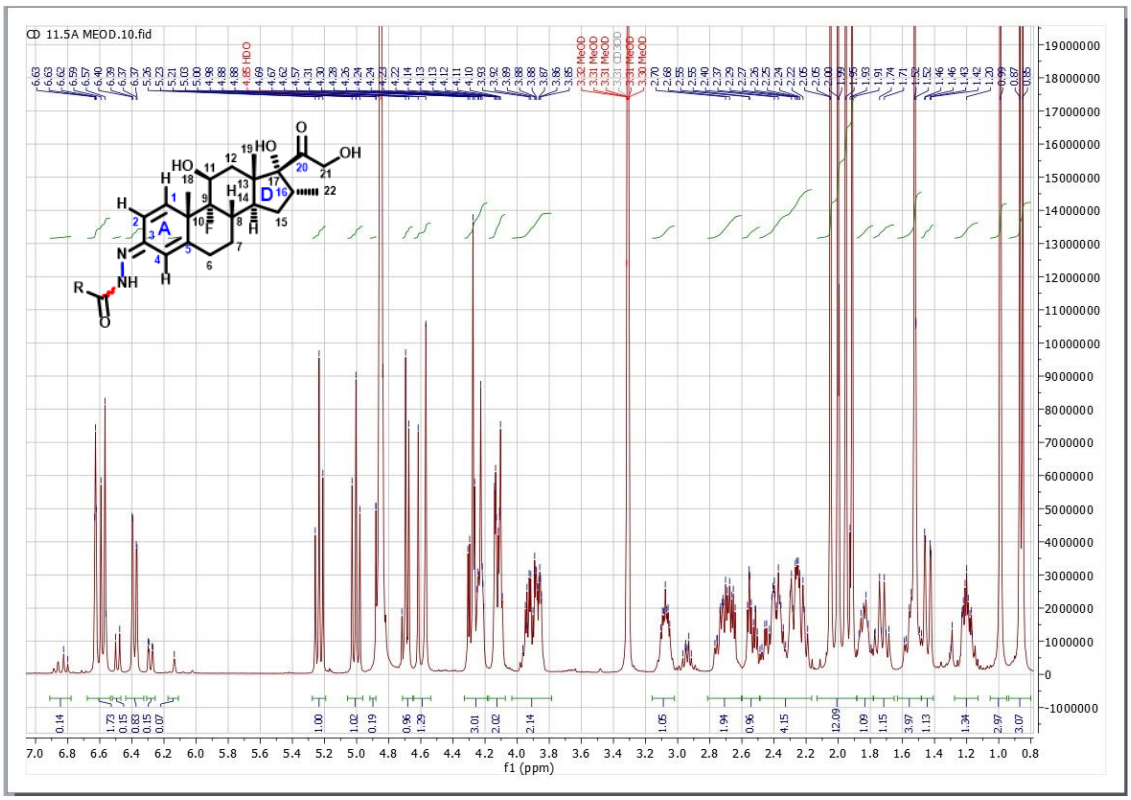

Figure S.8: ^{1}H NMR of Compound 6.9.A in CD_3OD

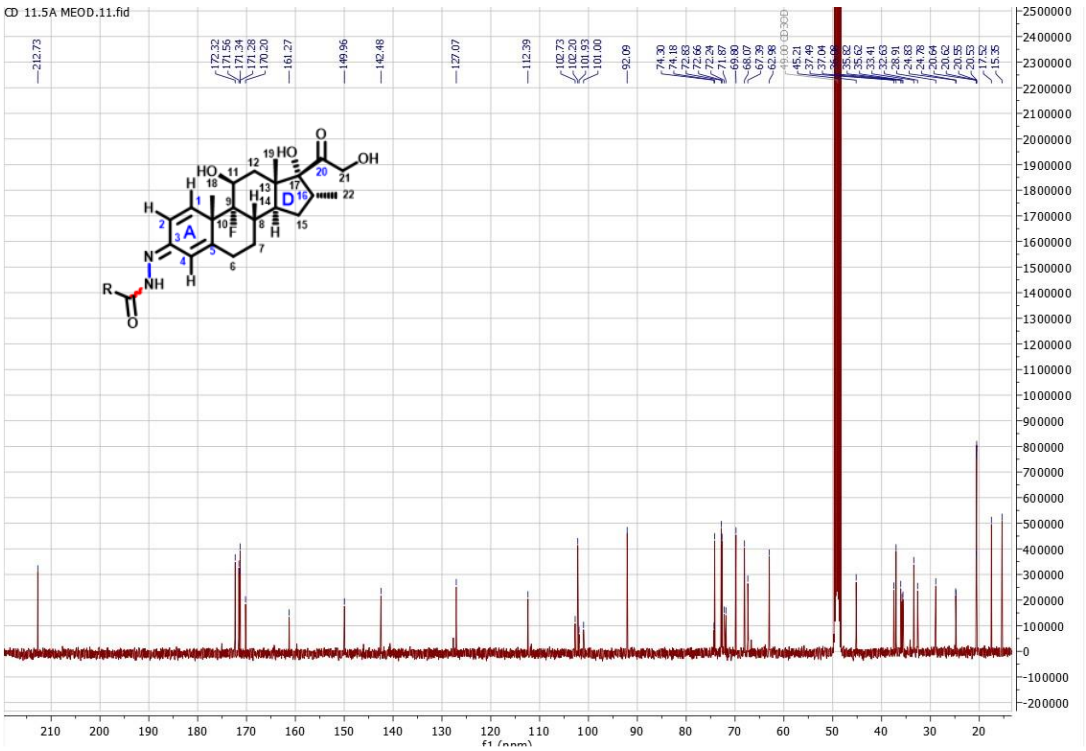

Figure S.9: ^{13}C NMR of Compound 6.9.A in CD_3OD

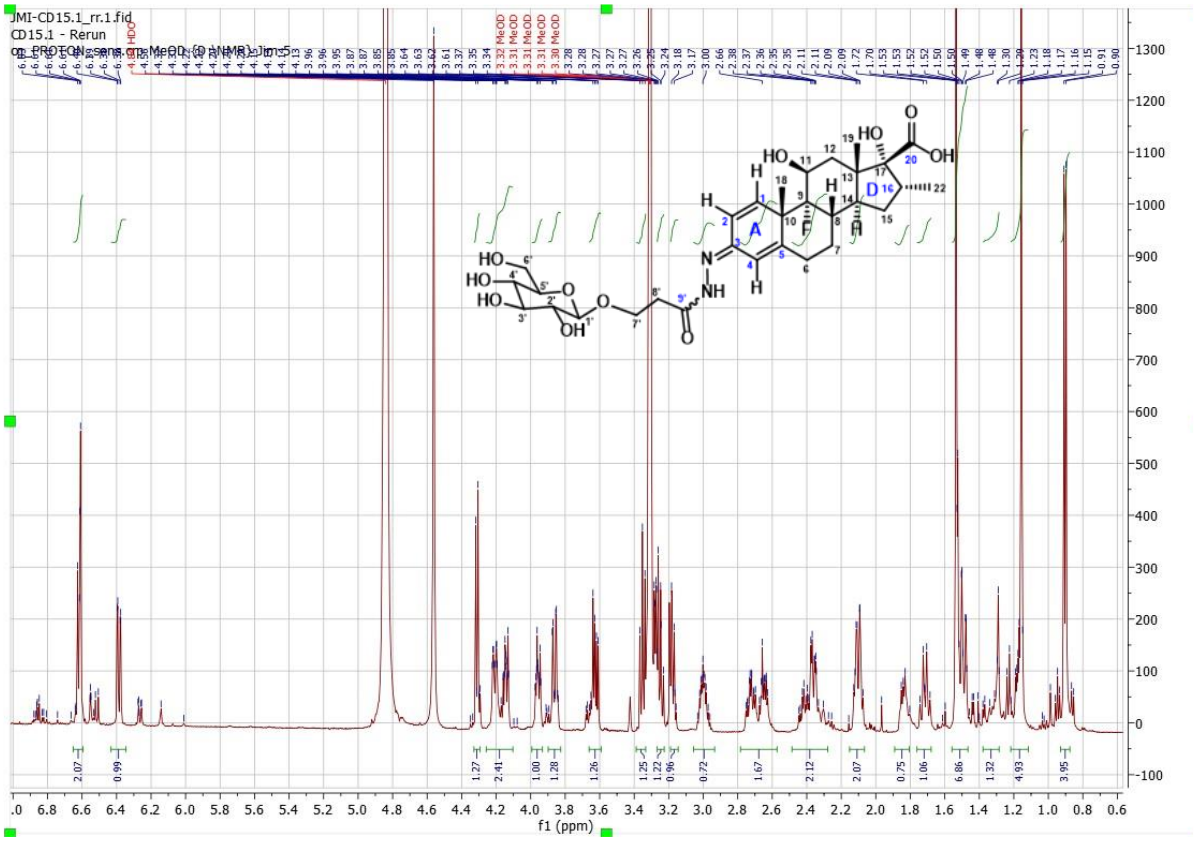

Figure S.10: ^{1}H NMR of Compound 6.12 in CD_3OD

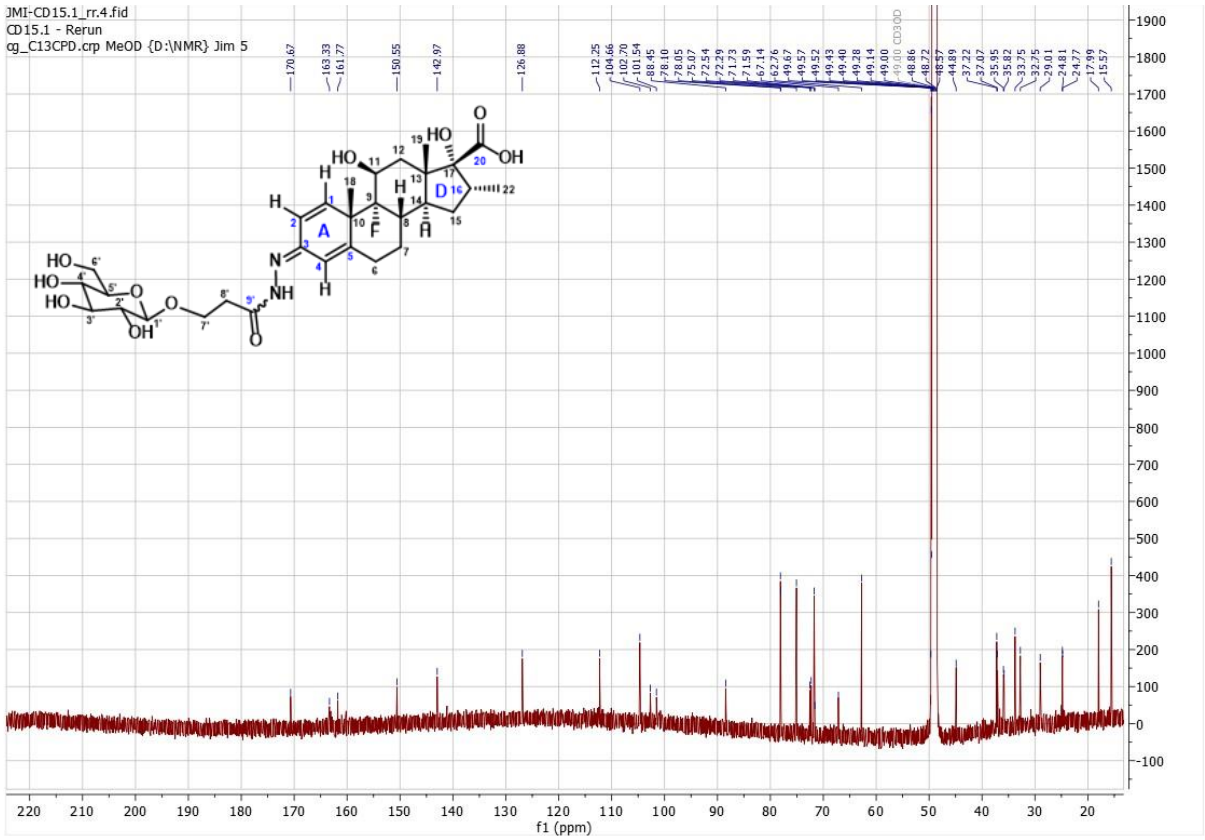

Figure S. 11: ^{13}C NMR of Compound 6.12 in CD_3OD